

IEK-3 Report 2015

Systems Research and Technology
for a Sustainable Energy Supply



Energie & Umwelt /
Energy & Environment
Band / Volume 279
ISBN 978-3-95806-077-7

Forschungszentrum Jülich GmbH
Institute of Energy and Climate Research
Electrochemical Process Engineering (IEK-3)

IEK-3 Report 2015

Systems Research and Engineering
for a Sustainable Energy Supply

Schriften des Forschungszentrums Jülich
Reihe Energie & Umwelt / Energy & Environment

Band / Volume 279

ISSN 1866-1793

ISBN 978-3-95806-077-7

Bibliographic information published by the Deutsche Nationalbibliothek.
The Deutsche Nationalbibliothek lists this publication in the Deutsche
Nationalbibliografie; detailed bibliographic data are available in the
Internet at <http://dnb.d-nb.de>.

Publisher and
Distributor: Forschungszentrum Jülich GmbH
Zentralbibliothek
52425 Jülich
Tel: +49 2461 61-5368
Fax: +49 2461 61-6103
Email: zb-publikation@fz-juelich.de
www.fz-juelich.de/zb

Cover Design: Grafische Medien, Forschungszentrum Jülich GmbH

Printer: Grafische Medien, Forschungszentrum Jülich GmbH

Copyright: Forschungszentrum Jülich 2015

Schriften des Forschungszentrums Jülich
Reihe Energie & Umwelt / Energy & Environment, Band / Volume 279

ISSN 1866-1793
ISBN 978-3-95806-077-7

The complete volume is freely available on the Internet on the Jülicher Open Access Server (JuSER)
at www.fz-juelich.de/zb/openaccess.

Neither this book nor any part of it may be reproduced or transmitted in any form or by any
means, electronic or mechanical, including photocopying, microfilming, and recording, or by any
information storage and retrieval system, without permission in writing from the publisher.

Forward	2
1 Contributions to International Conferences	5
1.1 Preparation, organization and result of ICEPE 2013	6
1.2 Scientific coordination of TRENDS 2015	10
2 Education and Training	13
2.1 University education	14
2.2 Provision of information and further education	19
3 Scientific and Technical Reports	23
3.1 Solid oxide fuel cells	24
3.2 Fuel processing and systems	37
3.3 High-temperature polymer electrolyte fuel cells	48
3.4 Direct Methanol Fuel Cells	61
3.5 Polymer Electrolyte Membrane Electrolysis	72
3.6 Process and Systems Analysis	85
3.7 Physicochemical and electrochemical principles	93
3.8 Quality assurance	103
4 Selected Results	105
4.1 Diffusion and ion conduction along ceramic interfaces	106
4.2 Mobile fuel processing systems with middle distillates for HT-PEFCs	111
4.3 Water distribution in the HT-PEFC	120
4.4 Efficiency aspects of high-pressure water electrolysis	123
4.5 Market launch of fuel cells for cars with renewable hydrogen	129
5 Ausblick auf neue FuE-Vorhaben	137
5.1 Development of a reversible system based on an SOFC	138
5.2 Metallic bipolar plates for HAT-PEFCs	143
5.3 The electrolysis pilot project at the JuHY hydrogen demonstration facility	148
5.4 More flexibility using integrated energy supply systems	153
6 Facts and Figures	159
6.1 IEK-3: Institute of Electrochemical Process Engineering	160
6.2 Overview of department expertise	163
6.3 Publikationen, Technologietransfer und Ressourcen	167
6.4 Committee work	169
6.5 Contributions to trade fairs and exhibitions	172
6.6 How to reach us	174
6.7 List of Abbreviations	177

Forward

Dear reader,

In the following I would like to give you a short overview of the activities of the institute in the years 2013 and 2014 and report some selected results, which I hope will encourage you to read further.

In the years 2013 and 2014, the institute continued to focus on the topic of the Energiewende (energy transition). The status of water electrolysis as the most important technology for the storage of renewable energy was reiterated and the systems analysis activities of the IEK-3 were further developed. Alongside acidic water electrolysis, alkaline water electrolysis was also included in the research program. Building on the work with ceramic fuel cells, bifunctional operation in both the fuel cell and electrolysis modes was also further researched. Successful project acquisitions have also succeeded in extending the systems analysis work in such a way that the German energy system can be investigated and illustrated. Within this framework, a consortium with 19 institutes of RWTH Aachen University and the Forschungszentrum Jülich has also been set up to engage in systems analysis. In addition, the IEK-3 has joined a virtual institute for research into “electricity to gas and heat”.

With regard to the reforming of kerosene and diesel to synthesis gas, further reactors have been developed in recent years alongside the actual reformer. A stable reforming process has been demonstrated in recent years. Remaining barriers to the commercialization of such aggregates include the dynamics and partial load capacity. Therefore, the injection of fuel remained a focus and thus injection nozzles were designed with an industrial consortium. This enabled spreading in the range of 15-100% of the rated load. Similarly, our development of the ceramic high temperature fuel cell focused on thermal cycling, which is also a commercialization barrier. By means of experiments and simulation of the mechanical stress, a 700 W stack could be improved such that it could withstand 100 thermal cycles. Even if this number would already be sufficient for some installations, work on thermomechanical stability will continue. On this basis, it was possible to describe the uptake of acidic electrolytes by basic polybenzimidazole. This behavior has particular practical significance for the filling of polybenzimidazole with phosphoric acid for the high temperature polymer electrolyte fuel cell. A 5 kW high temperature polymer electrolyte fuel cell stack was successfully operated with both hydrogen and synthetic reformat. The breadth of the institute's technical competencies constitute a good foundation for systems analysis. In this area of work, a regeneration-based energy supply concept for Germany was developed and verified through simulation. In light of the need to balance resources and costs, a coupled sector has been established that connects the electricity and transportation sectors via suitable gas infrastructures. Several of the dissertations that describe the complex, partial dynamic models with a high temporal resolution and high degree of specification of the physics were awarded prizes.

The Alexander Kuznetsov Prize of the Electrochemical Society for theoretical electrochemistry, which is internationally recognized in the electrochemical research field, was awarded to Professor Andrei Kulikovskiy in 2013 for his analytical models describing elementary fuel cell processes. I myself have received the Sir William Grove Award from the International Association of Hydrogen Energy.

I would like to thank my colleagues from the IEK-3 for their dedicated work, many good ideas and collaborative commitment. This was only possible through personal engagement, focused cooperation and fruitful exchange amongst scientists, as well as effective cooperation in technical and administrative areas. I would like to thank the BMBF for our basic funding and the many third party donors for the trust placed in our institute.



Jülich, June 2015

Dieter Polster



1

WHEC 2010

Contributions to the 18th World Hydrogen Energy Conference 2010

- Scientific coordination
- Coordination of accompanying events
- IEK-3 contributions
- Editing of books and publications

1.1 Preparation, organization and result of ICEPE 2013

ProcessNet – an initiative of DECHEMA e.V. and VDI-GVC – organizes events on the topics of process engineering, chemical engineering and industrial chemistry. Considering the heated discussions on the “Energiewende” – or transformation of the German energy sector – and the appropriate positioning of ProcessNet, the focus of the 3rd International Conference on Energy Process Engineering in 2013 was on the transition to renewable energy systems. In this context, the conference presentations targeted scientists and those from the industrial and political sectors with an interest in the topic. The aim was to present sustainable technologies and elements of a future energy supply system capable of achieving the G8 CO₂ mitigation targets of an 80% reduction in emissions by 2050 with a prevailing share of renewables from 2030 onwards. The 3rd ICEPE 2013, which took place from 3–6 June 2013 in Frankfurt am Main was attended by some 120 participants from 19 countries. The organizing committee was chaired by Prof. Detlef Stolten and Prof. Viktor Scherer was co-chairman.

1.1.1 Scientific coordination

The conference was opened by chairman of the organizing committee Prof. Stolten and the welcome address was given by Parliamentary State Secretary Schütte. This was followed by five presentations on the driving forces and greatest challenges characteristic of the transformation process aiming for a transition to renewable energy systems. The remaining ten plenary presentations on the first day with speakers from seven countries dealt with technical solutions and coherent strategies for a transition to renewable systems in various energy sectors as well as for the transition to a fully sustainable global energy system.

	Tue, June 4	Wed, June 5	Thu, June 6
09:00	Registration		
10:00		Plenum	Plenum
11:00	Plenum		
12:00		Parallel Session	Parallel Session
13:00	Lunch & Poster Exhibition	Lunch & Poster Exhibition	Lunch & Poster Exhibition
14:00		Plenum	
15:00			Parallel Session
16:00	Plenum	Parallel Session	
17:00			Closing Plenum
18:00			
19:00	Reception & Poster Exhibition	Reception, Conference Dinner & Poster Award	
20:00			

Table 1: Overview of the program for the 3rd ICEPE 2013

The second day began with four plenary presentations on energy savings potentials and technologies in the industrial sector, economic aspects of the transformation, an introduction to transmission networks and pumped-storage hydropower. Four parallel sessions followed on advanced batteries, biomass, chemical storage and sustainable buildings, each of which opened with an introductory presentation on the topic at hand. After lunch, the second day continued with two plenary presentations on natural gas pipeline systems and a future hydrogen infrastructure. They were followed by four parallel sessions on photovoltaics, electrochemical H₂ production, power to gas and emerging and developing countries. Four more parallel sessions on solar and geothermal power, geological gas storage and biomass for power production brought the second day to a close. The third and final day of the conference opened with a plenary presentation introducing transmission grid components, energy storage technologies and a comprehensive transition concept. The subsequent parallel sessions focused on maritime power production, the future role of fossil power plants, smart grids and sustainable buildings in Europe. After lunch, three plenary presentations looked at onshore and offshore wind power as well as hydropower. The final four parallel sessions concentrated on e-mobility, biofuels, chemical gas production and the near-surface gas storage of hydrogen. At the heart of the conference were the 50 15-minute scientific and technical presentations on some 20 overarching topics. Each of these topics was first introduced in a 30-minute presentation. An additional twelve plenary presentations aimed to provide delegates with additional information and were either directly related to a specific subtopic or supplemented the topics covered at the conference. Table 1 and Table 2 provide an overview of the conference program as well as the topics.

Topic Field	Power Generation	Gas Production	Biomass & Biofuels	Energy Storage	Energy Distribution	End-user Technologies	Other
Topic	Onshore Wind Power	Chemical Gas Production	Globale Aspects & Resources	Pumped Storage Hydropower	Smart Grid Power-to-Gas Technology	Sustainable Buildings - Europe	Emerging & Developing Countries
	Offshore Wind Power	Electrochemical Gas Production	Biomass for Power Production	Geological Gas Storage		Sustainable Buildings	
	Photovoltaic Power	Photoelectrical Gas Production	Biofuels	Near Surface Gas Storage		E-Mobility	
	Solarthermal Power			Advanced Batteries			
	Maritime Power						
	Hydro Power						
	Geothermal Power						
Futur Role of Fossil Power Plants							

Table 2: Overview of overarching conference topics

As part of the conference's poster program, almost 50 posters were presented during lunch breaks and on the first evening of the conference, providing interested delegates with an opportunity to discuss the various topics with the authors. Poster prizes were awarded by the organizers to the three best posers at the conference reception.

1.1.2 Conference contributions from IEK-3

IEK-3 scientists working on R&D topics relevant for renewable energy systems were involved in ICEPE 2013 on various levels. The program featured four presentations and two posters from IEK-3. Table 3 provides an overview of the different conference contributions. In his plenary presentation, Prof. Stolten presented the results of quantified path analyses to emphasize the central role of hydrogen in the extensive deployment of renewables. Introductory presentations in the plenary sessions on the status of technologies for hydrogen production by water electrolysis, power-to-gas processes and geological storage by Mr Mergel, Dr. Schiebahn and Dr. Wackerl were further highlights of the conference. Two posters rounded off the contributions made by IEK-3 to ICEPE 2013.

Presentation Typ	Session Topic	Presentation Topic	Speaker
Overview	Plenum	Carbon Capture Options for Coal Power Plants	Detlef Stolten
	M2	Physical Absorption Materials for CO ₂ Capture	Sebastian Schiebahn
Parallel	P4	Cascaded Membrane Processes for Post-Combustion CO ₂ Capture	Li Zhao
	P5	Oxygen Supply for Oxyfuel Power Plants by Oxy-Vac-Jül Process	Michael Weber
Poster	P6	Integration of Water-Gas Shift Membrane Reactor in IGCC for Pre-Combustion Capture	Sebastian Schiebahn
	P7	CO ₂ Separation from a Thermodynamic Viewpoint: 100% - Pure - Reversible	Ernst Riensche
	P7	CO ₂ Absorbition by MEA Scrubbing: Impact of Process Design Parameters on the Thermal Energy Consumption	Alexander Otto

Table 3: Presentations and posters by IEK-3 scientists

1.1.3 Books and series of publications

Together with the conference documentation, delegates received the first edition of the WILEY-VCH book “Transition to Renewable Energy Systems”, edited by the conference chairmen Prof. Stolten and Prof. Scherer. The 969-page book comprises the full texts of the key plenary and introductory presentations given at the 3rd ICEPE 2013. It is intended as a comprehensive reference work with data and publications for the experienced expert as well as a good introduction to the topic for the inexperienced, interested individual. It contains a total of 43 articles with an average length of 20 pages broken down into the following sections:

- Renewable Strategies
- Power Production
- Gas Production
- Biomass
- Storage
- Distribution
- Applications

IEK-3 scientists wrote five of the introductory articles, thus making a significant contribution to the book.

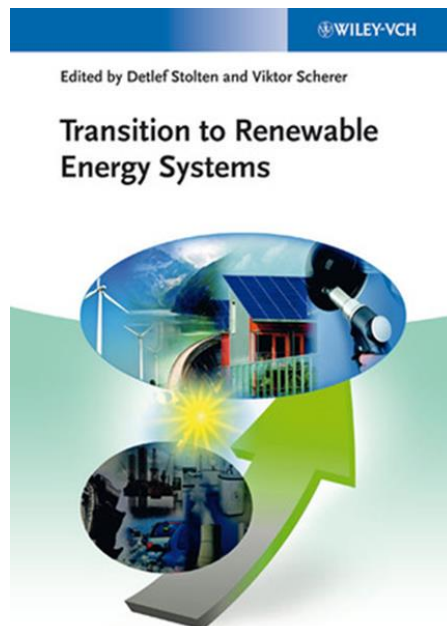


Fig. 1: Book with the plenary and introductory articles

1.2 Scientific coordination of TRENDS 2015

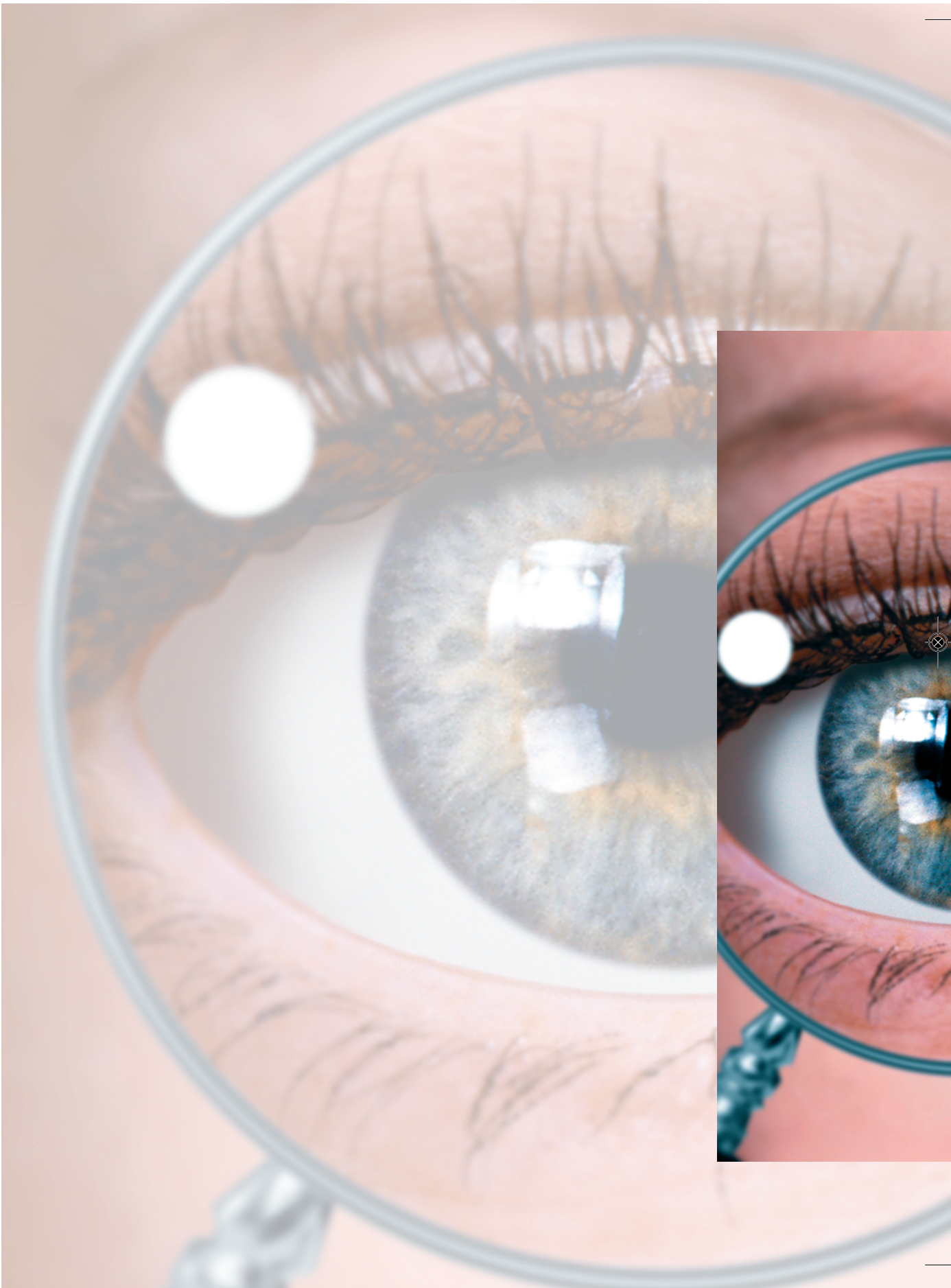
The round table discussion “TRENDS 2015” (Transition to Renewable Energy Devices and Systems) will take a closer look at topics that play an important role in the transition from existing fossil-based fuel chains to renewables. The discussion forum will be held in Aachen on 3 and 4 December 2015. The forum aims to identify pioneering developments and missing links that will make it possible to achieve the G8 targets of an 80% reduction in CO₂ emissions by 2050 and a prevailing share of renewables by 2030. The discussion forum will focus on fuels for the transportation sector and respective technology in vehicle drives and auxiliary power supply. The interaction between the fuel and the application will be emphasized. On the fuel side, a realistic quantitative assessment of the potential of alternative fuels and their production paths will be discussed. Cost aspects are important in this transition.

The first day of the discussion forum will analyze the potential of global biomass, alternative fuel strategies and the integration of biomass in conventional refinery processes and their distribution chains. The second day will be dedicated to discussing the corresponding process technologies from a production and application point of view. Table 4 provides an overview of relevant topics.

3 December 2015	4 December 2015
Global biomass potential	Auxiliary power for on-road and rail vehicles, ships and aircraft
Future energy paths for passenger transport	Systems analysis
Biorefineries with no waste water	Thermal management of electrical drives
Economic analyses	Drive systems for trucks
Future trends for jet engines	Bio-oils
International fuel strategies	Bio-based oxygenates
Hydrogen as a future energy carrier	Networks and services for battery vehicles, hybrids and fuel cell vehicles
Hydrotreatment of vegetable oils for future fuels	

Table 4: Overview of topics

Each topic will first be outlined in an introductory presentation covering the basic principles, technological implementation, latest developments in science and technology and references. This will be followed by extensive and in-depth discussion.

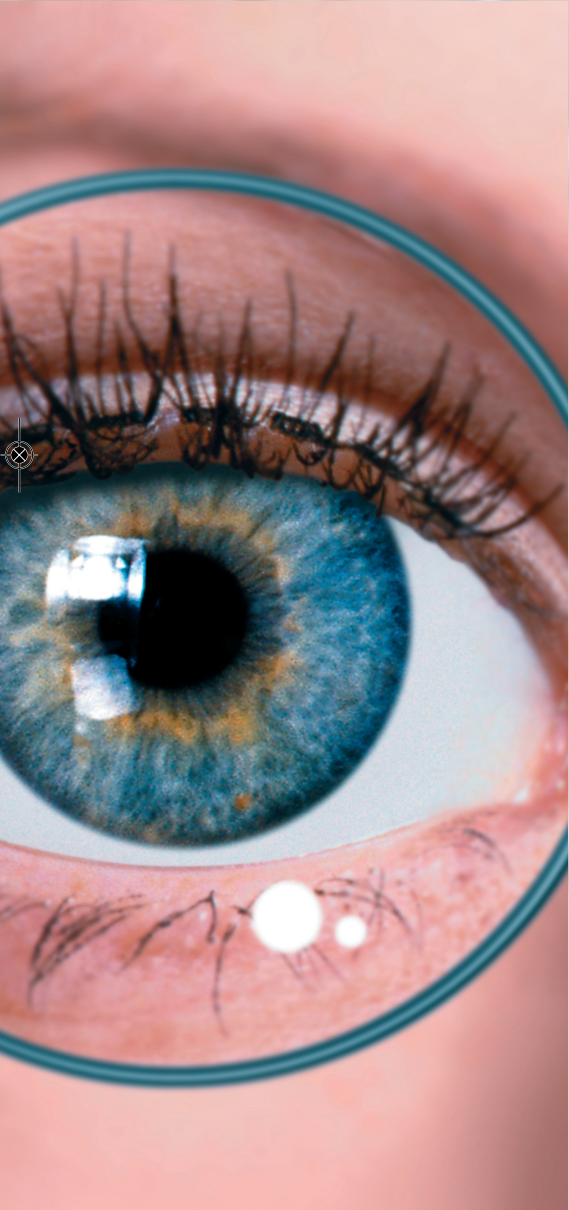


2

Education

Education and Training

- University education
- Contributions to information provision, further education and training



In addition to propagating knowledge on pioneering energy conversion technologies, several scientists at IEK-3 are involved in education and training for specific target groups. They give lectures and seminars at universities and also support and supervise doctoral students' projects. Students enrolled in dual study programs for laboratory technicians and mathematical-technical software developers are guided and trained at the institute. School children in grade 10 and above also benefit from lessons on energy technology given by IEK-3 employees.

2.1 University education

Teaching at universities is a fundamental responsibility of selected research scientists at IEK-3 in addition to their research and development work. Within the framework of the Jülich model, IEK-3 has one full professorship (grade W3) at RWTH Aachen University, which is currently held by Prof. Dr.-Ing. Detlef Stolten. Dr. Martin Müller supports Prof. Stolten, teaching seminars that accompany the lectures and conducting oral examinations at undergraduate level. Prof. Dr. rer. nat. Werner Lehnert is a grade-W2 professor at RWTH Aachen University in the Scientific Faculty. Privatdozent Dr. rer. nat. Carsten Korte lectures at Justus Liebig University Gießen. Two other grade-W2 professorships are held at Aachen University of Applied Sciences Campus Jülich by Prof. Dr.-Ing. Ralf Peters and Prof. Dipl.-Ing. Ludger Blum. Since winter semester 2012/2013, Dr.-Ing. Murat Peksen has been lecturing at Aachen University of Applied Sciences Campus Jülich and Dr.-Ing. Dipl.-Wirt.Ing. Thomas Grube works together with Prof. Peters teaching seminars accompanying his lectures and conducting oral examinations at undergraduate level. Fig. 2 shows the Internet addresses of the four universities at which IEK-3 scientists teach the next generation of scientists.



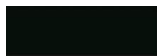
<http://www.rwth-aachen.de/>



<http://www.uni-ulm.de/>



<http://www.uni-giessen.de/>



FH AACHEN
UNIVERSITY OF APPLIED SCIENCES

<http://www.fh-aachen.de/>

Fig. 2: Universities where IEK-3 scientists lecture

The spectrum of topics taught ranges from the fundamentals of science and theoretical modeling and simulation methods to detailed technical knowledge and the characterization of technical applications. Each semester, one block seminar, five lecture courses and three seminar courses are taught. An additional half-day practical course is offered every summer semester. Up to eighty students take the various individual courses each semester. IEK-3 scientists also play an important role in supervising semester papers, undergraduate dissertations and doctoral theses. In 2013, nine bachelor's dissertations, thirteen diploma/master's dissertations and six doctoral theses were successfully completed. In 2014, ten bachelor's dissertations, seventeen diploma/master's dissertations and six doctoral theses were successfully completed.

2.1.1 Courses taught by professors

Table 5 provides an overview of the courses taught at universities by IEK-3 professors.

Name	Subject area	Type/hours Semester		University
Prof. Dr. D. Stolten	Principles and Technology of Fuel Cells	V/2 Ü/2	WS	RWTH Aachen
Prof. Dr. W. Lehnert	Modeling in Electrochemical Process Engineering	V/2 Ü/2	WS	RTWH Aachen
Prof. Dr. R. Peters	Basics and Applications of Chemical Reaction Theory – Simulation of Dynamic Processes in Energy Systems with Matlab/Simulink	V/2 Ü/2	WS	Aachen Univ. of Applied Sciences Campus Jülich
Prof. L. Blum	Fuel Cells – The Future of Decentralized Energy Supply!?	V/2	WS	Aachen Univ. of Applied Sciences Campus Jülich
	Fuel Cells – The Future for Dispersed Power Supply!?	V/2	WS	

Table 5: Courses taught by professors

2.1.1.1 Principles and Technology of Fuel Cells

Prof. Dr.-Ing. Detlef Stolten holds the Chair for Fuel Cells at RWTH Aachen University. The courses offered deal with the conversion of renewable and fossil energy carriers for use in fuel cells in portable, stationary and mobile applications. The process engineering and systems technology aspects include high-temperature and low-temperature fuel cells, as well as the processing of fuels specifically for fuel cells. These aspects are accompanied by an examination of the basic physical and chemical principles involved. Systems analyses of energy process engineering, which include cost estimates, serve as a comprehensive examination with a view to future market launch. During the 2013/2014 winter semester,

89 students attended the lectures and seminars. As part of the existing cooperation with Forschungszentrum Jülich, students have the opportunity to write semester papers and undergraduate dissertations at Jülich and to work on projects as research assistants.

2.1.1.2 Modeling in Electrochemical Process Engineering

Prof. Werner Lehnert teaches modeling in electrochemical process engineering at RWTH Aachen University. His lecture course focuses on the mathematical description of electrochemical converter systems. In addition to the basic approach to modeling, different modeling techniques are also outlined. Using low- and high-temperature fuel cells as examples, 1D, 2D and 3D models with varying degrees of complexity are developed and their validity is then discussed. These examples of application form the basis for mathematical descriptions of the interactions of mass and heat transport with the electrochemical processes. Particular attention is paid to the description of processes in the porous components of fuel cells. The lecture course was offered for the second time in winter semester 2013/2014 and was attended by eight students.

2.1.1.3 Basics and applications of chemical reaction theory – simulation of dynamic processes in energy systems with MATLAB/Simulink

Prof. Ralf Peters teaches energy process engineering at Aachen University of Applied Sciences Campus Jülich. The course “Basics and applications of chemical reaction theory – Simulation of dynamic processes in energy systems with Matlab/Simulink” links the basic principles of chemical process engineering with dynamic simulations of reactors. The lectures and seminars look at the examples of fuel cell systems for hydrogen-powered vehicles and systems combined with fuel processing for auxiliary power supply based on diesel. The course is compulsory for the 30–40 students enrolled in the Master of Science in Energy Systems.

2.1.1.4 Fuel Cells – The Future of Decentralized Energy Supply!?

Prof. Ludger Blum teaches fuel cell technology at Aachen University of Applied Sciences, Campus Jülich. The optional subject “Fuel cells for decentralized energy supply” in the bachelor’s course on energy and environmental technology and the Master of Science in Energy Systems covers the function, construction, behavior, advantages and disadvantages of different types of fuel cells. It also lays the groundwork for the process engineering design of fuel cell systems. The topics include: basic principles of fuel cells; fuel supply; efficiency, function and construction of different types of fuel cells; fuel cell system requirements; process engineering of various fuel cell systems for different applications; energy balance of a fuel cell system; and modern plant engineering. An average of 20–30 students in the master’s program and an average of 10 in the bachelor’s program took these courses.

2.1.2 Lehrveranstaltungen von Lehrbeauftragten an Hochschulen

Table 6 provides an overview of the courses taught at universities by IEK-3 lecturers.

Name	Subject area	Type/hours Semester		University
PD Dr. C. Korte	Physical and Chemical Methods for the Preparation and Characterization of Thin Films	S/2 Block	SS	Justus Liebig University Gießen
Dr. Martin Müller	Principles and Technology of Fuel Cells	Ü/2	WS	RWTH Aachen
Dr. M. Peksen	Multiphysical Modeling of Functional Materials and Components	V/2	WS	FH Aachen
Th. Grube	Basics and Applications of Chemical Reaction Theory – Simulation of Dynamic Processes in Energy Systems with Matlab/Simulink	Ü/2	WS	Jülich Office

Table 6: Courses taught by university lecturers

2.1.2.1 Physical and Chemical Methods for the Preparation and Characterization of Thin Films

PD Dr. Carsten Korte teaches a seminar course at Justus Liebig University Gießen in the Faculty of Biology and Chemistry. The seminar provides a comprehensive introduction to the preparation and analysis of thin oxide-ceramic films and their use in technical applications. It is aimed at all interested students taking master's courses in chemistry, physics and materials science, as well as at doctoral students in the same fields. The course looks at the most important vacuum evaporation processes, including thermal evaporation, sputtering methods, chemical vapor deposition (CVD), molecular beam epitaxy (MBE) and pulsed laser deposition (PLD). Particular emphasis is placed on pulsed laser deposition (PLD). Other topics from the field of preparation are the growth modes for large and small layer thicknesses, which determine layer morphology, and the dependence of these modes on surface energy and surface diffusion. The analytical methods covered are X-ray diffraction (XRD, pole figures, reflectometry), electron microscopy (SEM, TEM) and the associated electron diffraction techniques (EBSD, SAED). A concluding seminar looks at examples from the literature and discusses them. Fourteen students took the block seminar offered in summer semester 2013.

2.1.2.2 Multiphysical Modeling of Functional Materials and Components

Computational modeling has become an important tool for predicting and simulating the multiphysical behavior of complex engineering systems. Dr. Peksen's lecture course therefore aims to familiarize students with theoretical and practical approaches to multiphysical modeling. The necessary skills for analyzing technical problems using numerical simulation products are taught. The lecture course covers the methodology for modeling coupled physical interactions as well as the simulation and analysis of materials

and components. The fundamentals of computational modeling are detailed. Thermofluid-structural coupling is discussed using advanced techniques. The linear and non-linear behavior of materials and components under thermofluid, static and dynamic load is elucidated. Advanced modelling topics are taught. The lecture course is held during winter semester for students enrolled in the Master of Science in Energy Systems. Students are expected to successfully complete a written exam and an additional computational project. In winter semester 2013/2014, four students took the course.

2.2 Provision of information and further education

As in previous years, IEK-3 organized a variety of different events, was involved in external events on various levels and worked with other institutions preparing, coordinating and offering support. The expansion and consolidation of these activities is the aim of existing and planned partnerships focusing on providing interested target groups with information and further education.

2.2.1 Organization of tours, seminars, work experience, information events and visits to the institute

The topics dealt with at the events are tailored to the requirements and requests of each target group. The events range from information events and training courses for secondary-school students, university students, teachers, tradesmen, technicians, engineers and scientists to practical courses on career choice and work experience for secondary-school students, as well as vocational training and study-related placements for undergraduates and postgraduates. The duration of the events ranges from a half-day to several weeks depending on the situation. The tasks assigned to secondary-school students and university students during a placement include shadowing technical and scientific personnel at the institute as well as supervised independent work on selected practical projects.

- Information events and visits to the institute for individuals interested in Jülich's contribution to research and development for fuel cell and hydrogen technology. Every year, around 60 tours are organized at IEK-3 with an average of 20 people per tour. Tours are given by two doctoral students.
- Work experience and placements for secondary-school students from local schools focusing on specialist careers in the area of fuel cell and hydrogen technology (2013: three students on placement; 2014: six students on placement). A broad interdisciplinary range of topics are covered. Placements for secondary-school students are generally for one or two weeks depending on requirements.
- A day of work experience as part of Boy's Days 2013 for two local school students.
- Several single days of experiments dealing with fuel cells as part of the JuLab Schools Laboratory research week "Energy – Researching for the Future" – for eleven school students aged between 15 and 17 from 29 July to 2 August 2013 and for sixteen school students from 7 July to 11 July 2014.
- Several single days of project work on a fuel cell R&D topic as part of JuLab's work experience program on the world of fuel cells – for ten school students aged between 15 and 18 from 22 July to 26 July 2013 and from 21 July to 25 July 2014.

2.2.2 Involvement in external events

Several scientists from IEK-3 gave introductory presentations and specialist presentations as invited speakers on fuel cells and hydrogen at diverse external events including training courses, workshops and continuing professional development courses.

- Courses for developers and users on fuel cells and hydrogen technology as part of the WBZU events in Ulm: the courses were run in April 2013 and March 2014. One IEK-3

scientist gave two presentations on each of the specialist topics of “Lifetime Aspects of PEFC” and “Hydrogen Supply”.

- Summer school on renewable energy at the University of Bonn: two IEK-3 scientists performed laboratory experiments on low-temperature fuel cells in July 2013 with students from the USA, Canada, Poland and Lebanon. In July 2014, students from Australia, USA, Singapore, Lebanon and Canada conducted similar experiments.
- International Summer School “Advanced Studies of Polymer Electrolyte Fuel Cells”: the sixth event in the series took place in August 2013 in Yokohama, Japan. An IEK-3 scientist gave two presentations on “Basics of electrochemistry and modeling of PEFC”. In September 2014, the seventh event was held in Graz, Austria, where an IEK-3 scientist gave two presentations on “Modeling of Fuel Cells”.
- Joint European Summer School on Fuel Cell, Battery, and Hydrogen Technology (JESS 2013): at the event in September 2013 in Athens, Greece, an IEK-3 scientist gave four presentations on the history, thermodynamics, principles, materials, properties, challenges and future of alkaline and PEM water electrolysis. In September 2014, the summer school took place in Rethymno, Greece. The nine presentations given by an IEK-3 scientist on low-temperature water electrolysis dealt with the topics of electrolyte, cathode and anode materials, cell and stack design, manufacturing, material design, systems engineering, degradation and new trends.

2.2.3 Collaboration with other organizations

In creating and implementing further education and training and continuing professional development in the field of fuel cell and hydrogen technology, a new topic has been integrated: how applications with fuel cells and hydrogen infrastructures can be launched on the market. This development is occurring at a rapid pace in response to growing interest in expertise in the areas of fuel cells and hydrogen on the part of the manufacturing industry and the relevant educational establishments. In order to cater for this demand, special initiatives have been launched. The combination of specialist knowledge and existing opportunities provides an excellent basis for collaboration.

- Involvement in the Fuel Cells Qualification Initiative (IQ-BZ), which aims to implement information and training measures for fuel cell and hydrogen technologies.
- Promotion and sale of a “Fuel Cells” CD-ROM through the Federal Technology Centre for Electrical Engineering and Information Technology (Oldenburg) and Vogel Industrie Medien GmbH (Würzburg) which is designed to provide information, increase the acceptance of fuel cells, and promote further training and education.
- Adaptation of existing teaching modules to meet relevant consumer demands.
- Assessment of the theoretical and practical results of 20 teams of school students in the final round of the competition for school students “Fuel Cell Box”, which is organized annually by the EnergyAgency.NRW. In Fig. 3, the winning teams in 2013 and 2014 are pictured holding their certificates together with the organizers.



Fig. 3: Presentation of certificates to the winning teams in 2013 (left photo) by State Secretary Knitsch from NRW MKULNV (left) and in 2014 (right photo) by Mr Mees NRW MKULNV (right)

- Assessment of the theoretical and practical results of work in the disciplines of technology, the working world, and geo- and space science in the regional competition “Jugend forscht”, which takes place once a year at Forschungszentrum Jülich. In 2014, there was high team participation: eight school teams and three projects by teenagers in the three disciplines. Fig. 5 shows the teams in 2014 together with their supervising teachers and the judges.

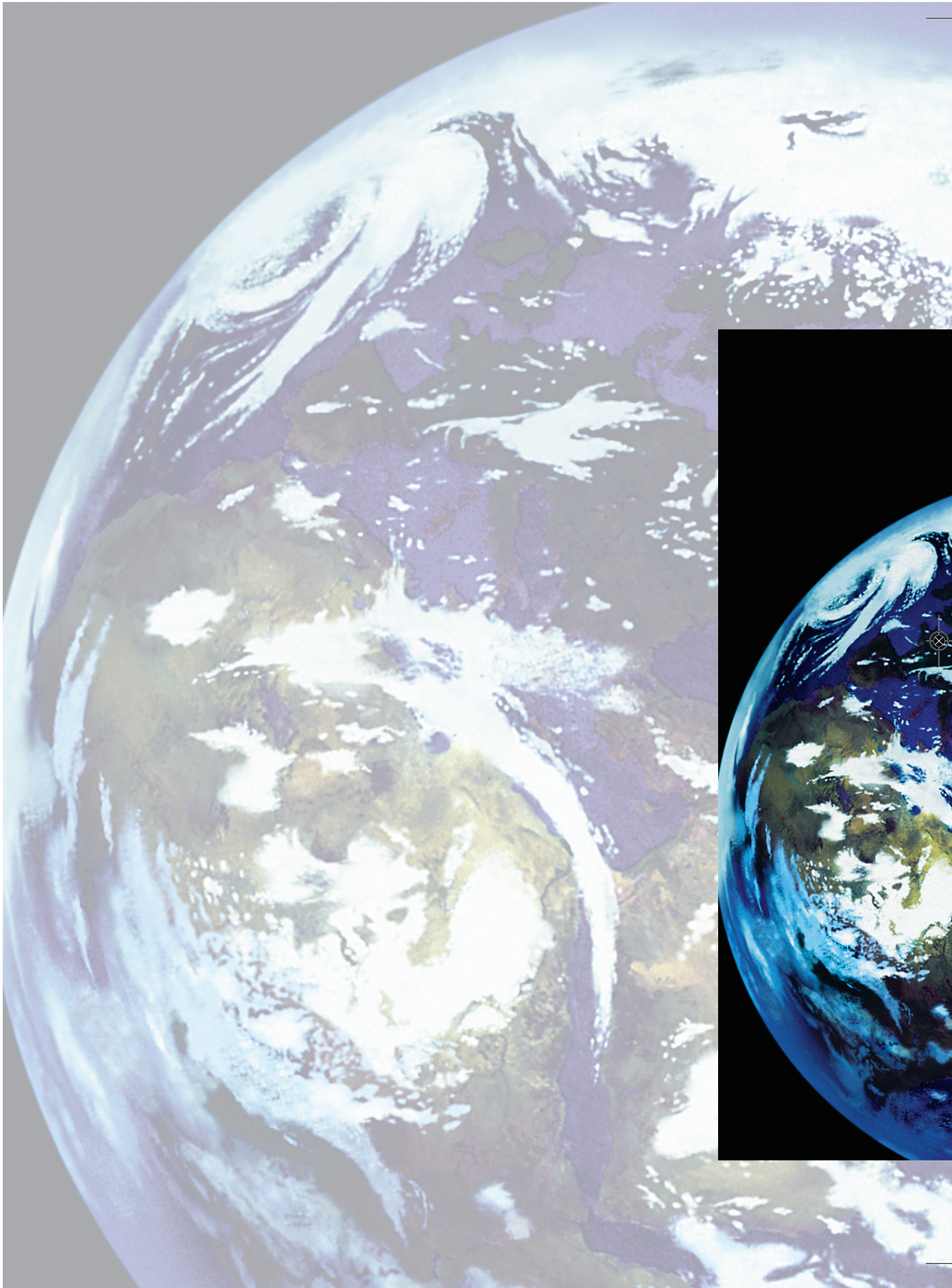
In the competition for younger school students, Chiara Hackfort (left, Fig. 4) and Maria Mendéz Sturm (right, Fig. 4) from the Inda-Gymnasium secondary school in Aachen came first in the category of geo- and space science with their project “Not Covered at High Tide – Mobile Flood Control” and qualified for the next round of the competition (state competition for North Rhine-Westphalia).



Fig. 4: First place in geo- science category in the competition for younger school students



Fig. 5: Group photo of participants in the 2014 regional competition of “Jugend forscht” in the lecture theatre at Forschungszentrum Jülich



3

Reports

Scientific and Technical Reports

- Direct methanol fuel cells
- High-temperature polymer electrolyte fuel cells
- Solid oxide fuel cells
- Fuel processing and systems
- Process and systems analysis
- Analysis
- Quality management

3.1 Solid oxide fuel cells

3.1.1 Objectives and fields of activity

Within the program topic of fuel cells, cells, components, stacks and systems are being developed for high-temperature fuel cells with a solid oxide electrolyte (SOFCs). Strategically, this topic aims to provide electric energy in a highly efficient manner for mobile and stationary applications, both distributed and centralized, on a scale ranging from a few kilowatts to several hundred kilowatts. Work focuses on increasing power density, long lifetimes, the identification of degradation mechanisms in the stack and preventing them, advanced design and highly integrated system engineering. The results of this development work include materials for cells, thermomechanically improved stacks and highly integrated system components, as well as the very first 20 kW system. Important supporting activities include the modeling of mechanical and thermal component loads as well as the development and characterization of components for fuel cell systems and their evaluation using process engineering analyses.

3.1.2 Important results

3.1.2.1 Tests with cassette stacks

One of the newer areas of research is cassette or lightweight stacks, which are being developed for use in vehicle auxiliary power units (APUs). This application is particularly demanding in terms of the thermal cyclability of the stacks.

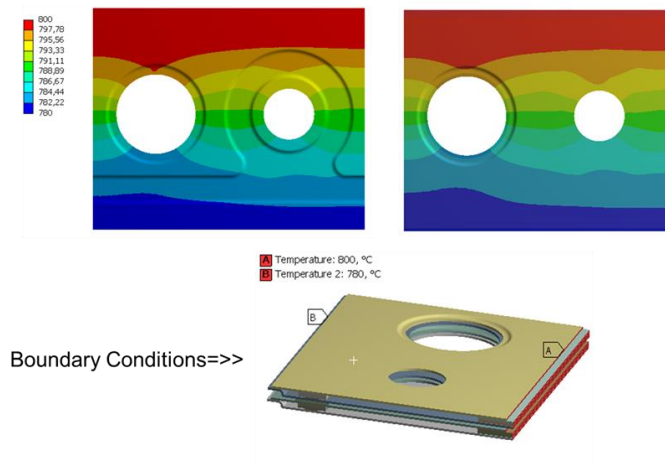


Fig. 6: Boundary conditions and resulting temperature distribution for both designs (left: CSIV with swage; right: CSII)

Nachdem Untersuchungen am aktuellen Leichtbau Design (CS^{II}) nach 100 tiefen Thermozyklen (750 °C → 50 °C → 750 °C) mit einer Heizrate von 10 K/min beim abschließenden

Following tests on the current lightweight design (CS^{II}) comprising 100 deep thermal cycles (750 °C → 50 °C → 750 °C) with a heating rate of 10 K/min, the stack was removed from the test stand for subsequent leak tests, which revealed considerable internal and external leaks. The design was subsequently reworked in the EU project MMLCR with the aim of optimizing the joining technique. Firstly, potential improvements to the mechanical robustness were analyzed using FEM. One modification that had already been implemented in a previous project (CS^{IV}) was the addition of a swage to reinforce the sheet contour and thus reduce the thermally induced stress in the join. To test this, a FEM comparative analysis was conducted. Fig. 6 shows the sections analyzed together with the calculated temperature distribution. It is based on the calculation of a full stack in steady-state operation.

Three different analyses were performed to investigate the effect of the swage. The first was a coupled thermomechanical analysis of the operating state; the second was a thermomechanical analysis accounting for an artificially produced additional shear stress; and the third analysis investigated stress at room temperature after the stack had cooled down from the reference temperature, which was 800 °C in all cases. None of the analyses showed a significant difference between the designs with and without a swage. As the swage involved considerable additional expenditure during manufacture and assembly and also significantly increased the risk of a short circuit between the sheet metal parts, it was decided to dispense with the swage in the new design.

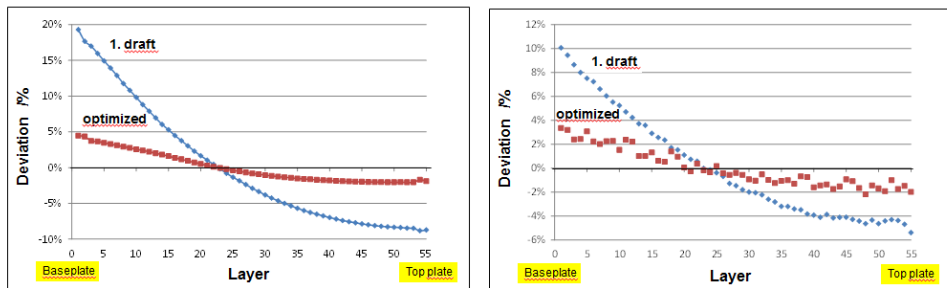


Fig. 7: Flow distribution on the anode and cathode side in the stack with 55 layers

Based on experience with other stack designs, the construction was further optimized for the glass seal. For the flow-field design, the target was defined as a 3 kW stack comprising 55 layers. On this basis, the manifold dimensions necessary for a sufficiently good distribution of the fuel gas and air across each layer were calculated (see Fig. 7). Based on these results, the design was finalized and the first parts were produced. A first short stack with two layers was successfully operated with performance data comparable with other lightweight stacks (see Fig. 8).

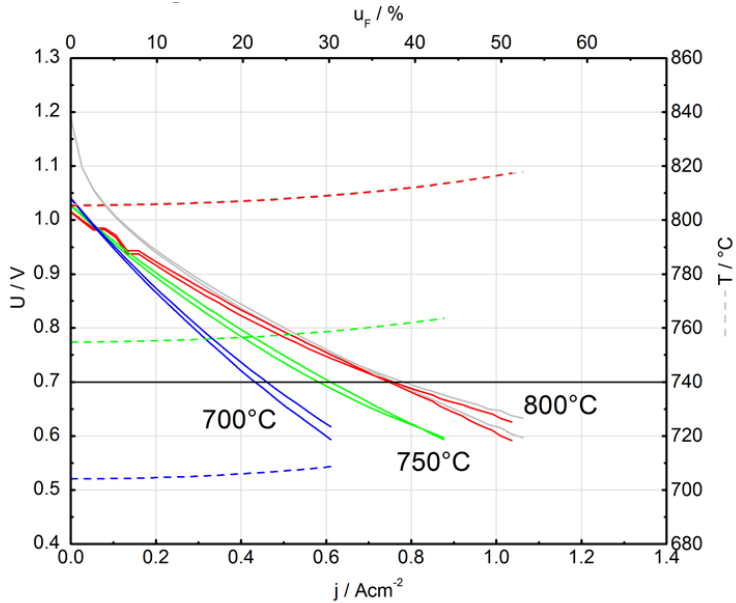


Fig. 8: Stack CSV02-01 – Current-density curves at different temperatures

To analyze the conditions during rapid heating of the lightweight stack in more detail, a 3D CFD model was used to calculate the temperature distribution within a multilayer stack. The boundary conditions concerning the gas volumes and inlet temperatures were taken from heating tests. The stack design is shown in Fig. 9.

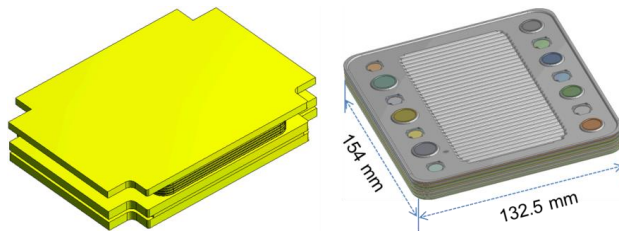


Fig. 9: Fuel cell stack: geometry and interior

The resulting temperature distribution was analyzed for different time steps and the outlet temperatures were in good agreement with the measured values. The results show that the highest temperatures and temperature gradients occur in the inlet area between the manifold and cell (see Fig. 10). Towards the end of the heating time, the larger mass flows of hot gases cause higher temperature gradients at the cell outlet. These findings led to an improved understanding of the damage profiles at the end of the test and permitted specific design improvements

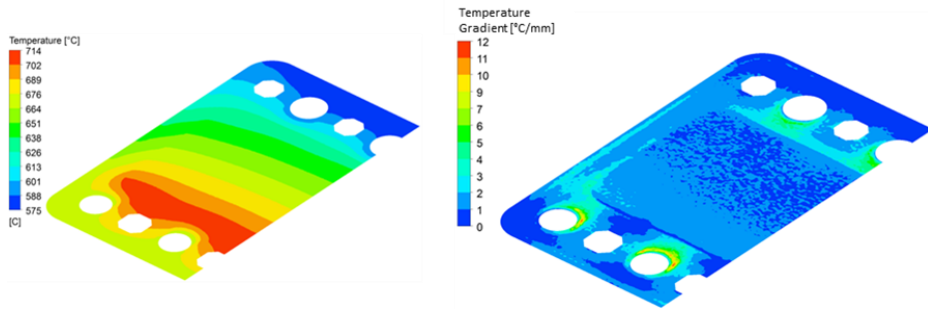


Fig. 10: Temperature distribution and temperature gradients in a cell layer after 8015 s

3.1.2.2 Stack technology in the kW class with improved performance

Cyclability

Stack development concentrated on verifying a stack design suitable for use under real conditions that achieves a high efficiency with various fuels. Stacks with larger cells with external dimensions of 20 x 20 cm² and an effective electrode area of 360 cm² have been tested since 2000. In the last test phase, the thermomechanical robustness was improved to the point that 5 kW stacks could be operated in the 20 kW system.

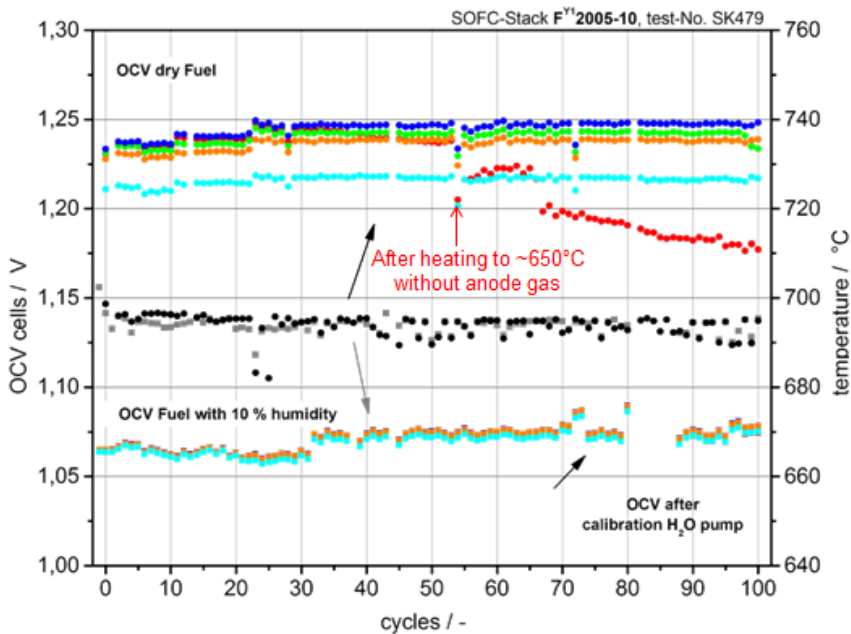


Fig. 11: FY12005-10: Behavior of OCV as a function of thermal cycles

Based on FEM analyses in the last period under review, the stack design was again modified and the cyclability tested with a 1 kW stack (F^{Y1}2005-10). The stack was first operated for 617 h with H₂ (u_F 80%) The thermomechanical loading was increased with larger temperature gradients and the stack was subsequently operated for approx. 900 h with CH₄ (u_F 30/50/70%) at a current density of 0.5 A/cm² and 700 °C. After it was removed from the test stand, the stack showed no leaks. When the test was resumed, the stack was cycled between 200 °C (sometimes 100 °C) and 700 °C with a furnace heating rate of between 2 K/min and 6 K/min. After cycle 5, 10 and 21, the stack was removed and tested for leaks. No changes were observed in relation to the very good starting values. After cycle 56, the stack was heated without fuel due to a test-stand malfunction. Cell 1 subsequently exhibited a slightly lower open circuit voltage (OCV). From cycle 67 onwards, this decreased continuously (albeit still a very good level). The OCV value of the other cells remained stable as did the dew point of the exiting fuel gas. After 100 thermal cycles, the test was stopped. The progression of the OCV values is shown in Fig. 11. All values remained at a very good level even at the end. However, a final leak test revealed a leak in the area around the fuel gas outlet which had not been detected by measurements when it was still in the test stand. Despite this leak, the result still constitutes a considerable improvement from previous designs, and requirements for CHP application with respect to the number of cycles were fulfilled.

Stack design and modeling

In the next phase, stacks with an output of at least 15 kW are the aim, which should in turn facilitate the assembly of larger systems with fewer stacks. Another aim is to utilize cells from external manufacturers. However, discussions with cell manufacturers made it clear that cells with dimensions of 200 x 200 mm² are not available. A design was therefore developed to enable the use of several smaller cells (here the standard dimensions were 100 x 100 mm²). This “window design” is shown in Fig. 12.

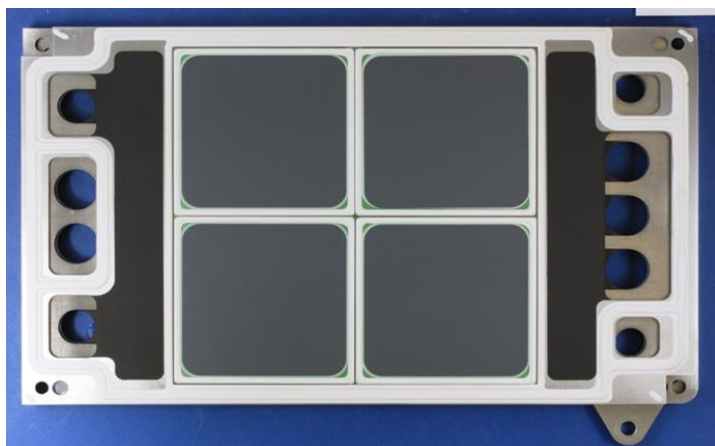


Fig. 12: Window design with four cells in one layer

Here, four cells are connected in parallel in one layer resulting in an electrode area of 320 cm². The first tests on stacks with five layers revealed performance data comparable with short stacks with one cell per layer. To create stacks with an output of 15 kW on this basis, 120 layers must be stacked on top of each other. For the flow-field design, H₂ operation in parallel flow was assumed. The manifold geometry was optimized resulting in a scattering of flow rate values per layer on the air side from +4/-2% across the 120 layers and on the fuel gas side of ±1%. On this basis, the revised design was completed.

The thermomechanical loading of the stack is determined by the design, operating conditions and the operating environment. In the development phase, the stacks were first operated in a heated environment, i.e. in a furnace. During later operation in a real system, they would be thermally insulated, i.e. ideally in an adiabatic environment. Using the 3D model of an F20 stack with six active cell layers, a comparative calculation was performed which first calculated the temperature distribution in the stack layer for furnace operation and for operation in adiabatic insulation. Based on these temperature distributions, the voltages in the steel and the glass seal were calculated. The radiative exchange between the furnace heating and stack surface was taken into account as was the thermoplastic behavior and the creep of steel. The inlet temperatures of the gases were 500 °C for the fuel gas and 630 °C for air at a furnace temperature of 700 °C. The stack was operated in counter flow with 10% pre-reformed methane at 500 mA/cm². The waste heat of the reaction was incorporated as a heat source in the active cell area.

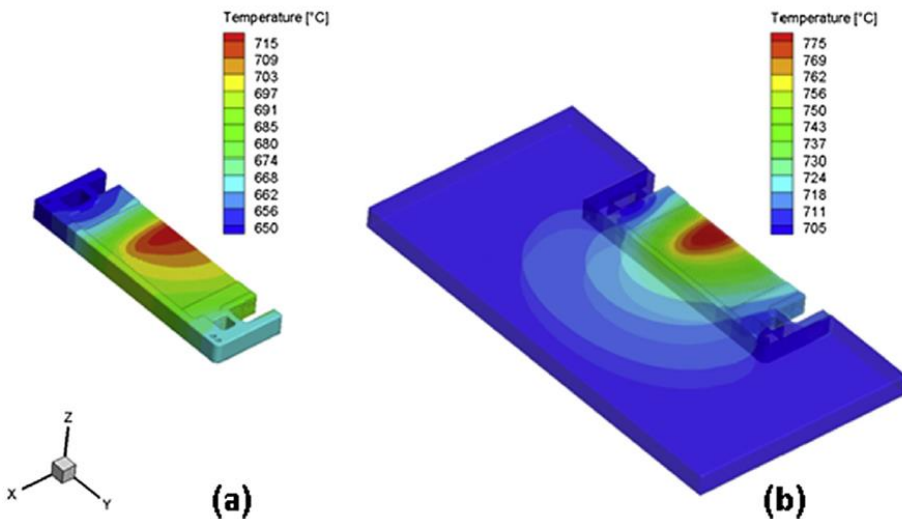


Fig. 13: Temperature distribution in the stack during operation in (a) a system environment and (b) a furnace

Fig. 13 compares the temperature distribution. During operation in the furnace, the temperature in the manifolds is dominated by the furnace temperature of 700 °C and was between 705 °C and 720 °C on both sides. The maximal temperature was detected near the center of the cell in the electrochemically active area and was 775 °C. In this area, the temperature decreased towards the edges to 740 °C, which means that the inner region of

the stack is around 35 K hotter than the stack surface. During operation with adiabatic surfaces, the manifold temperature on the air inlet side was dominated by the air temperature and was 650 °C. On the fuel gas inlet side, the internal reforming had a cooling effect. However, this effect was diminished by air that was heated as it flowed through, resulting in a manifold temperature here of approx. 670 °C. The maximum temperature in the cell area was detected at a similar point as for operation in the furnace but was only 715 °C. In this area, the temperature decreased towards the edges to 690 °C, which means that the inner region of the stack is around 25 K hotter than the stack surface. This temperature distribution caused an elastoplastic deformation of the metal parts. At high temperatures, this elastic deformation was transformed by creep into a permanent deformation, which for longer periods caused an increase in the tensile stress in the rigid glass sealant. Fig. 14 shows the distribution of the main stresses in the glass seal after an hour of loading as described above. It is clearly visible that the maximal tensile stress occurs in the side seals where the maximal temperature causes the highest thermal strain. Further areas with high tensile stress are around the edges of the cell seal and at various points in the manifold. The maximal tensile stress level for operation in the furnace was approx. 20% higher than for operation in the system environment.

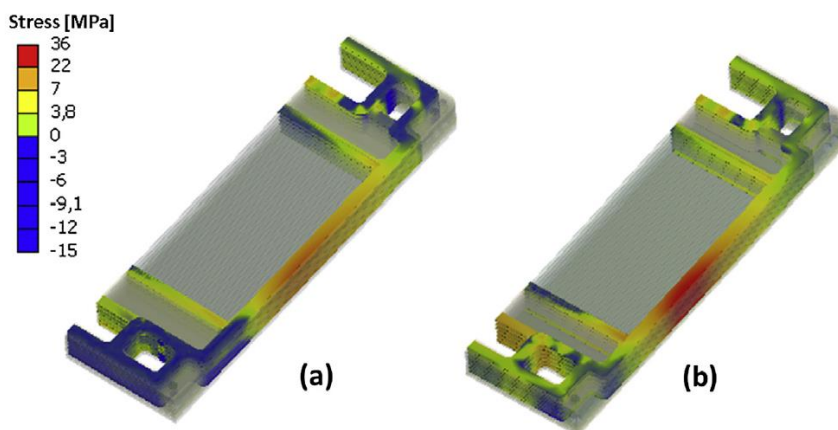


Fig. 14: Maximal main stresses in the glass seal during operation in (a) a system environment and (b) a furnace

Stack tests

For operation under real conditions, operation with higher fuel utilization is essential to achieve high system efficiencies. For this, two stacks of different design (F1004-39 and F^{Y1}2005-12) were operated in the furnace with fuel utilizations of up to 90% with humidified hydrogen (20% humidity) and natural gas (10% pre-reformed). Both stacks showed comparable behavior and were operated without problems in a temperature range of 750–800 °C with a fuel utilization of up to 85%. However, a fuel utilization of 80% and higher led to a clear increase in polarization losses (see Fig. 15).

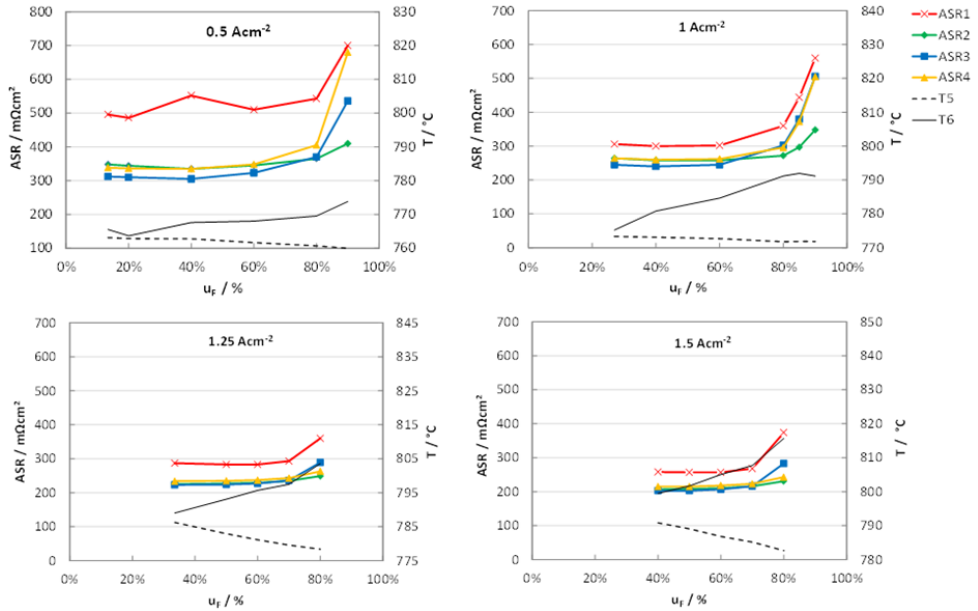


Fig. 15: ASR of the cells in stack F1004-39 at different fuel utilizations and current densities

At a fuel utilization of 90%, in addition to an even higher polarization partial reoxidation of the anode was detected in comparable areas (see Fig. 16).

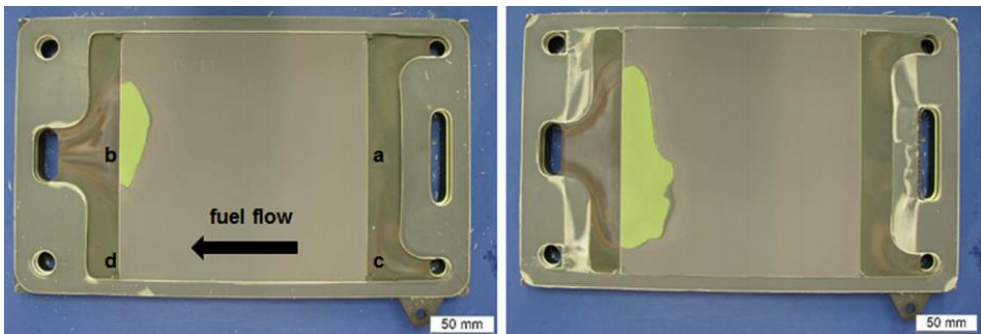


Fig. 16: Reoxidation of cell 1 (left) and cell 2 (right) near the fuel gas outlet in stack FY12005-12

First calculations based on a 1D stack model showed that even smaller temperature differences of 20 °C between the stack interior and the edge regions caused by the lower area specific resistance (ASR) of the cells gave rise to a 10% higher gas utilization, which can lead to partial reoxidation. Without design modifications, the fuel utilization should not exceed 85%.

3.1.2.3 Systems engineering

20 kW system

As outlined in the last report, a 20 kW test facility comprising four 5 kW stacks was successfully operated in 2012. The objectives were achieved with 21.3 kW at an electrical system efficiency of 42%. However, the stacks underwent high thermomechanical loading due to various malfunctions in the peripherals (control failure, electronic load, sensors, sealant in the peripherals), which is why the system could only be operated with half of the stacks after 550 hours of operation. After a total of 5000 hours, one stack was so degraded that it had to be replaced (see Fig. 17). The system was put back into operation but this time the two stacks were connected in series instead of in parallel in order to take account of the different operating periods. This verified that the system can also be operated when the stacks are connected in series, which is very positive for the inverter design due to the higher input voltage.

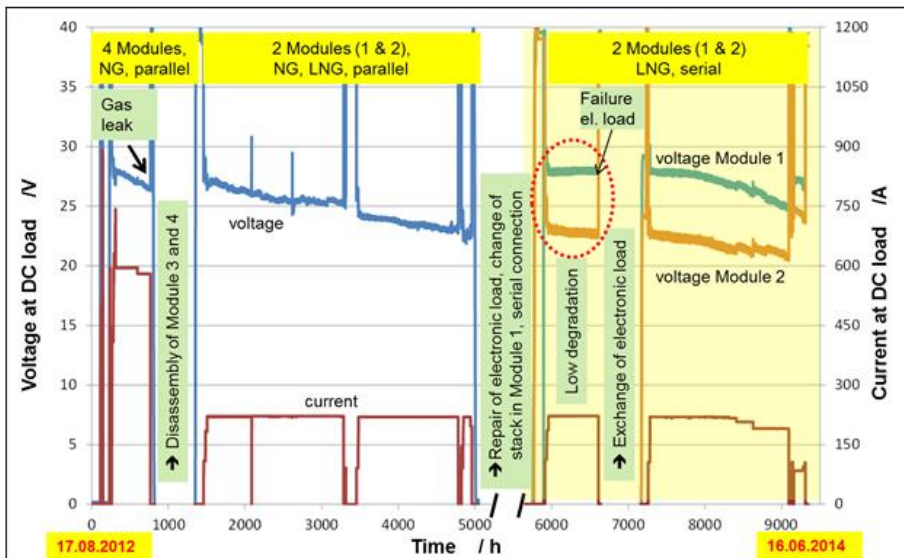


Fig. 17: 20 kW system: voltage and current over time

After another 700 hours of continuous operation with low degradation (see Fig. 17 period between 6000 and 6700 hours), the system had to be shut down again due to the failure of the electronic load. After a new load had been installed and the system restarted, considerably increased degradation was detected after several hundred hours, particularly in module 1. After approx. 1000 operating hours, the load was decreased gradually in order to test temperature control and to optimize the control parameters. In this phase, the block voltage E4 (sum of the cell voltages 19 to 24 in module 1) exhibited unstable behavior (see Fig. 18). Following automatic shutdown due to a sharp drop in the voltage of the laboratory power supply, E4 showed a drastic voltage drop. This led to the test being terminated after a total of 6800 hours under load and after 7500 hours at operating temperature.

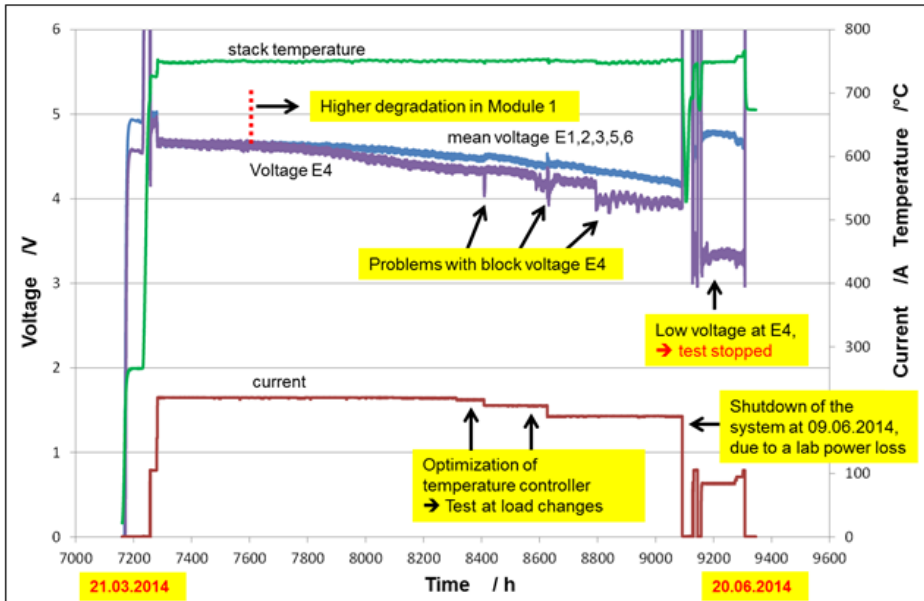


Fig. 18: 20 kW system: block voltage and current of module 1 over time in the final phase of operation

System design – Concepts for anode recirculation

In order to investigate the impact of fuel gas management on the system's electrical efficiency and on the supply of steam for the reforming process, a total of 220 system variants were analyzed. All systems analyzed had a high efficiency (all in relation to the lower heating value of natural gas):

Electrical efficiency:	50–66%
Thermal efficiency:	26–49%
Total efficiency:	76–106%

Depending on the operating parameters, the electrical efficiency of systems with anode gas recirculation was up to 16 percentage points higher than systems without such anode gas recirculation. Electrical and thermal efficiencies are influenced by fuel utilization u_F and the anode gas recirculation ratio RR.

In systems operated with natural gas, the electrical efficiency can also decrease with higher u_F and RR. This is caused by greater quantities of air and the resulting higher compressor power. However, high u_F and RR are needed to avoid carbon formation in the reformer. Therefore, depending on the system's actual consumption, the optimal parameter combination is RR = 70% and u_F = between 60% and 80%.

In comparison, system configuration, fuel and cell type (anode substrate or electrolyte substrate) have much less of an impact on system efficiency. This means that other criteria

must be taken into account in defining the most promising system configuration, for example, number of system components, complexity of the system, and so on.

System design – Part-load behavior of fuel-driven or steam-driven ejectors for anode recirculation in SOFC systems

To analyze the part-load behavior of SOFC systems, calculations were performed where fuel gas or steam was used as the feed gas for ejectors in anode gas recirculation. The part-load capability of a system with a fuel-driven ejector is determined by the carbon formation threshold. As the fuel utilization indirectly influences carbon formation through the amount of steam produced electrochemically, the part-load capability was analyzed in dependence on fuel utilization. Assuming a fuel utilization of 70% and suitable ejector geometry, a part load of 77.8% can be achieved. A concept for a steam-driven ejector was developed to improve the part load behavior. Calculations resulted in a part-load capability of 37.8% for a simultaneously higher efficiency. The results of the simulations achieved with MATLAB/Simulink[®] and Cycle-Tempo are shown for both versions in Fig. 19. The most important results of the simulations are as follows:

- Fuel utilizations above the fuel utilization design point reduce the part-load capability due to a reduction in the primary steam pressure at the ejector.
- The higher the fuel utilization design point, the lower the achievable part load as increased steam production in the fuel cell causes a higher O/C ratio.
- The main challenge for the fuel-driven ejector is preventing carbon formation. This is why the part-load capability is limited to 78%.
- The main challenge for the steam-driven ejector is controlling the condensation temperature to achieve a positive mass flow difference between the condensed water from the recirculated anode off-gas and the feed water flow to the ejector on the primary side. Without additional water, a part load of about 38% is possible.
- The electrical system efficiency of the steam-driven ejector is 3.2 percentage points higher than the efficiency of the fuel-driven ejector because the water pump consumes less energy than the fuel compressor.
- The fuel compressor consumes approx. 2% of the electrical energy produced by the stack.

The advantage of a fuel-driven ejector is a low number of components. The disadvantage is poorer part-load capability. The system with a steam-driven ejector enables the lower part load threshold to be halved and the system efficiency to be increased, but requires at least five additional system components: condenser, pump, evaporator and two additional heat exchangers. Thus, the system costs for a steam-driven ejector system are higher.

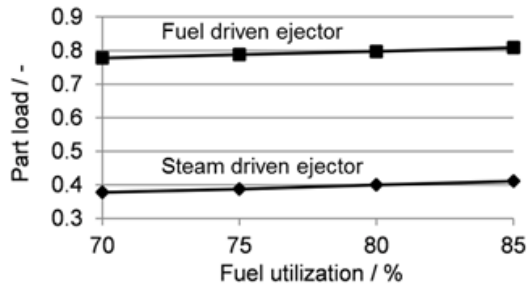


Fig. 19: Part-load capability as a function of fuel utilization for fuel-driven and steam-driven ejectors for SOFC systems with anode gas recirculation

3.1.3 Staff members and fields of activity

Name	Tel (02461-61-) e-mail Adresse	Field of activity
Prof. L. Blum	6709 l.blum@fz-juelich.de	Head of Solid Oxide Fuel Cells
A. Al-Masri	3774 a.al-masri@fz-juelich.de	Simulation of SOFC stacks, CFD and FEM
R. Deja	5291 r.deja@fz-juelich.de	System simulation, development and testing of SOFC system components
M. Engelbracht	4652 m.engelbracht@fz-juelich.de	System simulation, development and testing of SOFC system concepts
Dr. Q. Fang	1573 q.fang@fz-juelich.de	Head of SOFC Electrochemical Measurement Technique, electrochemistry, testing and analysis
I. Hoven	4053 i.hoven@fz-juelich.de	Electrical engineering, measurement data acquisition and systems control
Fr. A. Kind	3850 a.kind@fz-juelich.de	Software development, modeling
Dr. V.N. Nguyen	8393 v.n.nguyen@fz-juelich.de	Chemical process engineering, development and testing of system components
Fr. U. Packbier	5170 u.packbier@fz-juelich.de	Testing of SOFC stacks and test evaluation
Dr. M. Peksen	8732 m.peksen@fz-juelich.de	Simulation of stacks and high-temperature system components, CFD and FEM
Ro. Peters	4664 ro.peters@fz-juelich.de	Head of SOFC Systems Technology, component development, system design, system engineering and system testing

3.1.4 Important publications and patents

Important publications

Nguyen, V.N.; Blum, L.; Peters, R.;

Operational behavior and reforming kinetics over Ni/YSZ of a planar type pre-reformer for SOFC systems

International Journal of Hydrogen Energy 39 (13) (2014) 7131-7141

Blum, L.; Packbier, U.; Vinke, I.C.; de Haart, L.G.J.

Long-term Testing of SOFC Stacks at Forschungszentrum Jülich

Fuel Cells, 13 (4) 2013, pp. 646–653, DOI: 10.1002/fuce.201200151

Fang, Q.; Blum, L.; Batfalsky, P.; Menzler, N.H.; Packbier, U.; Stolten, D.

Durability test and Degradation behavior of a 2.5 kW stack with internal reforming of LNG

International Journal of Hydrogen Energy, 38 (36) 2013, pp. 16344-16353, DOI: 10.1016/j.ijhydene.2013.09.140

Nguyen, V.N.; Fang, Q.; Packbier, U.; Blum, L.

Long-term tests of a Jülich planar short stack with reversible solid oxide cells in both fuel cell and electrolysis modes

International Journal of Hydrogen Energy, 38 (11) 2013, pp. 4281 - 4290, DOI: 10.1016/j.ijhydene.2013.01.192

Peksen, M.; Al-Masri, A.; Blum, L.; Stolten, D.

3D Transient Thermomechanical Behaviour of a Full Scale SOFC Short Stack

International Journal of Hydrogen Energy, 38 (10) 2013, pp. 4099-4107, DOI: 10.1016/j.ijhydene.2013.01.072

Peters, R.; Blum, L.; Deja, R.; Hoven, I.; Tiedemann, W.; Küpper, S.; Stolten, D.

Operation Experience with a 20 kW SOFC System

Fuel cells, 14 (3) 2014, pp. 489-499, DOI: 10.1002/fuce.201300184

Important patents

Patents granted:

Principal inventor	PT	Description
L. Blum	1.2175	Gas distribution plate for a high-temperature fuel cell
J. Nazarko	1.2341	Device and method for reducing CO ₂ emissions from the waste gases of combustion plants
W. A. Meulenber	1.2366	Power plant that uses a membrane and method for operating the same
R. Deja	1.2503	Solid oxide fuel cell system and method for operating the same

3.2 Fuel processing and systems

3.2.1 Objectives and fields of activity

The availability of hydrogen is a prerequisite for the use of fuel cells in mobile and stationary applications. An option for passenger cars, buses and fleets of vehicles in the delivery sector is to combine electric motors with hydrogen-driven fuel cells. However, the infrastructure for hydrogen as a future energy carrier first has to be established. In future, hydrogen will be produced from renewable and solar power using electrolysis. With a pressure tank at 700 bar, a range of approx. 350–400 km can be achieved. Such ranges are insufficient for trucks, ships and aircraft. Due to the poor storage properties of liquid and gaseous hydrogen compared to today's fuels (i.e. gasoline, kerosene and diesel), liquid fuels are preferable for the aforementioned areas of application. The tank system as a whole with its mass- and volume-specific power densities must be considered in analyses. The aforementioned energy carriers are mainly produced today from the fossil primary energy carrier crude oil. In the long term, biomass will be used to produce some of the liquid energy carriers currently needed. Another option involves producing fuel from carbon dioxide, e.g. from industrial exhaust gases and renewable hydrogen.

Fuel cells are not available in the power classes needed for drives in maritime applications or aviation (i.e. larger than 1 MW_e). In driving mode, the diesel engines used in the truck sector are extremely efficient and have a high mass- and volume-specific power density. When running at idle speed, a power of 3–5 kW_e is generated to operate air conditioning or electrical heating as well as to power electrical devices on board. Under these load conditions, diesel engines have an efficiency of only 10–15%; special power units – small internal combustion engines – have slightly better efficiencies of 20–30%. In aviation, on-board power on the runway and sometimes at the gate is generated by auxiliary power units with efficiencies of approx. 20%. These applications are the target of ongoing research and development work conducted by the fuel processing and systems group.

At IEK-3, research in the field of fuel processing concentrates on reforming middle distillates, the desulfurization of kerosene and system development for on-board power supply in combination with HT-PEFCs. Reformers are also being developed for high-temperature SOFCs. All areas of work are supported by relevant modeling. CFD simulations on the Jülich supercomputer JUROPA and system simulations using the Simulink program are crucial tools for optimizing dynamic behavior during load cycling and for start-up strategies.

3.2.2 Important results

3.2.2.1 Desulfurization

Kerosene and sulfur-containing diesel fuels were desulfurized using liquid-phase hydrotreatment with presaturated hydrogen, which is contained in the product gas of a reforming process. The process operating conditions were pressures of 30–70 bar and temperatures of 330–390 °C. The space velocities in the liquid phase were 0.3–1.2 h⁻¹. Kerosene with a total sulfur content of 813 ppmw and diesel with 950 ppmw were desulfurized over 600 operating hours with a hydrogen-containing reformat to values below 10 ppmw with no catalyst degradation (see Fig. 20). When pure hydrogen was used, the

sulfur content was approx. 1 ppmw and for reformat operation at a water partial pressure of 21 bar the value was 5 ppmw. The hydrogen sulfide produced must be separated from the kerosene. Without post-treatment, the sulfur content in the product stream from hydrotreatment (50 bar, 390°C, H₂ operation, 0.6 h⁻¹) was 43.7 ppmw. Air flushing at 80 °C for 10 h led to a sulfur content of 1.7 ppmw. Flushing with pure oxygen achieved a slightly higher value of 1.8 ppmw, whereby the flush volume was higher by a factor of 278 than the volume of fuel cleaned.

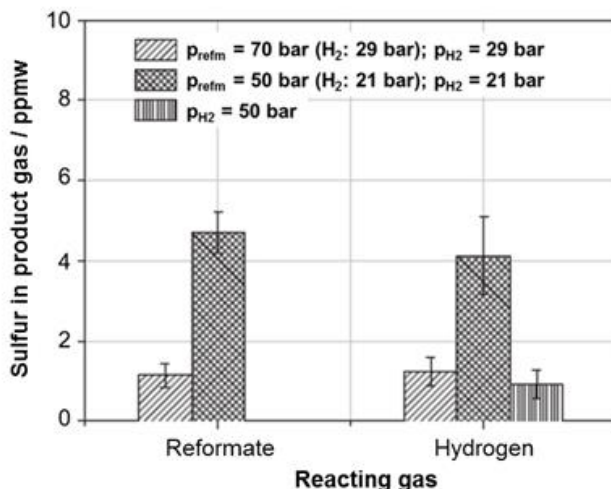


Fig. 20: Desulfurization of kerosene with a sulfur content of 813 ppmw using liquid-phase hydrodesulfurization at pressures of 50–70 bar and a temperature of 390 °C. The space velocity was 0.27 h⁻¹. Hydrogen was presaturated in the fuel. Pure hydrogen or reformat were used sources.

3.2.2.2 Catalytic burner

A series of catalytic burners was developed for low-emission combustion of the fuel cell anode exhaust gas. In addition to combustion, these burners must also guarantee the supply of hydrogen for autothermal reforming. The thermal power of the burners was 4.2 kW_{th} for CAB 2, 6.5 kW_{th} for CAB 3 and 2.6 kW_{th} for CAB 4. In addition to normal operation, CAB 4 was operated with diesel reformat. All reactors were experimentally investigated. The thermal power in this testing phase was 5.7 kW_{th}. The space velocities in the gas phase were 20,000–30,000 h⁻¹ for system operation with fuel cell exhaust gas and 30,000–40,000 h⁻¹ in diesel operation. The maximal adiabatic temperatures achieved at air ratios of 1–1.5 in system operation were 620–680 °C and at an air ratio of 3 in diesel operation 800–850 °C. The gravimetric and volumetric power densities of the burner in relation to the thermal power of the associated systems were 1.8–4.7 kW_{th}/kg and 2.1–6.3 kW_{th}/l, respectively. The new design of CAB 4 for a truck APU and the related reduction in sheet thickness to 1 mm of all inner metal parts enabled a three-fold increase in power density. For the distribution and vaporization of the water sprayed onto the hot surface of the upper burner chamber wall, a

hemispherical head is ideal. The design was expedited by CFD simulations, which were used to optimize specifications for the distance between the nozzle and the hemispherical head as well as the structure of the deflecting sheet on the burner chamber side. The burner types developed were all capable of supplying superheated steam pulsation-free. The following was tested:

- a typical diesel reformat downstream of a water-gas shift reactor with 2700 ppm CO, 2900 ppm CH₄, 16.2% (mol) CO₂, 21.2% H₂O and 31.5% H₂,
- the anode exhaust gas of a PEFC system with 30 ppm CO, 3700 ppm CH₄, 21.5% (mol) CO₂, 28.3% H₂O and 8.2% H₂,
- the anode exhaust gas of a HT-PEFC system with 1.4% (mol) CO, 1700 ppm CH₄, 20.3% (mol) CO₂, 31.9% H₂O and 7.7% H₂ and
- in a dehydrated state at 45 °C: 1.8% (mol) CO, 2200 ppm CH₄, 26.9% (mol) CO₂, 9.6% H₂O and 10.2% H₂.

First, experiments with a catalytic burner type CAB 2.2 with a nominal power of 4.2 kW_{th} were conducted with a fuel gas 4 according to a dehydrated state (last line). The air ratio of the burner was 1.1. A share of 70% of the steam required for the ATR was supplied by the burner. The reaction in the burner was ignited at 100 °C. Ignition was complete after 60 s and it took up to 20 min to achieve steady-state conditions due to the high thermal mass. The burner temperature was 800 °C. The superheated steam reached temperatures in excess of 350 °C; the exhaust gas almost 400 °C. The heat balance led to a reaction heat of 4160 W, which can be broken down into 2160 W for steam generation, 1900 W in the exhaust gas and 100 W as heat losses.

The thermal efficiency of steam generation in the burner at a vaporization temperature of 350–400 °C was approx. 45%. Substoichiometric operation led to a drop in the steam temperature. Preliminary tests showed that under such conditions methane is not emitted but rather converted in a partial oxidation process into hydrogen and carbon monoxide. Diesel operation with an air ratio of 4.8 gave rise to an operating temperature in the combustion catalyst of 650 °C. Steam generation is possible under these conditions; the steam temperature was unstable at temperatures of 170–220 °C.

3.2.2.3 Autothermal reforming

A prerequisite for implementing the autothermal reforming of middle distillates in a system to utilize the syngas in fuel cells is the conversion of almost all of the fuel. Fuel conversion should ideally be greater than 99.99%. The quality of the reforming process is described better by the detected residual hydrocarbon content than by the conversion sum total. The level of tolerable residual hydrocarbon content depends on the properties of the catalyst in the downstream reactors (water-gas shift (WGS) and preferential oxidation (PROX) reactors) in the case of PEFCs and on the type of fuel cells (PEFC or HT-PEFC). Precise values are not generally known and must be determined step by step in experiments. In addition, reforming must be possible with as constant a conversion as possible over a target period of 20,000–40,000 operating hours.

Residual hydrocarbon content can be detected in the gas phase by coupled gas chromatography and mass spectrometry (GC/MS). Special filter analyses revealed the presence of single substances in the range of 250 ppbV (benzene C₆H₆) to 1000 ppbV

(ethane & ethene, C_2H_6 & C_2H_4). Taking a margin of error into account, robust concentration values are 1–2 ppmV depending on the substance. The excess water produced during reforming was condensed out before gas analysis. It contains dissolved organic substances. The total organic carbon (TOC) was determined in mg C/l using a water analysis method. The threshold value was 0.5 mg C/l; minimal values in preceding measurement series were 1–2 mg C/l. The analysis accuracy was evaluated using Monte Carlo simulations taking into account characteristic concentration ratios. In dependence on the TOC analysis – 20 ppmv C or 1.5 mg C/l (aqueous phase) – the distribution functions resulted in mean conversions of 99.994 and 99.997%. IEK-3 will sink these limits even further in future as required.

Tests with an ATR 9.2 reformer showed that a synthetic fuel (GTL kerosene, Shell MDS with a final boiling point (90%) at 185 °C) was reformed over 5000 operating hours with a fuel conversion higher than 99.995%. For all measurements – unless otherwise specified – the following mixing ratios were used: $H_2O/C = 1.9$ and $O_2/C = 0.47$. The space velocity was approx. $30,000\ h^{-1}$. In the gas phase, no residual hydrocarbons were detected. In the aqueous liquid phase, 20 mg C/l was measured – here, as the value of non-purgeable organic carbon (NPOC). GC/MS measurements determined that of this, approx. 10 ppmw was acetic acid, 3–4 ppmw acetone and approx. 1 ppmw butanone. In dynamic operation with load cycling between 60% and 100% in stages of 10% with varying durations, no changes were observed in the hydrogen and carbon monoxide concentrations compared to steady-state operation. The temperature changes during load cycling must be considered as a function of the position of the thermocouples (cf. Fig. 21). In the lower mixing chamber, the temperature varied between 370 °C and 410 °C. 5 mm into the catalyst inlet area, the differences were much greater with values between 790 °C and 880 °C. In contrast to this, temperatures at the catalyst outlet varied little with values of 680–685 °C. This indicates that the chemical reaction zones in the catalyst are displaced during load cycling.

When the fuel was changed from GTL kerosene to Neste Oil BTL diesel with a final boiling point at 320 °C, higher concentrations of ethane, ethene, propene, butene, pentene, hexene, and benzene were found in the first 1000 operating hours (5000–6000 h). It should be noted that the operating parameters remained the same as for operation with GTL kerosene. For instance, an increased air ratio or the preheating of the ATR air would have led to more heat in the mixing chamber and thus to more heat in the catalyst. This would have counteracted the formation of these by-products. The cumulative concentrations in the gas phase were maximal 280 ppmV *non-methane hydrocarbons* (NMHC). The TOC values rose to maximal 90 ppmw in the same period.

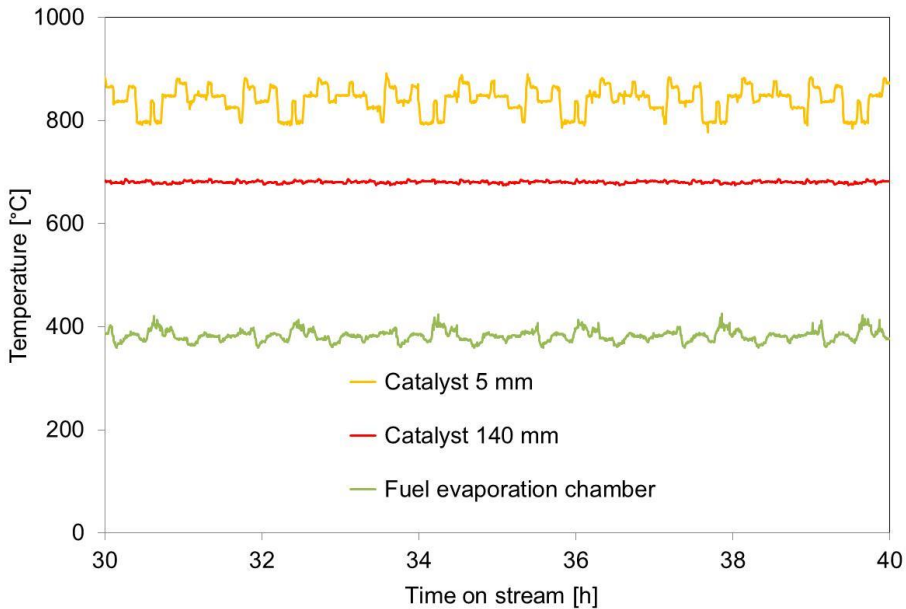


Fig. 21: Temperatures in the monolith and in the vaporization chamber during a load-cycling test with ATR 9.2 at an O_2/C molar ratio of 0.47 and a H_2O/C molar ratio of 1.9 for operation with GTL kerosene

The impact of fuel was evaluated separately using an autothermal reformer of type ATR 8 (cf. Fig. 22). NExBTL diesel (*Neste Oil*), Ecopar diesel (*ECOPAR*), GTL diesel *summer grade* (*SHELL*), GTL diesel *winter grade* (*SHELL*) and Ultimate Diesel (*ARAL*) were tested. Low NMHC concentrations of 13 ppmv and 16 ppmv were measured for NExBTL and Ecopar diesel, respectively. Much higher residual quantities of 261 ppmv and 310 ppmv NMHC were detected for the *SHELL* fuels GTL diesel *summer grade* and *winter grade*, respectively. The two *SHELL* fuels, just like the first two fuels, are free of aromatics. However, the final boiling point of the *summer grade* quality is higher at 350 °C. The final boiling point of the *winter grade* quality is lower at 307 °C (90% recovery) compared to *ECOPAR* at 338 °C. It also has a higher chain length of $C_{16}H_{34}$ compared to $C_{15}H_{32}$ (*ECOPAR*). The use of *ARAL* Ultimate Diesel increased the NMHC value to 915 ppmv. The reasons for this could be the aromatic content of 15% (mass), the higher boiling range with temperatures of 360 °C (90%) or the longer average chain length of $C_{19}H_{38}$. It was shown that the reforming quality decreases with increasing aromatic contents and with higher boiling temperatures.

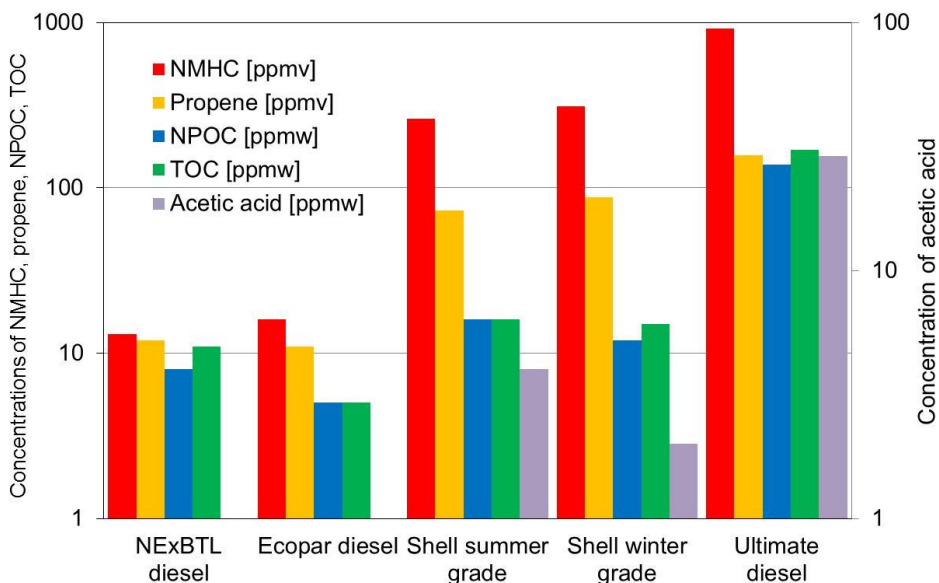


Fig. 22: Concentrations of by-products in the gas phase and in the liquid phase during operation of ATR 8 with five different fuels at an O_2/C molar ratio of 0.47 and a H_2O/C molar ratio of 1.9 for 100% reformer load

A conversion of approx. 98.5% was achieved, for example, for a residual hydrocarbon content of 400 ppmv ethene, 400 ppmv propene, and 200 ppmv benzene. Suitable countermeasures, such as preheating the air, can create a higher enthalpy input in the mixing chamber and thus a higher reaction temperature. The gravimetric power density of the developed reformer types is 2.2–3.2 kW_e/kg and the volumetric power density is 2.8–3.6 kW_e/l .

Fig. 23 shows the concentrations of H_2 , CO , CO_2 and CH_4 as a function of the test duration during a long-term experiment with ATR 9.2. GTL kerosene and NExBTL diesel were used as fuels. The O_2/C and H_2O/C molar ratios were 0.47 and 1.9, respectively, at a space velocity of $30,000 h^{-1}$. The total test duration was 10,000 hours. The figure clearly shows that the H_2 concentrations were very stable during the first 5000 hours of the test when GTL kerosene was used. They varied slightly between 37 vol% and 38 vol%. At the same time, the CO concentrations also varied little between 9 vol% and 10 vol%. This also applied to the CO_2 concentrations during the first 5000 hours of the test with GTL kerosene: values between 11 vol% and 12 vol% were measured. No changes were detected in the CH_4 concentrations in this period and values of approx. 0.5 vol% were measured. The concentrations over time, as shown in this figure, prove that the chemical and physical properties of GTL kerosene (low vaporization temperatures, no aromatics and no sulfur) are advantageous for autothermal reforming. In the second 5000 hour period in the test, BTL diesel was used and the concentrations of some of the components altered considerably. During the first 2300 hours of the test with BTL diesel, the H_2 concentrations decreased from 37.0 vol% to 32.5 vol%. At the same time, the CO concentrations rose from 12.0 vol% to 15.0 vol%. The CO_2 concentrations decreased during the same period from 11.0 vol% to

9.0 vol%. The CH₄ concentrations remained almost constant at values between 0.4 vol% and 0.5 vol%. These changes were due to a decreased catalyst activity in ATR 9.2 for the water-gas shift reaction. During the last 2700 hours of the test with BTL diesel, the concentrations of the targeted products of autothermal reforming remained almost constant. Several catalyst regeneration steps were performed during this period in an effort to restore the catalyst activity at least partially.

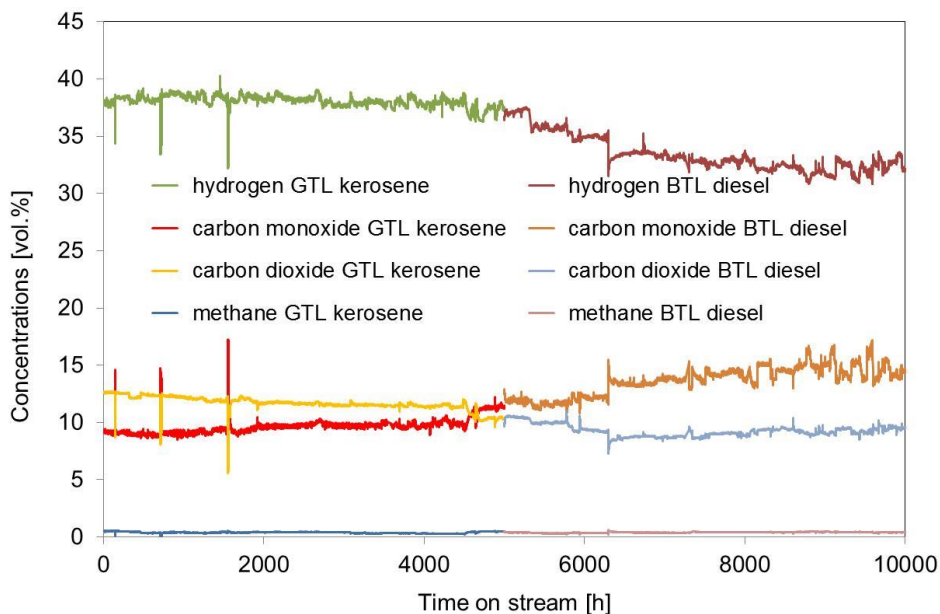


Fig. 23: Concentrations of H₂, CO, CO₂ and CH₄ as a function of test duration during a long-term experiment with ATR 9.2; fuel: GTL kerosene and NExBTL diesel, n(O₂)/n(C) = 0.47, n(H₂O)/n(C) = 1.90, GHSV = 30.000 h⁻¹

The long-term experiment with the reformer type ATR 9.2 also revealed important insights into the formation of by-products (cf. Fig. 24). At an operating time of 6368 hours, a pressure drop in the water supply caused an emergency shutdown. It is likely that the catalyst was permanently damaged. As a result, the total residual hydrocarbons (NMHC) rose from 280 ppmv at 6000 h to maximal 3154 ppmv at 7120 h. Regeneration measures helped to decrease the residual hydrocarbon content back down to NMHC concentrations of approx. 1500 ppmv. These measures involved feeding preheated air for 24 hours at temperatures of 250–280 °C and low space velocities of 12,000 h⁻¹ across the catalyst. After regeneration, the residual hydrocarbon content in the gas phase and in condensed water (TOC) decreased but then subsequently increased until the next regeneration phase. In the gas phase during the operating period 7000–10,000 h, there was a staggering of the alkene concentrations with 700–1650 ppmv C₂H₄, 350–700 ppmv C₃H₆, 200–400 ppmv C₄H₈, 40–95 ppmv C₅H₁₀ and 17–40 ppmv C₆H₁₂. In an analogous manner, 140–270 ppmv C₂H₆ and 20–40 ppmv C₃H₈ appeared. Benzene was found only in small concentrations of max. 13 ppmv. It should be noted that the fuel used – NExBTL – is free of aromatics.

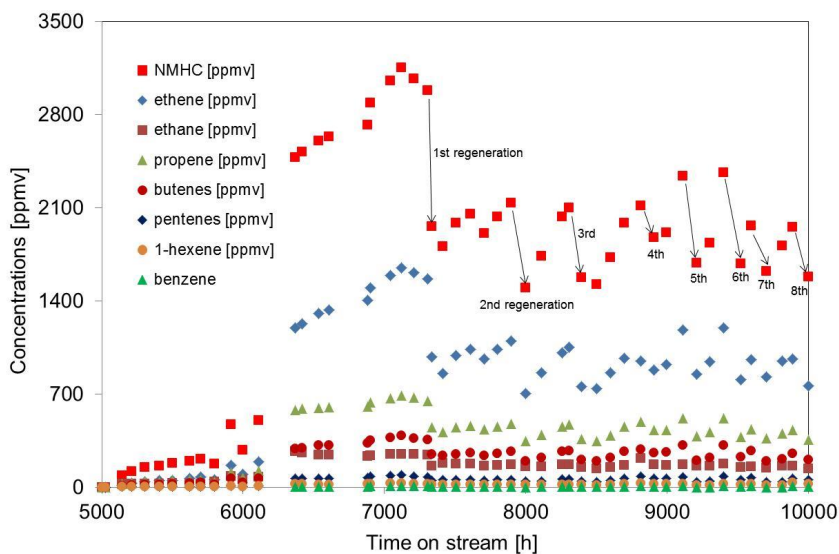


Fig. 24: Concentrations of by-products in the gas phase as a function of test duration during a long-term experiment with ATR 9.2 at an O_2/C molar ratio of 0.47 and a H_2O/C molar ratio of 1.9 using NExBTL diesel

The measured benzene concentrations in fuels containing aromatics (e.g. ARAL Ultimate Diesel and standard diesel SD 10) were considerably higher as soon as residual hydrocarbons were detected in the product gas. At 7042 operating hours, an organic liquid phase appeared above the aqueous phase. At this point in time, the conversion was only 95.8%. In cooperation with the Institute of Bio- and Geosciences (IBG-2), gas chromatography was used to analyze the liquid. The liquid organic residue had a composition that was almost identical to the main components of NExBTL diesel. A comparison with an alkane standard $n-C_{10} - n-C_{22}$ identified the n -alkanes $C_{15}H_{32}$, $C_{16}H_{34}$, $C_{17}H_{36}$, $C_{18}H_{40}$ and their isomers as the main constituents in NExBTL diesel. Smaller quantities of $C_{10}H_{22}$, $C_{11}H_{24}$, $C_{14}H_{30}$ were also found. Interestingly, $C_{11}H_{24}$ and $C_{12}H_{26}$ were not present. A small peak beside decene suggests nonane (C_9H_{20}). In addition to NExBTL components typical of diesel, the organic liquid phase contained small quantities of the substances 4-decene $C_{10}H_{20}$, 3-undecene ($C_{11}H_{22}$), 3-dodecene ($C_{12}H_{24}$), 6-tridecene ($C_{13}H_{26}$) and 7-tetradecene ($C_{14}H_{28}$). The regeneration measures suppressed the formation of an organic liquid phase and after 10,000 operating hours the conversion was again 98.2%. At 9600 hours, several polar components including furans, aldehydes, ketones, acids and alcohols were detected in the aqueous phase. Capillary electrophoresis identified formic acid and acetic acid. The TOC value at 10,000 hours was approx. 234 ppmv. If this is set against 1580 ppmv in the gas phase, then the balance flows can be used to calculate that of the inflowing 191 mol/h carbon in the form of diesel, a gaseous residual hydrocarbon flow of 2.57 mol C/h mainly in the form of ethene and propene and of 0.061 mol C/h in the form of oxygenates dissolved in water were present.

With respect to the reaction process over time, the literature indicates (Parmar et al., Fuel 89 (2010) 1212–1220) that alkanes are gradually degraded as CH_2^* is released to form CH_3^* adsorbate. Oxygen O^* oxidizes the CH_2^* adsorbate to form CH_2O^* and when hydrogen is added carbon monoxide is formed via CHO^* . Adsorbed oxygen is formed according to this

proposed reaction mechanism via the chemical sorption of steam. In a side reaction where H^* is released and desorbed, alkenes are formed and when H^* is added and desorbed, alkanes are formed. Our measurements indicate that alkene formation as a side reaction with shorter chain lengths is stronger. This can be interpreted as increased alkene formation with decreasing chain lengths or a lower desorption of adsorbates with longer hydrocarbon chains.

A striking feature is very different C chain lengths of the residual hydrocarbons in the gas phase and liquid organic phase. In the gas phase, short-chain alkenes – ethene to butene – are dominant, and in the liquid organic phase, the initial fuel remains chemically virtually unchanged. The oxygenates in the aqueous phase only play a subordinate role in the distribution of the absolute residual hydrocarbon content. At 7042 hours, for example, a liquid organic phase appeared for a short time. The fraction of residual hydrocarbon in the gas phase was 77.1%. A share of 21.4% of residual carbon was found in the liquid organic phase and only 1.5% was present in the liquid aqueous phase. To conclude, if a long-chain alkane molecule enters the reaction mechanism, then the carbon chain is almost always fully degraded, achieving C_2 or C_3 molecules. Alkanes that do not enter the reaction sequence leave the reformer almost unchanged. Therefore, the term “diesel slip” is fitting here.

Current and past measurements can be used to classify the conversion behavior:

- At extremely low conversions, e.g. during catalyst screening, there are such large quantities of non-converted fuel that the liquid separators fill up, preventing scientific measurement operation. It can be assumed that diesel slip is dominant here.
- For low conversions, e.g. <96%, diesel slip can occur causing the fuel to flow through the reactor almost unchanged. In parallel, high alkene concentrations, particularly of ethene and propene, occur in the gas phase.
- At relatively good to high conversions, 100–3000 ppmv NHMC – predominantly ethene and propene – occur. The residual hydrocarbon content in the gas phase is considerably higher than the C content in water at TOC values of 60–500 ppmw.
- At very high conversions, no hydrocarbon can be detected in the gas phase, while in the aqueous phase 1–20 ppmw can be found depending on the type of reactor. If ethene and propene appear, their concentrations increase as measurements continue to a much greater extent than the conversion deterioration as shown by the TOC values would have led us to expect. An identifiable residual hydrocarbon content of 1 ppmv ethene and 1 ppmv propene in terms of residual carbon is equal to a TOC value of 12 mg/l. In this conversion range, oxygenates are dominant in the aqueous phase.

3.2.2.4 System development

The results of system development are summarized in section 4.2.

3.2.3 Staff members and fields of activity

Name	Tel. (02461-61-) Email	Field of activity
Prof. Dr. R. Peters	4260 ra.peters@fz-juelich.de	Head of Fuel Processing Systems
Dr. J. Pasel	5140 j.pasel@fz-juelich.de	Head of Chemistry for Fuel Processing
Dr. R. C. Samsun	4616 r.c.samsun@fz-juelich.de	Head of Systems Engineering for On-Board Power Supply

3.2.4 Important publications, PhD theses and patents

Important publications

Pasel, J.; Samsun, R.C.; Peters, R.; Stolten, D.

Fuel Processing of Diesel and Kerosene for APU Applications

Energy & fuels, 27 (8) 2013, pp. 4836-4394, DOI: 10.1021/ef301976f

Peters, R.; Samsun, R.C.

Evaluation of Multifunctional Fuel Cell Systems in Aviation Using a Multistep Process Analysis Methodology

Applied energy, 111 2013, pp. 46 - 63, DOI: 10.1016/j.apenergy.2013.04.058

Meißner, J.; Pasel, J.; Samsun, R.C.; Scharf, F.; Wiethäge, C.; Peters, R.

Catalytic burner with internal steam generation for a fuel-cell-based Auxiliary Power Unit for middle distillates

International journal of hydrogen energy, 39 (8) 2014, pp. 4131-4142, DOI: 10.1016/j.ijhydene.2013.05.167

Samsun, R.C.; Pasel, J.; Janßen, H.; Lehnert, W.; Peters, R.; Stolten, D.

Design and Test of a 5 kW_e High-Temperature Polymer Electrolyte Fuel Cell System Operated with Diesel and Kerosene

Applied energy, 114 2014, pp. 238-249, DOI: 10.1016/j.apenergy.2013.09.054

Wang, Y.; Pasel, J.; Peters, R.

Hydrodesulfurization process with pre-saturation using reformat for application in a 5 kW fuel cell system

Fuel processing technology, 127 2014, pp. 59-65, DOI: 10.1016/j.fuproc.2014.05.032

Doctoral theses

Wiethäge, C

Mobile Fuel Processing Systems with Middle Distillates for High-Temperature PEFCs

Schriften des Forschungszentrums Jülich, Reihe Energie & Umwelt, Band 190, ISBN 978-3-89336-905-8, RWTH Aachen 2013

Important patents

Patents granted:

Principal inventor	PT	Description
D. Stolten	1.2168	Mixing chamber for a reformer and method for operating same
Z. Pors	1.2169	Mixing chamber for a reformer and method for operating same
Z. Pors	1.2272	Process for evaporating a liquid fuel and a mixing chamber for performing this process

3.3 High-temperature polymer electrolyte fuel cells

3.3.1 Objectives and fields of activity

Commercial vehicles, construction machines, ships and aircraft will continue to be run on diesel and kerosene even in the long term. Growing electrification will lead to more efficient power generation on board and thus substantial energy savings. In terms of practicability, these auxiliary power units (APUs) must be run on the fuel that is already on board, which means that these “middle distillates” will have to be reformed. The high-temperature polymer electrolyte fuel cell (HT-PEFC) combined with relevant reforming technology is ideal for this, efficiently generating electricity, even when the engine is not running.

The HT-PEFC, based on polybenzimidazole membranes doped with phosphoric acid, has a typical operating temperature of 160–180°C. Due to the high temperature level, it has a high CO tolerance, which makes it predestined for operation in combination with reformers. In contrast to Nafion-based polymer electrolyte membrane fuel cells, gases do not need to be humidified to ensure the protonic conductivity of the membrane. Another advantage of HT-PEFC technology is due to the considerable temperature difference between the stack and the ambient temperature, which facilitates a more compact cooling concept than is the case in conventional PEMFC systems.

Despite all of these advantages, the acid still has to be prevented from exiting the membrane. Operation in low temperature ranges where liquid water can be formed should therefore be avoided. This must be taken into account by operating strategies and the specific areas of application.

IEK-3 has been pursuing research and development activities on the HT-PEFC since 2005. Work covers basic electrochemical fields, electrode development and stack development. The laboratory infrastructure required for this was expanded and is shown in Fig. 25. In addition to enlarging the floor space in the laboratory, new equipment was also acquired.



Fig. 25: The platform with HT-PEFC test stands which was completed in 2014

In the area of stack development, different cooling concepts and temperature control concepts were investigated. In parallel to experimental stack development work, modeling and simulation were also performed. To describe HT-PEFC cells, models were developed

using the open source simulation tool OpenFOAM. Detailed simulations of mass transport in porous gas diffusion layers were performed using the lattice Boltzmann software tool JULABOS developed at IEK-3. Overall, it was apparent that closely coupling experiments with modeling/simulation led to significant progress in HT-PEFC research and development.

3.3.2 Important results

3.3.2.1 HT-PEFC cooling concepts

High-temperature polymer electrolyte fuel cell (HT-PEFC) stacks in the kW class require a special heat management system, which not only heats the stack during start-up to the necessary operating temperature (140 °C to 180 °C) but which also extracts excess reaction heat from the stack. Ideally, it should be possible to couple heat management in the stack with the system as a whole.

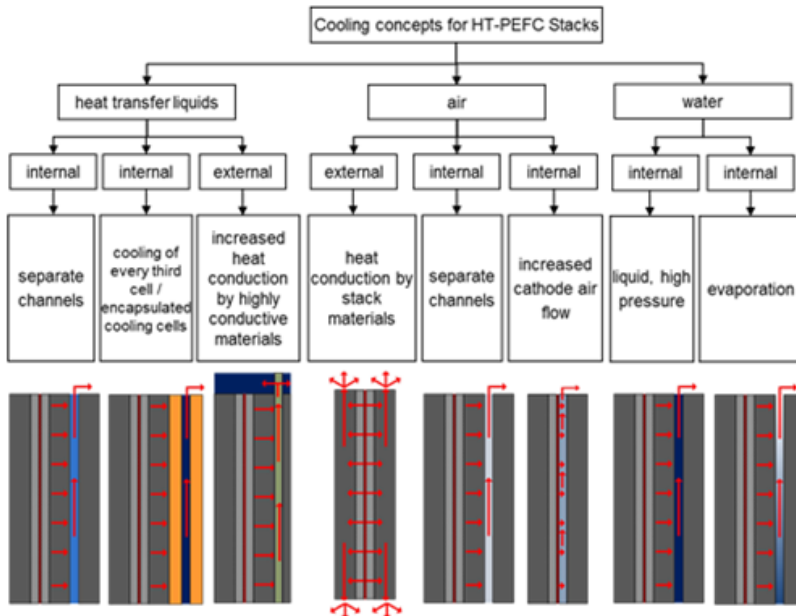


Fig. 26: Overview of the cooling concepts for HT-PEFC stacks

Fig. 26 shows possible concepts for cooling HT-PEFC stacks. Not all of these concepts are also suitable for heating the stack. Additional methods (e.g. electric heating) are necessary for this. The cooling concepts were first classified by the type of heat transfer medium and then by whether the heat transfer medium flows through the stack (internal) or not (external). Possible media for cooling are:

- heat transfer liquids, which remain liquid in the stack's operating range, e.g. polyglycol or a thermal oil
- ambient air

- water, where a distinction must be made between liquid cooling in pressure operation and cooling with phase change

With one exception, the heat transfer media have no direct contact with the membrane electrode assembly (MEA). In other words, heat is transported inside the stack from the source (MEA) via heat conduction to the adjacent bipolar plates (graphite composites or metals). The “internal concepts” have additional channels through which the heat transfer medium flows in or adjacent to the bipolar plates. These concepts can be realized for all heat transfer media with specific variations (e.g. enclosure of the cooling area). The aforementioned exception concerns air, which in one variant functions both as internal cooling medium and cathode air. Its mass flow is not designed for power generation but rather for heat extraction. Only in this case does the heat transfer medium have direct MEA contact.

The “external concepts” carry excess reaction heat out of the stack via thermally conductive materials (existing stack components such as bipolar plates or additional, highly thermally conductive elements such as heat pipes). Outside the stack, the heat is then either directly emitted into ambient air or is transferred to another heat transfer medium.



Fig. 27: HT-PEFC stacks for the experimental analysis of cooling concepts. Left: liquid cooling after each cell. Center: heat-pipe cooling with external heat transfer to a heat transfer liquid. Right: air cooling

After an intensive analysis of possible cooling concepts with some preliminary experiments or CFD simulations using Fluent®, stacks were assembled and tested for three different concepts. Fig. 27 shows the three test stacks. To ensure that the operating and cooling behavior could be compared, the stacks were assembled from similar components. Table 7 summarizes the most important parameters.

Components	Specifications
MEA	Celtec P-1000 [®] , BASF, active cell area: 200 cm ²
Bipolar plate	Graphite-composite material BBP 4, Eisenhuth Gas flow field with ten meanders on the anode and cathode side
Heat transfer medium	<u>Liquid cooling:</u> Polyglycol Fragoltherm [®] S-15-A, Fragol <u>Heat-pipe cooling:</u> Stainless steel jacket, diameter of 3 mm, heat pipe operating medium: water, external heat transfer to Fragoltherm [®] <u>Air cooling:</u> Ambient air

Table 7: Parameters for the experimental comparison of different cooling concepts for HT-PEFC stacks

The main task of the cooling system is to remove the reaction heat from the stack so that the local temperature distribution is sufficiently homogeneous. For the temperature during stack operation, a threshold of 160 °C to 180 °C was set. This threshold applies to the average value from cell to cell as well as to the entire active cell area.

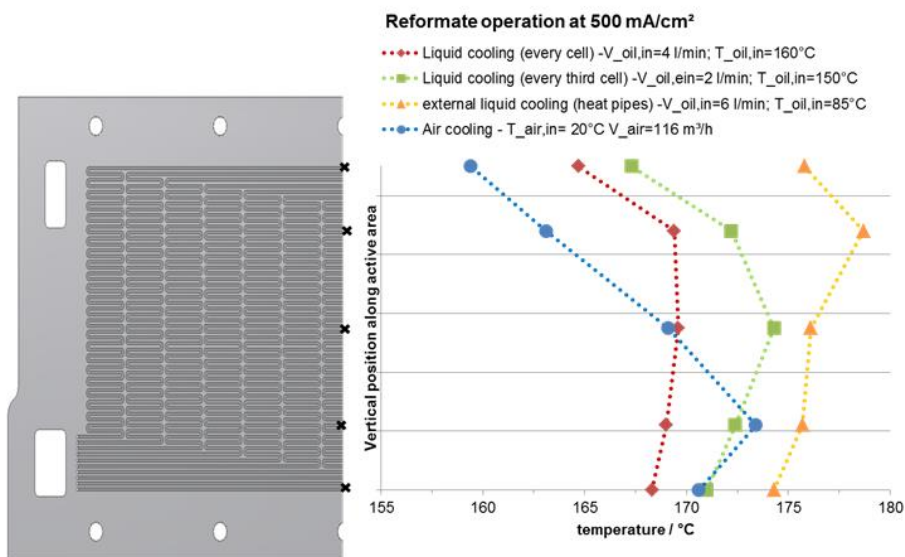


Fig. 28: Influence of the heat transfer medium and the cooling system on the temperature distribution in the MEA layer at a current density of 500 mA cm⁻²

Fig. 28 shows the temperature distribution at five selected points along the main flow direction in the MEA layer for the three different cooling concepts. Two variants were assembled for liquid cooling: cooling after each cell as well as cooling after every three cells.

In summary, all cooling concepts are theoretically possible. The limited temperature range was neither exceeded nor undershot. The temperature curves reveal specific differences

between the concepts. The largest temperature difference of around 14 K was found for air cooling. The reasons for this are the considerably lower heat capacity (approx. factor 2) and the smaller heat transfer coefficient (approx. factor 10) of air compared to liquid polyglycol. The typical temperature increase in the main flow direction of all media (parallel flow configuration from top to bottom) is recognizable and particularly pronounced for air flow. The temperature gradient is lowest for heat-pipe supported cooling. However, the temperature level is also close to the upper limit. The limiting factor here was the convective heat transfer from the heat pipes to the heat transfer liquid in the outer area of the stack.

3.3.2.2 Temperature distribution in a 5 kW HT-PEFC stack

As part of the project EFFESYS-BRINKS, a HT-PEFC stack was developed, assembled and tested for integration into an aircraft APU. The internal heat transfer liquid cooling every third cell with an enclosed cooling cell was identified as most suitable in preliminary investigations conducted by Jen Supra Fehler! Textmarke nicht definiert. as part of his doctoral thesis. The cooling system controls the temperature of a HT-PEFC stack in reformat operation with a power of 5 kW_{el}. To provide the required power, an active cell area of 320 cm² is used. An upscaling of experimental performance data of the stack concept predicted that 70 cells would be needed for this. The stack was designed modularly and comprised 5 modules with 12 cells each and 1 module with 10 cells. The advantage of this modular design is that if one cell fails, only the affected module and not the entire stack has to be disassembled.

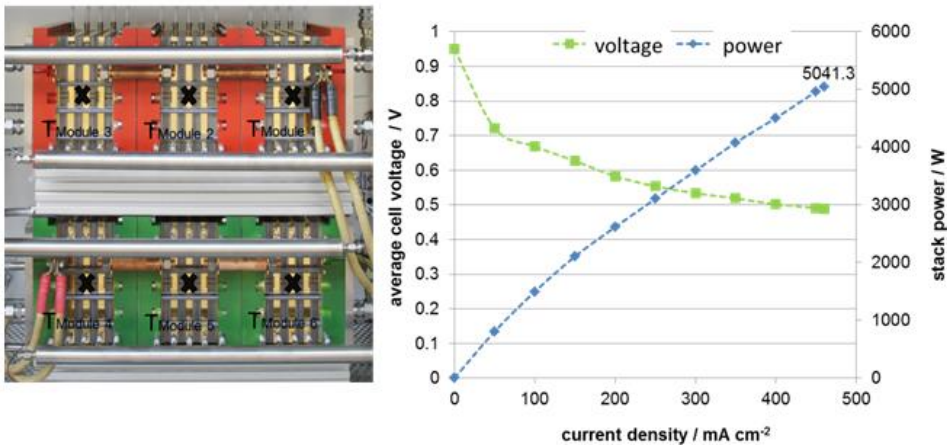


Fig. 29: Position of the thermocouples (left) and stack power (right) measured in reformat operation, $T_{coolant,in}=160\text{ }^{\circ}\text{C}$, $\dot{V}_{coolant,in}=18\text{ l/min}$, 70 cells, $\lambda_{ref/air}=2/2$

The thermal behavior was analyzed for the stack and each module in order to verify whether module behavior is also reflected in the full stack assembly. Therefore, the temperature in each module was first measured around the volumetric center. Fig. 29 depicts the measuring points and the performance curves of the entire assembly.

The current-density curves show that a total output of more than 5 kW_{el} was achieved at a current density of 460 mA cm⁻² for operation with synthetic reformat. Due to test stand restrictions, a total volume flow of the heat transfer liquid of maximal 18 l/min could be used

for cooling. This is equivalent to only half of the design value. The stack's operating window is therefore limited from a thermal perspective. The temperatures measured are shown in Fig. 30

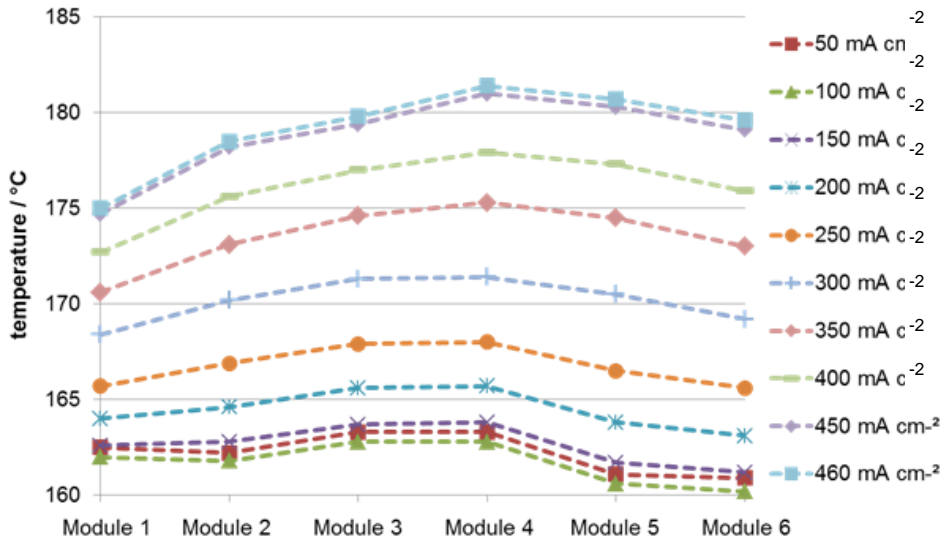


Fig. 30: Temperatures measured in the centers of each stack module as a function of current density

It can be seen that the temperature difference between the individual modules in the stack is sufficiently small, measuring a maximum of 6.4 K at a current density of 460 mA cm⁻². The temperature difference also decreases at low current densities. The temperature level at 50 mA cm⁻² was slightly higher than the temperature level at 100 mA cm⁻² because the dwell time until a steady-state temperature was achieved was too short.

In addition to the temperature difference between the individual stack modules, the temperature difference between the cells was also determined. An analytical model was created based on energy balances and a real stack module (see Fig. 31, left) with 12 cells and cooling after every 3 cells. For a stack with cooling every third cell and an active MEA area of 320 cm², the calculations resulted in the maximal temperature difference and heat flow to be removed, as shown in Fig. 31, right. From the diagram, it follows that a HT-PEFC stack module in reformate operation up to a current density of 450 mA cm⁻² is sufficiently cooled when the temperature is controlled every third cell. At this current density, the maximal temperature difference from cell to cell is 18.1 K. As was shown in a conceptual design, the temperature in the stack at this operating point was 160 °C when the heat transfer liquid had an inlet temperature of 140 °C. The maximal temperature in the stack at a temperature difference of 18.1 K therefore did not exceed the operating temperature threshold of 180 °C. At higher current densities and a constant inlet temperature of the heat transfer liquid, local temperatures above 180 °C would occur in the stack. Operation at current densities above 450 mA cm⁻² would be possible if the inlet temperature of the heat transfer liquid were to be decreased. In reformate operation, the stack efficiency for

producing power at current densities above 450 mA cm^{-2} was considerably lower than 50% meaning that steady-state operation is only an option from an energy perspective under certain circumstances.

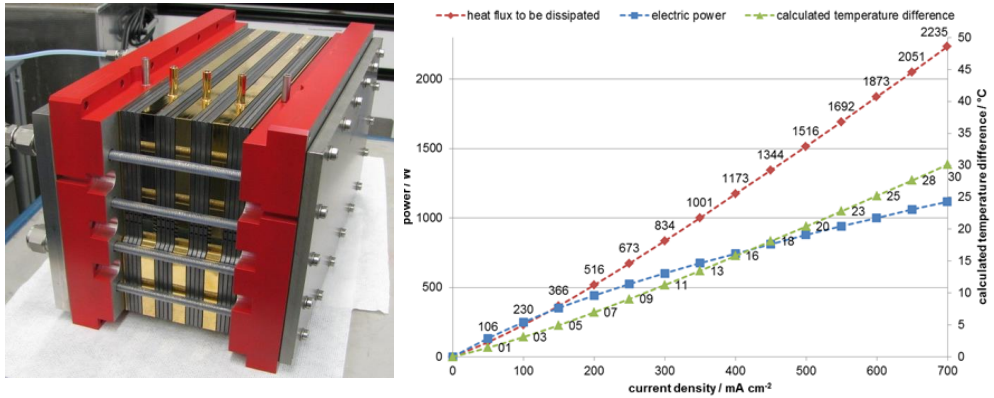


Fig. 31: Left: stack module with 12 cells, $A_{active}=320 \text{ cm}^2$. Right: one module's heat flow, calculated using the energy balance, and the maximal calculated temperature difference from cell to cell: reformate operation, full thermal insulation

These findings were verified in experiments with hydrogen or synthetic reformate and air at a stoichiometric ratio of 2. The variable parameters of supplying the heat transfer liquid were set to an inlet temperature of 160 °C and a volume flow rate of 6 l/min . An overview of the experimental operating conditions is given in Table 8.

Components/parameters	Specifications
Anode gas	Hydrogen or synthetic reformate (42% H_2 , 57% N_2 , 1% CO)
Cathode gas	Air
Stoichiometry	$\lambda_{\text{H}_2/\text{air}}=2/2$, $\lambda_{\text{ref}/\text{air}}=2/2$
$T_{\text{gas,in}}$	160 °C
$T_{\text{coolant,in}}$	160 °C
Volume flow of coolant	6 L min^{-1}
A_{active}	320 cm^2 per cell
MEA	BASF Celtec® P1000
Module	12 cells
Cooling	3 cooling cells + cooled end plates
Heat transfer liquid	Fragoltherm S-15-A

Table 8: Übersicht der experimentellen Betriebsbedingungen

Fig. 32 shows the local cell voltages and mean cell temperature along the stack axis. The temperature and cell voltage profiles are largely parallel and the influence of temperature on cell voltage is clear. At the same current density, the cell voltage for hydrogen operation with an average value of 0.52 V is 0.06 V higher than the cell voltage for reformate operation

(0.46 V). From the energy balance, it can be derived that the heat flow to be removed during reformat operation is 129.6 W higher than during hydrogen operation. As the inlet conditions of the heat transfer liquid are identical, it can be concluded that the temperature level of hydrogen operation is below that of reformat operation. Sufficient cooling is therefore possible up to a current density of 500 mA cm^{-2} ($\dot{Q}_{ab,Ref}=1516 \text{ W}$). In hydrogen operation, the higher voltage level means that an operating point at higher current densities is often selected. An appraisal using the energy balance showed that sufficient cooling during hydrogen operation is only possible up to current densities below 550 mA cm^{-2} ($\dot{Q}_{ab,H_2}=1549 \text{ W}$). In other words, the cooling concept outlined here is designed specifically for reformat operation.

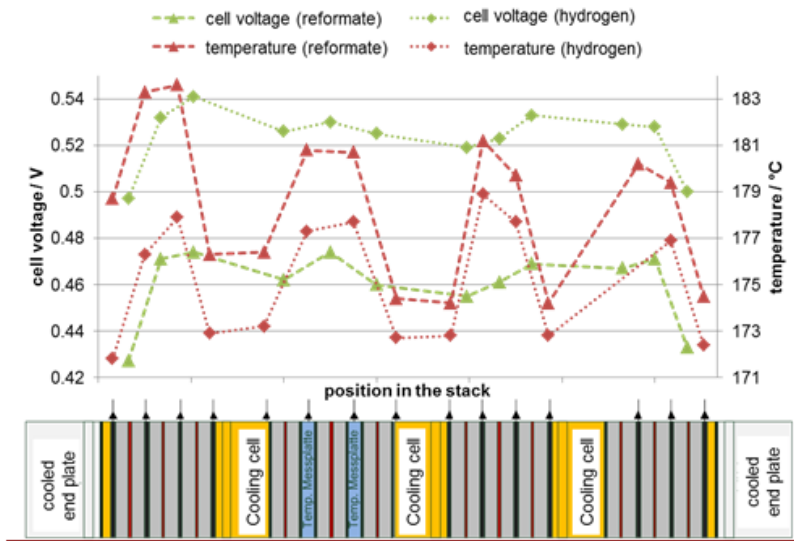


Fig. 32: Local temperature and voltage distribution from cell to cell. Comparison of reformat and hydrogen operation at a current density of 500 mA cm^{-2} $T_{\text{coolant,in}} = 160 \text{ }^\circ\text{C}$, $V_{\text{coolant}} = 6 \text{ l/min}$

3.3.2.3 Computational fluid dynamics in porous structures

On the mesoscopic scale, the lattice Boltzmann method was used to simulate transport processes in gas diffusion layers (GDLs). The underlying geometric structures came from two sources. At Helmholtz-Zentrum Berlin, the microstructure of GDLs was determined in the BESSY synchrotron and made available to IEK-3 for transport simulations. In addition, the Institute of Stochastics at Ulm University developed stochastic models of the microstructure of GDLs from different suppliers. These led to artificial structures that are stochastically equivalent to the real structure. These structures were also made available for transport simulations.

Gases are distributed across the active area of a fuel cell via suitable flow fields. Fig. 33 shows how the GDL is pressed together by the flow fields under the ribs and how under the channels parts of the microstructure can protrude into the channels.

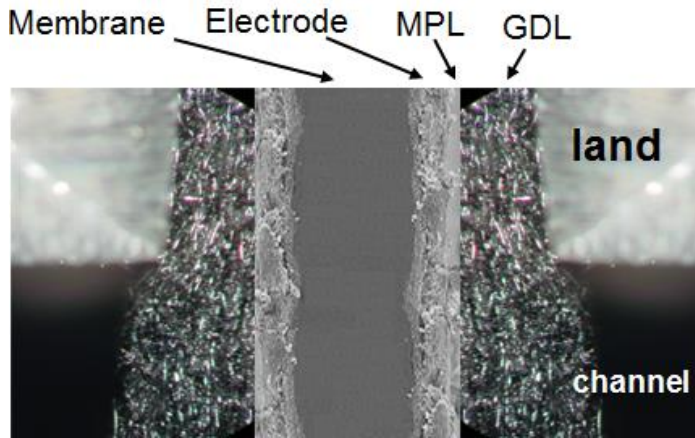


Fig. 33: GDL in the channel/rib area of a flow field

The channel-rib structure causes an imbalance in the gas supply to the electrode: an above-average supply below the channel and a below-average supply below the rib. The GDL enables the area below the rib to be utilized by making a cross-flow through the porous structure possible, which distributes the gas fairly homogeneously to the electrode.



Abb. 34: Left: clamping device for the controlled compression of porous structures. Right: part of a tomogram showing a GDL with 29% compression

The gas flow is influenced by the level of compression of the GDL, which correlates with the contact pressure between the bipolar plate and the GDL. The compression can be precisely adjusted on a laboratory scale using a clamping device (Abb. 34, left). A real GDL was investigated at Helmholtz-Zentrum Berlin in the BESSY synchrotron and geometries for a channel-rib scenario with varying degrees of compression were visualized. Abb. 34 (right) shows part of a 3D real structure with a channel running through the center.

With increasing compression, more fibers are forced into the channel area and the thickness of the material decreases. Fiber build-up occurs particularly under the rib. The level of

compression is equal to the volume fraction lost in the overall geometry due to compression. The influence of this compression on gas flow in a channel-rib scenario was analyzed in the microstructure using transport simulations. The scenario of the structural investigations was simulated in the BESSY synchrotron. The transport processes during fuel cell operation in the relevant area under the rib edge were simulated using the lattice Boltzmann method. A schematic of the simulation geometry is shown in Fig. 35.

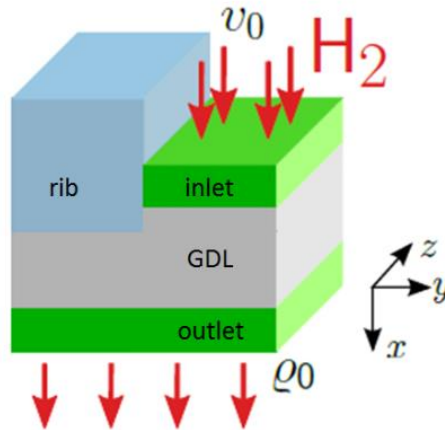


Fig. 35: Schematic of the simulation geometry

Hydrogen enters the GDL via the channel and is distributed through the porous structure so that it exits via the entire surface area at the electrode side. The operating point of the fuel cell was set by the velocity – and thus the mass – of the converted fuel, which enters the GDL from the channel side. For the simulation, real data from four compression levels between 0% and 29% were used.

Fig. 36 shows the x components of the local velocity v_x (which is proportional to the mass flow) at the interface to the electrode. It can be clearly seen how the GDL structure leads to the formation of local maxima and minima for v_x across the entire surface area. Furthermore, an imbalance in the y direction is obvious. This is more pronounced for the greater compression on the right-hand side: under the rib the supply is below average and under the channel it is above average.

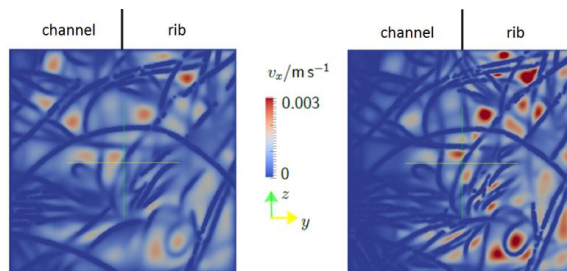


Fig. 36: Velocity profile y-z plane at the electrode side of a channel-rib geometry: compression=0% (left) and compression=29% (right)

As a qualitative result of the transport simulations at four levels of compression, it can be concluded that the gas supply to the electrode is not linear with respect to the compression. The transport simulations were performed using hardware (JUROPA) at the Jülich Supercomputing Centre (JSC).

3.3.3 Staff members and fields of activity

Name	Tel. (02461-61-) Email	Field of activity
Prof. Dr. W. Lehnert	3915 w.lehnert@fz-juelich.de	Head of High-Temperature Polymer Electrolyte Fuel Cells
J. Brinkmann	2177 j.brinkmann@fz-juelich.de	Lattice Boltzmann modeling on a cell-component level
Q. Cao	1923 q.cao@fz-juelich.de	Modeling of fuel cells with OpenFOAM
D. Froning	6676 d.froning@fz-juelich.de	Modeling of fuel cells, informatics, software engineering
Dr. H. Janßen	5082 h.janssen@fz-juelich.de	Head of HT-PEFC Stack Development
Prof. Dr. A. Kulikovskiy	5396 a.kulikovskiy@fz-juelich.de	Development of analytical and numerical models of HT-PEFCs, DMFCs and SOFCs
Fr. F. Liu	9036 f.liu@fz-juelich.de	Electrode development and characterization
Fr. S. Lee	1923 s.lee@fz-juelich.de	Modeling of fuel cells with OpenFOAM
Fr. Dr. W. Lücke	9073 w.lueke@fz-juelich.de	Electrode and MEA characterization
Fr. A. Majerus	3018 a.majerus@fz-juelich.de	Membrane and electrolyte characterization
Fr. Dr. M. Nullmeier	9074 m.nullmeier@fz-juelich.de	HT-PEFC fundamental chemistry
Dr. U. Reimer	3537 u.reimer@fz-juelich.de	Head of HT-PEFC Modeling and Simulation
Fr. B. Schumacher	5406 b.schumacher@fz-juelich.de	Development of designs for test stands for HT-PEFCs, testing of HT-PEFCs
J. Supra	6029 j.supra@fz-juelich.de	Development of HT-PEFC stacks, benchmarking of stack materials
V. Weißbecker	9576 v.weissbecker@fz-juelich.de	Corrosion investigations on metallic bipolar plates

3.3.4 Important publications, doctoral theses and patents

Publications:

Conti, F.; Willbold, S.; Mammi, S.; Korte, C.; Lehnert, W.; Stolten, D.

Carbon NMR investigation of the polybenzimidazole-dimethylacetamide interactions in membranes for fuel cells

New journal of chemistry, 37 (1) 2013, pp. 152-156, DOI: 10.1039/C2NJ40728K

Froning, D.; Brinkmann, J.; Reimer, U.; Schmidt, V.; Lehnert, W.; Stolten, D.

3D analysis, modeling and simulation of transport processes in compressed fibrous microstructures, using the Lattice Boltzmann method

Electrochimica acta, 110 (1) 2013, pp. 325-334, DOI: 10.1016/j.electacta.2013.04.071

Janßen, H.; Supra, J.; Lüke, L.; Lehnert, W.; Stolten, D.

Development of HT-PEFC Stacks in the kW range

International journal of hydrogen energy, 38 (11) 2013, pp. 4705-4713, DOI: 10.1016/j.ijhydene.2013.01.127

Kulikovsky, A.; Eikerling, M.

Analytical solutions for impedance of the cathode catalyst layer in PEM fuel cell: Layer parameters from impedance spectrum without fitting

Journal of electroanalytical chemistry, 691 2013, pp. 13-17, DOI: 10.1016/j.jelechem.2012.12.002

Liu, F.; Kvesic, M.; Wippermann, K.; Reimer, U.; Lehnert, W.

Effect of Spiral Flow Field Design on Performance and Durability of HT-PEFCs

Journal of the Electrochemical Society, 160 (8) 2013, pp. F892-F897, DOI: 10.1149/2.116308jes

Supra, J.; Janßen, H.; Lehnert, W.; Stolten, D.

Design and Experimental Investigation of a Heat Pipe supported External Cooling System for HT-PEFC stacks

Journal of fuel cell science and technology, 10 (5) 2013, pp. 051002-1 - 051002-7, DOI: 10.1115/1.4025052

Weißbecker, V.; Reimer, U.; Wippermann, K.; Lehnert, W.

A Comprehensive Corrosion Study on Metallic Materials for HT-PEFC Application

224th ECS Meeting, 58 (1) 2013, pp. 693-704, DOI: 10.1149/05801.0693ecst

Arlt, T.; Maier, W.; Tötze, C.; Wannek, C.; Markötter, H.; Wieder, F.; Banhart, J.; Lehnert, W.; Manke, I.

Synchrotron X-ray radioscopic in situ study of high-temperature polymer electrolyte fuel Cells - Effect of operation conditions on structure of membrane

Journal of power sources, 246 2014, pp. 290-298, DOI: 10.1016/j.powsour.2013.07.094

Doctoral theses

Kvesic, M.

Modellierung und Simulation von Hochtemperatur-Polymerelektrolyt-Brennstoffzellen

Schriften des Forschungszentrums Jülich, Reihe Energie & Umwelt, Band 158, ISBN 978-3-89336-835-8, RWTH Aachen 2013

Lüke, L.

Analyse des Betriebsverhaltens von Hochtemperatur-Polymerelektrolyt-Brennstoffzellen

Schriften des Forschungszentrums Jülich, Reihe Energie & Umwelt, Band 192, ISBN 978-3-89336-909-6, RWTH Aachen 2013

Maier, W.

Phosphorsäureverteilung in Membran-Elektroden-Einheiten dynamisch betriebener Hochtemperatur-Polymerelektrolyt-Brennstoffzellen

Schriften des Forschungszentrums Jülich, Reihe Energie & Umwelt, Band 157, ISBN 978-3-89336-830-3, RWTH Aachen 2013

Brinkmann, J.P.

Lattice-Boltzmann-Simulation in faserbasierten Mikrostrukturen

Schriften des Forschungszentrums Jülich, Reihe Energie & Umwelt, Band 232, ISBN 978-3-89336-995-9, RWTH Aachen 2014

Liu, F.

Interaction of Phosphoric Acid with Cell Components in High Temperature Polymer Electrolyte Fuel Cells

Schriften des Forschungszentrums Jülich, Reihe Energie & Umwelt, Band 219, ISBN 978-3-89336-972-0, RWTH Aachen 2014

Majerus, A.

Eigenschaften des Phosphorsäure-Polybenzimidazol-Systems in Hochtemperatur-Polymerelektrolyt-Brennstoffzellen

Schriften des Forschungszentrums Jülich, Reihe Energie & Umwelt, Band 210, ISBN 978-3-89336-947-8, RWTH Aachen 2014

Supra, J.

Kühlkonzepte für Hochtemperatur-Polymerelektrolyt-Brennstoffzellen-Stacks

Schriften des Forschungszentrums Jülich, Reihe Energie & Umwelt, Band 209, ISBN 978-3-89336-946-1, RWTH Aachen 2014

Important patents

Patent applications:

Principal inventor	PT	Description
J. Bohner	1.2569	Clamping means for a fuel cell stack and method for bracing a fuel cell stack
A. Kullikovskiy	1.2601	Method for characterising the catalyst structure in a fuel cell, and fuel cell design suitable for said method
O. Holderer	1.2630	Material testing of membranes for polymer electrolyte fuel cells
V. Weißbecker	1.2673	Bipolar plates for electrochemical cells and method for producing the same

Patents granted:

Principal inventor	PT	Description
H. Dohle	1.2375	High-temperature polymer electrolyte fuel cell system and method for operation of same
A. Kulikovskiy	1.2601	Method for characterising the catalyst structure in a fuel cell, and fuel cell design suitable for said method

3.4 Direct Methanol Fuel Cells

Direct methanol fuel cells (DMFCs) directly convert the liquid fuel methanol into electric current. In comparison to fuel cell systems operated with pure hydrogen or hydrogen-rich gases from reforming processes, the fuel is supplied directly in the form of liquid methanol. Simple system configuration enables unrestricted part-load operation, giving it an advantage over much more complex systems with reforming in the power range up to 5 kW. In addition to methanol's very high energy density, the DMFC offers easy handling and easy refueling of the liquid fuel.

The use of DMFCs for small mobile applications (e.g. in material handling as an alternative to lead-acid batteries) is interesting in the short to medium term. Another area of R&D involves developing kW-class DMFC systems for emergency power supply, which is particularly challenging in terms of stack durability. Robotics is yet another interesting application for DMFCs. Systems in this area are characterized by a compact structure and a high power density.

3.4.1 Objectives and fields of activity

DMFC research (cf. Fig. 37) covers the development of membrane electrode assemblies (MEAs), their usage in DMFC stacks, and the development of DMFC systems for the applications listed above. All work takes manufacturing aspects into account.

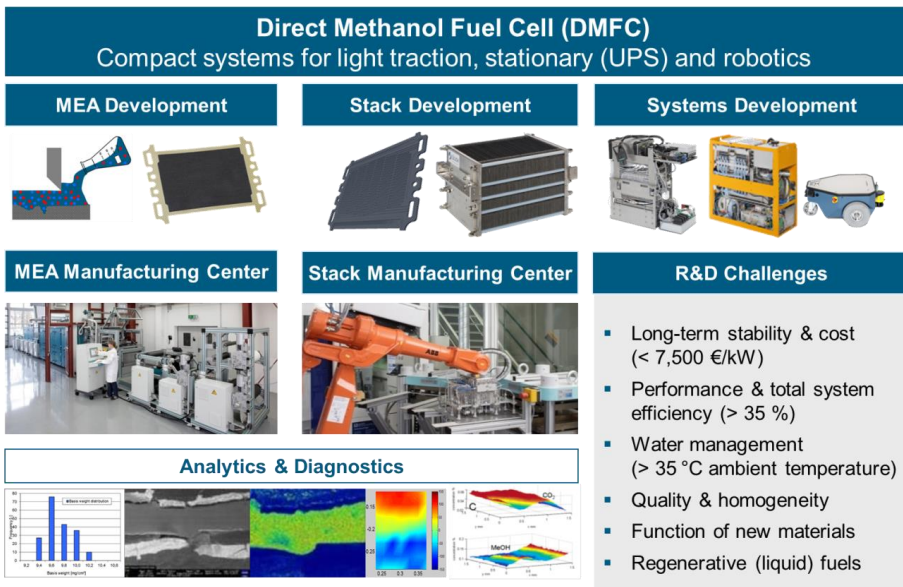


Fig. 37: DMFC research and development

Activities include investigating electrochemical reactions on optimized electrode structures, characterizing new membranes, optimizing cell components, such as the membrane electrode assembly (MEA) or the manifold structure and their fabrication methods,

characterizing MEAs, and developing stacks and systems. This work is supported by basic physicochemical investigations.

IEK-3 has been developing DMFC systems for different applications for more than 10 years (cf. Fig. 38). In this section, particularly interesting results of successful development work over the period under review will be presented.

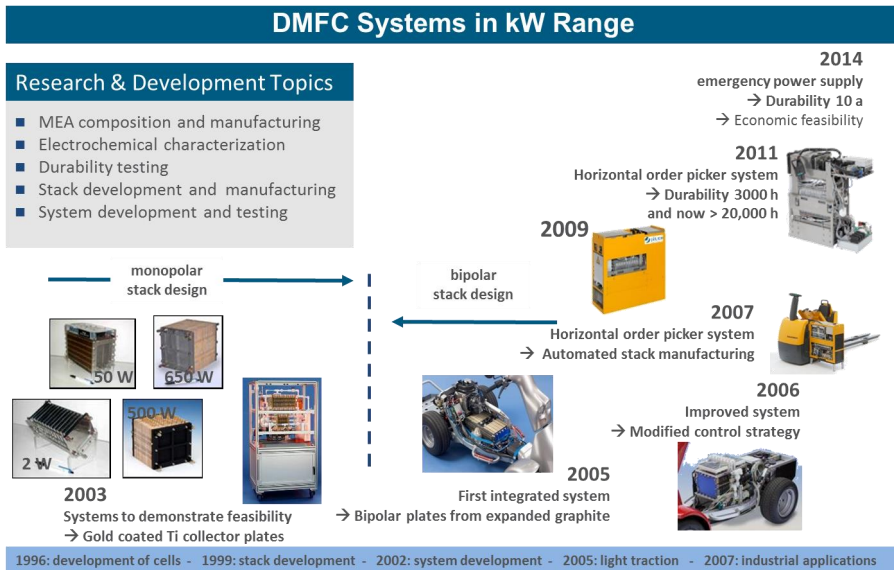


Fig. 38: History of the development of the direct methanol fuel cell at IEK-3

IEK-3 successfully replaced the battery tray of a forklift truck (ECE 220, Jungheinrich) with a kW-class DMFC hybrid system. The weight of the system was reduced by a factor of two and the range increased by a factor of three. An economic feasibility study verified that this type of system is suitable for use in a forklift truck and can be operated economically in three-shift operation.

The hybrid DMFC system comprises an active 1.0 kW DMFC system and 45 Ah lithium-ion high-power battery pack connected in parallel. This hybrid system can provide a peak load of 7 kW. The advantages of this energy-supply module compared to conventional lead-acid batteries are its higher range (24 h use with a 20 L methanol canister instead of 8 h with battery recharging) and its higher availability (it takes a few minutes to exchange canisters instead of hours to recharge the battery). To be economically efficient, the DMFC stack in the DMFC system V3.3-2 must have a lifetime of at least 10,000 h. IEK-3 has therefore focused its R&D over the last few years on identifying measures to improve the long-term stability of DMFC systems. To validate R&D results, two prototypes were assembled for dynamic lifetime testing using real load profiles until end of life (EOL) (cf. Fig. 39).

Durability of Direct Methanol Fuel Cells in the kW-Power Range

Prove of 20.000 h Lifetime

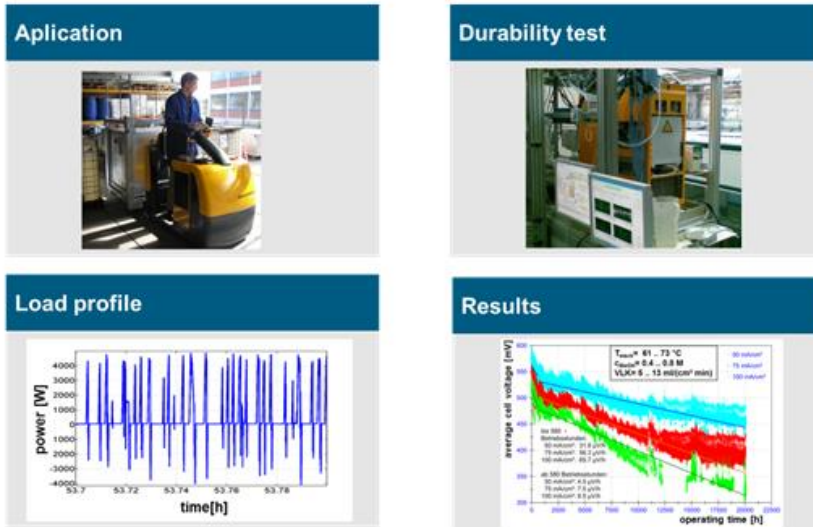


Fig. 39: Lifetime testing with a real load profile

The test duration was 25,200 hours and the hybrid system was operated for 20,000 of these. Operation for 20,000 hours is equivalent to the life cycle of a vehicle in the material handling sector. The development and validation of the DMFC system verified that it is suitable for use in a forklift truck and that it not only meets the techno-economic system requirements for commercialization but goes well beyond them. With a proven lifetime of 20,000 operating hours in a lifetime test with a realistic, highly dynamic load profile, a milestone has been achieved for the commercialization of DMFC systems in the light traction sector.

3.4.2 Important results

With funding from the Helmholtz Validation Fund, which the Helmholtz Association uses to support technologies close to commercialization, the DMFC system was further developed for use in telecommunication systems and other important devices which must be available even during a power failure as uninterruptable power supply (UPS). The DMFC system must start reliably in the case of a power failure and it must run without refueling for 72 hours or more.

In the DMFC-UPS validation project for reliable and uninterruptable power supply and emergency power supply, new challenges were encountered due to the application profile, which differs considerably from the light traction sector. The continuous output of these systems is around 2 kW and the necessary lifetime is some 10 years. During this period, the system is predominantly in standby and it must be ensured that there is no degradation of the electrochemically active during this period. Options for preventing degradation, particularly in standby phases, were therefore investigated.

3.4.2.1 Long-term stability of the membrane electrode assembly

The minimum lifetime of a DMFC system for uninterruptable power supply (UPS) or emergency power supply is 10 years. The MEAs must also be designed for this lifetime. A typical feature of UPS operation is the alternation between operating phases and standby phases. It is assumed that during the lifetime of 10 years (86,400 hours), the system will be operated for 5000 hours (see Fig. 40). During the rest of the time, the system is in standby. Continuous operating time is assumed to be 72 hours.

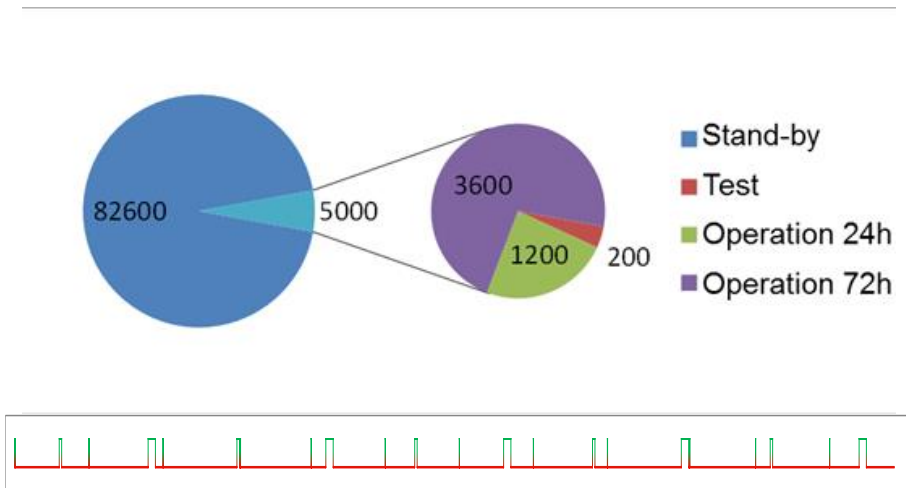


Fig. 40: Distribution of lifetime across various operating states (top) and schematic of operating and standby phases within a year (bottom)

As short periods of operation and regular system tests are expected to occur, it was assumed that some 220 start-up and shut-down cycles will occur during the lifetime. The aim of the lifetime tests was to verify the stability of the MEAs throughout the full lifetime with the necessary operating and standby phases as well as start-up and shut-down cycles. During the now completed project for the development of a DMFC system for a forklift truck, extensive insights were gained into the degradation of MEAs in continuous operation. However, the challenge for the UPS system was degradation during standby as well as frequent start-up and shut-down cycles. Operating strategies had to be developed to prevent an excessive reduction in the cell voltages. Tests were conducted on small cells and on short stacks comprising 5 cells with the same dimensions intended for the UPS stack.

3.4.2.2 Continuous operation

The system was designed for 5000 operating hours during its lifetime. A maximal degradation of $10 \mu\text{V/h}$ was therefore tolerable. As a realistic operating point, operation at 0.1 A/cm^2 and $70 \text{ }^\circ\text{C}$ with 0.75 M methanol solution was selected for all degradation measurements. MEAs from four different manufacturers were tested. The MEAs were run in using an established procedure and the performance characteristics were recorded. Then, the MEAs were loaded with 0.1 A/cm^2 in continuous operation and characteristics were

recorded every 500 hours after the running in procedure was repeated. As the performance improved during the first 500 hours, the characteristics after 500 hours were taken as the starting point. A decrease in the cell voltage was observed over 1000 hours. Within another thousand hours, a decrease of 0-10 mV was observed in the cell voltage of the MEAs used. The degradation rate was maximal 10 $\mu\text{V}/\text{h}$ in all cases. Fig. 41 shows this using an example.

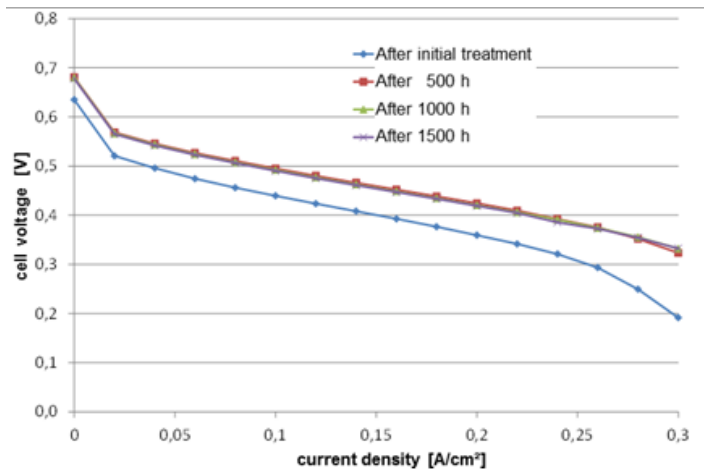


Fig. 41: MEA degradation during continuous operation. After an improvement in the first 500 hours, the cell voltage decreased gradually.

3.4.2.3 Standby

As the system will be in standby for more than 80,000 hours during its lifetime, only extremely low degradation rates are tolerable. The limit was set to 1 $\mu\text{V}/\text{h}$. In order to verify low degradation, tests lasting at least 5000 h are necessary to detect a decrease of <5 mV in the cell voltage. Smaller changes cannot be reproducibly detected.

In order to prevent wear and prolong the life of the MEAs during standby, different standby strategies were tested. Previous studies on degradation mechanisms have shown that if the potentials at the anode are too high, ruthenium contained in the catalyst oxidizes and diffuses to the cathode, where it then poisons the Pt catalyst. The cells were therefore dried with nitrogen to prevent diffusion of the dissolved species. In other variants, attempts were made to prevent an increase in the anode potential. This was done either by continuously supplying the anode with methanol solution, or by sealing the anode and cathode to prevent oxygen seeping in. In one test, the operating media were left in the cell, and in another, the cell was filled on both sides with water to displace the operating media. For comparison, the anode side was sealed in one cell while the cathode side was left open. Table 9 outlines the standby strategies investigated.

Description	Anode	Cathode
Wet	Sealed	Sealed
Dry	Dried with N ₂ , open	Dried with N ₂ , open
Water	Rinsed with water, sealed	Rinsed with water, sealed
Supplied, sealed	Methanol solution circulated	Sealed
Supplied, open	Methanol solution circulated	Open
Only turned off	Sealed	Open

Table 9: Standby strategies

It was shown that the degradation rate depends strongly on the selected standby strategy. The degradation rate during the first 2000 hours, in particular, can considerably exceed the maximal tolerable degradation rate of 1 $\mu\text{V}/\text{h}$ (see Fig. 42). This low degradation rate can be reached when the anode is continuously supplied with methanol. The methanol consumption was found to be negligible. The low starting voltage of a MEA was probably due to an incomplete running in at the beginning of the test. It can be assumed that the starting voltage was the same as for the other MEAs, namely 0.49 V. A similar effect can be achieved by filling the anode and cathode compartments during shut-down with water.

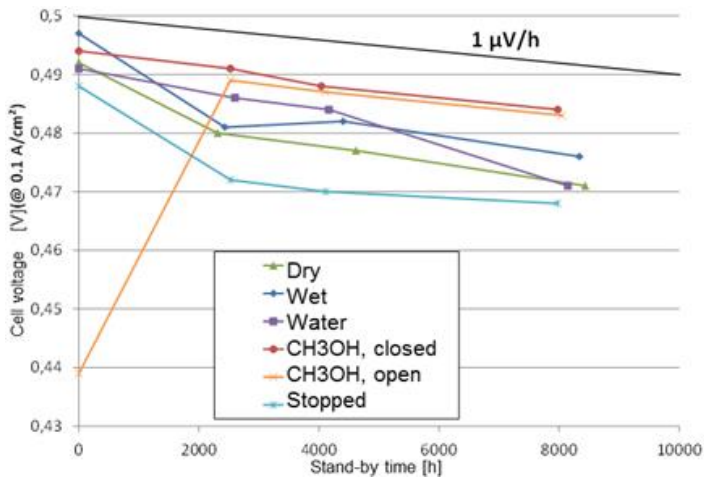


Fig. 42: Degradation for different standby strategies

However, in a real system, water would have to be provided, which is impractical. Simple techniques, which seal the cells or leave the cells unsealed during standby, cause strong degradation at the beginning and should therefore be avoided.

3.4.2.4 Interval operation

To investigate the impact of frequent start-up/shut-down of the system on the lifetime of the MEAs, the degradation was visualized for interval operation. The MEAs were operated every 12 hours for 3 hours and then shut down again. Within 10 weeks, 140 of these start-up/shut-down cycles were performed. In addition, 420 hours of operation and 1260 hours of standby were also achieved.

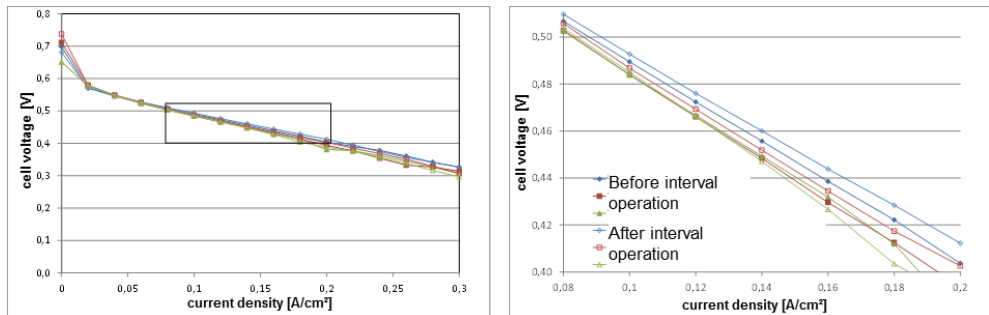


Fig. 43: Degradation during different standby strategies (left: complete characteristic curve; right: section)

As system start-up aims to produce power as fast as possible and system loading also accelerates the heating up process, the influence on degradation of the temperature from which the system is loaded was investigated. Loading of three MEAs began at temperatures of 25 °C, 30 °C and 35 °C, respectively, and the current was increased step by step. Nominal power for all three MEAs was achieved at temperatures 10 °C above the starting temperature. Based on the degradation measurements during standby and continuous operation, a decrease of 12 mV was expected in the cell voltage at 0.1 A/cm² during continuous operation. However, when the MEAs at temperatures of 30 °C or 35 °C were loaded, no decrease was observed in the cell voltage. For the MEA at 25 °C, a decrease of only 4 mV was observed (see Fig. 43). Instead of the feared additional degradation because of frequent start-up and shut-down, the degradation was actually reduced – above all when the MEA was not loaded at temperatures that were too low. Therefore, the MEAs are suitable for operation in a UPS system and loading is possible without damage from a temperature of 30 °C.

3.4.2.5 Reactivation

In the last section, observations showed that frequent start-up and shut-down led to a lower degradation of the MEAs than continuous operation or permanent standby. Therefore, interval operation was used to reactivate degraded MEAs after long standby times. The cells were loaded from a temperature of 35 °C. As shown in Fig. 44, the cell voltage increased after reactivation, particularly in those cells that had previously exhibited the worst degradation. The one cell with a decreased cell voltage was operated without methanol due to a test stand malfunction and was irreversibly damaged.

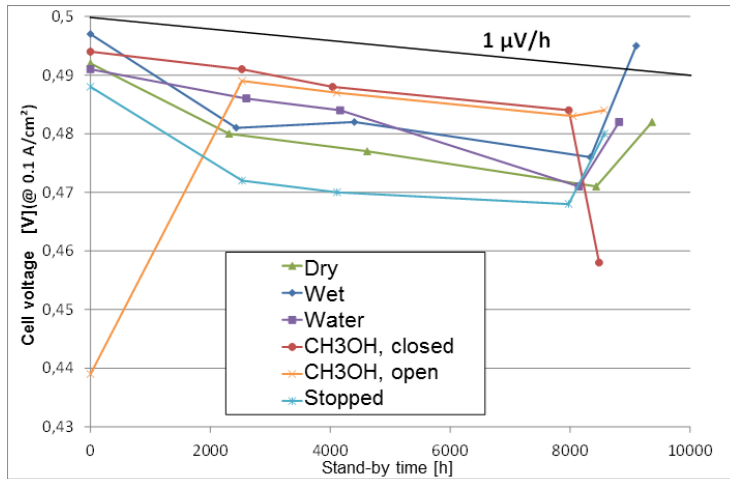


Fig. 44: Degradation for different standby strategies; each final data point was taken after one week of interval operation for reactivation

Based on the standby degradation investigations, there are two options for operation which achieve a tolerable degradation for a lifetime of 10 years: either the MEAs are continuously supplied with methanol solution to protect them from damage when put into standby or heavily degraded MEAs are reactivated in interval operation.

3.4.2.6 Degradation of short stacks

Selected measurements were performed on short stacks to ensure that the measurements on single cells also apply to the degradation behavior of a complete stack in a system. It was found that degradation can be minimized here in the same way as in the single cells when the stacks are continuously supplied with methanol during standby (see Fig. 45).

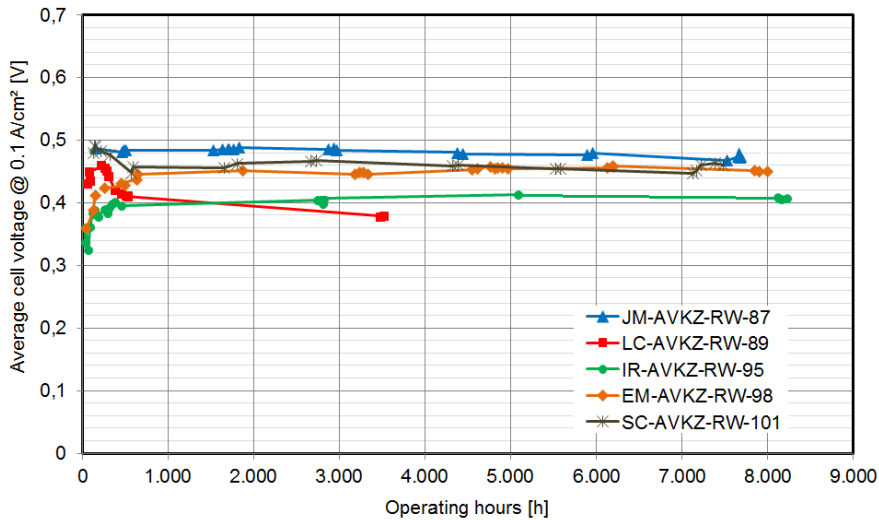


Fig. 45: Degradation of short stacks whose anode is supplied with methanol during standby

3.4.3 Staff members and fields of activity

Name	Tel. (02461-61-) Email	Field of activity
Dr. M. Müller	1859 mar.mueller@fz-juelich.de	Head of Direct Methanol Fuel Cells
N. Commerscheidt	5400 n.commerscheidt@fz-juelich.de	MEA development
Dr. A. Glösen	5171 a.gloesen@fz-juelich.de	MEA development
Fr. D. B. Günther	2378 d.guenther@fz-juelich.de	MEA fabrication techniques, quality management
M. Hehemann	5431 m.hehemann@fz-juelich.de	Stack and system development
Fr. N. Kimiaie	6484 n.kimiaie@fz-juelich.de	Head of Stack and System Development
Fr. R. Lambertz	5109 r.lambertz@fz-juelich.de	Stack and system development
A. Schulze Lohoff	1947 a.schulze.lohoff@fz-juelich.de	Stack and system development
R. Wegner	4832 r.wegner@fz-juelich.de	Stack and system development
W. Zwaygardt	2103	Stack and system development

3.4.4 Important publications, doctoral theses and patents

Important publications

Glüsen, A.; Müller, M.; Stolten, D.

Slot-Die Coating: A New Preparation Method for Direct Methanol Fuel Cells Catalyst Layers

Journal of fuel cell science and technology, 10 (4) 2013, pp. 044503 -, DOI: 10.1115/1.4024607

Hürter, S.; Wannek, C.; Müller, M.; Stolten, D.

1-Hexanol Based Catalyst Inks for Catalyst Layer Preparation for a DMFC

Journal of fuel cell science and technology, 10 (6) 2013, pp. 061008-1 - 061008-6, DOI: 10.1115/1.4025519

McIntyre, J.; Kulikovskiy, A.; Müller, M.; Stolten, D.

Large-scale DMFC stack model: The effect of a condensation front on stack performance

International journal of hydrogen energy, 38 (8) 2013, pp. 3373 - 3379, DOI: 10.1016/j.ijhydene.2012.12.028

Stähler, M.; Friedrich, I.

Statistical Investigations of basis weight and thickness distribution of continuously produced fuel cell electrodes

Journal of power sources, 242 2013, pp. 425-437, DOI: 10.1016/j.jpowsour.2013.05.073

Kimiaie, N.; Janßen, H.; Hehemann, M.; Trappmann, C.; Echsler, H.; Müller, M.

Influence of Contamination with Inorganic Impurities on the Durability of a 1 kW DMFC System

Fuel cells, 14 (1) 2014, pp. 64-75, DOI: 10.1002/fuce.201300047

Müller, M.; Kimiaie, N.; Glüsen, A.; Stolten, D.

The Long Way of Achieving a Durability of 20,000 h in a DMFC System

Advances in science and technology, 93 2014, pp. 56-60, DOI: 10.4028/www.scientific.net/AST.93.56

Doctoral theses

Hürter, S.

Einfluss neuer Membranmaterialien auf Herstellung und Betrieb von Direktmethanol-Brennstoffzellen

Schriften des Forschungszentrums Jülich, Reihe Energie & Umwelt, Band 240, ISBN 978-3-95806-013-5, RWTH Aachen 2014

Important patents

Patent applications:

Principal inventor	PT	Description
J. McIntyre	1.2616	Low-temperature fuel cell and method of operating same
A. Kulikovskiy	1.2644	Direct alcohol fuel cell with effective CO ₂

removal and method of operating such a direct alcohol fuel cell

Patents granted:

Principal inventor	PT	Description
H. Janßen	1.2196	Process for operating a direct methanol fuel cell stack
K. Wippermann	1.2318	Method for electrochemical activation of fuel cells
M. Stähler	1.2326	Exhaust gas purification system for a fuel cell or a fuel cell stack

3.5 Polymer Electrolyte Membrane Electrolysis

3.5.1 Objectives and fields of activity

Future energy conversion and storage is expected to be based on hydrogen produced and stored by means of water electrolysis¹. In this scenario, water electrolysis will play a key role in achieving an energy matrix based on renewable albeit intermittent power sources (e.g. wind turbines and photovoltaics). Hydrogen has the advantage that it is suitable for different uses – vehicle operation, chemicals, green production of fertilizers, regeneration of electricity in fuel cells, and bridging possible energy gaps via methanation by coupling it to carbon capture. In addition, the production, storage and distribution of hydrogen are possible both centrally and locally. At the moment, hydrogen provides the only solution for storing several gigawatt hours of energy¹.

At present, only alkaline and polymer electrolyte membrane (PEM) water electrolyzers are commercially available^{1,2}. To cover the future demand for water electrolyzers, the investment and operating costs must be cut dramatically. It is also essential that electrolyzers be developed for operation at high current densities, variable part load and overload, as well as start/stop cycles. These requirements are well met by PEM water electrolyzers coupled to intermittent power sources. In any case, the high costs of components for PEM water electrolysis (based on materials like platinum, iridium and titanium) still represent an obstacle for large-scale commercial application². Although research continues on PEM water electrolysis, the cost obstacle of the expensive materials must either be overcome or these materials must be completely replaced with cheaper variants².

The two groups Electrochemistry Electrolysis and Process Engineering Electrolysis develop industrial-scale electrolyzers with polymer electrolyte membranes (PEMs) in cooperation with leading industrial enterprises in this field. Cutting costs and increasing lifetime and power density are central aims. New types of membranes are being developed for PEM electrolysis to replace the 175 – 200 μm thick, extruded Nafion membranes currently used which do not possess sufficient mechanical or chemical stability for use in the planned industrial systems under pressures exceeding 50 bar. Another priority is to reduce and ideally completely replace the metals from the platinum group – iridium, ruthenium and platinum – which are commonly used today with a loading of up to 6 mg/cm^2 for catalytic reactions. For PEM electrolysis to be economic on a gigawatt scale for the storage of large quantities of energy produced from renewable power, a 90 % reduction is needed in the quantity of platinum group metals used combined with an increase in the overload capacity of membrane electrode assemblies to more than 6 W/cm^2 as well as a long-term stability of 40,000 hours. Another work package develops new cost-effective materials and coating techniques for metallic separator plates and current collectors with the aim of cutting the costs associated with these components, which presently account for 48 % of stack costs.

¹ J. Mergel, M. Carmo and D. Fritz. Transition to Renewable Energy: Status on Technologies for Hydrogen Production by Water Electrolysis, D. Stolten, V. Scherer, Editors, p. 423-450, Wiley-VCH, Weinheim (2013).

² M. Carmo, D. Fritz, J. Mergel and D. Stolten, International Journal of Hydrogen Energy, 38, 4901-4934 (2013).

3.5.2 Important results

3.5.2.1 Catalyst screening for PEM water electrolysis

Carbon-supported platinum Pt/C catalysts have long been used as the active material for the hydrogen evolution reaction in PEM water electrolysis. An approach was tested for reducing the platinum loading inside the electrodes by alloying platinum with cheap transition metals M (e.g. M = Ni, Co, Cu and Bi) or transition metal oxides (like SnO₂, TiO₂, WO₂). Ideally, the alloy is synthesized in a core-shell configuration: the core element comprises a cheap transition metal and the shell is the more noble and active element (here Pt). In general, catalysts with a large active surface area are advantageous for electrocatalysis. Multicomponent alloys are particularly promising for increasing the active surface area and thus increasing the electrochemical activity. While platinum in combination with transition metals shows a promising performance for the hydrogen evolution reaction, the long-term stability of the Pt-M electrodes in the acidic PEM environment has not yet been demonstrated. The following process was used for the fabrication and characterization of Pt-M catalysts here: Pt_xM_y alloys (with M = Bi, Co, Cu, Ni, Fe, 20 wt% metal on carbon black) were produced by reactive tempering in H₂ atmosphere. The resulting catalysts were physicochemically characterized using transmission electron microscopy (TEM), X-ray diffractometry (XRD), X-ray photoelectron spectroscopy (XPS) and inductively coupled plasma with mass spectrometry (ICP-MS). The catalysts were also electrochemically analyzed using cyclic voltammetry and linear sweep voltammetry. Polarization curves were recorded using 25 cm² single cells.

The transmission electron microscopy (TEM) analysis in Fig. 46 shows a dramatic increase in the electrochemically active surface areas (ECSA) of 5.3 m² g⁻¹ (before leaching) to 74.5 m² g⁻¹ (after leaching). This can be explained by the dissolution of the alloy in combination with the morphology of the carrier catalysts. The leaching or dissolution of the Pt-M catalyst alloys has already been utilized in PEM fuel cells as an effective method for increasing the surface area of catalysts, thus enhancing the catalyst activity³. This is achieved by preferential dissolution, removal or spinodal decomposition of the bimetallic alloys, where the less noble metal is dissolved while the more noble metal atoms remain as a porous skeleton structure.

³ Peter Strasser et al, Lattice-strain control of the activity in dealloyed core-shell fuel cell catalysts, *Nature Chemistry*, 2, 454–460 (2010) doi:10.1038/nchem.623.

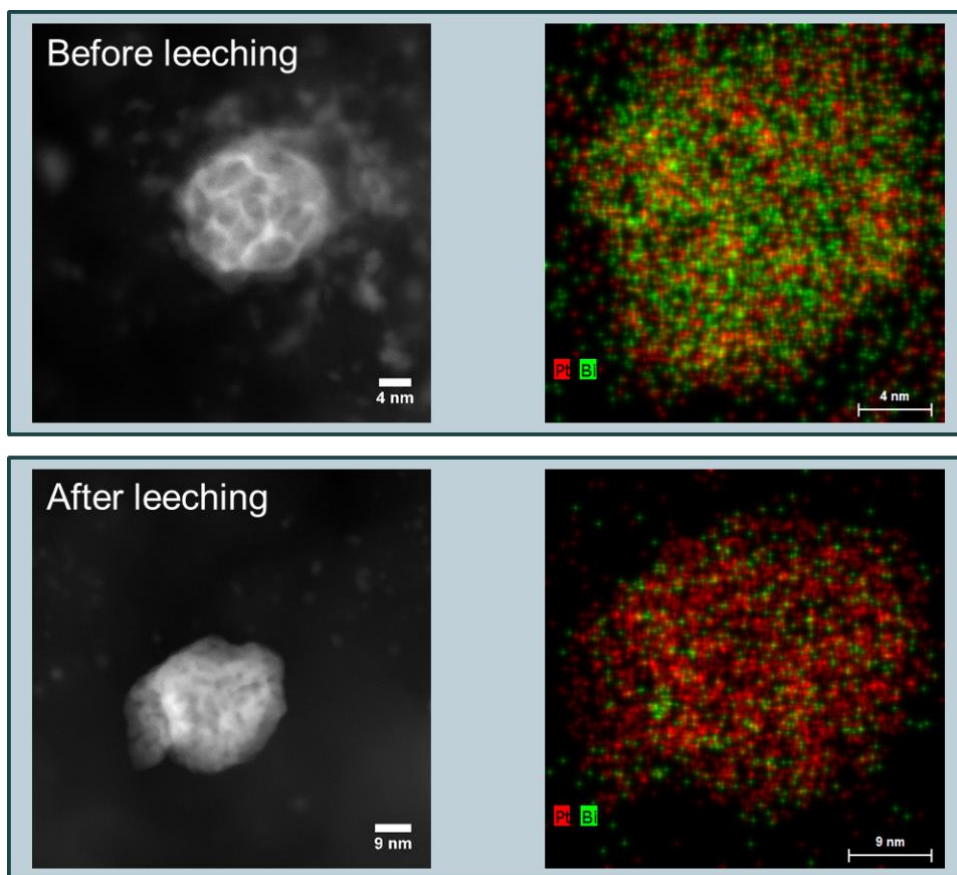


Fig. 46: Transmission electron micrographs of Pt₁Bi₃/C before leaching (top) and after leaching in H₂SO₄ (bottom). Due to the leaching of Bi, there is an increased concentration of Pt nanoparticles and a resulting increase in the electrochemically active surface area (ECSA).

Fig. 47 shows the mass activities of different Pt-M catalysts that were electrochemically characterized using a rotating disc electrode (RDE) in 0.5 M H₂SO₄. Of the 17 synthesized catalysts, PtBi (3:1) and PtNi (1:3) were found to be the most promising catalysts for the hydrogen evolution reaction in acid medium. The data acquired verify the information gained in the TEM investigations. The high mass activities determined by RDE for these two catalyst compositions can be explained by the high electrochemically active surface areas in both cases. Electronic and potential effects can also play an important role in increasing activity for the hydrogen evolution reaction. The alloying of Pt with other metals can decrease the electronic bonding energy of Pt, which strengthens the electrochemical reaction even at low overpotentials.

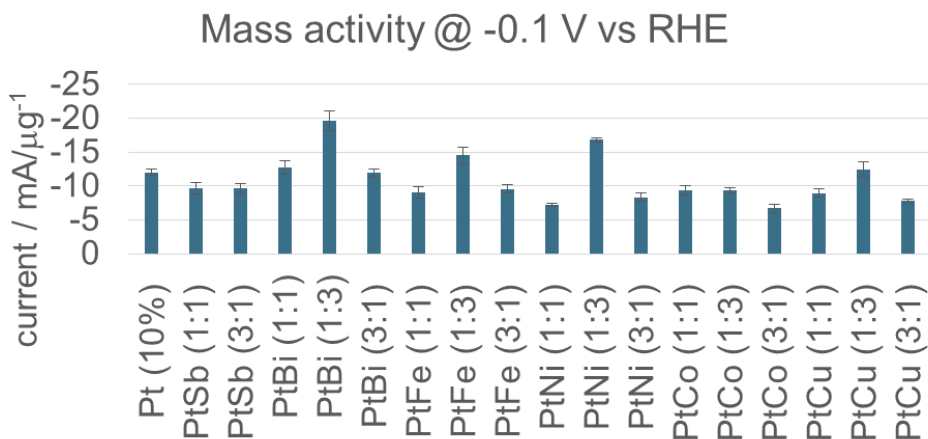


Fig. 47: Mass activities of the synthesized Pt-M catalysts analyzed using the rotating disc electrode (RDE) in 0.5 M H₂SO₄

3.5.2.2 Catalyst coated membranes (CCMs) with reduced Pt loading – Single cell tests

To compare commercially available materials and alternative catalysts for PEM electrolysis, it is important to set a benchmark. In this case, a conventional IrO₂ catalyst was used for the anode, a Pt/C catalyst for the cathode and Nafion 117 as the membrane. These materials were processed to CCMs and characterized electrochemically at 80 °C in single cells. A current density of 2 A/cm² and a cell voltage of 1.9 V were achieved. In producing these CCMs, an Ir loading of 2 – 3 mg_{Ir}/cm² and a Pt loading of 0.8 – 1.5 mg_{Pt}/cm² were standard in the past. Fig. 48 shows single-cell tests with the PtBi (3:1) and PtNi (1:3) catalysts, where the cathode loading was drastically reduced (from 0.8 mg_{Pt}/cm² to 0.025 mg_{Pt}/cm²) without influencing the cell performance. Work is under way on improving the durability of CCMs with reduced Pt loading to ensure that these Pt-M catalysts can be used in continuous operation in PEM electrolyzers.

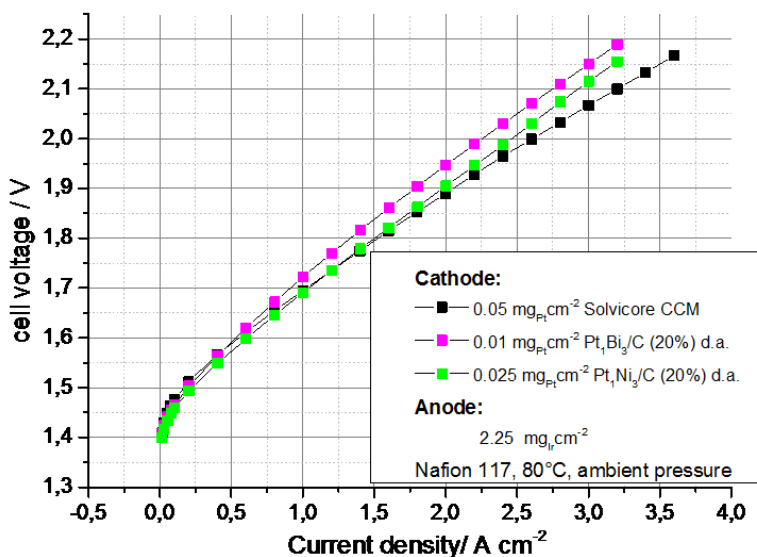


Fig. 48: Impact of Pt-M cathode loading on the performance of the PEM water electrolysis. The cell was operated at 80 °C and atmospheric pressure.

3.5.2.3 MEA fabrication technology

To evaluate the homogeneity of large-scale electrodes fabricated at IEK-3 by means of roll-to-roll processing, previous projects analyzed the thickness distribution of carbon substrates for the fabrication of membrane electrode assemblies (MEAs). A method was established for this, which determines the thickness distribution and the distribution of weight per unit area of square meter substrate samples. The investigations showed that commercial carbon substrates used for the gas diffusion electrode (GDE) route had thickness variations of up to 10 %. These variations are transferred during blade coating as variations in the catalyst loading of the resulting electrodes and are therefore unsuitable for production. Other substrate materials are needed for the fabrication process.

As carbon substrates cannot be used to fabricate anodes for polymer electrolyte water electrolysis because the carbon would oxidize during operation and decompose, work began on adapting the fabrication process for electrodes using the roll-to-roll machine from the GDE route to the electrode transfer route. Fig. 49 shows the differences between the GDE route and the electrode transfer route where the electrode must be easy to remove from the transfer film after drying. The challenges in applying the electrode transfer route in a roll-to-roll process is that the electrode must adhere strongly enough to the substrate so that it does not detach itself as it bends over the rolls. At the same time, the adhesion cannot be too strong because it must be possible to remove the electrode from the film after the transfer process. To produce homogeneous electrodes using blade coating combined with the transfer method, films must have a low thickness variation and a low surface energy.

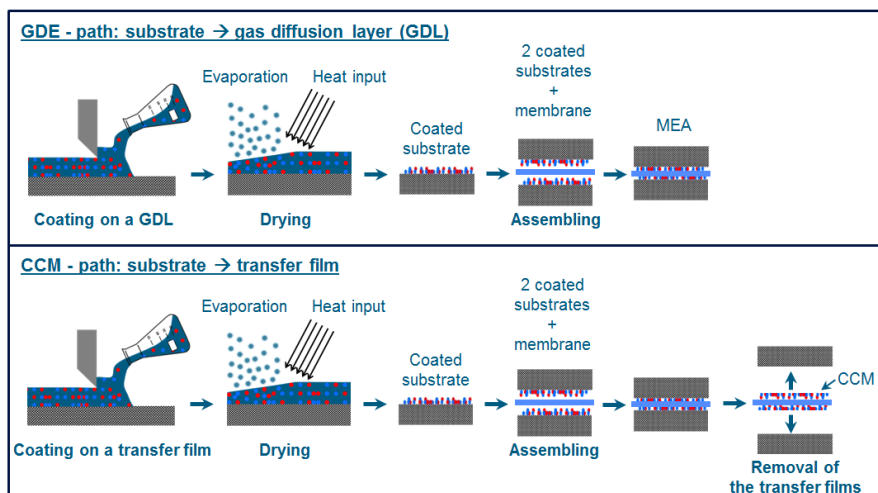


Fig. 49: Comparison of GDE route and electrode transfer route where the electrode is first coated on a substrate and dried before being transferred to the membrane. The transfer film must be removable. The catalyst coated membrane (CCM) produced in this manner can then be assembled with diffusion layers in order to produce a MEA similar to the GDE route.

First test series were conducted on commercial films. The thickness distribution of square meter specimens was analyzed. As the difference method was used to determine the coating distribution, films with a low variation in weight per unit area were essential. For this reason, the distribution of weight per unit area was also determined for the investigated films. The following table summarizes the results.

wpu: weight per unit area	wpu_{substrate}	stdev(wpu_{substr.})	d	stdev(d)
d: substrate thickness	mg/cm²	mg/cm²	μm	μm
commercial GDL	11,70	0,24	187	5
Kapton	17,90	0,08	125	2
Flexiso PET FI 1300	17,70	0,18	123	3
PTFE 70	14,63	0,12	74	2
PTFE 120	24,60	0,30	115	2
PTFE 200	43,71	0,32	205	3
Al 100 μm	27,10	0,24	102	1

Table 10: Mean values and standard deviation of weight per unit area (FG) and thickness (d) of the substrates. For each material, a substrate 2 m long and 50 cm wide was analyzed.

The measured values in Table 10 show that the Kapton, PTFE 70, and PTFE 120 films had a much smaller thickness distribution than the carbon substrate conventionally used. Only the aluminum film had even smaller thickness variations. Fig. 50 depicts the differences in the centered thickness frequency distributions of one of the films compared to the carbon substrate.

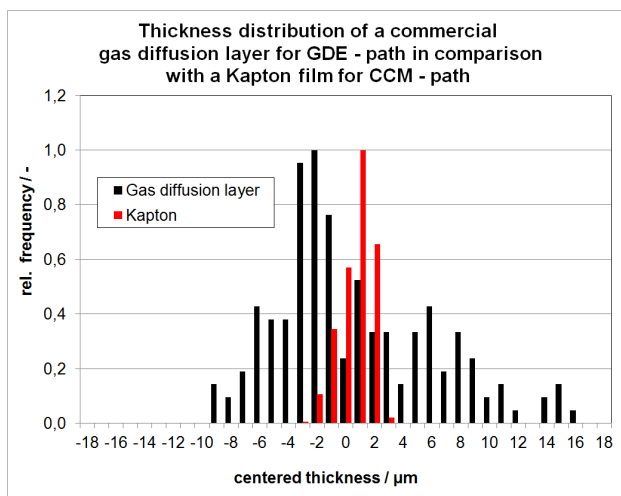


Fig. 50: Centered frequency distribution of the measured thicknesses of a Kapton film and the carbon substrate conventionally used.

The PTFE films have a small thickness variation and a low surface energy and thus fulfill the requirements in contrast to the aluminum films. Laboratory experiments show that the electrodes can be easily transferred from small coated films to the membrane. However, the adhesive forces are still too weak to transfer the laboratory process in full to the roll-to-roll machine. The large-scale homogeneous coating of the catalyst dispersion onto the PTFE film necessitates that the static and dynamic surface tension in the dispersion be adjusted to the surface energy of the film.

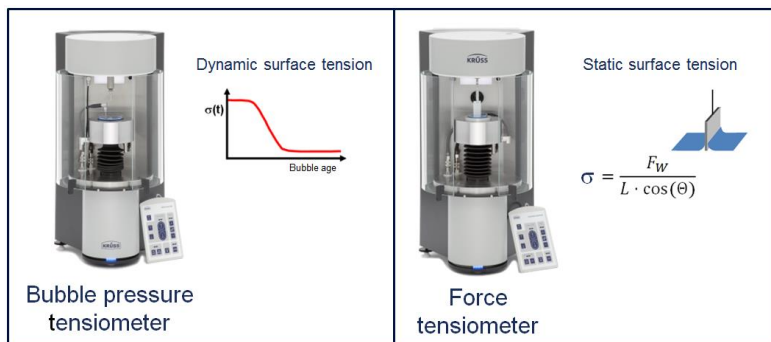


Fig. 51: Left: Bubble pressure tensiometer: determination of dynamic surface tension; Right: Force tensiometer: determination of static surface tension

For this purpose, the dispersion laboratory was equipped with new measurement technology to help adjust the surface tension to the substrate used. As part of ongoing work for a doctoral thesis, correlations are being investigated between the surface properties of the film,

the surface tension of the dispersion and the adhesion properties of the dispersion and/or the electrode on the substrate.

3.5.2.4 Stack and system development

Before PEM electrolysis can be realistically and sustainably launched on the mass markets for the storage of renewable energy from 2020 onwards, further technological progress is essential to improve insufficient stability and to cut the high costs associated with the technology as it currently stands.

One field of activity in the area of stack development is the development of low-cost materials and production processes. Table 11 shows the development goals for separator plates. The separator plates in PEM electrolyzers, which are currently produced from coated titanium, account for up to 25 % of the total costs of the system. An initial approach will therefore first optimize the performance and then replace expensive materials like titanium with cheap, corrosion-resistant materials. The use of metallic bipolar plates with a suitable coating should considerably cut the costs of flow fields and separator plates and thus drastically reduce their share in the total costs.

Lifetime 40,000 h
Pressure-resistant design for pressures > 50 bar
Integrated cooling system with an internal cooling flow field, if required
Optimal distribution structure for media
Fatigue strength for dynamic pressure change/temperature change
Replacement of titanium with cheap materials
Optimal surface pressure for contacting/minimization of internal resistance
High current carrying capacity
Integration of supporting structures for sealing systems
Integration into the complete system incl. end plates and tensioning technology

Table 11: Development goals separator plates

Using a corrosion measuring cell designed at IEK-3, the suitability of substrate and coating materials is evaluated for the fabrication of separator plates. Material characterization and degradation tests (lifetime tests) can be performed with this cell including electrochemical measuring techniques. The materials tested are subjected to a fixed potential in an electrolyte solution and changes in the surface condition of the material specimens are analyzed at a constant potential over time (cf. Fig. 52).

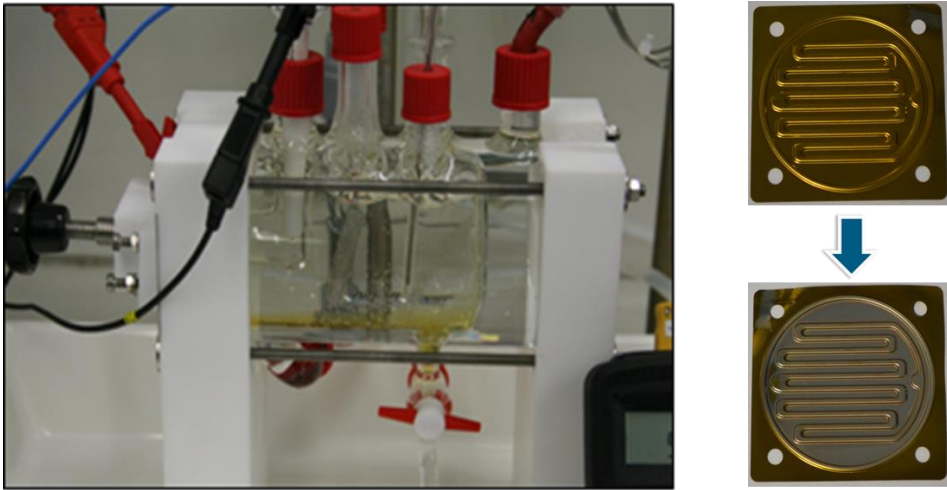


Fig. 52: Left: Corrosion measuring cell. Right: Before/after comparison of a stainless steel sample with a TiN coating in 0.005 M H₂SO₄ solution at 50 °C and a potential of 2.00 V (vs RHE).

To increase the performance and efficiency of PEM electrolysis, the design of the separator plates must be refined. Separator plate development focuses on achieving a reliable, uniform flow through all of the cells in the stack. The flow field design must fulfill this requirement under the boundary conditions of a low electrical resistance and a moderate pressure drop during through-flow. CFD analyses (cf. Fig. 53) are used to examine and optimize various flow aspects in the electrolyzers. This optimization aims to minimize the pressure drop and achieve a uniform velocity distribution across all channels to ensure that the catalyst layers are uniformly supplied with water and that cooling is adequate. Minimizing the flow loss simultaneously decreases the energy demand of the peripheral components (pumps etc.) in the system as a whole.

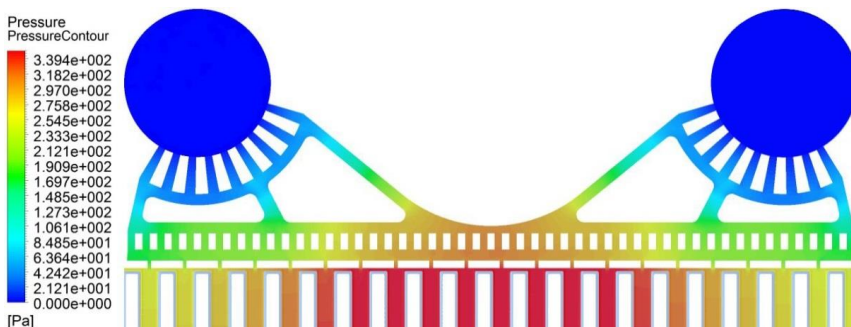


Fig. 53: CFD pressure distribution analysis for the outlet manifold in the frame.

The results of the CFD analyses were incorporated into the design of a sealing frame for a flow field. The channels connecting the manifold with the flow field were altered to achieve a uniformly distributed flow through the cells. Fig. 54 shows the design of two half cells in the

electrolysis stack. This design was developed to account for the formation of gas and a reliable discharge of the gas across the entire cell area. As the reaction water flows through a cell, the gas phase fraction increases in proportion to the liquid phase and so too does the flow velocity. To avoid potential problems associated with gas discharge at the outlet area, this design includes an inlet opening for reaction water supply and two outlet openings for reaction gas accumulation.

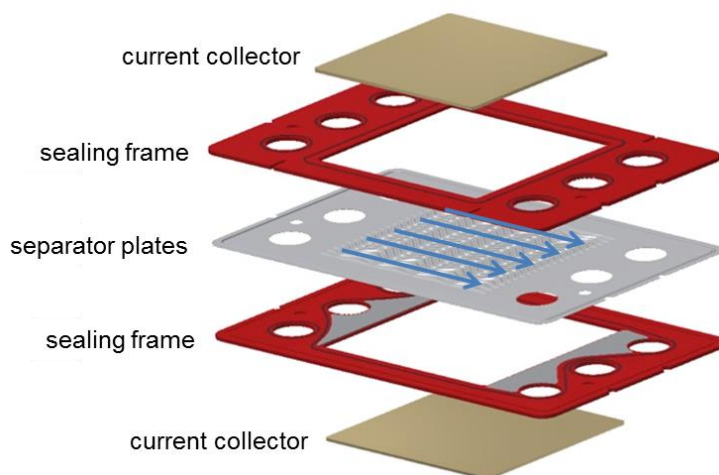


Fig. 54: Exploded view of the assembly of separator plates, sealing frame and current collector.

In PEM electrolyzers, the current collectors fulfill several functions: they stabilize the sensitive membrane and protect it from rupturing, they supply the electrons and they transport the liquid reactants and product gases while withstanding the highly corrosive environment and retaining their structure even under high pressures. Usually, porous titanium sintered plates are used as anodic current collectors. Resistance measurements, porosity analyses, and gas and water permeability measurements are performed on different materials to investigate uniform flow and media distribution on a cell level, particularly in a high current range. The physical parameters of the current collector were recorded and computer simulations were performed to learn more about mass transport. Fig. 55 shows the results of one simulation. It examined water distribution in a porous current collector under the influence of an injected waterfront. The original pore distribution was modified to create a pore diameter gradient from the separator plate (below) to the catalyst layer (top). The result from Fig. 55 is from a parametric study on pore size distribution aiming to achieve a pore size gradient at right angles, which means that the incoming water is uniformly supplied to the catalysts.

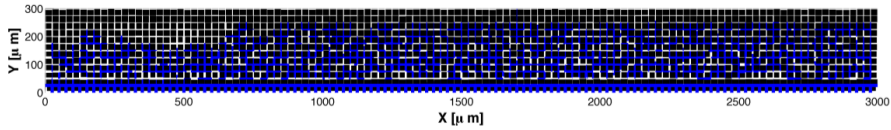


Fig. 55: Two-dimensional simulation of water penetration in a current collector made of sintered porous titanium with the aim of achieving an adjusted pore size distribution that will lead to a uniform supply of water to the catalyst layer.

All results were incorporated into the development of a stack design with suitable separator plates and current collectors for PEM electrolysis. At IEK-3, single cells and short stacks including the necessary end plates were designed and assembled for active surface areas of different dimensions. A seven-cell short stack (see Fig. 56) was assembled in an 100 cm² cell design. (Structure: bipolar plates, MEA, end plates). The stack design allows operation at equal pressure and differential pressure up to 50 bar. The stack was tested in constant and dynamic operation. Polarization curves were recorded to characterize the stack. An output of 5.0 kW was achieved and the voltage was 1.9 V at 2 A/cm².

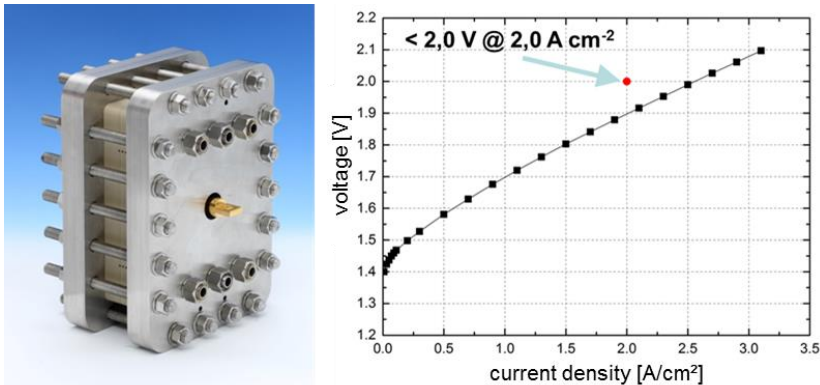


Fig. 56: Left: PEM electrolysis short stack in 100 cm² design. Right: Polarization curve.

To summarize, the simulations and designs were used to develop a reliably functioning cell with an active surface area of 100 cm², the operation of which was also verified in stacks. The pressure drop caused by the water flow agrees with the simulation results. The materials also fulfilled the corrosion stability requirements. Based on these results, the stack design will now be upscaled to an active cell area of 300 cm².

System development will examine the interaction between the necessary system components and develop optimized control strategies required for operating a PEM electrolysis stack. An example of these studies is outlined in section 4.4.

3.5.3 Mitarbeiter und Tätigkeitsfelder

Name	Tel. (02461-61-) Email	Field of activity
Dr. W. Lücke	9073 w.lueke@fz-juelich.de	Head of Electrochemistry Electrolysis
Dr. M. Müller	1859 mar.mueller@fz-juelich.de	Head of Process Engineering Electrolysis
Dr. M. Carmo	5590 m.carmo@fz-juelich.de	Head of MEA Development
Dr. M. Stähler	2775 m.staehler@fz-juelich.de	Head of MEA Manufacturing Technology
N. Kimiaie	6484 n.kimiaie@fz-juelich.de	Head of Stack and System Development
D. Günther	2378 d.guenther@fz-juelich.de	Documentation and characterization of ion exchangers
M. Hehemann	5431 m.hehemann@fz-juelich.de	Safety engineering of test stands
T. Höfner	9804 t.hoefner@fz-juelich.de	Development of membrane electrode assemblies for alkaline PEM electrolysis
M. Höh	9842 m.hoeh@fz-juelich.de	Simulation and development of porous layers
M. Langemann	9759 m.langemann@fz-juelich.de	Development and evaluation of suitable substrates and coatings for metallic bipolar plates in PEM electrolyzers
P. Paciok	9801 p.paciok@fz-juelich.de	Reduction and substitution of platinum group metals in hydrogen electrodes for PEM electrolysis
C. Rakousky	9803 c.rakousky@fz-juelich.de	Development of cheap and sustainable catalyst materials for oxygen electrodes in PEM electrolysis
M. Schalenbach	9802 m.schalenbach@fz-juelich.de	Development and evaluation of membranes with higher conductivity and mechanical and chemical stability for PEM electrolysis
F. Scheepers	2177 f.scheepers@fz-juelich.de	Analysis of the drying process of catalyst dispersions
A. Schulz	8965 a.schulz@fz-juelich.de	Analysis of the transfer processes for catalyst layers
G. Tjarks	4013	Simulation and development of PEM electrolysis systems

R. Wegner	g.tjarks@fz-juelich.de 4832 r.wegner@fz-juelich.de	Mechanical assembly of stacks and systems
-----------	--	---

3.5.4 Important publications and patents

Important publications

Carmo, M.; Fritz, D.; Mergel, J.; Stolten, D.

A comprehensive review on PEM water electrolysis

International journal of hydrogen energy, 38 (12) 2013, pp. 4901-4934, DOI: 10.1016/j.ijhydene.2013.01.151

Schalenbach, M.; Fritz, D.; Carmo, M.; Mergel, J.; Stolten, D.

Pressurized PEM water electrolysis: Efficiency and gas cross14921-14933

International journal of hydrogen energy, 38 (35) 2013, pp. 14921-14933, DOI: 10.1016/j.ijhydene.2013.09.013

Important patents

Patent applications:

Principal inventor	PT	Description
M. Schalenbach	1.2639	Electrochemical electrolytic cell and method for operating the same
M. Schalenbach	1.2642	Electrochemical electrolytic cell for the electrolysis of water and method for operating the same
M. Schalenbach	1.2661	Electrochemical separation of chemical elements from an electrolyte and apparatus for carrying out the process
M. Stähler	1.2678	Electrochemical cell and method for producing same
M. Schalenbach	1.2681	Fuel cell and method for operating the same
M. Schalenbach	1.2686	Method and apparatus for the separation of chemical elements (carrier fluid)
M. Schalenbach	1.2687	Method and apparatus for the separation of chemical elements

3.6 Process and Systems Analysis

3.6.1 Objectives and fields of activity

Process and systems analyses are performed on energy technologies as part of planning and consulting activities. Data searches and system simulations are used to determine energy and mass balances, performance data, emissions and costs to quantitatively compare energy systems. The priorities in the period under review were as follows:

- Fuel consumption of passenger cars with electric and conventional drive concepts

- Analysis of options for utilizing CO₂ in the chemical industry

- Design and cost of a hydrogen pipeline network to supply the road transport sector

- Further development of an energy strategy to meet the German federal government's targets for reducing greenhouse gas emissions

The last topic is dealt with in a separate section (4.5).

Wichtige Arbeitsergebnisse

3.6.1.1 Potential for reducing fuel consumption in passenger cars with different drives

With the aim of reducing greenhouse gas emissions and locally relevant pollutants, development efforts worldwide focus on drives with increasing electrification for passenger cars. Fuel cell electric vehicles (FCVs) facilitate local zero-emission driving while generally maintaining the usual performance data. Battery electric vehicles (BEVs), which also have zero emissions locally but a considerably reduced range, exhibit the lowest energy demand. Such vehicles are charged using mains power, which results in different regional environmental impacts. Drive systems with an internal combustion engine (ICE) are being further optimized. In hybrid electric vehicles (HEVs), electric drive components optimize the mode of operation of the combustion engine and reduce consumption by recycling braking energy.

To assess drive systems, the provision of fuel and/or electricity is analyzed (well-to-tank analysis, WTT) as is the energy utilization in the vehicle itself (tank-to-wheel analysis, TTW). The results presented here are from TTW analyses and were determined in a simulation environment developed at IEK-3⁴. The following car concepts were investigated:

- Internal combustion engine vehicle (ICV)

- Parallel hybrid passenger car with internal combustion engine and battery (parallel hybrid, PAH)

- Battery electric vehicle (BEV)

- Electric passenger car with fuel cells and battery (fuel cell vehicle, FCV)

⁴ Grube, T.: Potential der Stromnutzung in Pkw-Antrieben zur Reduzierung des Kraftstoffbedarfs. Technische Universität Berlin, Faculty V – Mechanical Engineering and Transport Systems, doctoral thesis. 2014

The analysis conducted here focused specifically on uniform specifications of vehicle parameters that are relevant for the power demand at the wheel as well as for other mechanical, thermal and electrical load profiles. The drive train was automatically dimensioned using uniform specifications for the targeted performance parameters of acceleration, top speed and range. To image the load-dependent operating behavior of the drive components, physical models, operating characteristics and in the case of batteries equivalent circuit diagrams were used. The analysis was performed for the scenarios “standard” and “future” in order to account for foreseeable development progress. Furthermore, the investigation included analyses for passenger cars classified as A segment (mini cars) and C segment (medium cars).

To illustrate the relevance of load profiles, Fig. 57 shows the mechanical energy demand for C-segment passenger cars in the “future” scenario. Positive values indicate the energy required to drive the vehicle forward and negative values indicate braking energy and thus the maximal energy available for regenerative braking.

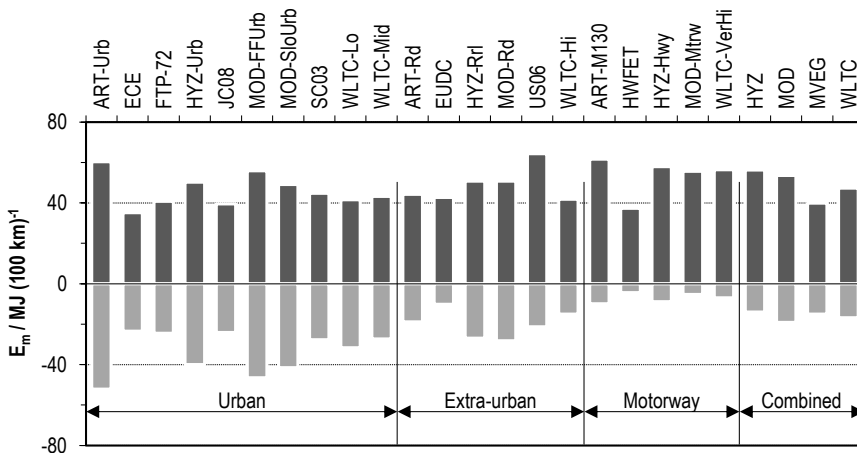


Fig. 57: Drive cycle-specific mechanical energy (E_m) at the wheels of a passenger car with a mass of 1251 kg, a cross-sectional area of 2.1 m² and an air drag coefficient of 0.32. ART.: ARTEMIS; FreeUrb: Free flow urban; Highw: Highway; HYZ: HYZEM; MOD: MODEM; Mtrway130: Motorway (maximal 130 km/h); Rur: Rural; SlowUrb: Slow urban; Urb: Urban⁴.

The time-dependent thermal load profiles result from the heat demand, which is determined using a thermal cabin model (see IEK-3 Report 2013⁵), while electrical load profiles concern the use of the vehicle’s electric devices. Based on the simulation runs, the range of fuel consumption as a function of the selected scenario and car segment can be given for all driving cycles and load profiles used here. Fig. 58 shows the value ranges for the “future” scenario and the C segment as an example.

It is evident that the zero-emission BEVs and FCVs have the greatest reduction potential, followed by parallel hybrids with diesel engines. The simulation results for the EU reference driving cycle MVEG and corresponding values from the literature are also shown. The comparison shows corroborative trends in the ranking of the drive systems. Individual values

⁵ Emonts, B. (Ed.) *IEK-3 Report 2013. Durable Electrochemical Process Engineering* Forschungszentrum Jülich GmbH, Central Library, Publishing House: Jülich, 2013. ISBN 978-3-89336-868-6

deviate considerably from each other due to different vehicle parameters, component efficiencies and operating strategies. There is insufficient information in the literature for a detailed analysis of the reasons for these deviations.

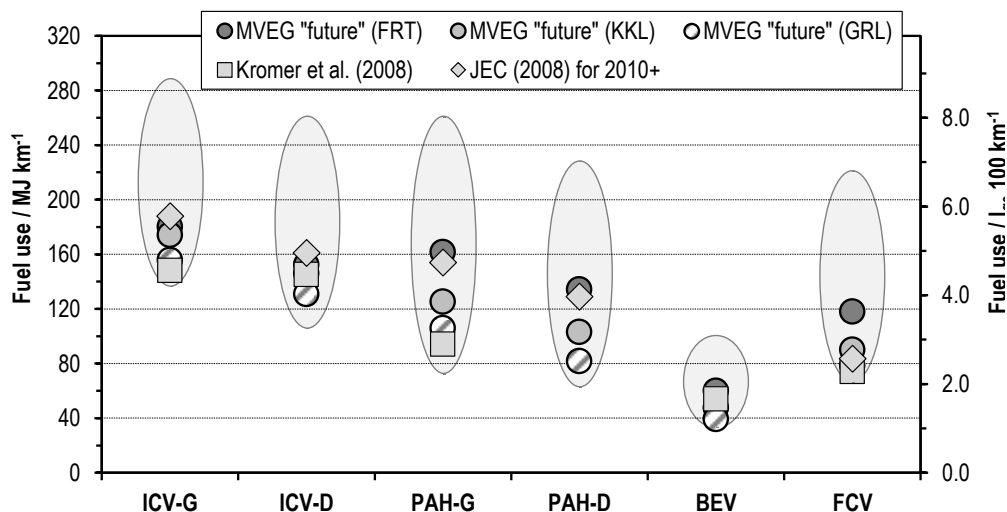


Fig. 58: Results of simulation-based fuel consumption analyses for various passenger car concepts⁴. Value ranges from consumption calculations⁴ are shown as ellipses for C-segment passenger cars in the “future” scenario. Individual values for the MVEG driving cycles are given for the APU load profiles “no air conditioning” (KKL), “frost” (FRT) and “only base load” (GRL); for definitions see⁴; lge: liters of gasoline equivalent.

3.6.1.2 Evaluation of carbon dioxide as a raw material in the chemical industry

The use of carbon dioxide as a raw material in the chemical industry is an alternative to geological storage, which is widely contested in Germany and legally limited. Scientific publications on CO₂ utilization reactions are generally concerned only with the viability of synthesis without considering the potential for reducing CO₂ or economic feasibility compared to similar conventional fabrication routes. Against this background, an evaluation procedure comprising several stages was used to identify, analyze and evaluate CO₂ utilization reactions in the literature. The focus was the chemical conversion of CO₂ into organic products as replacements for conventionally produced compounds. In the first step, 23 CO₂-based syntheses of bulk chemicals (production rates within the EU of more than 60 million t/a) and 100 CO₂-based syntheses of fine chemicals (production rates within the EU of approx. 1–2 million t/a) were taken from the literature and evaluated using specially defined criteria. The evaluation criteria accounted for the quantitative potential for reducing CO₂ as well as the possible economic interest in these reactions. As some selection criteria provided robust results specifically for bulk chemicals or fine chemicals, the evaluation criteria outlined in Table 12 were introduced for bulk and fine chemicals.

⁴ Ibid.

Bulk chemicals	Fine chemicals
<ul style="list-style-type: none"> ▪ Specific mass of CO₂ used as raw material ▪ CO₂ reduction potential ▪ Relative added value ▪ Independence from fossil raw materials 	<ul style="list-style-type: none"> ▪ Specific mass of CO₂ used as raw material ▪ Production volumes of the substance groups ▪ Relative added value ▪ Scientific relevance ▪ Technical availability

Table 12: Evaluation criteria for selecting the bulk and fine chemicals for analysis

Of the 23 bulk chemicals analyzed, formic acid, oxalic acid and formaldehyde met the evaluation criteria best, directly followed by methanol, urea and dimethyl ether. Of the 100 fine chemicals analyzed, methyl carbamate, 3-oxopentan dicarbonic acid, 2-imidazolidinone and ethyl carbamate came out on top in the preliminary selection.

In addition to evaluating the reactions, this first step also determined that a CO₂ avoidance potential of 1.3% of greenhouse gas (GHG) emissions within the European Union (EU) can be achieved if conventional processes are fully replaced by CO₂-based processes in the EU. The CO₂ avoidance potential of the 100 fine chemicals analyzed is much lower than 0.029% of the GHG emissions in the EU and is thus considerably lower than the avoidance potential of bulk chemicals. Therefore, they make little or no contribution to reducing CO₂ emissions. However, the advantage of the analyzed fine chemicals over the bulk chemicals is their much higher achievable added value.

In the second step, the potential CO₂-based process was directly compared with the conventional process for the bulk chemicals that fulfilled the selection criteria best – formic acid, oxalic acid, formaldehyde, methanol, urea and dimethyl ether. Using literature data and process designs and simulations in Aspen Plus, it was shown that the hydrogenation of CO₂ to methanol with 1.43 kg_{CO₂}/kg_{MeOH} and to dimethyl ether with 2.17 kg_{CO₂}/kg_{DME} achieved the greatest reduction in CO₂ compared to relevant conventional processes. A prerequisite for this, however, was that the hydrogen required for the reactions was produced via electrolysis with power from renewables. If the CO₂-based production processes for methanol and dimethyl ether were to fully replace conventional processes in the EU, they would help to achieve a 0.059% reduction in EU greenhouse gas emissions. Fig. 59 shows the process designed for the analyses including some simulation results from Aspen Plus for the hydrogenation of CO₂ to dimethyl ether.

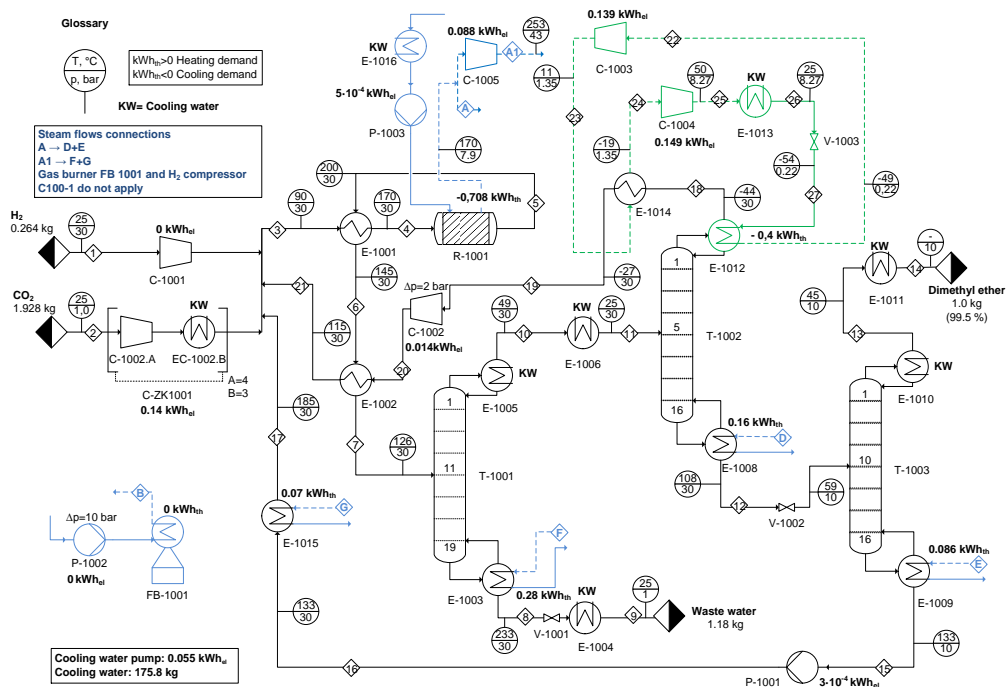


Fig. 59: Process design with simulation results from Aspen Plus for CO₂-based dimethyl ether synthesis at a reaction pressure of 50 bar, a reaction temperature of 200 °C and H₂:CO₂ molar ratios of 3 at the reactor inlet

In the third and final step of the evaluation, the production costs of the CO₂-based processes were analyzed. It was found that the costs of the CO₂-based synthesis of methanol and dimethyl ether were 3.3 and 2.3 times higher, respectively, than the relevant conventional processes. This resulted in CO₂ avoidance costs of € 540/t_{CO₂} for the CO₂-based synthesis of methanol and € 440/t_{CO₂} for dimethyl ether, which are 90 and 73 times higher, respectively, than the geological storage of CO₂ in aquifers. If the costs of the required hydrogen decreased from the assumed € 5.22/kg_{H₂} to € 1.22/kg_{H₂} or € 1.76/kg_{H₂}, respectively, then no avoidance costs would be incurred for the utilization of CO₂ as a raw material in the synthesis of methanol and dimethyl ether. Therefore, in addition to higher CO₂ allowance prices, the price trend of hydrogen produced via electrolysis would determine the future economic implementation of the two CO₂-based processes.

For the future chemical utilization of carbon dioxide as a CO₂ reduction option, the fabrication of bulk chemicals was identified as the most suitable option due to the high production volumes involved. However, for effective and economic implementation, the reactions must be performed with highly reactive Co reactants produced as cost-effectively as possible with simultaneously low CO₂ emissions. Although the syntheses of fine chemicals will not help to reduce CO₂ emissions, they do have great potential for economic implementation.

3.6.2 Staff members and fields of activity

Name	Tel. (02461 61-) Email	Field of activity
T. Grube	5398 th.grube@fz-juelich.de	Vehicle simulation, analysis of the provision of energy sources and process chains
B. Kumar	9743 b.kumar@fz-juelich.de	Alkaline electrolyzers for wind energy storage: integration and operation
S. Luhr	6689 s.luhr@fz-juelich.de	Membrane modules for carbon capture using polymer membranes
A. Otto	4113 a.otto@fz-juelich.de	CO ₂ utilization in the chemical industry, GHG reduction in industry, power to chemicals
M. Robinius	3077 m.robinius@fz-juelich.de	Alternative power market design, modeling of energy systems
S. Schiebahn	8731 s.schiebahn@fz-juelich.de	Power-to-gas concepts, reduction strategies for greenhouse gases
A. Schwane	1948 a.schwane@fz-juelich.de	Strategies for implementing a H ₂ supply infrastructure
Fr. V. Tietze	4113 v.tietze@fz-juelich.de	Techno-economic modeling of H ₂ supply infrastructure
Fr. L. Zhao	4064 l.zhao@fz-juelich.de	Membrane-based gas separation processes in energy technology

3.6.3 Important publications, doctoral theses and patents

Important publications

Schiebahn, S.; Grube, T.; Robinius, V.; Tietze, V.; Kumar, B.; Stolten, D.

Power to gas: Technological overview, systems analysis and economic assessment for a case study in Germany

International Journal of Hydrogen Energy 40 (2015), pp. 4285-4294

Tietze, V.; Luhr, S.

Near-Surface Bulk Storage of Hydrogen. In: Transition to Renewable Energy Systems

Wiley-VCH Verlag GmbH & Co. KGaA, 2013, pp. 659-690. ISBN 978-3-527-33239-7

Robinius, M.; Stolten, D.

Power-to-Gas: Quantifizierung lokaler Stromüberschüsse in Deutschland anhand unterschiedlicher Windenergie-Ausbaustufen

Proceedings: 9. Internationale Energiewirtschaftstagung 2015, Wien, 2015

Grube, T.; Höhle, B.

Costs of Making Hydrogen Available in Supply Systems Based on Renewables

Töpler, J.; Lehmann, J. (Hrg.), Wasserstoff und Brennstoffzelle, Springer Verlag Berlin Heidelberg, 2013, pp. 225-239

Topham, S., Bazzanella, A.; Schiebahn, S.; Luhr, S.; Zhao, L.; Otto, A., Stolten, D.

Carbon Dioxide. Ullmann's Encyclopedia of Industrial Chemistry

Wiley-VCH Verlag GmbH & Co. KGaA, 2014. ISBN 978-3-527-3067-32

Zhao, L.; Franz, J.; Schiebahn, S.; Riensche, E.; Scherer, V.; Stolten, D.

Investigating the influence of sweep gas on CO₂/N₂ membranes for post-combustion capture

International journal of greenhouse gas control, 13 2013, pp. 180-190, DOI: 10.1016/j.ijggc.2012.12.008

Doctoral theses

Grube, T.

Potential of Electricity Management Strategies for Reducing the Specific Energy Use of Passenger Cars

TU Berlin, 2014, Band 216, 255 pp, Dissertation / PhD Thesis

ISBN 978-89336-961-4

Schiebahn, S.

Efficiency-optimized CO₂ separation in IGCC power plants by water-gas shift membrane reactors

Schriften des Forschungszentrums Jülich, Reihe Energie & Umwelt, Band 213,

ISBN 978-3-89336-958-4, RWTH Aachen 2014

Important patents

Patent applications:

Principal inventor	PT	Description
S. Schiebahn	1.2584	Method for operating two sub-processes with different steam requirements in an overall process
S. Schiebahn	1.2585	Method for operating a subprocess in an overall process that requires steam

Patents granted:

Principal inventor	PT	Description
J. Nazarko	1.2341	Device and method for reducing CO ₂ emissions from the waste gases of combustion plants
R. Menzer	1.2381	IGCC power plant having flue gas recirculation and flushing gas
E. Riensche	1.2405	IGCC power plant having flue gas recirculation and flushing gas
J. Nazarko	1.2431	Apparatus and method for removing carbon dioxide (CO ₂) from the flue gas of a furnace after the energy conversion
J. Nazarko	1.2437	Power station and method for operating the same

3.7 Physicochemical and electrochemical principles

3.7.1 Objectives and fields of activity

In the physicochemical fuel cell laboratory, the basic structure-activity relationships of complex processes in electrochemical energy converters are investigated to identify ways of improving them. The focus is on the basic physicochemical properties and the electrochemical behavior of components and model cells. Various in situ and ex situ methods are used:

- Imaging analysis techniques (SEM/EDX, CLSM, optical microscopy), catalyst characterization using spatially resolved MS
- Spectroscopic methods (Raman, IR)
- Thermochemical and mechanical analysis techniques (TGA, DSC, elasticity/expansion measurements, BET, porosimetry, contact angle measurements)
- Electrochemical analysis techniques (EIS, CV, conductivity)

Existing methods are adapted and new methods are established as required for the scientific objectives. In addition to examining mechanical and thermomechanical conditions for application in fuel cells, another aim is to explain the fundamental principles and microscopic mechanisms of the redox kinetics of the electrodes and ion transport in the electrolyte membranes.

3.7.2 Important results

3.7.2.1 Adsorption isotherms of Fumapem AM-55®/H₃PO₄ and Raman spectroscopic studies

Measurements and model for adsorption isotherms

Using combined pH and Karl-Fischer titration, adsorption isotherms were determined for the PBI derivative Fumapem AM-55® for the uptake of phosphoric acid. The measured adsorption isotherms for the system Fumapem AM-55®/H₃PO₄ are shown in Fig. 60 together with adsorption isotherms taken from the literature for the systems *m*-PBI/H₃PO₄, AB-PBI/H₃PO₄, *m*-PBI/H₂SO₄ and *m*-PBI/H₃PO₄. All adsorption isotherms, literature data and in-house data can be fitted to a modified BET model. Such a model of the interaction of a protic (acidic) electrolyte with an ionogenic (alkaline) polymer is based on the assumption of two different intermolecular interactions between the electrolyte molecules and the polymer chains:

- Protonation of the alkaline groups of the polymer chains by an acidic electrolyte, strong ionic interactions between the positive charges on the polymer chains and the electrolyte anions
- Uptake of more electrolyte molecules by the formation of H bonds with N/O atoms in the polymer chains or with other bound electrolyte molecules

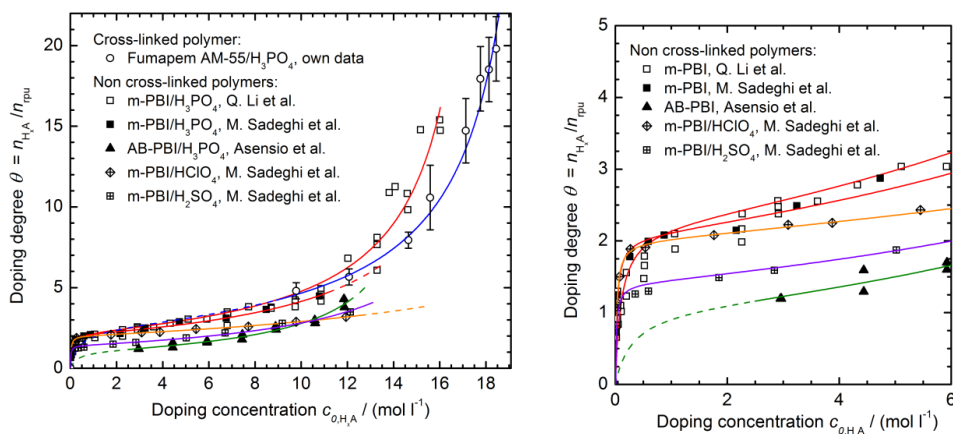


Fig. 60: Left: Adsorption isotherms of the systems Fumapem AM-55®/H₃PO₄ (10 °C), *m*-PBI/H₃PO₄, *m*-PBI/H₂SO₄, *m*-PBI/HClO₄ and AB-PBI/H₃PO₄ (all 25 °C). The solid curves have been fit to a modified BET model. The isotherms of the systems *m*-PBI/H₃PO₄, *m*-PBI/H₂SO₄, *m*-PBI/HClO₄ and AB-PBI/H₃PO₄ were taken from experimental studies⁵. Right: Section showing small doping degrees.

Each protonable group of polymer chains represents an adsorption site []_i, which permits multi-agent adsorption. For a polymer with *z* protonable groups per repeating unit, an equilibrium constant *K* for the adsorption of a first layer and *K'* for a multilayer-like adsorption results in the following expression for the doping degree θ :

$$H_xA + []_1 = [H_xA]_1 \text{ mit } K \quad \text{und} \quad H_xA + []_{i-1} = [H_xA]_i \text{ mit } K'$$

$$\theta(c_0) = \frac{z\alpha K'c_0}{(1 - K'c_0)[1 + (\alpha - 1)K'c_0]} \quad \text{mit} \quad \alpha = \frac{K}{K'}$$

The fit parameters *K*, *K'* and *z* contained in this model are shown in Table 13. For the systems *m*-PBI/H₃PO₄, AB-PBI/H₃PO₄ and *m*-PBI/HClO₄, the fit parameter *z* correlates well with the known number of protonable imidazole groups for these polymers. H₃PO₄ can be treated as a monoprotic acid, due to the low acidity of the H₂PO₃⁻ anion. In the case of Fumapem AM-55®/H₃PO₄ and *m*-PBI/H₂SO₄, the fit parameter *z* deviates by up to 40% from the expected values. In the case of Fumapem AM-55®/H₃PO₄, this is probably due to a lack of measured values for low doping concentrations *c₀*. In the case of *m*-PBI/H₂SO₄, the deviations indicate an incomplete transfer of the second proton from the sulfuric acid to the polymer. For the PBI-type polymers, an equilibrium constant *K'* of 10⁻² l mol⁻¹ was found for the multilayer uptake of strongly acidic protic electrolytes. The ratio of equilibrium constants for the uptake of the first adsorption layer *K* (protonation) and the multilayer uptake *K'* of other electrolyte molecules was consistently in the range between 10² and 10³.

⁵ Asensio, J.A., Borro, S. and Gómez-Romero, P., J. of the Electrochem. Soc. **151** (2), A304 (2004),
 Li, Q., He, R., Berg, R.W., Hjuler, H.A. and Bjerrum, N.J., Solid State Ionics **168**, 177 (2004),
 He, R., Li, Q., Jensen, J.O. and Bjerrum, N.J., J. of Polymer Sci A **45**, 2989 (2007),
 Sadeghi, M., Moadel, H., Khatmi, S. and Ghalei, B., J. of Macromol. Sci. B **49**, 1128 (2010)

Material	$M_{\text{pu}} /$ (g mol^{-1})	T / K	Fit parameter				Remarks
			z	α	$K / (\text{l mol}^{-1})$	$K' / (\text{l mol}^{-1})$	
<i>m</i> -PB/ H_3PO_4	308.34	25	2.2 ± 0.1	184 ± 102	9.9 ± 5.6	0.0539 ± 0.0005	non-cross-linked, Li and He et al.
<i>m</i> -PBI/ H_3PO_4	308.34	25	2.06 ± 0.04	648 ± 88	33 ± 5	0.050 ± 0.001	non-cross-linked, Saghedi et al.
<i>m</i> -PBI/ HClO_4	308.34	25	2.00 ± 0.01	1353 ± 66	42 ± 3	0.0312 ± 0.0006	non-cross-linked, Saghedi et al.
<i>m</i> -PBI/ H_2SO_4	308.34	25	1.40 ± 0.04	1041 ± 249	52 ± 14	0.050 ± 0.001	non-cross-linked, Saghedi et al.
AB-PBI/ H_3PO_4	116.12	25	1.1 ± 0.1	(55 ± 115)	(3.4 ± 7)	0.062 ± 0.002	non-cross-linked, Asensio et al.
Fumapem AM-55/ H_3PO_4	~ 400	110	2.5 ± 0.2	(59 ± 224)	(2.8 ± 11)	0.0478 ± 0.0005	cross-linked, own investigations

Table 13: Fit parameters for the systems fumapem AM-55/ H_3PO_4 , *m*-PBI/ H_3PO_4 , *m*-PBI/ H_2SO_4 , *m*-PBI/ HClO_4 and AB-PBI/ H_3PO_4 (see Fig. 60). Values that do not converge are given in brackets (very high margin of error).

Investigations using Raman spectroscopy

Raman spectra of Fumapem AM-55® with different H_3PO_4 doping degrees θ and the corresponding adsorption isotherms are shown in Fig. 61. The results of the Raman spectroscopic studies correlate well with the course of the adsorption isotherms. The symmetric stretching vibrations of the imidazole ring between 1550 cm^{-1} and 1576 cm^{-1} depend on the degree of protonation. Considerable changes in intensity changes occur up to a doping degree θ of 2, in accordance with the number of protonable groups per repeating unit. This corresponds to the first steep increase in the doping degree θ of the adsorption isotherms for low doping concentrations c_0 , described by the first equilibrium constant K . The stretching vibrations of the OH groups of the H_3PO_4 molecules and the H_2PO_4^- anions at 910 cm^{-1} intensify as the doping degree θ increases, i.e. when bulk-like H_3PO_4 is present. This corresponds to the second increase in the absorption isotherms for high doping concentrations c_0 , described by the second equilibrium constant K' .

The protonation of the ionogenic polymer by the protic electrolyte is obviously necessary for subsequent further uptake and for achieving high doping degrees. Comparable behavior is reported in the literature for the uptake of proton-conducting ionic liquids (PILs) by Nafion® or sulfonated polyimides (SPIs). Nafion® and SPIs are polymers with sulfonic acid groups and absorb only very small amounts of PILs. When the acidic polymers are pretreated with an organic base (e.g. alkylamine) and alkylammonium sulfonate is formed, the uptake is increased⁶. Compatibility with PILs improves considerably. The formation of a “polymer salt” with (cationic) charged polymer chains and counteranions probably creates a higher osmotic pressure compared to the doping solution, resulting in an increased uptake of the ionic liquid, respectively of phosphoric acid in case of PBI.

⁶ S.Y. Lee, A. Ogawa, M. Kanno, H. Nakamoto, T. Yasuda and M. Watanabe, *J. Am. Chem. Soc.* 132(28), 2183 (2010) bzw. V. Di Noto, E. Negro, J.Y. Sanchez and C. Iojoiu, *J. Am. Chem. Soc.* 132, 2183 (2010).

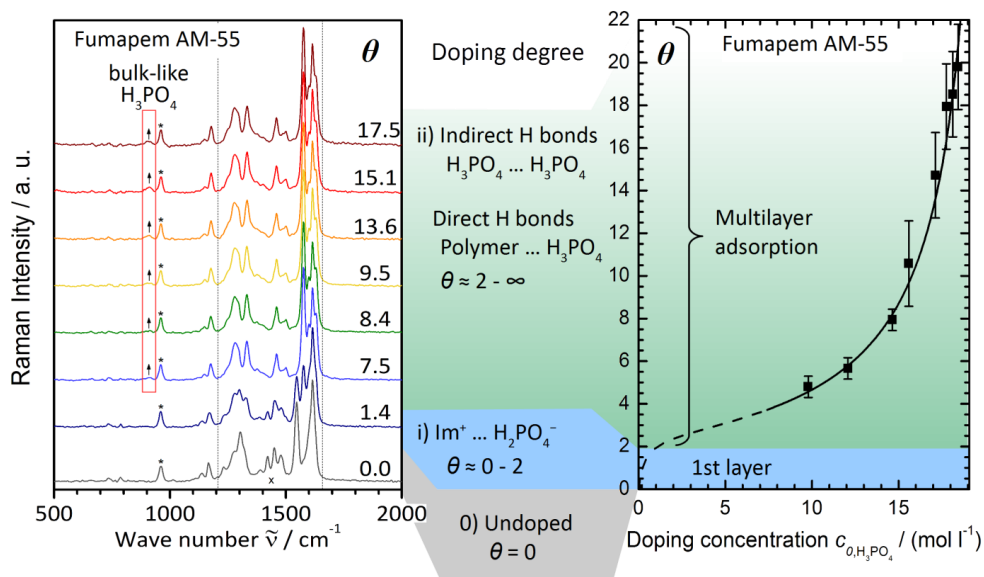


Fig. 61: Left: FT Raman spectra (25°C) of Fumapem AM-55® with various H_3PO_4 doping degrees θ . \uparrow : Raman bands at $\sim 910 \text{ cm}^{-1}$ of bulk-like H_3PO_4 . \times : Raman bands of the skeletal vibrations of the polymer. Right: Adsorption isotherms of the system AM-55/ H_3PO_4 (110°C , see also Fig. 60). Colored areas: undoped (gray $\theta = 0$), adsorption of the first layer (blue, $\theta \leq 2$), multilayer adsorption (green, $\theta > \sim 2$)

3.7.2.2 Ionic conduction in phosphoric acid above 100°C at varying water partial pressure

Phosphoric acid is currently the standard electrolyte for high-temperature polymer fuel cells (HT-PEFCs). It has a high proton conductivity, particularly in an environment with a very low water vapour pressure, good thermal stability, and good compatibility with PBI-type polymer materials. Although phosphoric acid has been the subject of many experimental studies since the mid-nineteenth century, the exact behavior of (concentrated, low-water) phosphoric acid in a temperature range of 120°C to 250°C is still not fully understood.

The main reason for this is the emergent polycondensation behavior of phosphoric acid. The state of thermodynamic equilibrium is determined only by the temperature and water partial pressure. The kinetics of the reactions depends on pH, concentration and temperature. However, it is often slow and it can take long periods of time, i.e. several days and even weeks, before equilibrium is established. In the HT-PEFC, a slow (and concentration-dependent) reaction kinetics, depending on the preceding load profile, can lead to different electrical characteristics being determined for identical operating conditions. This study investigated the kinetics at which the state of equilibrium was established in phosphoric acid for different temperature and humidity conditions relevant for the HT-PEFC. Time-resolved and frequency-resolved measurements were performed of the electrical conductivity of phosphoric acid in a measuring cell made of quartz glass during exposure to constant conditions in a climate chamber.

One result of the investigations is that there is not always a clear correlation between atmospheric conditions and the properties of the liquid phase above 120 °C (and <200 °C), most likely because of the different, metastable mixing ratios of ortho-, di- and triphosphoric acids etc. which emerge depending on the starting conditions. In accordance with the thermodynamic equilibria and reaction kinetics, there is only noticeable formation of these higher condensed species above 120 °C on a scale relevant for conductivity measurements (Fig. 62). At the measurement temperature of 150 °C, in the range of 10–15 mass% water, there was considerable scattering of the conductivity values. This cannot be explained by measurement uncertainties, but rather by to the different starting conditions before the equilibration step. This is indicative of different metastable mono/di/triphosphoric acid mixtures, which require long periods of time to achieve thermodynamic equilibrium appropriate for this temperature and composition (not achieved in these experiments).

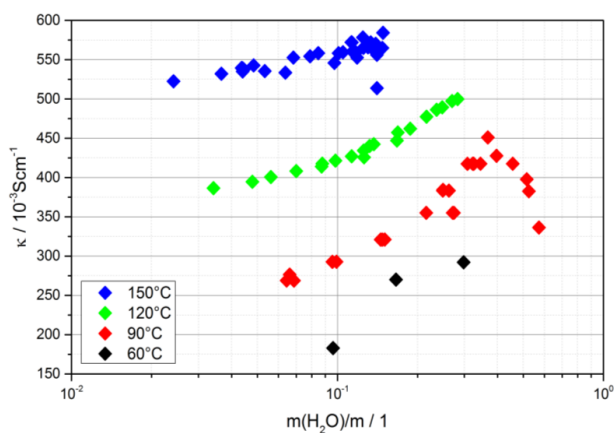


Fig. 62: Specific electrical conductivity κ of concentrated phosphoric acid as a function of the residual water content $m(\text{H}_2\text{O})/m_{\text{total}}$ and of temperature

Another finding was the strong dependence of the equilibration time for a certain atmospheric condition. As the experiment performed only permitted surface-limited implementation (small surface-to-volume ratio), equilibrium was established according to a simple exponential function and can therefore be presented as a half-life. To determine the half-life, determination of the water concentration would be desirable. However, this is not directly accessible. Therefore, the fact was used that a change in the water concentration causes a change in the heat of the solution due to the mixing enthalpy. For small changes in concentration, this is proportional and can thus be used for the determination. As shown in Fig. 63, clear jumps were observed due to the occurrence/disappearance of different phosphate condensates.

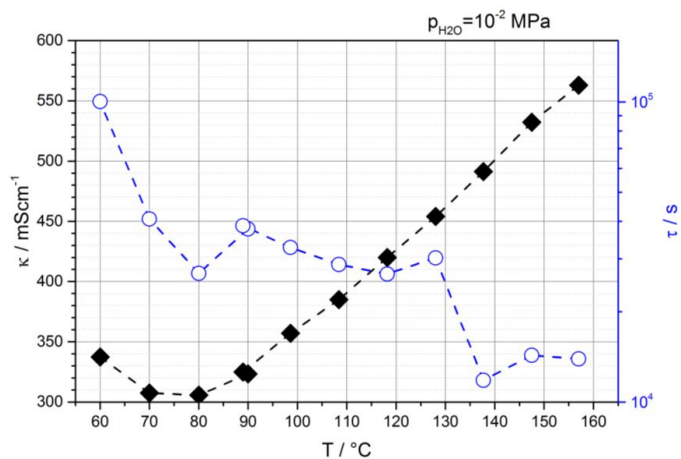


Fig. 63: Correlation between equilibration (half-life τ) and temperature θ of phosphoric acid for a defined water partial pressure $p_{\text{H}_2\text{O}}$

3.7.2.3 Ionic liquids as alternative electrolytes for the HT-PEFC

For high-temperature polymer electrolyte fuel cells (HT-PEFCs), proton-conducting membranes made of phosphoric acid-doped polybenzimidazole (PBI) are presently used as electrolytes. However, the presence of phosphoric acid or H_2PO_4^- anions considerably inhibits the platinum-catalyzed oxygen reduction reaction (ORR) at the cathode. At an operating temperature between 160 °C and 200 °C, the exchange current density is still one order of magnitude smaller than in conventional, Nafion-based fuel cells (PEFCs) operated at temperatures between 25 °C and 90 °C. Different experimental studies have shown that phosphoric acid and H_2PO_4^- anions block the electrochemically active centers on the platinum surface needed for the oxygen reduction. As an alternative to phosphoric acid, proton-conducting ionic liquids (PILs) are an option because they do not depend on water as ampholyte and are characterized by fast proton transfer processes. This means that they can be used at operating temperatures of 120 °C to 200 °C, which are envisaged in a HT-PEFC. In addition, ionic liquids typically exhibit good thermal stability, low volatility and low flammability.

In the period under review here, a new class of PILs based on amino alkyl sulfonic acids was identified. These compounds with a protonated amino alkyl sulfonic acid as a cation are a class of strongly acidic PILs that are suitable for use as an alternative electrolyte in HT-PEFCs. As a first candidate, 2-sulfoethyl ammonium trifluoromethanesulfonate (2-SeATfO, see Fig. 64) was synthesized and characterized.

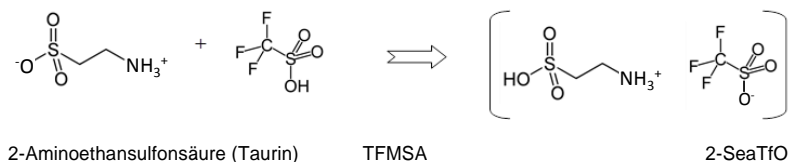


Fig. 64: Reaction scheme of the synthesis of 2-SeATfO

As water is formed at the cathode during operation of a HT-PEFC, a mixture of 95 wt% 2-SeATfO and 5 wt% water was prepared and the properties were compared with those of the 95 wt% phosphoric acid. The most important results of the physicochemical and electrochemical characterization of these new ionic liquids are: (i) in the practically relevant potential range, 2-SeATfO is electrochemically stable and thermally stable up to a temperature of 140°C, (ii) at temperatures ≥ 90 °C, higher current densities of the oxygen reduction are achieved with 2-SeATfO than with phosphoric acid, (iii) the specific conductivity of 2-SeATfO at 130 °C is around one order of magnitude below that of phosphoric acid.

3.7.2.4 Determination of thermal stability and calorimetric properties of ionic liquids

Ionic liquids (ILs) are salts with a low lattice energy. They have melting points below 100 °C. Some proton-conducting ionic liquids (PILs) are promising candidates for alternative electrolytes for the HT-PEFC (2-SeATfO). A unique feature of these ILs is that they can conduct protons even when water is not present. However, the melting point of such salts is not easy to determine and depends heavily on the residual content of dissolved water. An example is shown in Fig. 65, highlighting the influence of water on the heat capacity of the melt as well as on the melting point, which can be recognized as a jump in heat capacity. This work will be intensified and expanded in future.

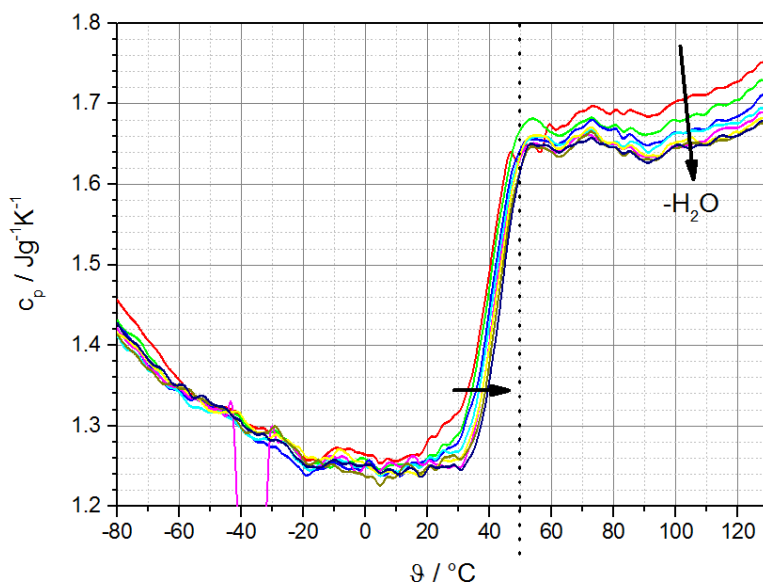


Fig. 65: Correlation between θ and heat capacity c_p during drying of an ionic liquid for application in a HT-PEFC (2-SeATfO).

3.7.2.5 Investigation of critical operational conditions in the direct methanol fuel cell

As part of the Canadian-German fuel cell cooperation funded by the Federal Ministry for Economic Affairs and Energy (funding number: 0327853A) with the project title “Improvement of the performance and durability of direct methanol fuel cells in the kW power range”, a

doctoral thesis was written by A. Löhmer entitled “Investigations of critical operation conditions in direct methanol fuel cells”. One of the priorities of this work was investigating an inadequate supply of methanol to the anode, which leads to irreversible, massive corrosion and degradation of the anode catalyst. Three successive degradation phases were identified for complete methanol depletion using a combination of electrochemical and mass spectrometry analyses. These phases were characterized by ruthenium and carbon corrosion (Fig. 66).

For a more comprehensive understanding of the degradation process, impedance spectra were recorded. These were fitted and analyzed using a model based on a differentiation between smaller primary pores (pores *in* the catalyst agglomerates) and larger secondary pores (pores *between* the catalyst agglomerates). The impedance analysis combined with porosity measurements gave rise to the following results: (i) the resistances of methanol oxidation, proton conductivity and mass transport in the anode catalyst layer increase after methanol depletion and verify the irreversible performance loss of up to 70%, (ii) the degradation of primary pores is particularly strong after the third phase of methanol depletion, which indicates a degradation process that begins in the secondary pores and ends in the primary pores.

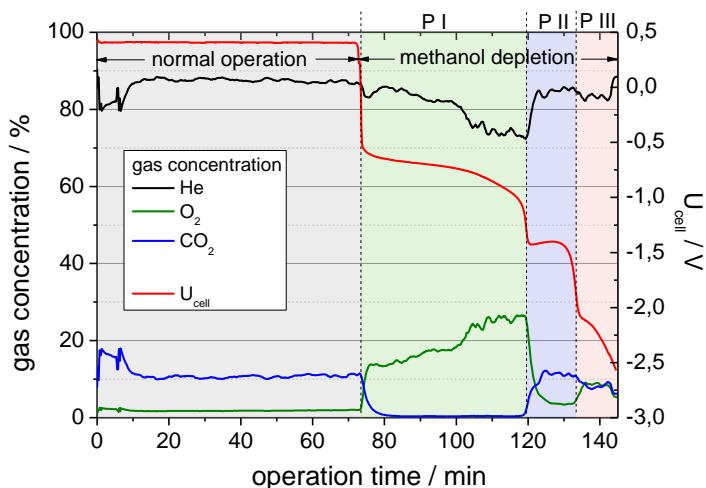


Fig. 66: The three phases of complete methanol depletion (PI – PIII) after methanol was replaced with water in a direct methanol fuel cell; cell voltage and composition of the anode exhaust gas over time at a constant flow of current (150 mA/cm^2)

3.7.3 Staff members and fields of activity

Name	Tel. (02461-61-) Email	Field of activity
PD. Dr. C. Korte	9035 c.korte@fz-juelich.de	Head of the Physicochemical Fuel Cell Laboratory

T. Bergholz	1891 t.bergholz@fz-juelich.de	System evaluation: Li accumulators in different fields of application, aging processes
J. Keppner	1891 j.keppner@fz-juelich.de	Basic research on ion conduction and diffusion along the phase boundaries in SOFC materials
Fr. K. Klafki	1895 k.klafki@fz-juelich.de	Conventional sample preparation
Dr. S. Kuhri	1891 s.kuhri@fz-juelich.de	Spectroscopic investigations: Raman/IR, imaging analysis techniques: SEM/EDX, CLSM
Fr. T. Mandt	1891 t.mandt@fz-juelich.de	Degradation processes in SOFCs, grain-boundary diffusion of Sr in CGO barrier layers
Dr. J. Wackerl	6228 j.wackerl@fz-juelich.de	Physical properties: DSC, TGA, mechanical properties, conductivity
K. Wedlich	9763 k.wedlich@fz-juelich.de	Electrical characterization of Li accumulators, aging processes
Dr. K. Wippermann	2572 k.wippermann@fz-juelich.de	Aging mechanisms in DMFCs, electrochemical investigations, spatially resolved measurements

3.7.4 Important publications and patents

Important publications

Schröder, A.; Wippermann, K.; Arlt, T.; Sanders, T.; Baumhöfer, T.; Markötter, T.; Mergel, J.; Lehnert, W.; Stolten, D.; Manke, I.; Banhart, J.

Water Evolution in Direct Methanol Fuel Cell Cathodes Studied by Synchrotron X-Ray Radiography

Fuel Cells 13-3 (2013) 371–379

Wippermann, K.; Löhmer, A.; Everwand, A.; Müller, M.; Korte, C.; Stolten, D.

Study of Complete Methanol Depletion in Direct Methanol Fuel Cells

Journal of the Electrochemical Society 161-4 (2014) F525-F534

Korte, C.; Conti, F.; Wackerl, J.; Dams, P.; Majerus, A.; Lehnert, W.

Uptake of protic electrolytes by polybenzimidazole-type polymers: absorption isotherms and electrolyte/polymer interactions

Journal of Applied Electrochemistry, online seit Mai 2015

Korte, C.; Keppner, J.; Peters, A.; Schichtel, N.; Aydin, H.; Janek, J.

Coherency strain and its effect on ionic conductivity and diffusion in solid electrolytes – an improved model for nanocrystalline thin films and a review of experimental data

Physical Chemistry Chemical Physics, 16 (2014) 24575-24591

Bergholz, T.; Nunez, T.; Wackerl, J.; Korte, C.; Stolten, D.

Magnetography: A novel Characterization Tool for Li-Ion-Batteries

2013 MRS Spring Meeting & Exhibit, 2013 2013, pp. 1544, DOI: 10.1557/opl.2013.724

Mandt, T.; Korte, C.; Breuer, U.; Weber, A.; Ziegner, M.; Uhlenbruck, S.; Menzler, N.; Stolten, D.

Sr-Diffusion in Ce_{0.8}Gd_{0.2}O_{2-d} Layers for SOFC Application

2013 MRS Spring Meeting & Exhibit, 1542 2013, pp. mrss13-1542-g11-05, DOI: 10.1557/opl.2013.629

Important patents

Patent applications:

Principal inventor	PT	Description
J. Wackerl	1.2583	Device and method for qualitative determination of the operational state of an object to be tested
K. Wippermann	1.2658	Electrolyte system for a fuel cell
T. Bergholz	1.2660	Electrolyte system for application in electrochemical components

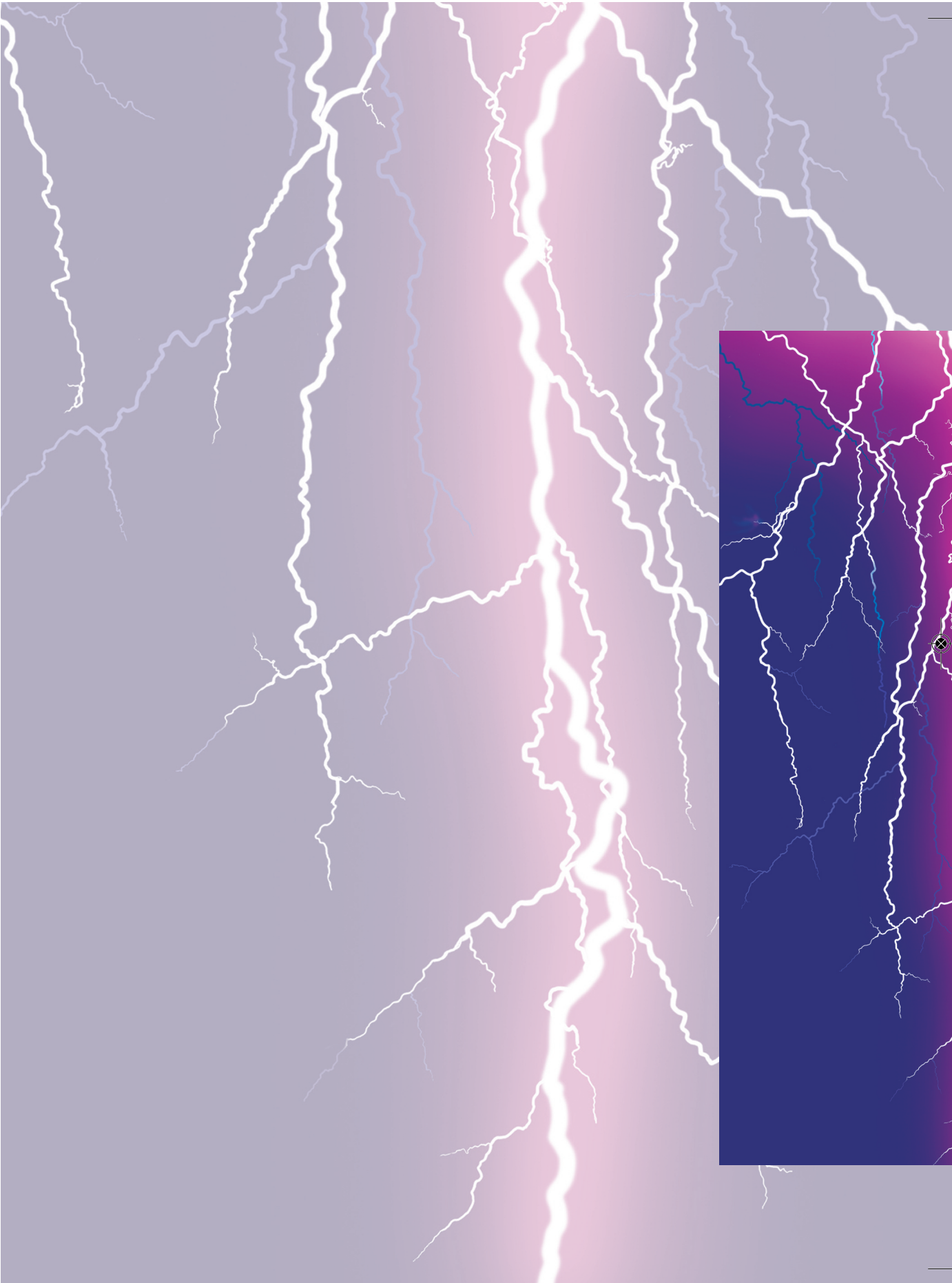
3.8 Quality assurance

Many aspects are important for the quality of work: these include safe operation of test facilities, documentation of results, organization of collaborative work, reproducibility of experiments, testing of materials received and much more. The central requirements of a quality management system involve measures for document control and quality records. DIN EN ISO 9001 demands this and documented procedure VA-RHLQ-01 of Forschungszentrum Jülich includes specifications defining how responsibilities are assigned for creating, revising, reviewing, approving, distributing and archiving documents and records. To meet these requirements, the centrally licensed ConSense information management system (licensed by Quality Management for Forschungszentrum Jülich) was implemented for the area of direct methanol fuel cells (DMFC). The aim was to gain experience with the ConSense software based on an existing and well established QM system and then to decide whether this system should be implemented in other QM subareas.

ConSense fulfils all requirements in DIN EN ISO 9001 pertaining to document management. For the DMFC area, necessary standard operation procedures (SOPs) were documented or adapted using the templates and entered into the system. The use of the QM software ensures that documents are created, verified and released by authorized persons only. In addition, the system organizes the information flow so that all of those involved in a process always have access to the most up-to-date document versions. Older versions are archived centrally and modifications are documented. Documents that apply to the whole of Forschungszentrum Jülich can also be accessed via the system. The software was implemented step by step in the department and achieves a high degree of transparency. It is now being implemented for the document management of quality assurance and safety-relevant documentation in other subareas. One example is the area of electrolysis. Here, one priority will be to use ConSense to describe all processes that are relevant for product fabrication and quality assurance. This will ensure clear-cut, transparent interfaces, which draw on existing experience and simultaneously represent new challenges. The aim is to extend the quality assurance measures in Process Engineering Electrolysis and to adapt these in line with the standards for quality assurance.

3.8.1 Staff members and fields of activity

Name	Tel. (02461-61-) e-mail	Field of activity
Fr. D.Günther	2378 d.quenther@fz-juelich.de	Documentation of workflows, quality management





4

Projects

Selected R&D Projects

- Low-cost DMFC systems with long-term stability in the kW class
- Auxiliary power supply with fuel cells for trucks
- Fuel cell APU for aircraft



4.1 Diffusion and ion conduction along ceramic interfaces

Ion conduction and diffusion along internal interfaces in ceramic solid electrolytes is still not fully understood. Compared to volume transport, far fewer experimental studies exist. Transport processes along grain and phase boundaries play an important role in the slow degradation processes in SOFCs, high- κ dielectrics and ceramic protective coatings. The influence of transport processes along interfaces increases due to a comparatively low activation energy at low operating temperatures. The most well-known model today describing accelerated transport processes in interfaces is based on the formation of space-charge zones. However, they do not account for the influence of possible elastic strains in the interface, misfit dislocations or decreased packing density. In technically important ceramic materials used as solid-state electrolytes or mixed conductors in fuel cells, sensors and batteries, space-charge models no longer apply because of the high concentration of charge carries brought about by doping.

In the period under review, the O^{2-} conductivity of Er_2O_3/YSZ , Dy_2O_3/YSZ and Sc_2O_3/YSZ multilayer systems was measured parallel to the phase boundaries as a function of layer thickness d . In addition, X-ray strain and texture measurements were performed on Y_2O_3/YSZ , Er_2O_3/YSZ , Dy_2O_3/YSZ and Sc_2O_3/YSZ multilayer systems. All multilayers were prepared using pulsed laser deposition (PLD) on (0001) Al_2O_3 substrates in cooperation with PGI-9/FZJ and the Institute of Physical Chemistry (PCI) at Justus Liebig University Giessen (JLU).

4.1.1 X-ray strain measurements

X-ray strain measurements expanded the available data basis for interfacially dominated systems to include lattice mismatches and interfacial strains. The results can be described with a simple model, which assumes exponentially decreasing strain/compression fields based on the strained interfaces caused by lattice mismatches.

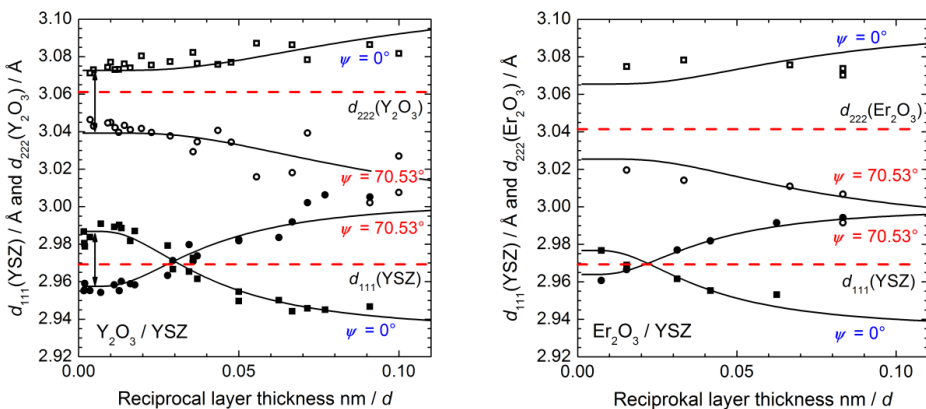


Fig. 67: Lattice plane spacing d_{111} and d_{222} of YSZ and SE2O3 in YSZ/SE2O3 multilayers (SE = Y, Er) as a function of inverse layer thickness $1/d$ for lattice planes \blacksquare, \square parallel (0°) and \bullet, \circ at an angle of 70.53° to the phase boundary (prepared at PGI-9/FZJ). Solid lines: fit according to Eq. (1).

For the (mean) lattice plane spacings perpendicular $d_{hkl,\perp}$ and parallel $d_{hkl,\parallel}$ to the substrate plane determined by x-ray diffraction (XRD), the model assumptions result in the following as a function of the thickness d of single layers:

$$d_{hkl,\perp} \approx d_{hkl} \left(1 - \frac{2\nu}{1-\nu} \varepsilon_0 \frac{1}{\cosh d/2\delta_0} \right) \quad \text{and} \quad d_{hkl,\parallel} \approx d_{hkl} \left(1 + \varepsilon_0 \frac{1}{\cosh d/2\delta_0} \right) \quad (1)$$

$$\delta_0 = \frac{1}{4} \sqrt{\frac{2(1-\nu)}{3(1+\nu)}} \cdot l$$

ν : Poisson's ratio
 l : mean diameter of layer crystallites
 d_{hkl} : lattice plane spacing in unstrained state
 ε_0 : lattice expansion/compression caused by misfit dislocations

In multilayers/layer systems with columnar nanoscale crystallites, strains caused by misfit dislocations are localized in areas near the interface. By fitting Eq. (1) with the measured data of the investigated multilayers, we get a value of around 10 nm for the mean spatial extent δ_0 of the strained regions (Fig. 67 und Fig. 68).

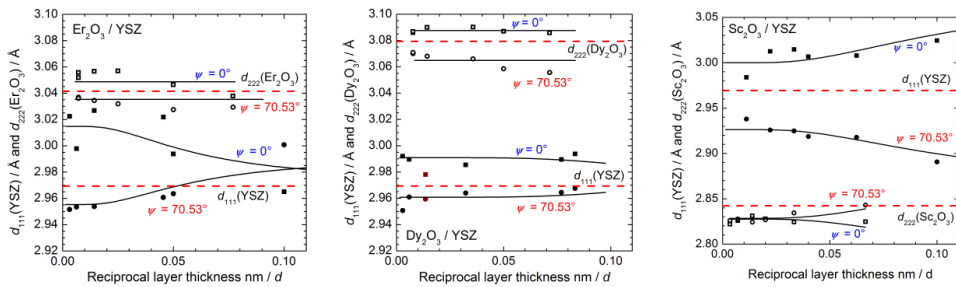


Fig. 68: Lattice plane spacing d_{111} and d_{222} of YSZ and SE₂O₃ in YSZ/SE₂O₃ multilayers (SE = Sc, Er, Dy) as a function of inverse layer thickness $1/d$ for lattice planes \blacksquare, \square parallel (0°) and \bullet, \circ at an angle of 70.53° to the phase boundary (prepared at PCI/JLU). Solid lines: fit according to Eq. (1).

4.1.2 Ionic conductivity and texture

The measured O²⁻ conductivity parallel to the YSZ layers shows a very strong dependence on the preparation conditions. The texture (grain boundaries) and the crystallite size of the layers can be identified as additional important parameters. It appears, that their influence is of the same order of magnitude as the influence of the local interfacial strain.

X-ray texture analyses (pole figures) showed that the YSZ/Y₂O₃ and YSZ/Er₂O₃ multilayers fabricated at a high substrate temperature at PGI-9/FZJ only exhibited a single crystallite orientation (Fig. 69):

$$i) \quad (111) \text{ YSZ} \parallel (111) \text{ SE}_2\text{O}_3 \parallel (0001) \text{ Al}_2\text{O}_3 \quad [1 \bar{2} 1] \text{ YSZ} \parallel [1 \bar{2} 1] \text{ SE}_2\text{O}_3 \parallel [\bar{1} 10] \text{ Al}_2\text{O}_3 \quad (2)$$

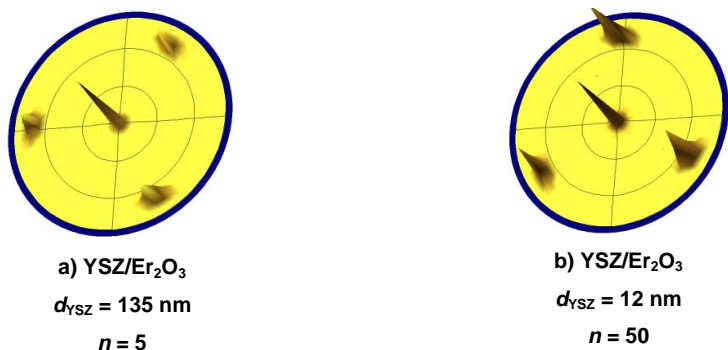


Fig. 69: Texture analysis of YSZ/Er₂O₃ multilayers on (0001) Al₂O₃ substrates fabricated at a high substrate temperature, low O₂ pressure and fast growth rate (PGI-9/FZJ). (111) YSZ pole figure a) of a multilayer with 135 nm and b) with 12 nm thick YSZ layers (Y₂O₃ layer between the first Er₂O₃ layer and Al₂O₃ substrate).

In contrast to this, the YSZ/Sc₂O₃, YSZ/Dy₂O₃ and YSZ/Er₂O₃ multilayers fabricated at a low substrate temperature at PCI/JLU exhibited two azimuthal crystallite orientations and transitions to fiber textures (Fig. 70):

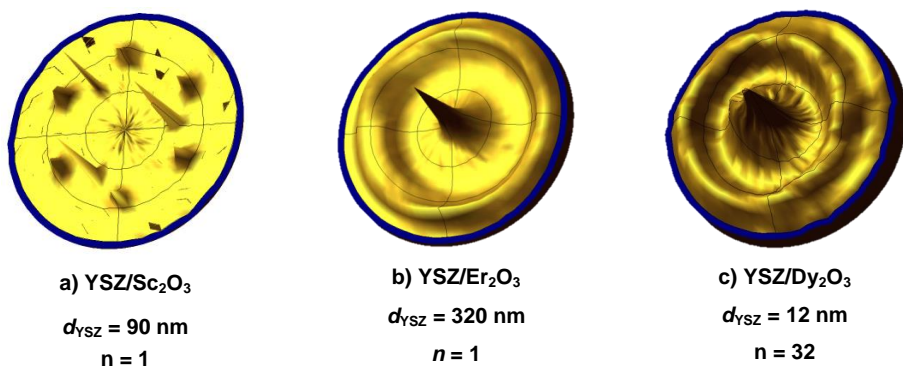
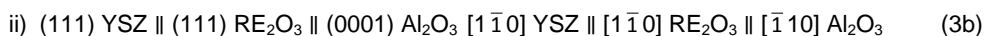
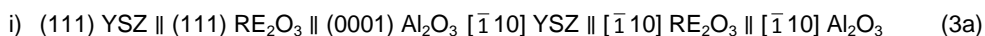


Fig. 70: Texture analysis of SE2O3/YSZ multilayers on (0001) Al₂O₃ substrates fabricated at a low substrate temperature, high O₂ pressure and slow growth rate (PCI/JLU). (200) YSZ pole figure a) of a Sc₂O₃/YSZ multilayer with a YSZ layer thickness of 90 nm, (111) YSZ pole figure b) of a Dy₂O₃/YSZ multilayer with a YSZ layer thickness of 125 nm and b) with a YSZ layer thickness of 12 nm thick YSZ layers.

The highly textured YSZ/Er₂O₃ multilayers with only one orientation of the layer crystallites exhibited a strong anisotropic ionic conductivity parallel to the YSZ layers (Fig. 71). The O²⁻ conductivity parallel and perpendicular to the substrate orientation $[100]$ Al₂O₃ differs by up to one order of magnitude.

In the YSZ/Sc₂O₃, YSZ/Dy₂O₃ and YSZ/Er₂O₃ multilayers fabricated at a low substrate temperature with two azimuthal orientations or transitions to fiber textures, no anisotropic effects were found due to a geometrical averaging (Fig. 72).

For the YSZ/Er₂O₃ multilayers with dilatationally strained YSZ layers, an increase in conductivity was ascertained as a function of inverse layer thickness $1/d$ (of the interface density). For the YSZ/Sc₂O₃ multilayers with compressively strained YSZ layers, a decreased conductivity was found.

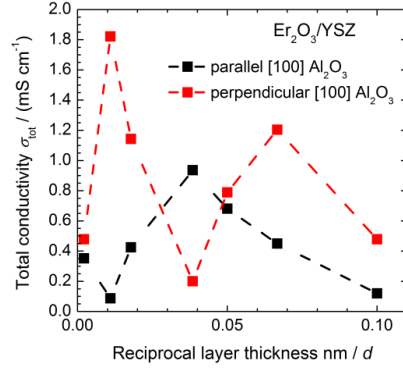


Fig. 71: O²⁻ conductivity σ_{tot} of YSZ/Er₂O₃ multilayers as a function of inverse layer thickness $1/d$ (layers prepared at PGI-9/FZJ; XRD strain analyses in Fig. 67, texture analyses in Fig. 69)

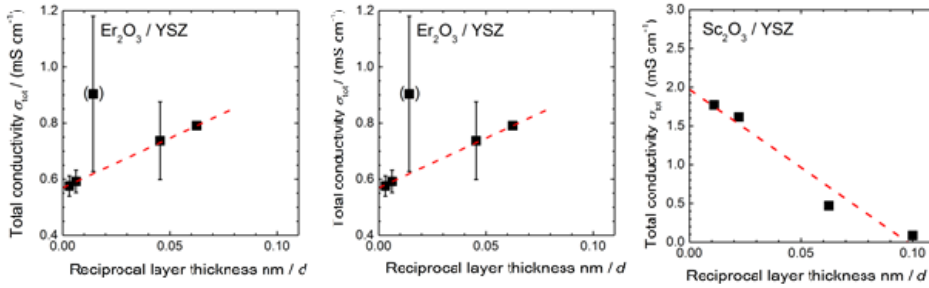


Fig. 72: O²⁻ conductivity σ_{tot} of YSZ/Er₂O₃, YSZ/Sc₂O₃ and YSZ/Dy₂O₃ multilayers as a function of inverse layer thickness $1/d$ (layers prepared at PCI/JLU; XRD strain analyses in Fig. 68, texture analyses in Fig. 70).

This behavior agrees with the aforementioned simple model of elastic strain fields exponentially decreasing from the interfaces and a pressure dependence of free activation enthalpy, following from transition state theory:

$$\frac{\sigma_{tot}(d)}{\sigma_{vol}} = \frac{2}{d} \int_0^{d/2} \exp\left(\alpha \varepsilon_0 \frac{\cosh z / 2\delta_0}{\cosh d / 2\delta_0}\right) dz \quad (4)$$

Eq. (4) describes the dependence of the ionic conductivity of a thin film, biaxial strained at its adjacent interfaces, as a function of its thickness d . By fitting the model with the layer-thickness-dependent O²⁻ conductivity data, we get similar values for the mean spatial extent δ_0 of the strained regions as with the X-ray studies.

For the YSZ/Dy₂O₃ multilayers fabricated at a low substrate temperature, no clear trend was visible for the O²⁻ conductivity as a function of the layer thickness. In line with the dilatational

strain of the YSZ layers, there should be, analogous to the YSZ/Er₂O₃ multilayers, an increase in conductivity as a function of the reciprocal layer thicknesses. For the YSZ/Dy₂O₃ multilayers – in contrast to the YSZ/Er₂O₃ and YSZ/Sc₂O₃ multilayers – the X-ray strain studies (Fig. 68) showed no clear variations in lattice parameters caused by elastic strain fields. In addition to the fiber texture, the YSZ/Dy₂O₃ multilayers also showed a stronger misorientation (tilting) of the (111) planes in relation to the substrate compared to the YSZ/Er₂O₃ multilayers (Fig. 70).

This tilting could lead to an additional reduction of the lattice mismatch at the interfaces. The reduced lattice mismatch and thus the hardly (by XRD) detectable elastic strain fields in these multilayer specimens therefore have only little influence on the ionic interfacial transport.

4.2 Mobile fuel processing systems with middle distillates for HT-PEFCs

4.2.1 Development of a full system

HT-PEFC technology combined with autothermal reforming is preferred for on-board power supply. An integrated HT-PEFC stack was assembled. In addition to two 2.5 kW_e HT-PEFC stacks, it comprises a fuel processing unit made up of an autothermal reformer, a water-gas shift reactor and a catalytic burner. Tests were performed with GTL kerosene (C₁₀H₂₂), BTL diesel (C₁₇H₃₆) and premium diesel (C₁₉H₃₈). Aiming for good efficiency, the target values were set to 83% for hydrogen utilization and 500 mA/cm² for the current density. A mass flow rate of 1670 g/h GTL kerosene was needed to produce 5 kW_e. This corresponds to an efficiency of 24%. Higher efficiency levels of 29.4% can be achieved at 50% part load. The envisaged output of 5 kW_e was achieved for all three fuels:

- GTL kerosene: 4.95 kW_e at 450 mA/cm² and 492 mV mean cell voltage and 77.1% hydrogen utilization.
- BTL diesel: 5 kW_e at 450 mA/cm² and 496 mV mean cell voltage and 74% hydrogen utilization.
- Premium diesel: 5.07 kW_e at 500 mA/cm² and 55.5% hydrogen utilization.

Efficiencies of 85.6% were also achieved for operation with GTL kerosene. Continuous aging was not detected. After 250 hours of operation, at an operating point with a current density of 250 mA/cm², the mean cell voltage dropped from initially 610 mV (0–72 h) to 577 mV. At all operating points, the design conditions of the heat exchanger concept were fulfilled and no external heat supply was required.

The core components, namely reformer and HT-PEFC stack, were robust and stable during the test series. In the tests with premium diesel (ARAL Ultimate Diesel), however, signs of degradation were detected on the water-gas shift reactor. At the beginning of the test, the CO content was reduced from 10.2 vol% in the ATR product gas to 0.8 vol%. Due to the exothermic reaction heat, the temperature increase in the high-temperature and low-temperature shift stage totaled 78 K (40 K (HTS) and 38 K (LTS)). A malfunction in the test stand peripherals caused degradation, which is indicated by the smaller temperature rise of 53 K and an increased CO concentration of 4 vol%. It should be noted that the quality of the ATR product gas was constantly very good; benzene appeared in concentrations of approx. 1 ppmv – above the detection limit.

To operate a fuel-cell APU, a start-up strategy must be prepared. The current HT-PEFC stack design requires a start-up time of approx. 37.5 min. The fuel processing unit is operational after 16.5 min. Fuel cell stack optimization combined with start burner modification leads to a range of 10–12 min. The emissions of the tested start burner are between 60 mg/m³ (3 kW part load) and 229 g/m³ (20 kW, full load for 10 s). The burner requires 2 min to reach its design temperature of 800 °C.

Detailed information on the development and characterization of an integrated HT-PEFC system and the autothermal reforming of diesel and kerosene in the 5 kW_e power class has been published in ⁷. Experience operating this system is discussed in ⁸. A start-up strategy for this system using a commercial ignition burner was developed in ⁹.

4.2.2 Development of fuel processing systems

Over the last few years, system development made considerable progress in packaging within the ADELHEID project. In package 1, into which reactor type AH1 was also integrated, the components are arranged sparsely. Reactors can also be installed that have not been specifically designed for the package. The package's performance class is limited to 12–18 kW_{th}. Package versions P2 and P3 were developed, designed and assembled for the EFFESYS project. The performance class for all components is consistently 28 kW_{th}. The components are arranged close together in the package in order to achieve a high power density. The components in the package can be exchanged but only with considerable effort. In package AH2, components were welded together so that they then count as a single component. The components cannot be exchanged. The reformer and shift reactor, for example, were welded together.

Reactor type AH1 was produced by Presswerk Struthütten and integrated into the existing package 1/AH1 for operational tests. In addition to a reformer type AH1, package AH1 comprises a shift reactor (WGS 3) and a catalytic burner (CAB 2.3). After integration into test module B, experimental testing began.

In the first few experiments, the system was operated with BTL diesel (NExBTL diesel) from Neste Oil. Fig. 73 shows the results of a test during which package AH1 was in operation for approx. 22 h. The reformer was operated at a H₂O/C molar ratio of 1.9 and an O₂/C molar ratio of 0.47. The concentrations of the main products in the dry product gas after the shift reactor are shown in Fig. 73. This analysis was performed using a mass spectrometer. At the beginning of the test (50–140 min), the system was operated with a diesel flow of 1013 g/h. In this part of the test, 600 g/h water was added between the shift stages for cooling. The CO concentration after the shift reactor was thus reduced to 1.0 vol%. However, this operational phase could not be continued as the water pump was not stable. The volume of water was therefore increased to 1000 g/h to ensure stable operation of the pump overnight. The inlet temperature in the LTS stage dropped as a direct consequence of this from approx. 300 °C to approx. 230 °C. This low temperature level led to an increased CO concentration in the product gas because of poorer reaction kinetics. As a counteractive measure, the mass flow of diesel was increased to 1350 g/h. This value is equivalent to the design point of package AH1. The water volume was kept constant for the LTS stage. As a result, the inlet temperature in the LTS stage rose only to 264 °C. This temperature is still lower than the

⁷ Samsun, R. C., Pasel, J., Janßen, H., Lehnert, W., Peters, R. and Stolten, D., "Design and test of a 5 kWe high-temperature polymer electrolyte fuel cell system operated with diesel and kerosene," *Applied Energy*, vol. 114, pp. 238-249, 2014.

⁸ Samsun, R. C., Pasel, J., Meißner, J., Janßen, H., Lehnert, W. and Peters, R., "Operational Experience from a 5 kWe HT-PEFC System with Reforming of Diesel and Kerosene," *ECS Transactions*, vol. 58, pp. 165-174, 2013.

⁹ Wiethage, C., Samsun, R. C., Peters, R. and Stolten, D., "Start-Up of HT-PEFC Systems Operating with Diesel and Kerosene for APU Applications," *Fuel Cells*, vol. 14, pp. 266-276, 2014.

design temperature of 300 °C. Operation of the shift reactor at its design point (GHSV: 30,000 h⁻¹) at this temperature led to a CO concentration of approx. 1.8 vol% at the reactor outlet. After stable operation of the system overnight (approx. 18 h), the quenching water volume was reduced in steps of 50 g/h down to 700 g/h. In this phase, decreasing CO and increasing CO₂ and H₂ concentrations were observed (see Fig. 73, from 1260 min). At 700 g/h water, the inlet temperature in the LTS stage increased to the design point of 300 °C.

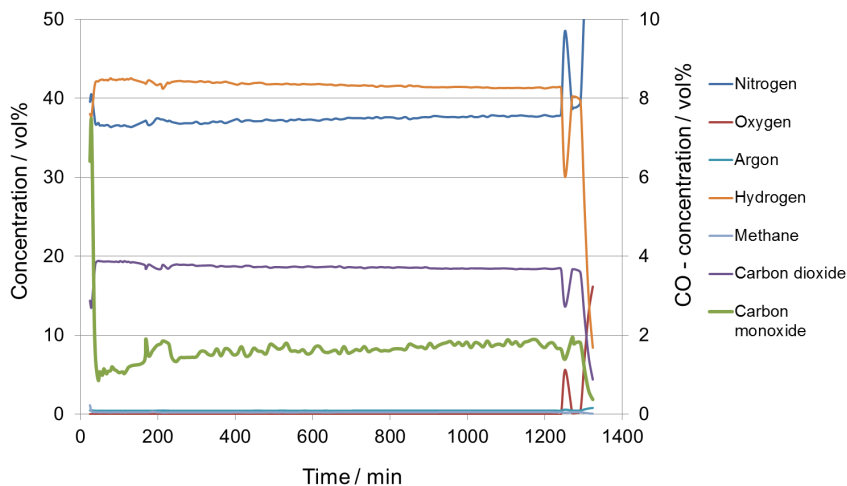


Fig. 73: Concentrations of the main products in the dry product gas after the shift reactor for operation of package AH1 with diesel. Analysis performed with mass spectrometry

In this period, the concentrations of CO and CO₂ after the shift reactor were analyzed by FTIR spectroscopy with a frequency of 1 s. The influence of the water volume and the inlet temperature in the LTS stage on the CO conversion in the shift reactor could therefore be dynamically investigated. Fig. 74 shows how the CO concentration continuously decreased in the period from 1260 min to 1290 min and as soon as a water volume of 700 g/h was achieved remained constant at 1.0 vol% in the dry product gas until the end of the test. This demonstrates that the target value of 1.0 vol% in the wet product gas was achieved and even exceeded for package AH1 for operation with BTL diesel at the package design point. The concentrations of higher hydrocarbons after the reformer and the shift reactor in the gas phase were at the detection limit of the analytical device.

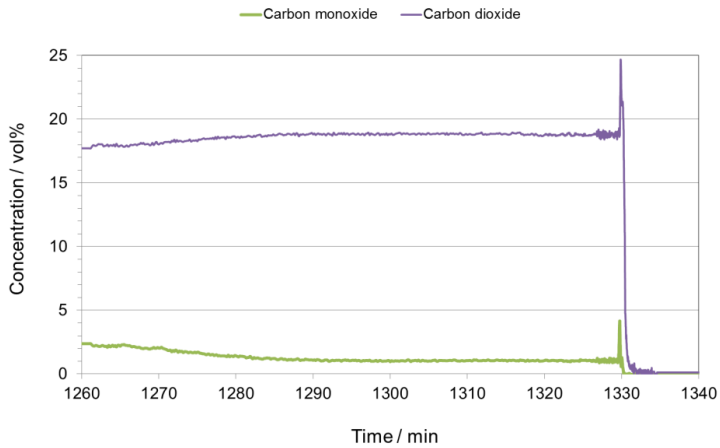


Fig. 74: Concentrations of CO and CO₂ in the dry product gas after the shift reactor for operation of package AH1 with BTL diesel. Analysis using FTIR

In addition to the analysis of the system in the steady state, the by-products after the shift reactor were also investigated for system start-up and shut-down by means of FTIR spectroscopy. During start-up, a maximal benzene concentration of 909 ppm was observed. The maximal concentrations of ethene (45 ppm), ethane (238 ppm) and propene (60 ppm) were lower. During system shut-down, the maximal concentrations of ethane (2974 ppm) and benzene (1168 ppm) were relatively high, while the maximal concentrations of ethene (11 ppm) and propene (18 ppm) were considerably lower. The influence of these by-products on the long-term stability of the system components is currently being investigated.

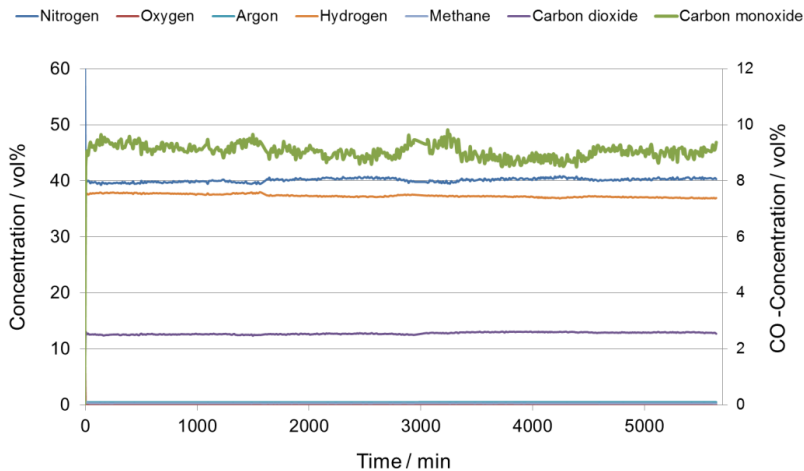


Fig. 75: Concentrations of the main products in the dry product gas after the reformer for operation of package AH1 with BTL diesel for a duration of 100 h. Analysis using mass spectrometry

In further tests, the long-term stability of the reformer ATR AH1 was investigated in system operation with different diesel and kerosene fuels. In all tests, the reformer was operated with a fuel flow of 1350 g/h with O_2/C and H_2O/C molar ratios of 0.47 and 1.9, respectively. Fig. 75 shows the course of the concentrations of the main products in the dry product gas after the reformer ATR AH1 during a test with BTL diesel (NExBTL diesel) for a duration of 100 h. It should be noted that all concentrations remained almost constant. No trends were observed in the reformer that could lead to possible deactivation. In this period, the reformer produced very small amounts of by-products, the concentrations of which were at the detection limit of the analytical device. Fig. 76 shows the concentrations of the main products in the dry product gas after the shift reactor. In this test, the CO concentrations were between 1.0 vol% and 1.5 vol%. Higher CO concentrations of up to 1.9 vol% were measured for a short period in the product gas. However, countermeasures in the system led to a drop in the CO concentration back down to between 1.0 vol% and 1.5 vol%. These countermeasures involved adapting the heating cartridge performance and the quenching water volume. The increase in CO concentration at the end of the test to approx. 1.5 vol% can be explained by problems supplying water to cool the reformat prior to the low-temperature shift reactor.

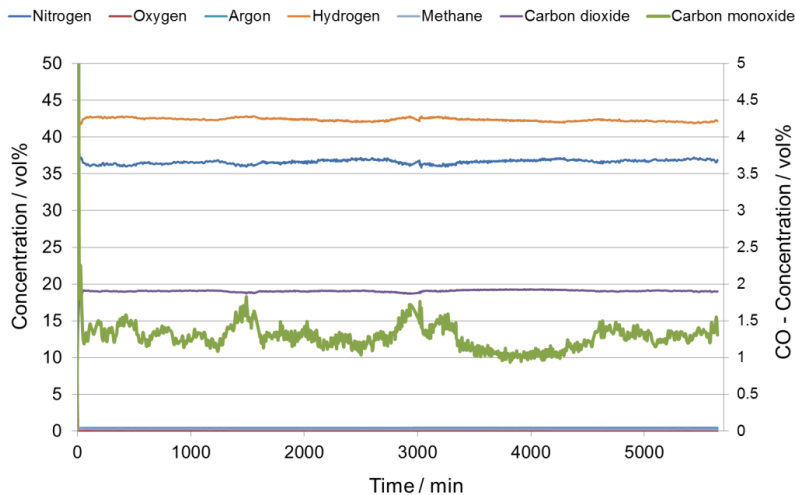


Fig. 76: Concentrations of the main products in the dry product gas after the shift reactor for operation of package AH1 with BTL diesel for a duration of 100 h. Analysis using mass spectrometry

For the rest of the test duration, the system was operated with other diesel and kerosene qualities. Table 14 shows the averaged concentrations of the main products of reforming for operation with NExBTL diesel (120 h), Ecopar diesel (120 h), HC kerosene (136 h) and Ultimate Diesel (13 h). The concentrations in the dry product gas were measured using mass spectrometry. For all tested fuels, the reformer ATR AH1 exhibited stable operation with no evidence of aging.

Fuel	Test duration	x(H ₂)	x(CO)	x(CO ₂)	x(CH ₄)	x(Ar)	x(N ₂)
	h	vol%					
NExBTL diesel	120	37.0	9.0	12.9	0.2	0.5	40
Ecopar diesel	120	37.0	9.4	12.6	0.2	0.5	40
HC kerosene	136	35.7	10.0	12.4	0.2	0.5	41
Ultimate Diesel	13	34.9	11.1	11.6	0.3	0.5	42

Table 14: Analysis of long-term stability of reformer ATR AH1 in system operation with different diesel and kerosene qualities. Concentrations of the main reforming products in the dry reformat measured by mass spectrometry

The reforming by-products were ascertained using FTIR spectroscopy. Table 15 shows the concentrations of ethene, ethane, propene and benzene in the reformat, averaged over the test duration for operation with different fuels. During the test with the fuels NExBTL diesel, Ecopar diesel and HC kerosene, the concentrations of the by-products were at a very low level at the detection limit of the analytical device. During operation with Ultimate Diesel, the by-product concentrations increased slightly but still remained at a subcritical value.

Fuel	Test duration	x(C ₂ H ₄)	x(C ₂ H ₆)	x(C ₃ H ₆)	x(C ₆ H ₆)
	h	ppmv			
NExBTL diesel	120	7	4	3	13
Ecopar diesel	120	6	4	3	14
HC kerosene	136	6	0	0	8
Ultimate Diesel	13	6	29	2	35

Table 15: Analysis of long-term stability of reformer ATR AH1 in system operation with different diesel and kerosene qualities. Concentrations of the by-products of reforming in the dry reformat measured by FTIR

As already mentioned, much higher concentrations of by-products were measured during start-up and shut-down. At the end of the test series, dynamic tests were performed to develop strategies for starting and stopping system operation with lower concentrations. It was found that starting the system with the O₂/C and H₂O molar ratios used for normal system operation and preheating the reforming air gave rise to lower concentrations of by-products.

At the end of system operation, almost no by-products were detected when during shut-down the volume of water supplied to the reformer was increased before the fuel supply was stopped at a constant air volume. This helped to identify promising operating strategies which must now be optimized in future work.

4.2.3 Spray pattern analysis at the nozzle of the ATR AH2

Fig. 77 shows the results of spray pattern analyses using the set arrangement of a fuel injection device comprising a pump manufactured by Thomas Magnete, a reservoir, a pressure regulator, a fast opening/closing magnetic valve manufactured by GSR Ventiltechnik and the pressure swirl nozzle before integration into the ATR AH2.

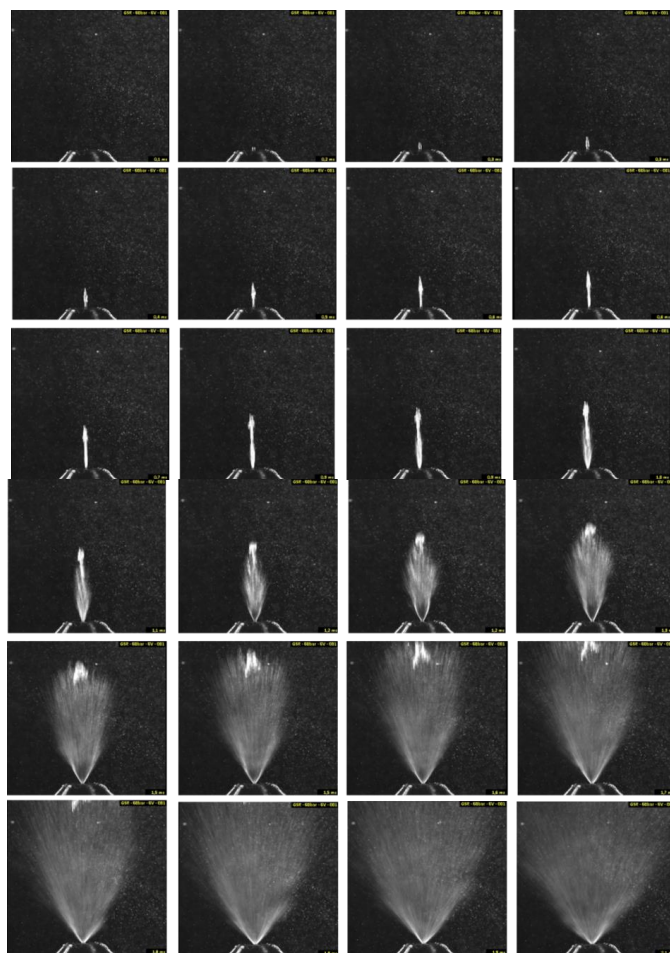


Fig. 77: Series of video stills recorded by the high-speed camera with a frame rate of 13300 fps during pulsed operation of the fuel injection device. This device is a combination of a pump manufactured by Thomas Magnete, a reservoir, a pressure regulator, a fast opening/closing magnetic valve manufactured by GSR Ventiltechnik and a pressure swirl nozzle. The storage pressure was 50 bar, the repetition rate was $16 \frac{2}{3}$ Hz corresponding to 60 ms per stroke. The valve was 50% open. The injection times for a minimal load of 15%, approx. 15% of 67 ms, were a time interval of 10 ms. The pressure swirl nozzle is at the bottom. The formation of the spray pattern is shown.

A video was recorded for each setting. Video rates were 4000–133000 fps (fps: frames per second). A real-time video is usually played back in avi file format at 15 fps. PAL formats or the US format NTSC use 30 fps. The time effect therefore causes an expansion by factors of between 13.67 and 267. The image series in Fig. 77 has a time interval of 75 μ s at 13300 fps for each image. The spray pattern formed in 1.5–2 ms. It is important that a liquid jet no longer appears after less than 1 ms. The development of the pump and magnetic valve in

combination with the technical layout was therefore successfully implemented. For a good-quality spray pattern, a constant operating pressure of 40–50 bar is ideal. The effective minimal load was 10%. The theoretically conceivable load of 5% was not possible. A load of 10% was only possible to a limited extent because the spray did not settle well. As shown in Fig. 77, during spray pattern formation, a small amount of water accumulated in the middle. The impacts of this were still unclear at the time of writing this report.

4.3 Water distribution in the HT-PEFC

The HT-PEFC is operated at 160 °C and normal pressure. The resulting product water therefore leaves the cell in a gaseous aggregate state. A large proportion of the product water is discharged directly via the cathode gas channel. However, the water is most likely formed in the liquid aggregate state in the electrode, which contains phosphoric acid as an electrolyte (to be more exact, a phosphoric acid-water mixture). Some of the product water diffuses within the electrolyte to the anode, where it is then discharged. This principle is shown in Fig. 78.

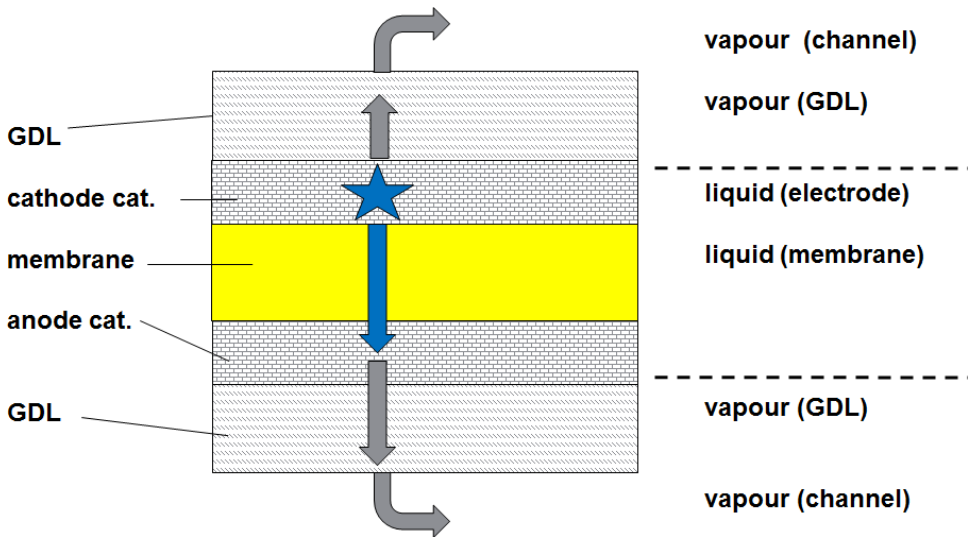


Fig. 78: Water distribution in the HT-PEFC

The distribution of the product water between the cathode and anode is dependent on the material properties of the electrode, the GDL and the membrane as well as on the balance between water production and water evaporation, and thus the local flow conditions.

Stoichiometry anode	Volume flow ratio (Cathode/anode)
2.0	4.3
4.0	1.4
6.0	0.9
<i>Hypothetical reformate operation¹⁰ (for comparison of volume flow)</i>	

¹⁰ Lüke, L., Janßen, H., Kvesić, M., Lehnert, W., Stolten, D., *Int. J. of Hydrogen Energy* **37** (2012), 9171

1.2	1.1
2.0	2.3

Table 16: Flow ratios at the cell outlet (without water, stoichiometry of the cathode = 2)

In a first step, the water distribution was characterized using a standard single cell. The cell has three meanders and an active cell area of 45 cm². A CELTEC P1000 manufactured by BASF was used as the MEA. The cell was operated in parallel configuration with pure hydrogen at the anode and dry air at the cathode. The stoichiometry of the cathode was set to a value of 2. The stoichiometry of the anode was varied in accordance with Table 16. This table shows that the volume flow ratios for operation with hydrogen differ considerably from operation with reformat. At the cell outlet, the product water at the anode and cathode sides is collected by a condenser, as shown in Fig. 79.

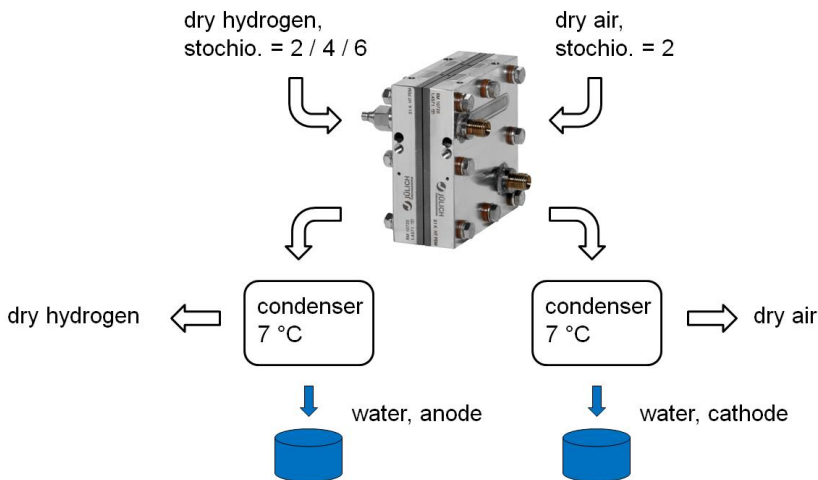


Fig. 79: Experimental setup to determine water distribution

For each operating point, the water was collected for approx. 70 hours in the two collecting vessels. The resulting product water mass flow is presented in Fig. 80. In accordance with Faraday's law, there is a linear relation between current density and water production. However, the slope of the straight line is much greater on the cathode side. This agrees well with the transport pathways depicted in Fig. 78, as water on the way towards the anode must first overcome a diffusion barrier.

If the mass flow ratios of cathode and anode are then plotted, a variation in behavior can be identified as a function of the volume flow (Fig. 81). For a high volume flow at the cathode (anode stoichiometry 2), independent of the current density, five times as much water is discharged via the cathode. If the volume flow ratio is more balanced (anode stoichiometry 4 and 6), then the water discharge at the cathode is only twice or three times that at the anode. The amount of water at the cathode continues to rise with increasing current density.

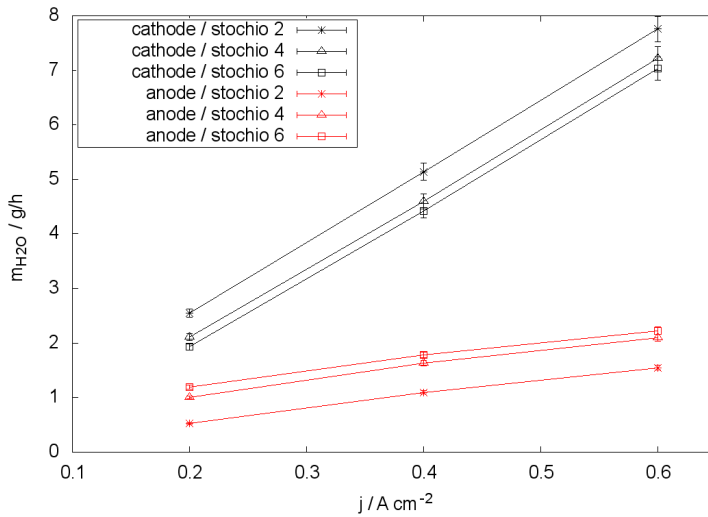


Fig. 80: Product water mass flow as a function of current density

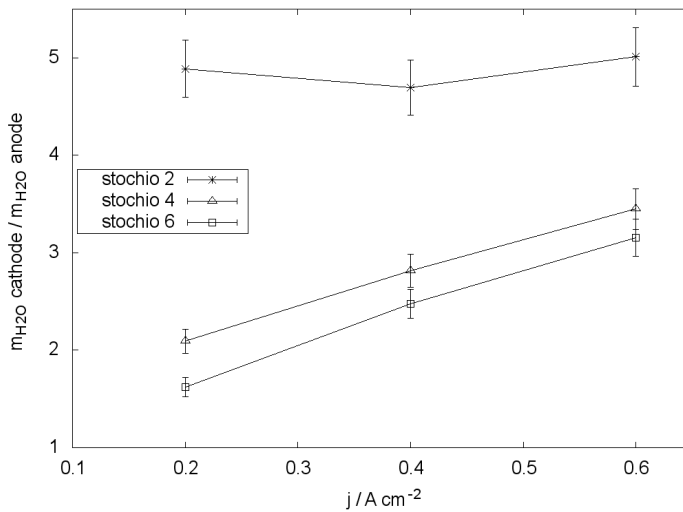


Fig. 81: Product water mass flow ratio

To summarize, the water diffusion flow through the membrane can be altered as a function of the volume flow. The proton conductivity of the membrane is therefore also expected to change. Gases dissolved in water may be transported in this way from the cathode to the anode, which would influence the “crossover effect”. Such effects are also dependent on the flow configuration and the geometry of the flow field.

4.4 Efficiency aspects of high-pressure water electrolysis

Industrial-scale energy storage can be achieved by producing and storing hydrogen. Water electrolysis systems make it possible to produce high-purity hydrogen efficiently and with low emissions. Aside from alkaline electrolysis, polymer electrolyte membrane electrolysis (PEM electrolysis) has developed over the last few years into a technical application for water electrolysis. IEK-3 is working on electrolysis systems and their integration into the energy infrastructure. System efficiency is one of the key development parameters in this context. Activities at IEK-3 aiming to increase the efficiency of water electrolysis systems are presented in this section. Particular attention is given to pressure operation of the electrolyzer.

4.4.1 Introduction and overview

The economic integration of electrolysis systems for hydrogen production hinges on the costs of producing hydrogen. These costs are made up of investment costs, plant utilization and the energy costs of supplying the systems with electric power. Through the efficiency of the system as a whole, the energy costs are transferred directly to the costs of hydrogen production. Increasing the efficiency is therefore an effective measure of cutting the costs of hydrogen production.

The water electrolysis system comprises the cell stack as well as various system components for supplying and cooling the cell and system components for gas conditioning. When considering system efficiency, these components must be taken into account. Fig. 82 shows the system setup. The efficiency of the stack as the central component is discussed first, followed by the system components.

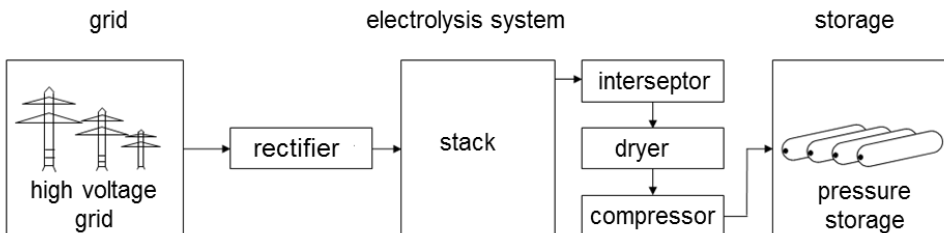


Fig. 82: Configuration and integration of water electrolysis systems

4.4.2 Stack efficiency

To increase the power density, single cells are connected to each other in stacks, which then serve as the central component of an electrolyzer. The stack efficiency in this set up is almost equal to the cell efficiency. The cell efficiency is the sum of the voltage efficiency and Faraday efficiency. The voltage efficiency is reduced by the heat produced during electrolysis. The Faraday efficiency is calculated from the loss of hydrogen produced in the cell, which is mainly determined by cross-permeation of the gases formed through the membrane. Both efficiencies are explained in the following and the impact they have on the total efficiency of the cell is determined.

4.4.2.1 Voltage efficiency

To electrochemically split water into hydrogen and oxygen, an electrical load is required. This is determined by the ratio of voltage to current, the current-voltage characteristics. This in turn is predominantly determined by the setup, the components used and the selected cell temperature. Ideally, the Nernst voltage should be all that is needed to split water. It is calculated from the Gibbs free energy for water electrolysis. In real situations, losses occur that increase with increasing current density. These include kinetic activation losses caused by the electrochemical reactions, ohmic losses and mass transport losses.

Activation losses

For activation losses, the condition of the electrodes is extremely important. Water electrolysis with an acidic polymer electrolyte membrane means that water is oxidized at the anode. The protons formed during this process are reduced at the cathode. These reactions are accelerated by catalysts, which are applied with a polymer carrier to the membrane. This then results in the electrodes.

The quality of the electrodes is therefore determined mainly by the catalyst. To reduce overpotentials, catalysts with a high activity are required for the electrolysis reaction. The catalyst should also have a large surface area to ensure a high utilization of the catalyst material. The electrode must be designed with the catalyst in such a way that degradation is minimized during electrolyzer operation. During operation, different mechanisms give rise to degradation, which then causes a drop in efficiency over operating time. For PEM electrolysis, platinum nanoparticles are used as the catalyst for the cathode and iridium oxide nanoparticles for the anode.

Ohmic losses

Ohmic losses occur in the cell during the conduction of protons and electrons. The ohmic resistance of a cell is determined mainly by the proton conductivity of the membrane. The cell resistance is therefore roughly proportional to the membrane thickness. Not only the membrane but also the electrodes must exhibit a high proton conductivity. This is achieved by means of a polymer electrolyte binder, which is applied with the catalyst material to the membrane. This binder also serves as the catalyst's mechanical interface. The electron conductivity of the electrode is realized by the catalyst material. To ensure that the electrode has a high proton and electron conductivity, an optimal ratio of polymer binder to catalyst material must be chosen. All of the components that supply media downstream of the electrodes must also have a high electron conductivity. This also applies to the contact points to ensure low contact resistances.

Mass transport losses

The cell is supplied with water and gases produced are removed via porous layers and a channel structure on the anode and cathode sides. These components also support the membrane mechanically during pressure operation of the electrolyzer. At increasing current densities, an adequate supply to the cell is essential. If this cannot be ensured, losses occur known as mass transport losses. Mass transport losses limit the possible current density for large current ranges.

Fig. 83 shows the loss mechanisms of the cell and the resulting current-voltage characteristics. Ongoing research activities at IEK-3 focus on methods of reducing these losses in order to increase the voltage efficiency. The degradation mechanisms of different components are also investigated so that the cell design can be adapted accordingly to achieve long lifetimes and high efficiencies.

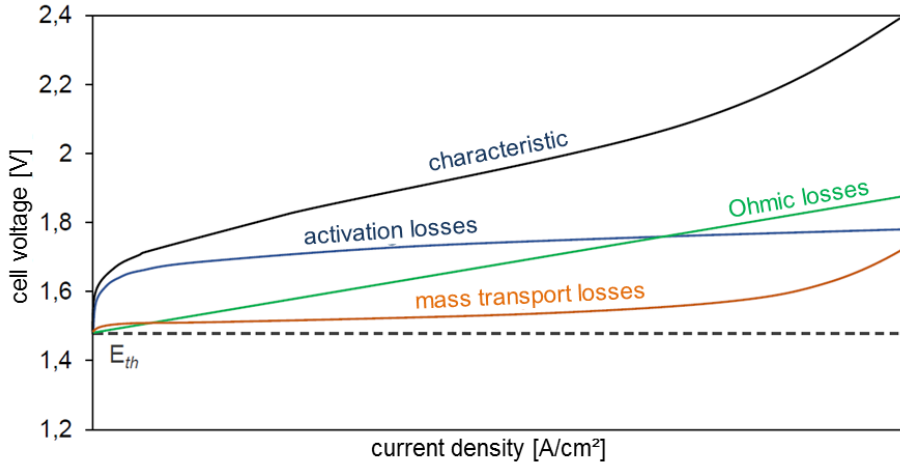


Fig. 83: Current-voltage characteristics and loss mechanisms of PEM electrolysis

4.4.2.2 Faraday efficiency

During electrolyzer operation, the gases produced cross-permeate through the membrane. This is mainly caused by diffusion, which is determined by the concentration gradients of the gases across the membrane. In addition to the gas concentration, which is controlled by the set pressures, cross-permeation is dependent on the permeability of the membrane (material property) and its thickness. Fick's law of diffusion means that gas permeation is inversely proportional to the membrane thickness.

Hydrogen, which permeates into the anodic chamber, cannot subsequently be used and must therefore be considered a loss. In addition to safety issues, the mixing of hydrogen and oxygen also causes a drop in efficiency. Oxygen also continues to enter the cathode chamber. Here, the oxygen is catalytically combusted with the prevailing hydrogen by the platinum catalyst. The hydrogen converted during this process is therefore also lost, which means that oxygen permeation also causes a drop in efficiency.

For subsequent technical application, hydrogen is stored under pressure. As an almost adiabatic compression can be realized within the electrolyzer, the energy required for compression inside the electrolyzer is lower than that required for mechanical post-compression. However, this mechanism is limited by gas permeation because the pressure increase causes an increase in the concentration gradients. Increased concentration gradients therefore cause increased gas permeation and thus lead to a lower Faraday efficiency. To counteract this loss, the equal pressure principle was developed to bring the oxygen side up to the same pressure level as the hydrogen side. It was shown that this does indeed increase gas purity. However, this is accompanied by increased oxygen permeation

which means that the efficiency continues to decrease. In practice, an optimal pressure level must therefore be found.

4.4.2.3 Faraday

The cell configuration must account for the aforementioned mechanisms. The thickness of the membrane is a particularly important design parameter. It also determines the ratio of cell resistance to gas permeation. While the cell resistance increases proportionally with membrane thickness, the gas permeation is inversely proportional to the membrane thickness.

The current density has little impact on gas permeation through the membrane. However, if more hydrogen is produced at higher current densities, then an almost constant loss caused by permeation is relatively less pronounced: accordingly, the percentage of hydrogen lost due to permeation through the membrane decreases with increasing current density. The membrane thickness should therefore be adjusted in line with the following properties:

- ohmic resistance for proton conductivity,
- hydrogen and oxygen permeability,
- temperature, which determines the first two properties,
- pressure at the cathode and anode sides,
- applied current density.

Such optimization of membrane thickness has been dealt with in a separate publication¹¹. The properties of proton conductivity and hydrogen and oxygen permeability were determined separately outside the electrolysis cell and were taken as starting parameters for the model. These calculations are independent of the electrochemical properties of the electrodes.

In addition to the efficiency loss, hydrogen permeation through the membrane also causes a safety risk: a gas mixture in excess of 4% H₂ in O₂ is an explosive mixture, the formation of which must be prevented by process management. With the increasing current density, the hydrogen content in the gas mixture decreases because although the permeation rate of oxygen through the membrane is almost constant, the production rate of the oxygen is higher. The anodic gas mixture is therefore shifted to the oxygen side.

¹¹ Schalenbach, M., Carmo, M., Fritz, D. L., Mergel, J. & Stolten, D. Pressurized PEM water electrolysis: Efficiency and gas crossover. *Int. J. Hydrogen Energy* 38, 14921–14933 (2013).

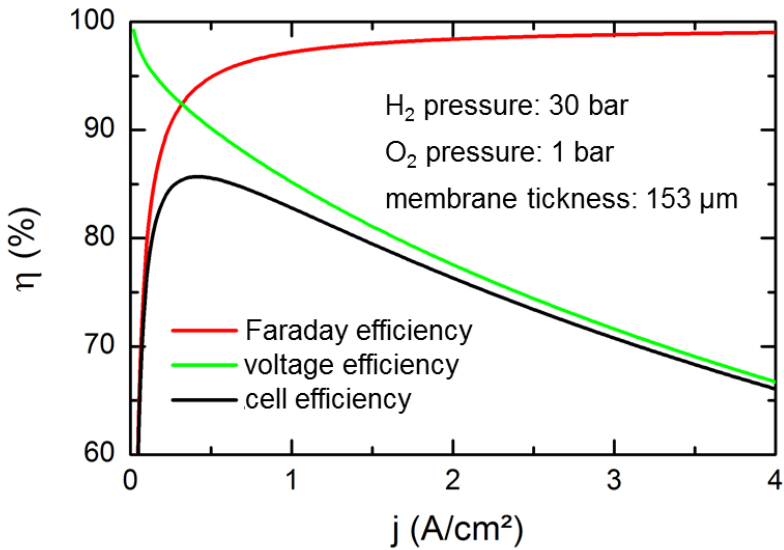


Fig. 84: Modelled efficiency of a PEM electrolyzer for differential pressure operation

The voltage efficiency, Faraday efficiency and cell efficiency curves are shown as a function of current density in Fig. 84. As discussed above, the heat produced by the overpotentials increases with current density, which lowers the voltage efficiency. The Faraday efficiency increases with increasing current density. Optimum cell efficiency therefore depends on the operating conditions of the electrolyzer.

4.4.3 System efficiency

To operate an electrolysis stack, further system components are needed but their power consumption reduces the total efficiency of the system. The individual system components are shown in Fig. 82. A rectifier unit is usually needed to supply the stack with power. This unit exhibits a load-dependent efficiency. Using established technologies, such as chloralkali electrolysis, efficiencies above 98% have already been achieved. However, this loss must still be accounted for in the overall chain because it occurs before the actual electrolysis and therefore directly reduces the available power.

The waste heat produced by overpotential must be dissipated to prevent damage to the components, particularly to the membrane. Cooling circuits on the anode and cathode sides fulfill this function. The cooling circuits also provide the anode side with water for the reaction. They are operated with pumps, which also reduce the efficiency of the system as a whole.

The product gases are separated from the water after the electrolyzer, but they are still saturated with water vapor. The produced hydrogen must therefore be dried for storage. It was found that gas cooling makes it possible to remove large quantities of water by means of condensation. This considerably reduces the energy required for subsequent fine drying. Fine drying is usually performed with an adsorption unit by changing the temperature.

The subsequent mechanical compression has a substantial impact on the total efficiency. Thermodynamically, the energy required for gas compression is calculated from the

compression ratio. This means that a relatively high expenditure of energy is required to achieve a low pressure level. Therefore, low pressure levels should already be achieved during electrolysis operation because a higher efficiency can be achieved here during compression. However, with an increasing pressure level, the Faraday efficiency decreases, also resulting in an optimum. An additional reduction in the energy expenditure is possible by means of multistage compression with cooling between each stage.

An optimal design therefore depends on the requirements for pressurized storage. IEK-3 will use models to develop an electrolyzer design optimized for operating parameters, particularly for the pressure level in the electrolyzer.

4.5 Market launch of fuel cells for cars with renewable hydrogen

The growing installed capacity of renewable energy means that future energy systems can be assumed to have an increasing range of both positive (energy shortage) and negative (excess energy) residual loads. Power-to-gas concepts exploit excess power to produce hydrogen and oxygen via water electrolysis. This excess power will increasingly be supplied by renewables in the future energy mix. Fig. 85 shows three ways the hydrogen produced in this way can be used^{12 13}:

- Feeding limited quantities of hydrogen directly into the natural gas grid.
- Methanation of hydrogen and methane feed-in into the natural gas grid.
- Direct use of hydrogen in the transportation sector or in industry, accompanied by the expansion of appropriate hydrogen infrastructure.

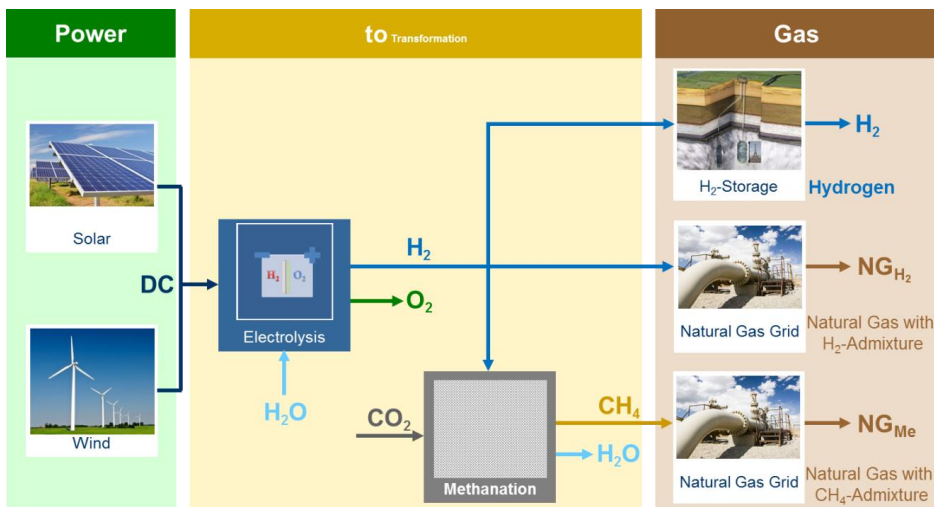


Fig. 85: Power-to-gas concept. NG_{H_2} : natural gas with H_2 admixture; NG_{Me} : natural gas with methane admixture.

IEK-3 showed that directly using hydrogen in the transportation sector utilizing a hydrogen pipeline network is the most economically attractive variant (before-tax analysis) of all three pathways¹². The reason for this is two-fold (cf. Fig. 86).

- The low reference costs of natural gas at approx. 4 c/kWh preclude the economic integration of hydrogen (production costs: 15 c/kWh) and methane (production costs: 23 c/kWh).
- The comparatively high investment costs of hydrogen at the filling station of 16 c/kWh and 22 c/kWh (costs of gasoline at 8 c/kWh and halved fuel consumption of fuel cell

¹² Schiebahn, S. et al., Power to Gas in: Stolten, D.; Scherer, V. (Eds.), Transition to Renewable Energy Systems, Wiley-VCH, 2013, pp. 813-849. ISBN 978-3-527-33239-7

¹³ Robinus, M.; Stolten, D.: Power-to-Gas: Quantifizierung lokaler Stromüberschüsse in Deutschland anhand unterschiedlicher Windenergie-Ausbaustufen. 9. Internationale Energiewirtschaftstagung Vienna, 2015.

vehicles) make an economic integration of hydrogen practicable in the transportation sector.

Even if hydrogen can be transported from the production plants to the filling stations in trailers during the early phase of market launch, it still makes sense to think about pipeline transport when larger quantities are involved.

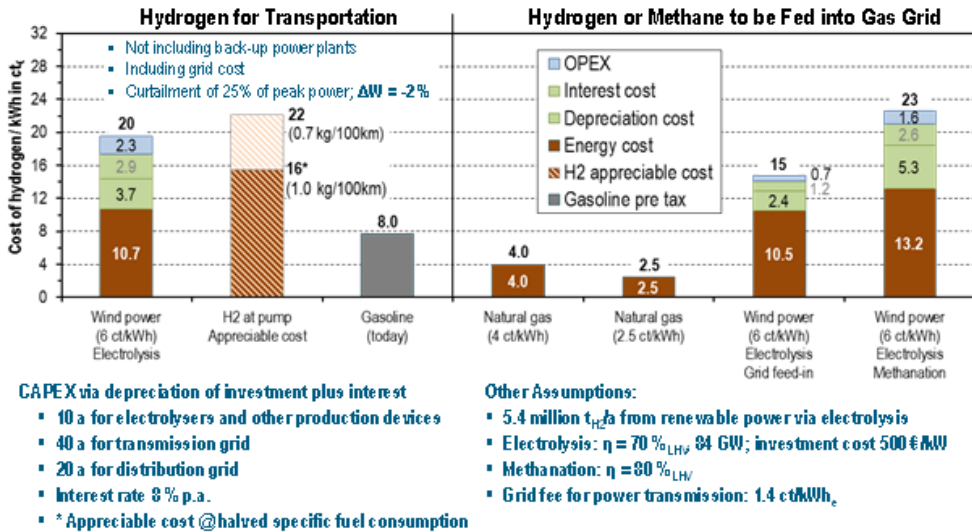


Fig. 86: Cost analysis of power-to-gas pathways from Fig. 85. Hydrogen feed-in into the existing natural gas grid (far right), methanation of hydrogen and feed-in into the natural gas grid (second from the right) and utilization of hydrogen in the transportation sector via a hydrogen pipeline network (far left)¹².

The hydrogen pipeline network designed at IEK-3 is capable of supplying 75% of passenger cars in Germany with a total demand of 5.4 megatonnes hydrogen (cf. Fig. 87, left)¹⁴. It comprises a transmission network (12,000 km long) and a distribution network with a length of between 31,000 km and 47,000 km. If this hydrogen pipeline network (transmission and distribution) is fully expanded and if electrolyzers and storage are installed in response to demand, then the break-even point (before tax) will be reached somewhere between 2.2 megatonnes and 1.6 megatonnes [8]. The higher value applies to a mean hydrogen consumption of the FCV of 0.7 kg/100 km, and the lower to a consumption of 1.0 kg/100 km. If in addition to electrolyzers, the distribution network and filling stations were also expanded in response to demand, a surface plot results showing the before-tax costs for each phase of expansion (cf. Fig. 87, right).

Cost-optimized expansion is represented by the bold black curve in the foreground.

¹² ibid.

¹⁴ Krieg, D.: Konzept und Kosten eines Pipelinesystems zur Versorgung des deutschen Straßenverkehrs mit Wasserstoff. 228 pages. Forschungszentrum Jülich, Central Library: Jülich, 2012. ISBN 9783893368006

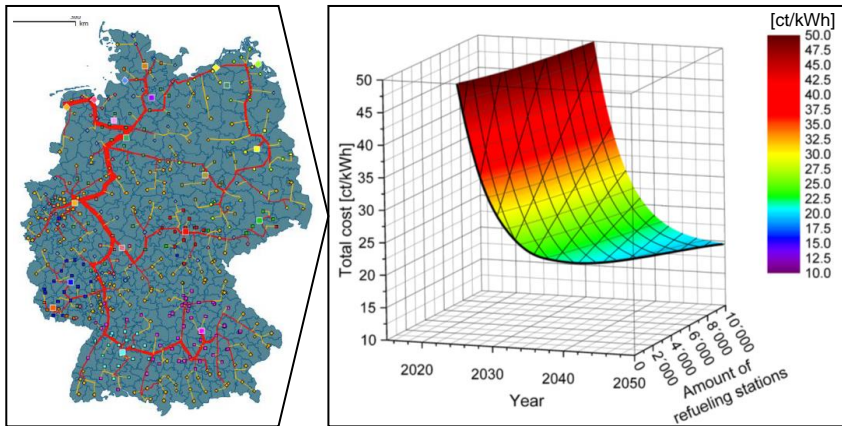


Fig. 87: Hydrogen pipeline network supplying the transportation sector with hydrogen (left) and cost-optimized configuration (right)^{14 15}.

In previous infrastructure analyses (e.g. ¹⁴), the most important production sites for hydrogen were in North Rhine-Westphalia (coal gasification) and in the north of Germany (offshore wind power). For a future scenario, more heavily based on renewable power, the supply sources must be adapted accordingly. IEK-3 is currently developing a model that will determine the residual load from renewables at a municipal level (cf. Fig. 88). For example, the grid load¹⁶ and provision of power from onshore and offshore wind energy¹³ are included in the residual load calculation.

¹⁵ Stolten, D., et al.: The Potential Role of Hydrogen Technology for Future Mobility How Can this Improve Our Life? In: International Federation of Automotive Engineering Societies: (2014).

¹⁶ Robinius, M., et al.: Lastmodellierung und -visualisierung mittels Geoinformationssystemen. http://portal.tugraz.at/portal/page/portal/Files/i4340/eninnov2014/files/lf/LF_Robinius_Lastmodellierung.pdf. Last updated: 7 January 2015.

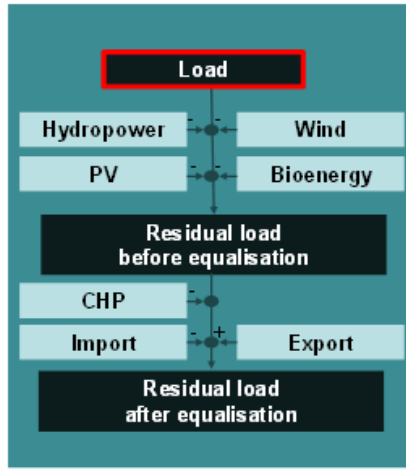


Fig. 88: Residual load calculation

Fig. 89 shows the highest and lowest loads calculated for 2010, which was the year with the highest power consumption (513 TWh) in the period from 2010 to 2013. The analysis of load distribution showed that positive residual energy (power demand for controllable power stations) in the load centers, such as the Ruhr area, clearly dominate and negative residual energy, i.e. power surplus, is mainly concentrated in the north of Germany. In addition to the population density, the technical and economic potential for the installation of plants utilizing renewables is decisive.

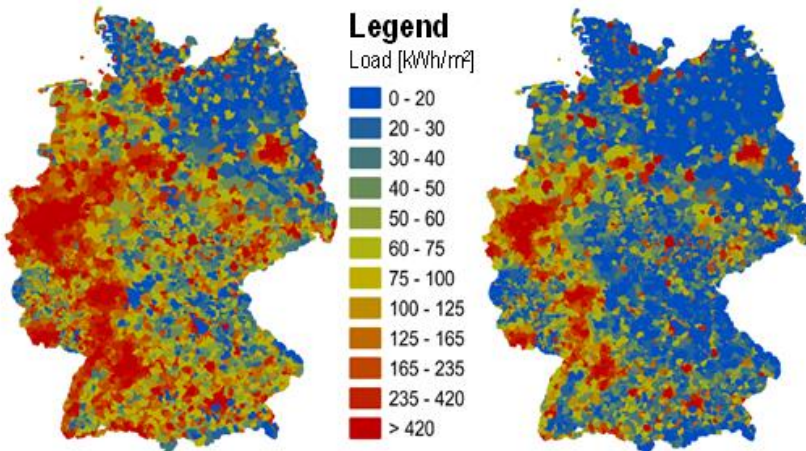
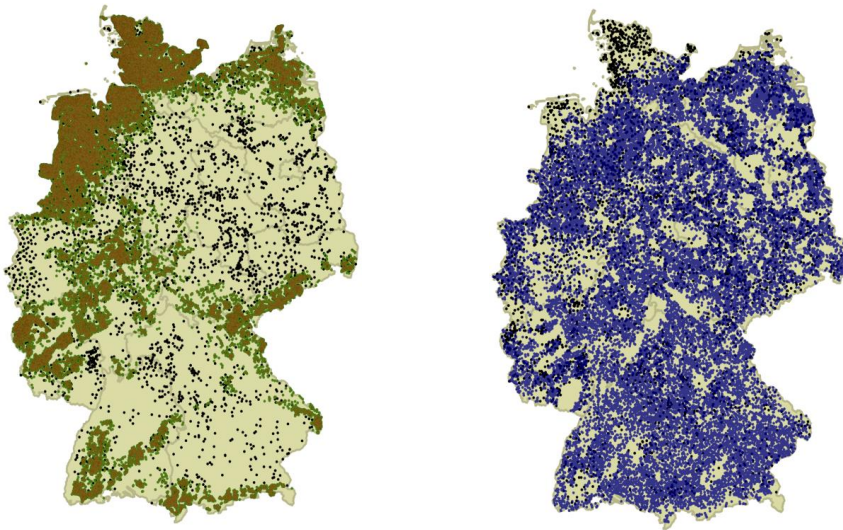


Fig. 89: Load per square kilometer in 11,268 municipalities in Germany at the point in time when load was greatest (84 GW) on 1 December 2010 at 18:00 (left) and when load was smallest (36 GW) on 6 June 2010 at 18:00¹³.

Fig. 90 shows the distribution of the sites of onshore wind turbines according to different investment decision-making parameters: (i) cost optimization, (ii) profit maximization, (iii)

maximum compensation and (iv) site quality in 2006. The cost-optimized expansion (i) basically corresponds to the profit-maximized (ii) or energy-optimized expansion (cf. Fig. 90, top left). This means that although the site quality has an effect on the level of compensation per kWh, this is cancelled out by the higher number of full-load hours. The maximum compensation defined by the EEG 2012 (iii) (Fig. 90, top right) and EEG 2014 (Fig. 90, bottom left) accounts for other sites than those in reality. If the expansion is modelled according to EEG compensation, then in contrast to the actual expansion, wind turbines would be erected at far less suitable sites. Finally, the real distribution of site qualities in 2006 (iv) [¹⁷, p. 19] is used as the basis for a random erection of wind turbines (Fig. 90, bottom right). The distribution of wind turbines in this case adequately reflects the situation in 2014. Therefore, it was shown that the expansion of wind energy on land to date has tended to follow the expansion targets of the federal states and cost optimization and profit maximization featured less as motivation. It should, however, be noted that a cost-optimized expansion of wind energy in this model does not fully represent an economic expansion. The costs of integrating wind energy into the system would then have to be considered, for example, the cost of network integration.



¹⁷ Agora Energiewende: Vergütung von Windenergieanlagen an Land über das Referenzertragsmodell. http://www.agoraenergiewende.de/fileadmin/downloads/publikationen/Studien/Referenzertragsmodell_Wind/Studie_Referenzertragsmodell_Wind_WEB.pdf. Last updated: 18 November 2014.

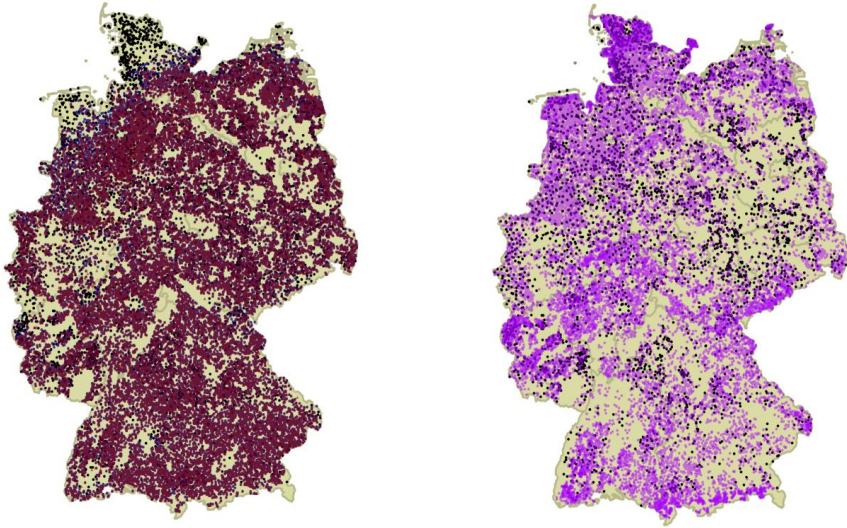


Fig. 90: Sites of wind turbines according to optimization criteria: costs (top left, green), profit (top left, red), and compensation (top right and bottom left, blue) and site qualities as of 2006 (bottom right, purple); 24,762 real sites in 2014 (all images, black dots).





5

Outlook

Outlook for New R&D Projects

- Energy storage and hydrogen initiatives in the Helmholtz Association
- Hydrogen system solutions
- Batteries for future energy sectors



5.1 Development of a reversible system based on an SOFC

5.1.1 Initial situation and objectives

Fluctuating power production associated with utilizing excess wind or solar power for hydrogen production is a big challenge that electrolysis systems must overcome. A system capable of producing hydrogen during periods of excess power and of producing power during off-peak periods would be extremely advantageous. In principle, the combination of a high-temperature fuel cell (SOFC) and high-temperature electrolysis (SOE) has the potential to do just this. The first tests with small SOFC stacks have already shown that the same stack can be easily operated in electrolysis mode with a reversed current direction simply by applying an external voltage. However, these tests also revealed that the materials used must be optimized in order to achieve the required low degradation, particularly for high current densities in the range of 1 A/cm². The system must also be engineered to allow the same unit to be switched (rSOC = reversible solid oxide cell) without modifications from fuel cell operation to electrolysis operation. R&D at IEK-3 aims to realize this for a 5 kW rSOC system within the next three years.

5.1.2 Priority at IEK-3

IEK-3 is working on the design and electrochemical characterization of the stack, as well as system configuration, including the necessary components as well as the realization and testing of the 5 kW system.

5.1.3 Methodology

For stack characterization in electrolysis mode, two test stands for short stacks were modified to additionally enable operation in electrolysis mode as well as automatic switching from fuel cell operation to electrolysis operation. Two new test stands were set up for the same tests but with larger stacks in the kW range. In addition to standard characteristic measurements at different temperatures and long-term measurements at different current densities and temperatures, stack impedance measurements are also becoming more important in analyzing the long-term behavior of individual cell and stack components. Together with experts from the other institutes involved in the development, the stack undergoes intensive post-test examination, ranging from chemical analysis using SEM/EDX to TEM investigations. The behavior of the stack is also analyzed with CFD and FEM modeling. This modeling provides important information on weaknesses and indicates where improvements could be made in the design and operation.

System development builds on experience with SOFC system engineering and begins with the development of simulation tools for the individual system components. These are then combined in a full system simulation. This is the basis for developing a simple system concept together with the appropriate operating strategy for fuel cell and electrolyzer operation, at best simply by switching the current direction. Following this, the critical system components are designed (e.g. steam generator, preheater, heating) with the aid of a dynamic system simulation based on Matlab/Simulink and tests in special component test setups. These results are subsequently incorporated into the real system dimensioning and design. Finally, the system is set up and operated. Sophisticated instrumentation and

measurement technology combined with test results enable further optimization of the stack and systems engineering.

5.1.4 Results

A two-layer short stack in the standard F10 design was operated in both fuel cell and electrolysis mode (see Fig. 91). The cells were based on a fuel electrode made of a 1 mm thick Ni/8YSZ substrate coated with a 10 μm thick 8YSZ electrolyte and a 40 μm thick air electrode made of lanthanum strontium cobalt ferrite (LSCF) sintered onto a diffusion barrier layer made of gadolinium-doped cerium oxide (GDC). First, the stack was operated continuously for 4000 h in the fuel cell mode at 750 $^{\circ}\text{C}$ and 0.5 A/cm^2 , during which aging was 0.6%/kh. Operation was subsequently switched to steam electrolysis and the stack was operated at -0.3 A/cm^2 for 2000 h at 810 $^{\circ}\text{C}$. No measurable aging was detected.

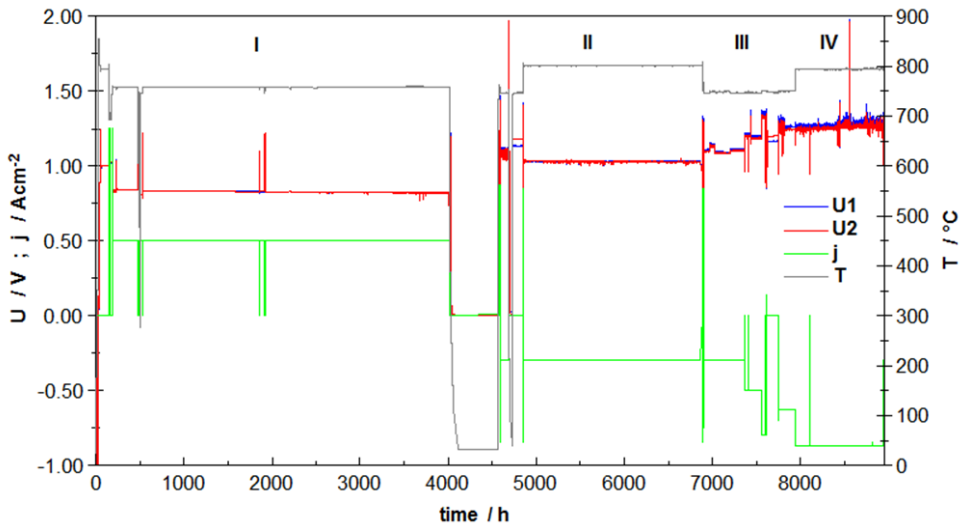


Fig. 91: Voltage, current density and temperature as a function of operating time in SOFC and SOE mode of operation: phase I – SOFC operation at 0.5 A/cm^2 and 750 $^{\circ}\text{C}$; phase II – SOE operation with $\text{H}_2/\text{H}_2\text{O}$ 1:1 at -0.3 A/cm^2 and 810 $^{\circ}\text{C}$; phase III – SOE operation with $\text{H}_2/\text{H}_2\text{O}/\text{CO}_2$ 2:1:1 at -0.3 to -0.8 A/cm^2 and 760 $^{\circ}\text{C}$; phase IV – SOE operation with $\text{H}_2/\text{H}_2\text{O}$ 1:1 at -0.875 A/cm^2 and 810 $^{\circ}\text{C}$

In the next phase between 6900 h and 7600 h (Fig. 91, III), the stack was operated with hydrogen, steam and CO_2 in co-electrolysis mode at -0.3 A/cm^2 and -0.5 A/cm^2 (and for a short time at -0.8 A/cm^2). The furnace temperature was 760 $^{\circ}\text{C}$. For the different and sometimes relatively short operating times at the various settings, aging was between 1%/kh and 6%/kh. The reason for increased aging in the co-electrolysis mode has yet to be investigated. During the different tests in co-electrolysis mode, gas chromatography was used to measure the composition of the syngas at the stack outlet. There was very good agreement with the calculated equilibrium compositions. The reverse shift reaction was

completed in full and the methane contained in the product gas was negligible at high operating temperatures. Finally, the stack was operated for 1000 h again at 810 °C in steam electrolysis mode but this time at -0.875 A/cm^2 (Fig. 91, IV). Aging in the time interval between 8000 h and 9000 h was $1.5\%/kh$.

Fig. 92 shows the current-voltage characteristics of the stack for fuel cell and electrolysis operation at a furnace temperature of 800 °C and a $\text{H}_2/\text{H}_2\text{O}$ gas composition of 1:1. It depicts the curves before and after 2000 h operation in the steam electrolysis mode at -0.3 A/cm^2 (phase II in Fig. 91), for which no aging was detected, and the concluding characteristics after 9000 h, for which only a small deterioration was detected.

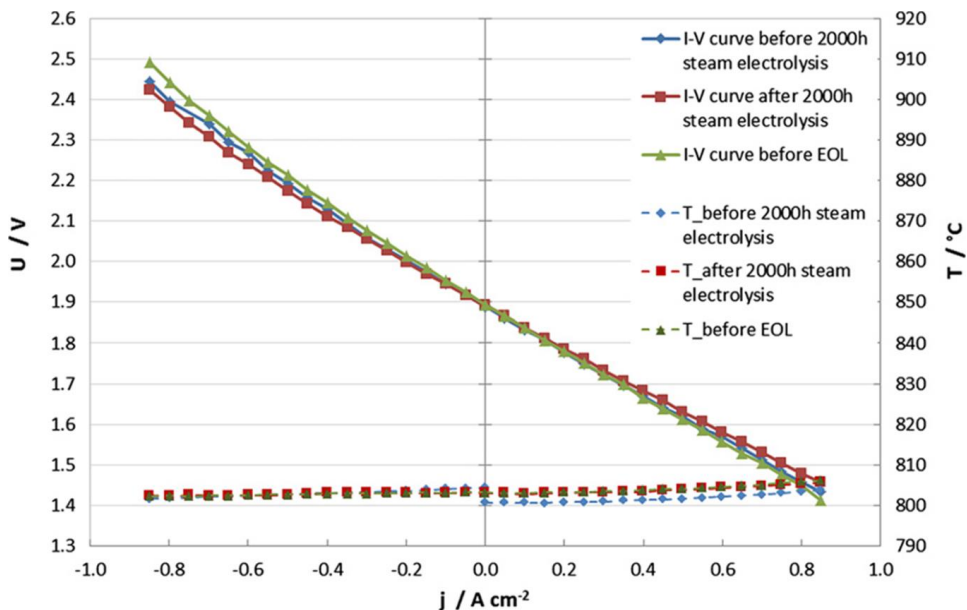


Fig. 92: Current-voltage characteristics of the two-layer short stack at a furnace temperature of 800 °C and gas composition of $\text{H}_2/\text{H}_2\text{O}$ of 1:1

The basic feasibility of reversible operation was also demonstrated with a two-layer short stack. The stack was operated with one-hour cycles alternating between fuel cell and electrolysis mode with one minute idling between each switch. A total of 310 cycles were run at 0.3 A/cm^2 and 700 °C, 750 °C and 800 °C and aging was comparable to pure fuel cell operation. After 1100 hours of operation, a malfunction in the test stand caused a breakdown in the steam supply. This gave rise to a considerably poorer performance and increased aging after the system was restarted (phases 4 and 5 in Fig. 93) due to damage caused by the short phase of electrolysis operation with insufficient steam supply.

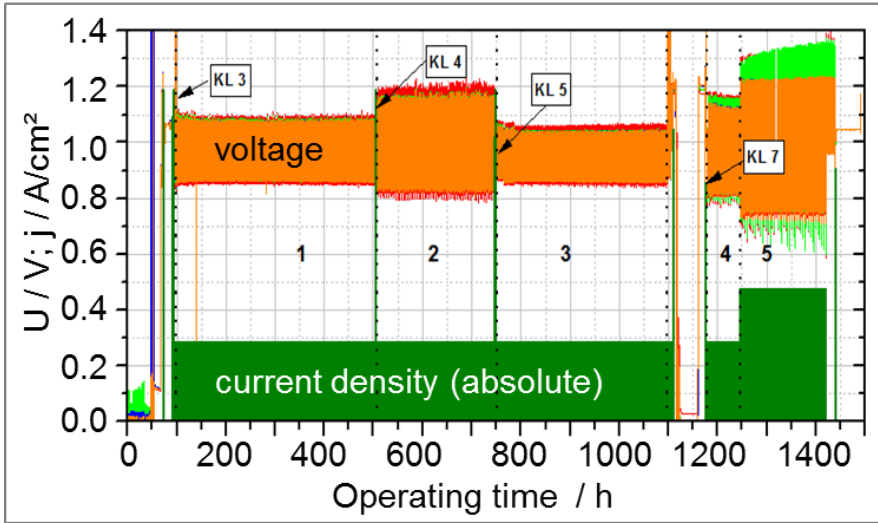


Fig. 93: Current density and mean cell voltage over time of a two-layer short stack at a furnace temperature of (1) 750 °C, (2) 700 °C and (3) 800 °C and a gas composition of H₂/H₂O of 1:1 during reversible operation (1 h fuel cell – 1 minute idling – 1 h electrolysis)

As high-temperature electrolysis has the potential for a particularly high electrical efficiency, promising system configurations and operating parameters were investigated in an energy systems analysis. To ensure comparable results, four efficiencies were defined for different energy consumptions.

η_1 is the relationship between the calorific value of the hydrogen produced and the power consumption of the electrolyzer stack ($P_{\text{electrolyzer}}$), the air blower and fuel recirculation blower ($P_{\text{Cp},i}$) and all other power consumers in the system (P_{Add}). Low- and high-temperature heat for steam generation and superheating of the gases are provided in other processes. The hydrogen is produced at atmospheric pressure.

$$\eta_1 = \frac{H_u^0}{P_{\text{Electrolyzer}} + \sum_{i=1}^2 P_{\text{Cp},i} + P_{\text{Add}}}$$

To effectively store the hydrogen, it must be compressed. A three-stage compressor with intermediate cooling is represented by η_2 .

$$\eta_2 = \frac{H_u^0}{P_{\text{Electrolyzer}} + \sum_{i=1}^2 P_{\text{Cp},i} + P_{\text{Add}} + \sum_{i=3}^5 P_{\text{Cp},i}}$$

As waste heat is not available in most cases at sufficiently high temperature levels (at least 800–900 °C), this additional energy must be incorporated as additional consumption. This is done by η_3 as $P_{\text{HT},i}$ for the fuel gas and air sides.

$$\eta_3 = \frac{H_u^o}{P_{\text{Electrolyzer}} + \sum_{i=1}^2 P_{\text{Cp},i} + P_{\text{Add}} + \sum_{i=3}^5 P_{\text{Cp},i} + \sum_{i=1}^2 P_{\text{HT},i}}$$

If at least some of the low- and medium-temperature heating energy must be provided by the system itself, P_{MT} in η_4 can be used. Optimum heat use in the system is included in this.

$$\eta_4 = \frac{H_u^o}{P_{\text{Electrolyzer}} + \sum_{i=1}^2 P_{\text{Cp},i} + P_{\text{Add}} + \sum_{i=3}^5 P_{\text{Cp},i} + \sum_{i=1}^2 P_{\text{HT},i} + P_{\text{MT}}}$$

An important variable in these calculations is the cell voltage. Three cases were considered:

- the cell voltage is less than the thermoneutral voltage – the stack must be heated externally (high-temperature heat is required)
- the cell voltage is equal to the thermoneutral voltage – the stack must neither be heated nor cooled (no high-temperature heat required)
- the cell voltage is greater than the thermoneutral voltage – the stack must be cooled (increased mass flow on the air side)

System calculations gave rise to the following results:

- The efficiency η_1 is between 90% (operation above the thermoneutral voltage) and 104% (operation below the thermoneutral voltage).
- The efficiency η_2 is between 82% (operation above the thermoneutral voltage) and 93% (operation below the thermoneutral voltage). Compression of the produced hydrogen to 7 MPa is included here.
- The efficiency η_3 is between 74% (operation above the thermoneutral voltage) and 80% (operation below the thermoneutral voltage). All of the energy for steam generation is provided by an external process. The high-temperature heat is fed into the system by an electrical heating unit.
- The efficiency η_4 is approx. 74% in all cases as long as the stack is directly electrically heated when operated below the thermoneutral voltage. If the waste heat is not utilized in the system, the efficiency decreases in all cases to approx. 63%.

5.2 Metallic bipolar plates for HAT-PEFCs

At present, graphitic bipolar plates are used for HT-PEFCs due to aggressive operating conditions. The advantage of graphitic materials is long-term stability, but this is often offset by low volumetric and gravimetric power densities as well as high manufacturing costs. These power densities can be increased using metallic bipolar plates. The material properties and low material thickness of the bipolar plates give rise to design options for flow distributors that cannot be applied to graphitic materials.

An important aspect in the transition to metallic materials is the selection of materials. The very aggressive conditions within the stack (phosphoric environment, temperature approx. 160 °C) make it necessary to test the suitability and plasticity of materials and combinations of materials. In future, work will therefore focus on researching corrosion phenomena. In addition, known coatings will be evaluated and new coatings developed for metallic bipolar plates. The influence of phosphoric acid on corrosion phenomena in model systems will be presented in the following. In further work, tests will be performed under real operating conditions on single cells.

5.2.1 Influence of temperature on degradation of passivation layers

The free corrosion potential E_{cor} is used here to investigate the temperature dependence of passivation layers on the metal surfaces. E_{cor} describes the mixing potential of the corrosion elements between the oxidation and reduction reaction when no external potential is applied. In general, the higher the E_{cor} , the greater the electrochemical stability of the metallic substrate in aggressive media. The experiments aimed to understand the temperature-dependent formation and degradation of passivation layers in phosphoric acid, which influence the contact resistance at the interface between the bipolar plates and gas diffusion layer and thus also have a considerable impact on the cell performance. Measurements of the fuel cell were made under open circuit voltage (OCV) with no polarization current.

Simulated HT-PEFC conditions were used in a three-electrode measurement setup with a volume of 175 ml 85 wt% H_3PO_4 . The high electrolyte volume prevented the saturation of the electrolyte with metal ions, which would lead to reduced corrosion processes. After the mechanical and electrochemical erosion of the oxide layer formed upon contact with atmospheric oxygen, measurements of E_{cor} began at room temperature. After 20 h, the temperature increased with a heating rate of 1 °C min⁻¹ (within 2 h) to 130 °C and remained at this level for another 2 h. Later in this section, exposure tests at temperatures up to 160 °C are described. They were conducted in an open vessel with 50±1 g phosphoric acid. In this system, after only a few hours, a H_3PO_4 concentration of >95 wt% was found, which also corresponds to the electrolyte composition in the HT-PEFCs. The relatively high electrolyte volume is also intended to ensure subsaturated conditions.

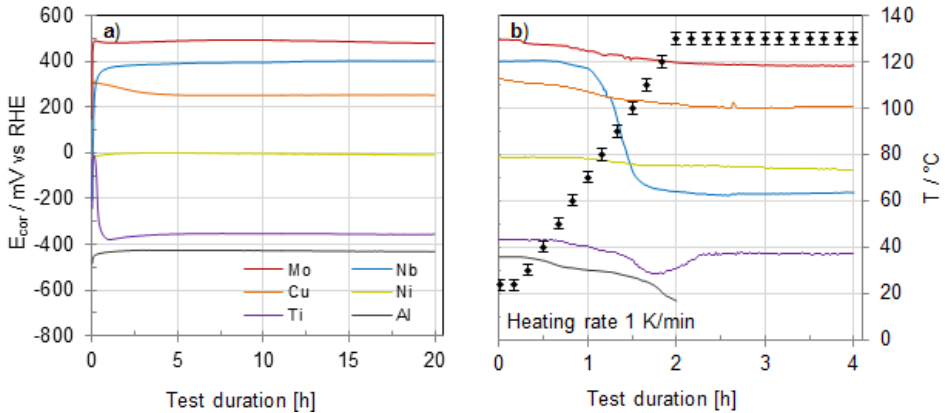


Fig. 94: E_{cor} in 85 wt% H₃PO₄ of technical metals over time at a) room temperature and b) a temperature rise up to 130 C.

Fig. 94 a) shows the E_{cor} of the metals investigated – molybdenum, copper, titanium, niobium, nickel and aluminum – over 20 h. These are industrial metals with a purity of >99.5 wt%. It can be seen that the E_{cor} increases sharply within a few minutes and after about 2 h remains at an almost constant level. The free corrosion potentials are -425 mV (Al), -355 mV (Ti), -0 mV (Ni), 255 (Cu), 395 mV (Nb) and 495 mV (Mo). The potential behavior differed only for Ti and Cu. The E_{cor} for Ti increased initially from approx. -250 mV to -5 mV before decreasing to -355 mV after 2 h. The E_{cor} for Cu decreased linearly over 4.5 h from 320 mV to 255 mV and subsequently remained constant. The clear increase in E_{cor} at the beginning of the measurements can be explained by the passivation of the metal surfaces in concentrated H₃PO₄. The resulting passivation layer functions like a kinetic barrier, preventing the release of metal ions. As the electrode potential is characterized by the electrochemical permeation reactions at the phase boundary, the electrode potential moves with increasing stability to more noble potential ranges. It can be concluded that the resulting passivation layers have the highest protective effect in the case of Mo and Nb, and the lowest reduction in the permeation of metal ions in the case of Ti and Al. In the case of Ti, the increase and decrease in E_{cor} observed within the first hour additionally indicates that the passivation layer formed at the beginning is not stable in the long term and is degraded again within ~1 h. Cu has a standard potential E^0 of 350 mV. The concentration dependence of the electrode potential can be determined with the Nernst equation. As the activity of the oxidized species $a_{Cu^{z+}}$ is very low in the electrolyte, $a_{Cu^{z+}} \ll a_{Cu}$ applies, where the logarithmic term of the Nernst equation is negative and the electrode potential is shifted to smaller values. This explains the deviation of the measured electrode potential from the electrochemical standard potential.

Fig. 94 b) shows E_{cor} over time for a linear increase in temperature to 130 °C and a subsequent constant temperature. In the case of Mo, Cu and Al, E_{cor} began to decrease from approx. 35 °C onwards, and in the case of Nb, Ni and Ti, from approx. 60 °C. When 130 °C was reached after 2 h, a constant corrosion potential once more emerged. After 4 h, Mo had the highest corrosion potential (390 mV) and Ti the lowest (-430 mV). The largest potential

difference of 575 mV was observed for Nb and the lowest of 40 mV for Ni. The free corrosion potential of Al dropped after 2 h to -615 mV and the material sample dissolved completely. As the temperature-dependent decrease in E_{cor} reflects an increase in the corrosion kinetics and the degradation of the passivation layer, it can be concluded that Nb passivation exhibits the lowest temperature stability while Mo exhibits the most effective passivation effect. Ti again exhibits contrary potential behavior over time. After an initial decrease, E_{cor} reaches a potential minimum of -515 mV at 1.7 h before subsequently increasing to a constant value of -430 mV. One possible explanation for this dynamic passivation behavior is the comparatively high porosity of Ti oxides. The linear decrease in E_{cor} in the case of Cu can be explained by the temperature dependence of the electrode potential using the Nernst equation.

5.2.1 Influence of corrosion on the surface structure

This section compares the corrosion behavior at higher H_3PO_4 concentrations with the findings from the former section at 85 wt% H_3PO_4 . The metals Mo (highest E_{cor} value), Nb (strongest influence of temperature on E_{cor}), Ti (lowest E_{cor}) and Ni (relatively stable E_{cor} at ~ 0 V) were exposed to room temperature, 80 °C and 160 °C for 24 h. Table 17 compares the masses m of the material samples after exposure and the free corrosion potential E_{cor} from Fig. 94. To prevent phosphoric acid residues on the metal surface, the material samples were washed before their masses were determined for 30 min at 80 °C in 100 ml Milli-Q® water. Ti dissolved completely in phosphoric acid at 80 °C. After 24 h at 80 °C, Ni only had 32% of its initial mass. The Nb sample exhibited adequate corrosion resistance over 24 h at 160 °C with a mass loss of ~ 20 wt%. Mo showed exceptionally high stability in phosphoric acid at increased temperatures. Even after 24 h at 160 °C, it had no mass loss. Comparing the findings with E_{cor} values confirms that the corrosion resistance is predominantly determined by the protective passivation layer and the level of E_{cor} .

	$m_{Rest,RT}/\%$	$m_{Rest,80^\circ C}/\%$	$m_{Rest,160^\circ C}/\%$	$E_{cor,80-130^\circ C}/mV$
Mo	100,0 \pm 0,1	100,0 \pm 0,1	99,9 \pm 0,1	445 – 380
Nb	100,1 \pm 0,1	99,1 \pm 0,1	80,9 \pm 0,1	300 – -170
Ni	99,0 \pm 0,1	32,4 \pm 0,1	0	-(20 – 60)
Ti	98,9 \pm 0,1	0	0	-(395 – 425)

Table 17: Mass m of Mo, Nb, Ni and Ti after exposure tests in 30 ml concentrated H_3PO_4 as well as the free corrosion potential E_{cor} in the temperature range 80–130 °C.

To assess degradation processes on the metal surface caused by acid attack, SEM micrographs were taken. These are shown in Fig. 95 to Fig. 97 for Ti, Ni and Nb, respectively. Due to the high corrosion stability of Mo, no topographical changes were determined by SEM. For Ti, which has the lowest free corrosion potential and the lowest passivation layer stability, clear surface damage and increasing porosity were evident after 24 h exposure in 85 wt% H_3PO_4 at room temperature (Fig. 95). The Ti substrate dissolved fully at 80 °C.

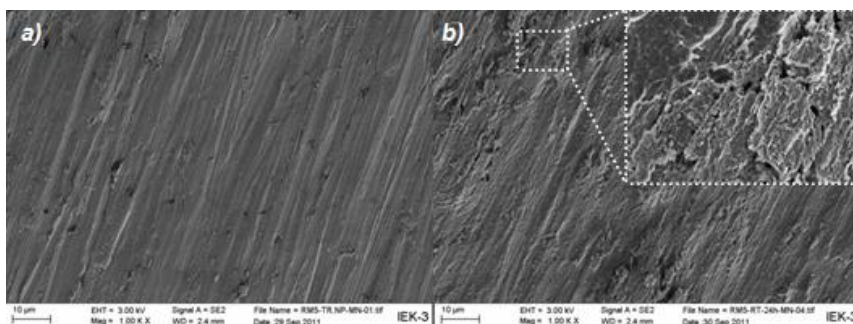


Fig. 95: SEM micrographs of Ti a) before exposure, b) after 24 h at room temperature in 30 ml 85 wt% H₃PO₄.

For Ni, which exhibits a negative E_{cor} behavior with increasing temperature, there is a much smaller degree of surface corrosion in concentrated H₃PO₄ after 24 h at room temperature than for Ti. However, a fine and uniform roughening of the surface is evident. At an exposure temperature of 80 °C, the passivation protection fails completely and there is high Ni oxidation resulting in considerable surface damage, as shown in Fig. 96 c) and d). After 24 h, the material dissolves at ~70 wt%.

When the temperature rises above ~80 °C, the corrosion potential of Nb decreases significantly from approx. 300 mV to -170 mV at 130 °C. Exposure tests with Nb show no corrosion damage in H₃PO₄ at room temperature. After 24 h at 80 °C, the first signs of aging appear in the passivation layer in the form of local corrosion areas and they lead to the aforementioned decrease in E_{cor} . After 24 h at 160 °C, there is increased dissolution of the passivation layer. The bare metal underneath cannot withstand the acid attack and the dissolution of the metal proceeds (see Fig. 97 b-d). For Nb, the loss of ductility was striking after the exposure tests at 160 °C. This can be explained by the tendency of Nb to become brittle. The diffusion of protons inside the metal structure and the subsequent recombination to hydrogen create stress-induced cracks causing material brittleness. Such physical corrosion of Nb must be taken into account for application as a bipolar plate material.

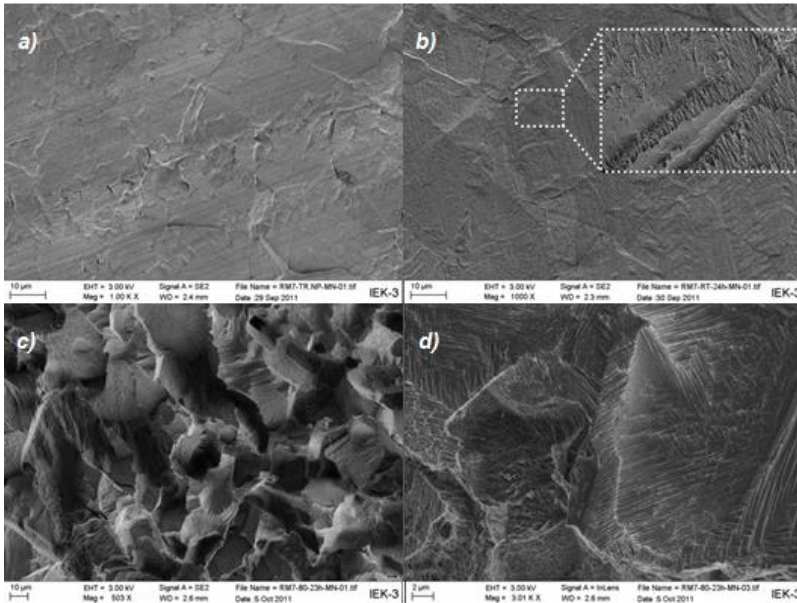


Fig. 96: SEM micrographs of Ni a) before exposure, b) after 24 h at room temperature and c, d) each after 24 h at 80 °C in 30 ml H₃PO₄ (>85 wt%).

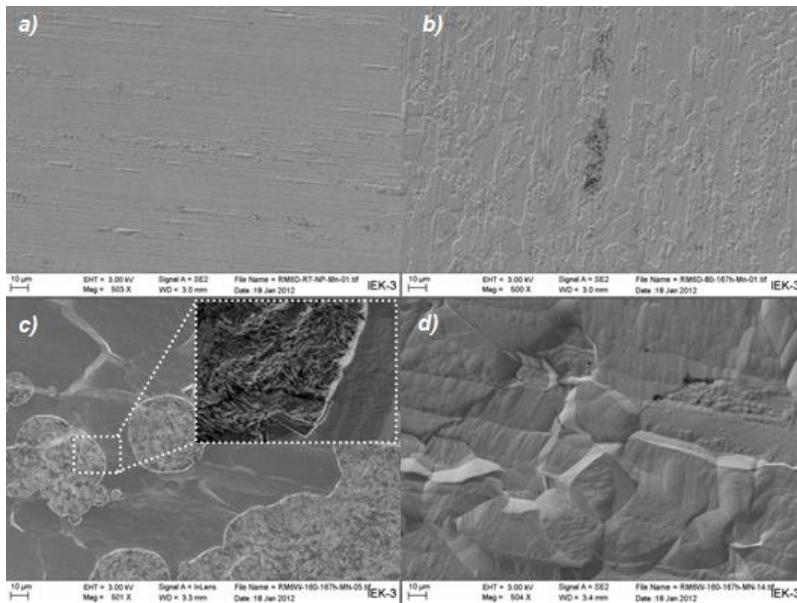


Fig. 97: SEM micrographs of Nb a) before exposure, b) after 24 h at 80 °C and c, d) each after 24 h at 160 °C in 30 ml H₃PO₄ (>95 wt%).

5.3 The electrolysis pilot project at the JuHY hydrogen demonstration facility

Climate change and the cap on CO₂ emissions heralded the huge transition to renewables that energy technology is currently undergoing. In contrast to fossil energy, renewables are not time-independent. To continue to guarantee power supply when there is a large proportion of renewable energy in the power grid, the power grids must be expanded and large storage solutions must be created for electrical energy.

This necessary transition was addressed by the German Federal Government in its 2010 Energy Concept, which declares a reliable and affordable energy supply based on renewables as a future goal. Various types of energy storage are being discussed for storing large quantities of energy, including pumped-storage power plants, batteries and compressed air storage. The high energy density involved means that chemical storage media, such as hydrogen produced by electrolysis using renewable power is a promising option. As shown in Fig. 98, potential markets for hydrogen produced by electrolysis from renewable power are transportation, direct conversion back into electric energy, methanation and feed-in into the natural gas grid as well as use as a raw material in industrial processes.

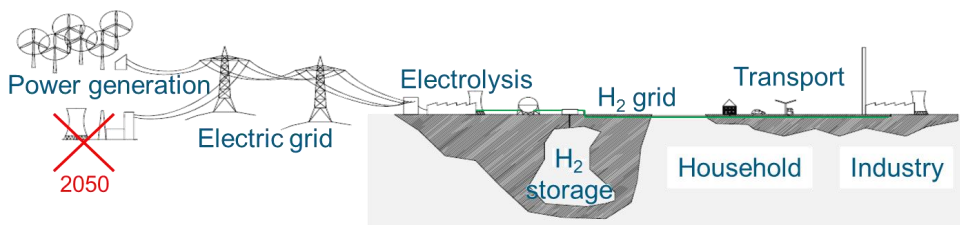


Fig. 98: Hydrogen as a storage medium for a future energy system based on renewables

Water electrolysis has been used for over 100 years to produce hydrogen and oxygen from water. However, the high costs mean that only 4% of all hydrogen is produced by electrolysis. Hydrogen produced from natural gas (77%) and coal (18%) dominates the market, despite the resulting CO₂ emissions, because of the low production costs¹⁸.

Building on the expertise and experience gained in the R&D project PHOEBUS Jülich on alkaline electrolysis with operating pressures up to 200 bar and in research on fuel cells with polymer membranes, an R&D priority was created in 2012 for the verification of large-scale PEM electrolyzers. A new test platform is planned to test more powerful electrolyzers than was possible in the past. The planned test system aims to realize a bifunctional setup to enable the production of hydrogen using acidic and alkaline electrolysis. The dimensions involved will also allow tests to be conducted on systems on a scale relevant for energy technologies. In addition, close links will be established with the Energy Lab 2.0 with whom data will be exchanged.

The Energy Lab 2.0 is a virtual platform to analyze the interaction of real individual components of future energy systems. Fig. 99 shows the links within the Energy Lab 2.0. The

¹⁸ Wöhrle, D.: Wasserstoff als Energieträger – Eine Replik. Nachrichten aus Chemie, Technik und Laboratorium, 39 (1991), pp. 1256-1266.

Energy Lab 2.0 aims to accelerate the Energiewende by testing new approaches for stabilizing the power grids in a realistic manner. A network of facilities pools electrical, thermal and chemical energy flows as well as new information and communication technologies. Project partners are the Karlsruhe Institute of Technology (KIT), the German Aerospace Center (DLR) and Forschungszentrum Jülich (FZJ), all members of the Helmholtz Association.

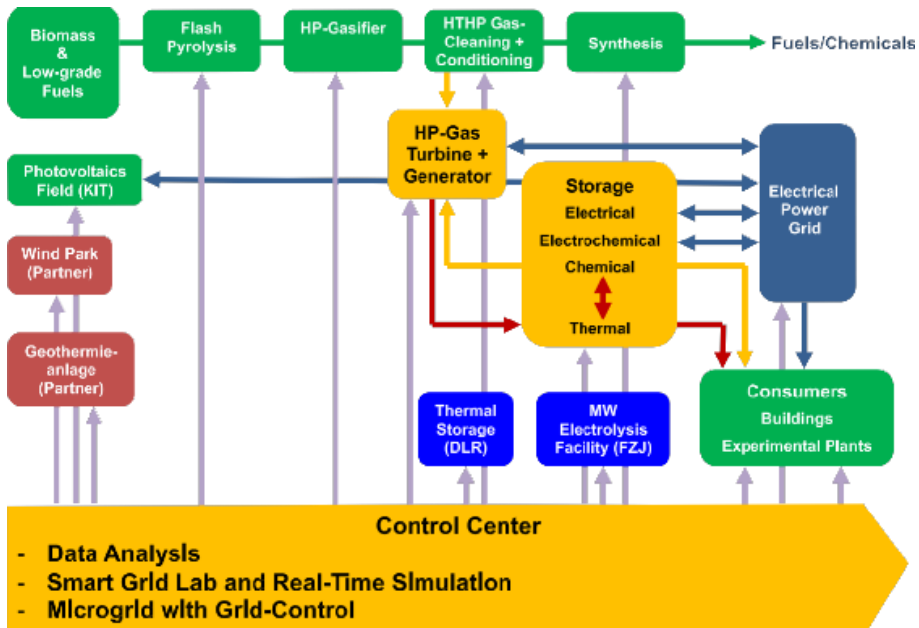


Fig. 99: EnergyLab (Source: KIT)

5.3.1 Integration of modular electrolysis systems into the energy infrastructure

Today, there are two commercial electrolysis products:

- alkaline electrolysis and
- proton exchange membrane electrolysis (PEM electrolysis).

In alkaline electrolysis, potassium hydroxide (KOH) with a concentration of 20–40 wt% is used as the electrolyte. The anode and cathode are separated by diaphragms. In most cases, Zirfon® (a zirconia-based diaphragm) is used. The diaphragm facilitates the transport of hydroxide ions (OH⁻) while simultaneously preventing the mixing of the gases produced at the anode and cathode. Ordinary Raney-nickel catalysts are used as electrodes. Raney nickel is a nickel-aluminum alloy. The gas diffusion electrodes are applied to a nickel perforated plate using a vacuum-based coating technique. Once the electrode has been fabricated, it is activated. The aluminum constituents are dissolved out of the alloy to produce as large an active electrode surface area as possible.

The PEM electrolysis cell is operated with distilled water which is electrolytically split into hydrogen and oxygen. Instead of a diaphragm, a proton-permeable (H⁺) polymer membrane separates the anode and cathode. The electrodes are connected directly with the membrane

by a catalyst coated membrane. Carbon-supported platinum is employed as the standard cathode catalyst and iridium oxide as the standard anode catalyst.

Alkaline water electrolysis	PEM electrolysis
<p>Advantages:</p> <ul style="list-style-type: none"> • established technology • no noble metal catalysts • high long-term stability • high output already achieved 	<p>Advantages:</p> <ul style="list-style-type: none"> • high power density • high efficiency • simple system configuration • dynamic operation • extremely fast system response → grid stabilization • compact design facilitates high-pressure operation
<p>Challenges:</p> <ul style="list-style-type: none"> • increase current density • expand part-load range • faster dynamics of the system as a whole • system dimensions and complexity (footprint) • reduction of gas purification efforts • total material required (stacks currently on a scale of several tonnes) 	<p>Challenges:</p> <ul style="list-style-type: none"> • identification of costs for a 1 MW system • determination of where costs could be cut, e.g. reduction and substitution of platinum-group metals and other costly components • demonstration of long-term stability • scaling up of stack and peripherals • optimized balance of materials used, power density, operating point and operating strategy (long-term stability, maintenance, etc.)

Table 18: Comparison of the advantages and disadvantages of alkaline and PEM electrolysis

Both of the available commercial electrolysis technologies have specific advantages and disadvantages, which are listed in Table 18. In terms of using electrolysis technology to store renewable power, however, neither is favored at present. Both technologies are being further developed both by research and industry. This is why the test facility described below will make it possible to characterize and refine both alkaline and PEM electrolyzers with the system configuration shown in Fig. 100. The data obtained in this process will then be made available to the Energy Lab 2.0 for the validation of the virtual power plant.

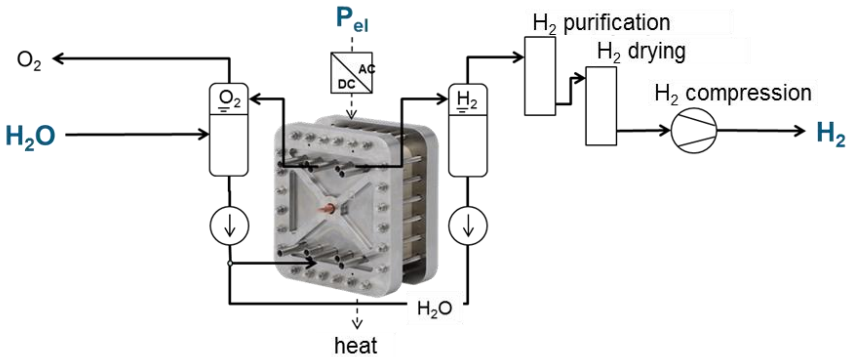


Fig. 100: Configuration of a system to characterize PEM electrolyzers

5.3.2 Integrated experimental facility and multifunctional test facility

The aim is to create a research platform to enable realistic testing of various electrolyzers on a scale of >100 kW. Electrolyzers will be tested in different configurations to identify the best options for integrating modular electrolysis systems into the energy infrastructure. The hydrogen demonstration plant with the planned 0.5 MW test platform will make in operando characterization of electrolyzers (acidic and alkaline) possible on a scale relevant for the energy industry. Research priorities are the analysis of the following points:

- interactions between system components,
- long-term experiments in dynamic operation,
- up-scaling of the technology,
- definition of technically interesting operating conditions,
- validation of simulation models.

The automated specification of relevant operating parameters and the automated recording of measurement data as well as the processing of these data is closely linked to other topics dealt with at the Energy Lab 2.0. The research platform itself is composed of different submodules for energy and media supply, which enable operation of the electrolyzers. The experimental facility comprises:

- coupling to the power grid
- direct current supply
- water purification
- control system
- multifunctional stack and system test facility (alkaline and acidic electrolytes)

The enclosed test facility is the core component of the test platform with different experiments and analytical instruments. An electricity supply (around 0.5 MW) will be set up to reproduce different power generation profiles. The aim is to replicate future power grids characterized by volatile renewable feed-in. Electrolyzers can thus be operated under realistic profiles, providing reliable results on the functioning and economic viability of each module.

An important starting material for electrolysis and other conversion processes is water. High-purity water is essential for long-term stable operation of the electrolyzers. This water will be centrally prepared for the test platform. Centralized provision is cost-effective and simultaneously means that the water quality can be centrally analyzed to guarantee a high quality, thus creating the prerequisites for stable long-term operation.

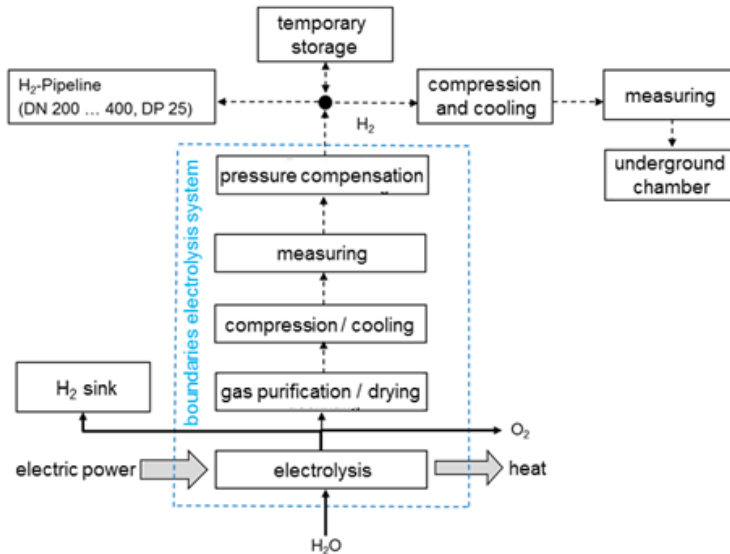


Fig. 101: Integration of electrolysis into the hydrogen infrastructure

A decisive factor in designing the electrolyzers and coupling them to renewables is their connection to and integration into the hydrogen infrastructure. Fig. 101 illustrates the components that are necessary for proper integration. Of the conceivable options for integrating electrolysis into the hydrogen infrastructure, direct coupling to a pipeline is particularly interesting in the long term because this would allow the hydrogen to be transported to a wide range of potential users. Another interesting option is direct connection to hydrogen storage.

The test platform will help to determine important parameters for the various configurations and incorporate these into existing simulations. The most technically simple module is the hydrogen sink, which safely converts hydrogen (particularly during incidents) or highly contaminated hydrogen into uncritical steam. This torch or other system must always be available as a safety-relevant component.

The test facility is controlled via a central control system. It sets the operating parameters of each module and records and processes the measurement data centrally so that they can be transferred to the Energy Lab for further use. It is planned to analyze all electrolysis technologies in different power classes at this test facility. Suitable operation scenarios and system boundaries will therefore be defined for the planned investigations.

5.4 More flexibility using integrated energy supply systems

The targets set by the German Federal Government for reducing greenhouse gases (GHGs) are a clear indication of how ambitious the project Energiewende in Germany is with its planning horizon of 35 years. The German energy system is facing important challenges both technically and structurally. A systematic evaluation of the structure, components and interactions of the energy supply system is therefore essential. In addition, the interactions between the industrial sectors and the energy sector as well as relationships with neighboring countries must be incorporated into a system-wide analysis. Criteria that must be included in the quality analysis of a future energy system are stability, economic viability, sustainability and acceptance.

An important factor driving the transformation of the energy system is the massive expansion of the non-controllable generation of power from renewables, which are characterized by a fluctuating availability and a considerably lower annual duration of use. An energy supply that has been altered in this manner needs adapted energy infrastructures based on improved modern systems and above all the use of new, pioneering technologies. However, these new technologies must be sufficiently mature by 2030. In this way, not only will viable technological solutions be identified with a view to achieving the targets but their market penetration by 2050 will also be guaranteed.

5.4.1 Potential electrochemical systems for more flexible energy markets

With respect to energy storage and energy transport, hydrogen-based energy supply systems have considerable advantages over conventional systems in terms of efficiency, flexibility and wear. The production of hydrogen by means of electrolysis, its storage, continuous transport, widespread distribution and utilization in different areas of application are therefore extremely important for sustainable energy management. In addition to the option of using it as a fuel for vehicle drives, hydrogen has very varied uses (Fig. 102). Renewable energy can thus be transferred from the power sector to the transportation and industrial sectors, which would otherwise find it difficult to achieve the Federal Government's GHG reduction targets. Electrolysis could help to make the power supply more flexible. Local excess power which is not directly utilized to cover demand in power grids could thus be fed into suitable storage where it could be held until needed. Such a pan-sector supply of energy and raw materials demands the interconnection of power and gas infrastructures including new industrial-scale storage solutions. The type and scope of the technological options that will be used for this depend on how intensively renewables can be used taking technical, economic and ecological factors into account. This aspect could be accompanied by the import of renewables.

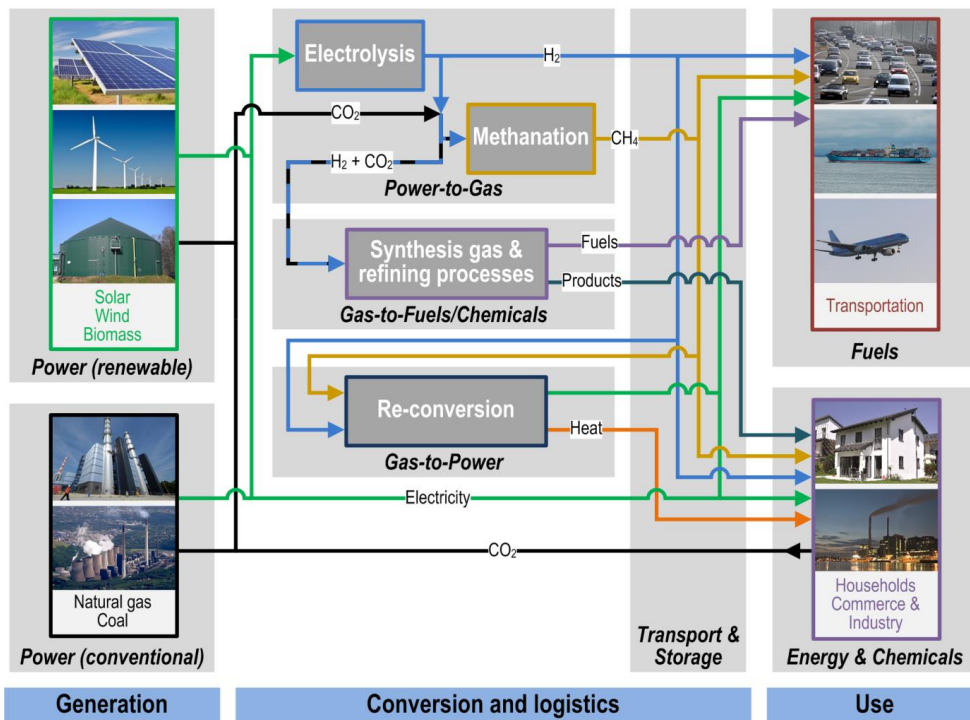


Fig. 102: Energy and raw material pathways with hydrogen

5.4.2 Evaluation of new technologies in the context of the system as a whole

Achieving application and market maturity of electrochemical systems involves great challenges in researching and developing targeted detailed solutions. This also applies to the components of a future hydrogen supply infrastructure. An important task that will be dealt with in future process and systems analyses involves the qualified evaluation of these new technologies in the context of the changing energy economy system as a whole. These activities are also being pursued within the HGF initiative Energy System 2050 and at RWTH Aachen University as part of the project Technology-Based Energy Systems Analysis (TESA). The complexity of the energy economy system as a whole has been broken down based on the subgoals of the planned activities and will be explained in more detail in the following:

- Draft concepts for integrated energy supply systems
- Model development and evaluation process
- Achievable greenhouse gas reduction

Draft concepts for integrated energy supply systems

The greenhouse gases emitted by the polluter spheres of power generation, transportation, households, industry, commerce and trade will be taken as the basis to develop technological concepts and processes for reducing greenhouse gases. Ways of achieving the envisaged 80% reduction in GHGs compared to levels in 1990 will also be identified. The draft concepts will then be roughly compared and promising concepts for the provision and utilization of renewables and hydrogen will be selected. Existing modelling tools for the time-dependent and spatially resolved determination of residual loads will be further developed to incorporate industrial-scale gas storage, power and gas grids, and sector-specific energy and raw material usage, allowing a sustainable energy system to be designed as a whole. An important element here is the analysis of how much power and gas is consumed by households, small consumers and industrial customers, which could change substantially in response to increasing self-sufficiency by means of decentralized renewable energy systems and storage. In addition, sector-specific spatially and temporally resolved quantification of the demand for hydrogen as energy and as a raw material is part of the analysis. Distinguishing features of the draft concepts here include the development of the use of renewables, the potential applications and the resulting necessary infrastructures.

Model development and evaluation process

A unique feature associated with the research topic described here is the development and application of models with the required level of detail. Particularly complex and highly dynamic systems will be modelled in submodels with a high temporal resolution and/or a high level of physical and technical detail. To evaluate the draft concepts and scenarios, in contrast, full models with a reduced level of detail are needed. Therefore, different evaluation procedures will be developed, for example, with respect to the economic viability of the draft concepts in relation to the target markets. A priority in this area involves adapting individual modelling approaches in order to display the power and gas supply in a full model. The aim is to use defined time steps on the way towards supplying all relevant hydrogen consumers in transportation and industry in order to derive measures for the economically optimized creation of an integrated power and H₂ supply infrastructure.

Achievable greenhouse gas reduction

Simulation runs will provide concept-specific data which will then be used to evaluate the results and derive recommendations for concept implementation. Full implementation of each of the draft concepts and scenarios will be assumed. These data will also be used as the basis for more in-depth analyses. In addition to the aforementioned work, the framework conditions that need to be considered when transferring results that are valid for Germany to the European or even global context will also be identified. An international network is currently being established for this.

Furthermore, the potential associated with renewables beyond the intensively debated power-to-gas pathway will also be analyzed and evaluated. For example, both heavy goods vehicles and industry will continue to use carbon-containing energy carriers in the long term. The availability of usable biomass must therefore be included in a strategic approach to such uses to allow optimal deployment with respect to economic and ecological criteria. A major

objective here is the drafting of a comprehensive fuel strategy resulting in a quantitative allocation of the limited renewables to the demand segments of the transportation sector.

Expected results

The research objectives outlined in this section will be verified by comprehensive data material in terms of system and process design, infrastructure costs, and temporally and spatially resolved energy flows. In addition, specific recommendations for action will also be derived. With the aim of developing a holistic energy concept to achieve the GHG reduction targets and with a particular focus on the role of hydrogen as a key element of future energy supply systems, the following results among others are expected:

- Realistic temporally and spatially resolved development of the availability of renewables as well as the demand for electricity and hydrogen
- Improved evaluation options for individual technologies on the basis of specially developed submodels with a high level of detail; the derivation of technology-specific R&D topics, e.g. regarding new materials
- Identification of expedient draft concepts by modelling the system as a whole with the aim of determining infrastructure adjustments over time
- Recommendations for action for stakeholders in politics and industry, e.g. with respect to establishing framework conditions for the swift marketing of hydrogen as a fuel and/or a raw material for industry or establishing market conditions in electricity markets with high proportions of renewables
- Chance of European or global market success of hydrogen technologies based on analyses of the spatially resolved potential of the utilization of low-GHG power generation



6

Data

Facts and Figures

- Institute of Energy and Climate Research – Fuel Cells (IEK-3)
- Overview of department expertise
- Publications, technology transfer and resources
- Committee work
- Contributions to trade fairs and exhibitions
- How to reach us
- List of abbreviations

6.1 IEK-3: Institute of Electrochemical Process Engineering

The developments at IEK-3 in the period under review (2013–2014) were influenced mainly by the migration process coordinated by the Helmholtz Association (HGF) from the second phase of program-oriented funding (PoF-II: 2010–2014) to the third phase (PoF-III: 2015–2019). Future work contents and objectives had to be newly defined together with the necessary institutional funding. The work program was restructured in keeping with the challenges associated with the Energiewende and the corresponding research policy targets. At IEK-3, this led to two major changes, the implementation of which will continue into the next review period.

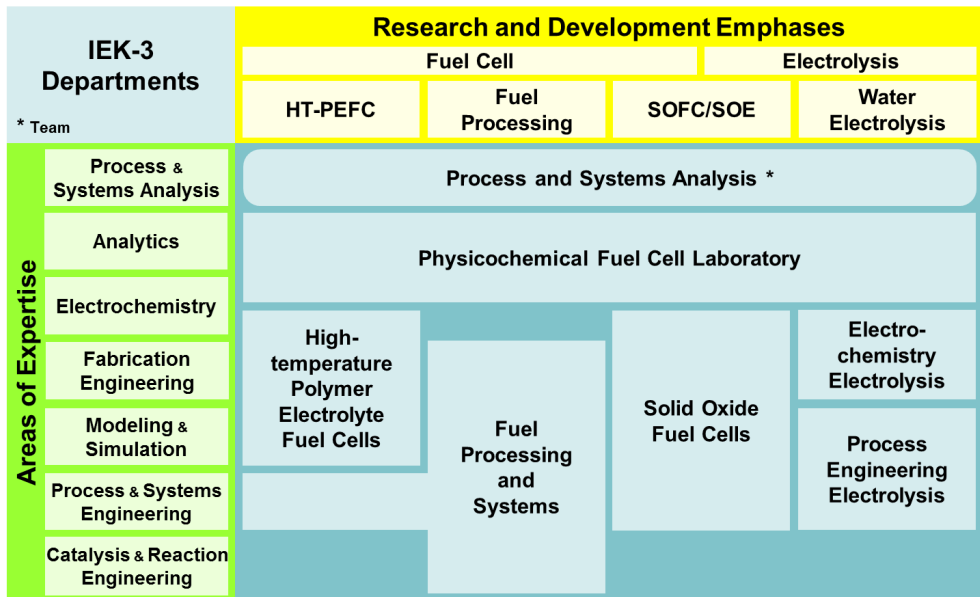


Fig. 103: Departments, areas of expertise and R&D priorities

The first change was the intensification of electrolysis research and development. As this change was implemented using resources for DMFC activities, DMFC research is currently limited to maintaining scientific and technical know-how. The existing units for DMFC and PEM electrolysis research were restructured as two departments for low-temperature electrolysis investigating electrochemical and process engineering issues. In future, more attention will be devoted to high-temperature electrolysis (SOE). A second development was brought about by realigning process and systems analysis to the technology-based evaluation of energy systems ranging from single units right up to the energy technology infrastructures of a country, such as the process and systems analysis of Germany. Sustainability in the form of utilizing renewables in all energy sectors is the focus of the analyses.

The PoF-induced objectives therefore led to IEK-3 cutting their R&D topics down to four. The high-temperature polymer electrolyte fuel cell (HT-PEFC), fuel processing using liquid energy carriers intended to supply fuel cells with hydrogen, the ceramic solid oxide fuel cell and electrolysis cell (SOFC/SOE), and low-temperature electrolysis are now part of the R&D portfolio at IEK-3. Fig. 103 shows the fields together with the respective areas of expertise. Focusing more closely on concrete areas of application enables IEK-3 to work on all aspects of each of these R&D topics from the basic phenomena to process engineering for entire systems with teams of supercritical size. Synergies between the specialized disciplines are exploited in this process which extends from theory to the pilot-plant stage. Technology-based process and systems analysis provides IEK-3 with its strategic orientation. Pioneering processes and energy systems are analyzed, drawn up, designed, evaluated and compared. The approach used here accounts for technical, economic and ecological aspects, and permits quantitative conclusions to be drawn on the performance efficiency and sustainability of an energy system. Application-oriented R&D activities are additionally accompanied by basic research aiming to clarify structure-activity relationships using selected advanced analysis methods. These activities are pooled in the physicochemical fuel cell laboratory, which works together with the technology-oriented departments within the institute.



Institute of Energy and Climate Research
IEK-3: Electrochemical Process Engineering
Forschungszentrum Jülich GmbH
52425 Jülich
Germany



Head of Institute
Prof. Dr.-Ing. Detlef Stolten
Tel: +49 2461 61-3076
Email: d.stolten@fz-juelich.de

Jülich has the largest institutional research team (approx. 150 employees) working on fuel cells and electrolysis in Europe. Of these 150 employees, around half work on the SOFC/SOE, and approx. one-fifth of these are involved in IEK-3 activities. Three other institutes also work in the SOFC/SOE field. IEK-1 is responsible for manufacturing materials, IEK-2 tests the materials and conducts steel research, and IEK-9 focuses on the electrochemical principles. The Central Institute of Engineering and Technology (ZEA-1) is responsible for stack construction. Of the some 104 IEK-3 employees, 88 work on technological developments for low-temperature fuel cells and electrolyzers as well as energy systems analysis. A coordinator is responsible for the fields of work at IEK-3, and is also available to answer generic questions.



**Deputy Head
of Institute and Scientific
Coordinator**

Dr.-Ing. Bernd Emonts

Tel: +49 2461 61-3525

Email: b.emonts@fz-juelich.de

6.2 Overview of department expertise

High-Temperature Polymer Electrolyte Fuel Cells

Fuel Processing Systems

Fields of work, range of services

Work on the HT-PEFC extends from the electrode to the stack and is conducted in cooperation with internal and external partners. New electrode structures and preparation methods are developed, and MEAs are fabricated and electrochemically characterized. Structure-activity relationships of electrode layers are also investigated. Extensive modeling enhances process understanding. Simulations of components, cells and stacks support the development of air-cooled and liquid-cooled stacks with high volume-specific and weight-related power densities.

H₂ produced from commercially available fuels expedites the early introduction of fuel cell technology. Work here concentrates on reforming in the power classes of 3 kW_{el} and 50 kW_{el} of middle distillates (kerosene, diesel and heating oil) and diesel-like biofuels. In developing mobile on-board power supply systems, in-house HT-PEFC 5 kW_{el}–10 kW_{el} stacks are preferred. In addition, PEFC and SOFC systems with diesel reforming are evaluated in cooperation with project partners and within the framework of systems analyses.

Facilities, processes, methods

Equipment

- Test stands for the electrochemical characterization of MEAs
- Test stands for electrochemical studies on stacks up to 5 kW_{el}
- Equipment for the fabrication of gas diffusion electrodes

Models

- Simulation models to describe mass, charge and heat transport processes in cells and stacks
- Characterization of porous structures
- Support using high-performance computing (HPC)

Equipment

- Test stands for the examination of reactors and whole systems
- Test stands for the screening and examination of catalyst activity and selectivity
- Analytical devices for the determination of reaction gas concentrations (GC, GC/MS, NDIR, FTIR)
- Apparatus for fractional distillation of fuels

Models

- CFD simulation programs for reactor and system design

Contacts



Prof. Dr. Werner Lehnert
Tel.: 02461-61-3915
e-mail: w.lehnert@fz-juelich.de



Prof. Dr.-Ing. Ralf Peters
Tel. 0261-61-4260
e-mail: ra.peters@fz-juelich.de

Solid Oxide Fuel Cells

Electrochemical Electrolysis

Fields of work, range of services

A key area of scientific and technical expertise is the development and optimization of stacks and systems for high-temperature fuel cells for stationary and mobile/portable applications. Stacks, systems and system components are devised, designed, constructed and tested. To optimize concept evaluation, the experimental studies are accompanied by the development of thermomechanical and process-engineering models. Priorities here are the electrochemical characterization of stacks and the development of new system concepts, control technology concepts and components in cooperation with industry, which are also tested and evaluated.

Advanced PEM electrolyzers facilitate the economic production of H₂ from excess renewable electricity. With support from project partners in research and industry, development work concentrates on membrane electrode assemblies (MEAs) in which the platinum group metals required for catalytic reactions are either reduced or fully replaced while retaining comparable performance. New types of membranes aim to lend planned large-scale systems sufficient stability. Further topics include the identification of cost-effective materials and the development of replicable fabrication techniques for MEA development and production.

Facilities, processes, methods

Test stands

- Characterization: high-temperature heat exchangers up to 850 °C @ 200 m³ air/h
- Characterization: reformers and afterburners for stacks up to 5 kW
- Characterization: 20 kW system
- Electrochemical characterization: 100 W–10 kW stacks in fuel cell and electrolysis operation

Models

- CFD/FEM models to determine flow and voltage distribution in stacks and system components
- Simulation models for the design of fuel cell systems

Equipment

- Test stands for the characterization of electrocatalysts (rotating disc electrode)
- Test stands for the characterization of membranes (gas permeation measurements, fluorine release rate)
- Test stands for the electrochemical characterization of CCMs
- Test stand for electrochemical studies up to 30 kW_{el}
- Coating facility (roll-to-roll) for continuous electrode fabrication

Contacts



Prof. Ludger Blum
Tel.: 02461-61-6709
e-mail: l.blum@fz-juelich.de



Fr. Dr. Wiebke Lücke
Tel. 0261-61-9073
e-mail: w.lueke@fz-juelich.de

Fields of work, range of services

Using ideas for new concepts, electrolysis stacks and systems are developed and modeled. The aim is to improve efficiency, power density and lifetime while simultaneously reducing the amount of material needed. Work is validated in component tests and by characterizing entire stacks and systems. In cooperation with project partners, coatings, stack components, stacks and systems are optimized and characterized. Combined with automated fabrication on an industrially relevant scale, this work builds a bridge between science and technology.

As the technical development of new pioneering energy systems progresses, scientific work is becoming increasingly important for understanding basic phenomena. The department therefore focuses on fully elucidating material and structural properties as well physico-chemical and electrochemical processes. Imaging, physical and spatially resolved analysis techniques are used to determine chemical and structural changes, mechanical and thermodynamic suitability, and fluid dynamic and electrochemical performance.

Facilities, processes, methods

Equipment

- Test stands for electrochemical studies of electrolyzers up to 100 kW_{el} and fuel cells (DMFCs)
- Visualization tests
- Corrosion test stands for the evaluation of coatings
- Analysis of ion-exchange materials with media containing specific impurities
- Laser coating for local modification of surfaces
- Robot facility for the reproducible fabrication of stacks

Models

- Description of mass, charge and heat transport

Equipment and methods

- Imaging analysis techniques: high-resolution scanning electron microscope (H-SEM) with EDX analysis, optical microscope, confocal laser scanning microscope
- Spatially resolved analysis techniques: segmented cell technology (SCT), magnetic imaging and mass spectroscopy (SRMS)
- Physicochemical analysis techniques: thermogravimetric analysis (TG, TGA), differential scanning calorimetry (DSC), contact angle measurement (KF analysis), impedance spectroscopy/CV, RDE, climate cabinet, tensile testing machine with climate chamber, BET and standard porosimeter, particle size measuring unit

Contacts



Dr.-Ing. Martin Müller
Tel.: 02461-61-1859
e-mail: mar.mueller@fz-juelich.de



PD Dr. Carsten Korte
Tel.: 02461-61-9035
e-mail: c.korte@fz-juelich.de

Process and Systems Analysis

Fields of work, range of services

Selection, development and implementation of future energy systems demand approaches analyzing and evaluating the sustainability and economic viability of entire systems. Techno-economic comparisons of competing technologies for energy conversion and storage are the foundation for this. The broad experimental basis and extensive modeling at IEK-3 make it possible to design energy systems, describe them in models and compare them with competing technologies under realistic conditions as well as to identify development potential and shortcomings. Studies for industry are also conducted with protection of information and policy recommendations are derived on a neutral basis.

Facilities, processes, methods

Methods

- Process analysis and optimization (Fluent, AspenPlus)
- Energy system modeling (databases, Matlab)
- Dynamic simulations (Matlab/Simulink)
- Well-to-wheel analyses (spreadsheets)
- Evaluation of energy yields (databases, GIS)
- Technology-based benchmarking
- Economic evaluations (SWOT, WACC, CAPM, Monte Carlo simulations)

Contacts



Dr.-Ing. Thomas Grube
Tel.: 02461-61-5398
e-mail: th.grube@fz-juelich.de

6.3 Publikationen, Technologietransfer und Ressourcen

The results of scientific and technical work carried out at IEK-3 are published in relevant journals and presented to interested specialist audiences at national and international conferences. Important journals in which three or more peer-reviewed papers from IEK-3 were published during the period under review were the Journal of Hydrogen Energy (2013: 13, 2014: 8), the Journal of the 13th International Symposium on SOFCs (2013: 5), Electrochimica Acta (2014: 4), the Journal of Power Sources (2013: 3; 2014: 3) the Journal of the Electrochemical Society (2013: 2, 2014: 3), the Journal of Fuel Cell Science and Technology (2013: 3) and Fuel Cells (2014: 3).

The most important conferences with IEK-3 involvement in 2013 were the 13th International Symposium on SOFCs in Okinawa, Japan, with 8 contributions, the 4th European PEFC & H₂ Forum in Lucerne, Switzerland, with 7 contributions, the European Summer School on Fuel Cell, Battery and Hydrogen Technology in Athens, Greece, with 6 contributions, the 3rd ICEPE: Transition to Renewable Energy Systems in Frankfurt with 5 contributions and the 224th ECS Meeting in San Francisco, USA, with 5 contributions. In 2014, IEK-3 presented 11 papers at the 20th WHEC in Gwangju, Korea, and 4 papers at the 11th European SOFC & SOE Forum in Lucerne, Switzerland. IEK-3 was also represented in Karlsruhe at the annual meeting of the ProcessNet Subject Division Energy Process Engineering with 3 contributions as well as at the 11th Symposium on Fuel Cell and Battery: Modelling and Experimental Validation in Winterthur, Switzerland. Various departments at IEK-3 also contributed papers and presentations to numerous other specialist conferences both in Germany and abroad.

During the period under review (2013–2014), 9 PhD theses were completed on HT-PEFCs (7), DMFCs (1) and fuel processing (1) as were two undergraduate dissertations evaluating pioneering energy systems. Tab. 19 details the publications in each year.

To foster a successful knowledge and technology transfer, IEK-3 was and is involved in numerous national and international R&D projects (2013: 44; 2014: 40; see Tab. 19) with funding from the European Commission (EC; 2013: 11; 2014: 11), the German Federal Ministries of Economics (BMW; 2013: 11; 2014: 7), of Education and Research (BMBWF; 2013: 6; 2014: 10) and of Transport, Building and Urban Development (BMVBS; 2013: 1) as well as from various ministries of North Rhine-Westphalia and Bavaria (2013: 4; 2014: 4), the German Research Foundation (DFG; 2013: 2; 2014: 2) and industry (2013: 9; 2014: 6). Some of these projects were headed and coordinated by IEK-3.

Additional funding from the Helmholtz Association was used during the two-year period under review to substantially support four basic research and system-oriented R&D projects on batteries, electrolyzers and membranes and to help the respective research institutions, including IEK-3, prepare for implementation in the new PoF program structure which was launched in 2015. Further elements of technology transfer during the period under review were patent applications (2013: 9, 2014: 12; see Tab. 19) and patents granted (2013: 11, 2014: 6; see Tab. 19).

Year		2013	2014
Publications	Peer-reviewed journals ¹⁾	37	37
	Books and journals	20	3
	Papers in a book	9	6
	Theses and dissertations	4	7
Technology transfer	Ongoing projects with third-party funding	44	40
	HGF initiatives & portfolios	4	4
	Patent applications	9	12
	Patents granted	11	6
Resources²⁾	Personnel (PoF ³⁾ /third-party funding)	110 (66/38)	104 (55/42)
Explanatory notes	¹⁾ According to ISI citation index ²⁾ Data in PY/a ³⁾ PoF: Program-oriented funding		

Tab. 19: IEK-3 core data for 2013 and 2014

During the period under review, the number of employees at IEK-3 fluctuated between 110 (2013) and 104 (2014). They were financed through the Helmholtz Association's (HGF) program-oriented funding (POF) as well as by third-party funds. Some of these employees work on a part-time basis, which results in an effective personnel capacity of 104 PY/a in 2013 and 97 PY/a in 2014 (cf. the figures in brackets in Tab. 19).

6.4 Committee work

IEK-3's national and international reputation as leading experts on fuel cells and hydrogen technology is reflected in the fact that IEK-3 scientists are members of and collaborate with national and international committees. An internationally visible achievement was the role played by Prof. Stolten as Chairman of the 3rd International Conference on Energy Process Engineering 2013 and by IEK-3 scientists in coordinating the conference. Numerous scientists at IEK-3 hold executive positions on various committees and work as members of different annexes of the Advanced Fuel Cells (AFC) Implementing Agreement of the International Energy Agency (IEA). On the national level, Prof. Stolten is a member of the Executive Board and Advisory Council of the VDI Society for Process Engineering and Chemical Engineering, Chair of the ProcessNet Subject Division Energy Process Engineering and member of the Steering Committee of the ProcessNet Section SuPER. Committee work performed by IEK-3 employees is set out in detail below.

IEA Advanced Fuel Cells Implementing Agreement

since 2000, Prof. Dr.-Ing. D. Stolten

Head of the German Delegation in the Executive Committee

since 2002, Prof. Dr.-Ing. D. Stolten

Vice-Chairman of the Executive Committee

since 2009, Dr.-Ing. R.C.Samsun

Member of the Executive Committee

2009–2014, Dr.-Ing. M. Müller

Operating Agent for Annex 27

since 2011, Prof. Dr.-Ing. D. Stolten

Chairman of the Executive Committee

since 2011, Prof. Dr.-Ing. D. Stolten

Operating Agent for Annex 36 Systems Analysis

since 2011, Dr.-Ing. R.C.Samsun

Member of Annex 35 Systems Analysis

since 2013, Prof. L. Blum

Member of Annex 32 Solid Oxide Fuel Cells

since 2014, Prof. Dr. S. Beale

Operating Agent for Annex 37 Modeling of Fuel Cell Systems

since 2014, Prof. Dr.-Ing. D. Stolten, Prof. L. Blum, Dr. W. Lüke, Dr. M. Müller

Members of Annex 30 Electrolysis

since 2014, Prof. Dr. W. Lehnert

Member of Annex 31 Polymer Electrolyte Fuel Cells

since 2014, Dr.-Ing. T. Grube

Member of Annex 34 Fuel Cells for Transportation

since 2014, Dr.-Ing. M. Müller

Member of Annex 35 Fuel Cells for Portable Applications

since 2014, Prof. L. Blum, D. Froning, Prof. Dr. A. Kulikovskiy, Prof. Dr. W. Lehnert, Dr. U. Reimer

Members of Annex 37 Modeling of Fuel Cell Systems

Working Group of Electrochemical Research Facilities (AGEF)

since 2000, Prof. Dr.-Ing. D. Stolten
Member

ProcessNet Subject Division Energy Process Engineering

since 2003, Prof. Dr.-Ing. D. Stolten
Member of the Subject Division

since 2006, Prof. Dr.-Ing. D. Stolten
Vice-Chair of the Subject Division

since 2008, Prof. Dr.-Ing. D. Stolten
Chair of the Subject Division

Fuel Cell Qualification Initiative

since 2005, Dr.-Ing. B. Emonts
Member of the Executive Committee

BREZEL Expert Committee of the Association of German Engineers

since 2005, Prof. L. Blum
Member of the Expert Committee

Global Roundtable on Climate Change, Columbia University, New York

since 2006, Prof. Dr.-Ing. D. Stolten
Member

WILEY-VCH Fuel Cells Journal

since 2006, Prof. Dr.-Ing. D. Stolten
Member of the Advisory Board

National Organization for Hydrogen and Fuel Cell Technology

2007–2013, Prof. Dr.-Ing. D. Stolten
Member of the Advisory Board and HGF representative for research

N.ERGHY in EU FCH Undertaking

since 2008, Prof. Dr.-Ing. D. Stolten
Representative of full member Forschungszentrum Jülich

since 2008, Prof. Dr.-Ing. R. Peters
Member of the Working Group for AA Transport and Refuelling Infrastructure

ProcessNet Section SuPER

since 2008, Prof. Dr.-Ing. D. Stolten
Member of the Steering Committee

Renewable Energy Research Association (FVEE)

since 2009, Dr.-Ing. B. Emonts
Representative of Forschungszentrum Jülich for Fuel Cells

h2-netzwerk-ruhr

since 2009, Dr.-Ing. B. Emonts
Member of the Advisory Board

since 2012, Dr.-Ing. B. Emonts
Vice-Chair of the Advisory Board

IEA Experts' Group on Science for Energy (EGSE)

since 2009, Prof. Dr.-Ing. D. Stolten
Co-Chairman

Working Group of Electrochemical Research Facilities (AGEF)

since 2010, Dr. K. Wippermann
Member

Max Planck Institute for Dynamics of Complex Technical Systems Magdeburg

since 2011, Prof. Dr.-Ing. D. Stolten
Member of the Scientific Advisory Board

Society for Chemical Engineering and Biotechnology e.V. (DECHEMA)
since 2011, Prof. Dr.-Ing. D. Stolten
Member

VDI Society for Process Engineering and Chemical Engineering (VDI-GVC)
since 2011, Prof. Dr.-Ing. D. Stolten
Member of the Executive Board and Advisory Council

German Hydrogen and Fuel Cell Association (DWV)
since 2011, Prof. Dr.-Ing. D. Stolten
Representative of full member Forschungszentrum Jülich

Fuel Cells and Hydrogen Network NRW
since 2012, Dr.-Ing. B. Emonts and Dr.-Ing. T. Grube
Chairmen of the hydrogen platform and the working group for H₂ systems

Wuppertal Institute for Climate, Environment and Energy
since 2012, Prof. Dr.-Ing. D. Stolten
Member of the Supervisory Board

International Association of Hydrogen Energy (IAHE)
since 2012, Prof. Dr.-Ing. D. Stolten
Vice President for Europe

Applied Energy Journal Elsevier
since 2012, Prof. Dr.-Ing. D. Stolten
Member of the Editorial Board

3rd International Conference on Energy Process Engineering 2013: Transition to Renewable Energy Systems, Frankfurt am Main
2012–2013, Prof. Dr.-Ing. D. Stolten
Chairman of the Organizing Committee

2012–2013, Dr.-Ing. B. Emonts
Member of the Organizing Committee

Hydrogen Power Storage & Solutions East Germany (HYPOS)
since 2013, Prof. Dr.-Ing. D. Stolten
Member of the Board

VDMA Fuel Cells Group PG HT-BZ (SOFC)
since 2013, Prof. L. Blum
Member

Journal of Hydrogen Energy Elsevier
since 2014, Prof. Dr.-Ing. D. Stolten
Member of the Editorial Board

6.5 Contributions to trade fairs and exhibitions

IEK-3 showcases its innovativeness and R&D results at trade fairs and exhibitions which provide an excellent environment for establishing contact with interested visitors and exchanging information with partners and experts with similar specializations. During 2013, IEK-3 took part in three trade fairs and exhibitions in Hannover, Lucerne and Hamburg. Details of these fairs and exhibitions are listed below.

2013

Hannover Trade Fair 2013

08.–12.04.2013, Hannover

Fuel cell research and technology development

4th European PEFC & H₂ Forum

02.–5.07.2013, Lucerne, Switzerland

Polymer electrolyte membranes for fuel cells and electrolyzers

f-cell

30.09.–02.10.2013, Hamburg

Electrolyzers and battery-supported fuel cell systems

The annual highlight is the joint stand on hydrogen and fuel cells at the technology trade fair in Hannover (see Fig. 104, left). In 2013, IEK-3 showcased the latest technological developments in the areas of hydrogen as a future energy vector and technologies for the utilization of biofuels.



Fig. 104: Hannover Trade Fair 2013 – Jülich's stand (left) and interview with Prof. Ralf Peters (right)

Reactors for a fuel processing system and HT-PEFC stacks with different cooling concepts demonstrated the development status of on-board power supply in the transportation sector. A service robot also showed how multifaceted the DMFC is as a battery replacement. A Plexiglas demonstrator impressively showed how a PEM electrolysis cell is set up and operated for hydrogen production. The potential for converting H₂ back into electrical energy

was illustrated by a model of the SOFC test stand. As part of the Public Forum, Prof. Peters was interviewed (Fig. 104, right) on the topic of fuel cell systems for the utilization of biofuels.

An overview of the events in which IEK-3 participated in 2014 and the topics concerned is given below.

2014

Hannover Trade Fair 2014

07.–11.04.2014, Hannover

Efficient electricity generation and H₂ for energy storage and mobility

20th World Hydrogen Energy Conference 2014

15.–20.06.2014, Gwangju, South Korea

Research for the efficient production and use of hydrogen

11th European SOFC Forum

01.–04.06.2014, Lucerne, Switzerland

SOFC research and technological development

ProcessNet Annual Meeting

30.09.–02.10.2014, Aachen

Jülich research for a sustainable energy provision

f-cell 2014

06.–08.10.2014, Stuttgart

Battery-supported fuel cell systems and electrolyzers for commercial energy storage

Under the motto of materials research and electrochemical process engineering for the Energiewende, IEK-3, IEK-1 and ZEA-1 exhibited at the Hannover Trade Fair 2014. The exhibits ranged from cell components, cells and stacks to PEM electrolysis, SOFCs and HT-PEFCs and from a fuel processing module to a functioning DMFC system for uninterruptable power supply (see Fig. 105, left). A highlight at Jülich's stand was a visit from Minister Svenja Schulze (see Fig. 105, right).



Fig. 105: Hannover Trade Fair 2014 – Jülich's stand (left) and visit from Minister of Innovation, Science and Research Svenja Schulze (right)

6.6 How to reach us

6.6.1 By car

Coming from Cologne on the A4 motorway (Cologne–Aachen) leave the motorway at the Düren exit, then turn right towards Jülich (B56). After about 10 km, turn off to the right onto the L253, and follow the signs for “Forschungszentrum”.

Coming from Aachen on the A44 motorway (Aachen–Düsseldorf) take the “Jülich-West” exit. At the first roundabout turn left towards Jülich, and at the second roundabout turn right towards Düren (B56). After about 5 km, turn left onto the L253 and follow the signs for “Forschungszentrum”.

Coming from Düsseldorf Airport, take the A52 motorway (towards Düsseldorf/Mönchengladbach) followed by the A57 (towards Cologne (Köln)) to Neuss-West. Then take the A46 (towards Jüchen/Grevenbroich), before turning onto the A44 (towards Aachen). Continue as described in “Coming from Düsseldorf”.

Coming from Düsseldorf on the A44 motorway (Düsseldorf–Aachen) you have two choices:

1. (Shorter route but more traffic) turn right at the Jülich-Ost exit onto the B55n, which you should follow for approx. 500 m before turning right towards Jülich. After 200 m, before the radio masts, turn left and continue until you reach the “Merscher Höhe” roundabout. Turn left here, drive past the Solar Campus belonging to Aachen University of Applied Sciences and continue straight along Brunnenstrasse. Cross the Römerstrasse junction, continue straight ahead onto Wiesenstrasse, and then after the roundabout and the caravan dealers, turn left towards “Forschungszentrum” (signposted).
2. (Longer but quicker route) drive until you reach the “Jülich-West” exit. At the first roundabout turn left towards Jülich, and at the second roundabout turn right towards Düren (B56). After about 5 km, turn left onto the L253 and follow the signs for “Forschungszentrum”.

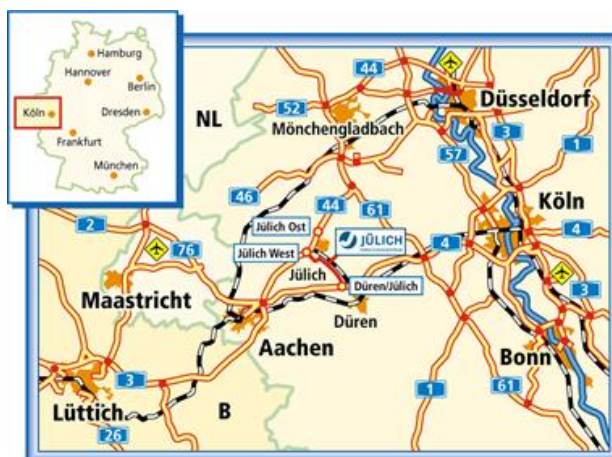


Fig. 106: Euregio Rheinland map

Navigation systems: In your navigation system, enter “Wilhelm-Johnen-Strasse” as the destination. From here, it is only a few hundred meters to the main entrance – simply follow the signs. Forschungszentrum Jülich itself is not part of the network of public roads and is therefore not recognized by navigation systems.

6.6.2 By plane

Cologne Bonn Airport: From the railway station at the airport, either take the S13 to Cologne main train station (Köln Hauptbahnhof) and then continue with the regional express to Düren, or go to Köln-Ehrenfeld by regional express and then take the S12 to Düren. Continue from Düren as described under “By train”.

By train from Düsseldorf Airport: From the railway station at the airport, travel to Cologne main train station (Köln Hauptbahnhof) and then continue on to Düren. Some trains go directly to Düren whereas other connections involve a change at Cologne main train station. Continue from Düren as described under “By train”.

6.6.3 By train

Take the train from Aachen or Cologne to Düren’s main train station (Hauptbahnhof). Then take the local train to Jülich (“Rurtalbahn”) and get out at the “Forschungszentrum” stop. From here, you need to keep right and walk towards the main road before turning right towards Forschungszentrum Jülich. The main entrance to Forschungszentrum Jülich is about 20 minutes by foot.



Fig. 107: Forschungszentrum Jülich campus map

6.7 List of Abbreviations

ADELHEID	NRW-Projekt „Aus dem Labor heraus in die Lüft“
ADELHEID	NRW project – from the laboratory into the air
AFC	Advanced Fuel Cells Implementing Agreement of the International Energy Agency
AGEF	Working Group of Electrochemical Research Facilities e.V.
APU	auxiliary power unit
ASR	area specific resistance
ARTEMIS	Assessment and Reliability of Transport Emission Models and Inventory Systems
ATR	autothermal reforming
BBP	benzyl butyl phthalate
BESSY	Berlin Electron Storage Ring – Society for Synchrotron Radiation
BET	analytical technique for the determination of surface area (Brunauer-Emmett-Teller)
BEV	battery electric vehicle
BGS	Department of Fuel Processing Systems
BMBF	Federal Ministry of Education and Research
BMWi	Federal Ministry for Economic Affairs
BMVBS	Federal Ministry of Transport, Building and Urban Affairs
BREZEL	fuel cells expert committee of the Association of German Engineers (VDI)
BTL	bio-to-liquid
FC	fuel cell
CAB	catalytic burner
CAPM	capital asset pricing model
CCM	catalyst coated membrane
CFD	computational fluid dynamics
CGO	cerium-gadolinium oxide: $Ce_{0.8}Gd_{0.2}O_{2-\delta}$
CHP	combined heat and power
CLSM	confocal laser scanning microscope
CO	carbon monoxide
CONCAWE	Conservation of Clean Air and Water in Europe
CS	cassette-substrate concept
CV	cyclovoltametry
CVD	chemical vapor deposition
DECHEMA e.V.	Society for Chemical Engineering and Biotechnology e.V.
DFG	German Research Foundation
DIN EN ISO	sector-independent certification standard for quality management systems
DLR	German Aerospace Center
DME	dimethyl ether
DMFC	direct methanol fuel cell
DSC	differential scanning calorimeter
DWV	German Hydrogen and Fuel Cell Association
EBSD	electron backscatter diffraction
ECE	Jungheinrich horizontal order picker: lift 1.25 m; load 2.0–2.5 t
ECE-15	urban driving cycle (Economic Commission for Europe)

ECS	Electrochemical Society
ECSA	electrochemically available surface area
EDX	energy-dispersive X-ray spectroscopy
RE	renewable energy
EEG	German Renewable Energy Act
EEL	Department of Electrochemistry Electrolysis
EFFESYS-BRINKS	project for the development of a stack for an aircraft APU
EGSE	Experts Group on Science for Energy
EIS	electrochemical impedance spectroscopy
Energy Lab	HGF research project investigating large-scale energy systems for grid stabilization
EOL	end of life
EU	European Union
EUDC	extra-urban driving cycle
FCH	fuel cell and hydrogen
FCV	fuel cell electric vehicle
FEM	finite element modeling
FG	weight per unit area
FRT	frost day
FTIR	Fourier transform infrared spectroscopy
FTP	driving cycle USA (Federal Test Procedure)
FVEE	German Renewable Energy Research Association
FZJ	Forschungszentrum Jülich GmbH
GC/MS	gas chromatograph coupled with a mass spectrometer
GDE	gas diffusion electrode
GDL	gas diffusion layer
GHG	greenhouse gas
GHSV	gas hourly space velocity
GIS	geographic information system
GRL	base load
GTL	gas-to-liquid
GVC	Society for Process Engineering and Chemical Engineering
HEV	hybrid electric vehicle
HGF	Helmholtz Association of German Research Centres
HPC	high-performance computing
H-SEM	high-resolution scanning electron microscopy
HT	high-temperature
HT-PEFC	high-temperature polymer electrolyte fuel cell
HTS	high-temperature section
HWFET	Highway Fuel Economy Test
HYPOS	Hydrogen Power Storage & Solutions East Germany
HYZEM	European driving cycle with a high proportion of speed changes (Hybrid Technology Approaching Efficient Zero Emission Mobility)
IAHE	International Association of Hydrogen Energy
IBG-2	Institute of Bio- and Geosciences – Plant Sciences
ICEPE	International Conference on Energy Process Engineering
ICP-MS	inductively coupled plasma mass spectrometry
ICV	internal combustion engine vehicle
IEA	International Energy Agency

IGCC	integrated gasification combined cycle
IQ-BZ	qualification initiative for fuel cells
IEK-1	Institute of Energy and Climate Research – Materials Synthesis and Processing
IEK-2	Institute of Energy and Climate Research – Microstructure and Properties of Materials
IEK-3	Institute of Energy and Climate Research – Electrochemical Process Engineering
IEK-9	Institute of Energy and Climate Research – Fundamental Electrochemistry
IL	ionic liquid
JC08	Japanese driving cycle
JSC	Jülich Supercomputing Centre
JuHY	Jülich's hydrogen demonstration facility
JuLab	Jülich Schools Laboratory
JULABOS	Jülich's Lattice-Boltzmann software tool
JUROPA	Jülich supercomputer
KIT	Karlsruhe Institute of Technology
LSCF	lanthanum strontium cobaltite ferrite
LNG	liquefied natural gas
LTS	low-temperature shift
MATLAB	programming language for technical calculations
MBE	molecular beam epitaxy
MEA	membrane electrolyte assembly
MeOH	methanol: CH ₃ OH
MODEM	empirically determined driving cycle (Modelling of Emissions and Fuel Consumption in Urban Areas)
MS	mass spectrometry
MVEG	Motor Vehicle Emissions Group
Nafion®	registered trademark for a sulfonated tetrafluorethylene polymer
NDIR	non-dispersive infrared adsorption analyzer
N.ERGHY	New European Grouping on Fuel Cells and Hydrogen
NESTE Oil	Finnish refinery and marketing company
NExBTL	fuel based on palm oil
NMHC	non-methane hydrocarbons
NMR	nuclear magnetic resonance spectroscopy
NPOC	non-purgeable organic carbon
NRW	North Rhine-Westphalia
OCV	open cell voltage
OpenFOAM	Open Source Field Operation and Manipulation
ORR	oxygen reduction reaction
PAH	parallel hybrid passenger car with internal combustion engine and battery
PBI	polybenzimidazole
PCI	Institute of Physical Chemistry at Giessen University
PEFC	polymer electrolyte fuel cell
PEM	polymer electrolyte membrane
PEM-EL	polymer electrolyte membrane electrolysis
PEMFC	polymer electrolyte membrane fuel cell

PHOEBUS	Jülich research and development project on photovoltaics, electrolysis, fuel cells and systems engineering
PIL	proton conductive ionic liquids
PLD	pulsed laser ablation/deposition
PoF	program-oriented funding
ProcessNet	initiative of DECHEMA and VDI-GVC
PROX	preferential oxidation
PTFE	polytetrafluoroethylene
PtG	power-to-gas
QM	quality management
RHE	reversible hydrogen electrode
RDE	rotating disc electrode
RR	anode gas recirculation ratio
rSOC	reversible solid oxide cell
RWTH	RWTH Aachen University
SAED	selected area electron diffraction
SC03	driving cycle, part of the Supplemental Federal Test Procedure (SFTP), accounts for vehicle air conditioning
SCT	segmented cell technology
SD	standard diesel
SeaTfo	2-sulfoethyl ammonium trifluoromethanesulfonate
SEM	scanning electron microscope
SOE	solid oxide electrolysis
SOFC	solid oxide fuel cell
SOP	standard operation procedure
SPI	sulfonated polyimide
SRMS	magnetic imaging and mass spectroscopy
SuPER	ProcessNet Section Sustainable Production, Energy and Resources
SWOT	analysis of strengths, weaknesses, opportunities and threats
TEM	transmission electron microscope
TESA	collaborative project for technology-based energy systems analysis
TG	thermogravimetric analysis
TGA	thermogravimetric analyzer
TOC	total concentration of total organic carbon
TRENDS	Expert Group for the Transition to Renewable Energy Devices and Systems
TTW	tank-to-wheel
US06	driving cycle, part of the Supplemental Federal Test Procedure (SFTP), accounts for aggressive driving behavior
UPV	uninterruptable power supply
VDI	Association of German Engineers e.V.
VEL	Department of Process Engineering Electrolysis
VA-RHLQ	Jülich documented procedure for the creation, revision, reviewing, approval, distribution and archiving of documents
VSA	Process and Systems Analysis Team
WACC	weighted average cost of capital
WBZU	Education and Training Centre for Innovative Energy Technologies Ulm e.V.
WGS	water-gas shift reactor

WHEC	World Hydrogen Energy Conference
WILEY-VCH	WILEY chemistry publisher
WLTC	Worldwide Harmonized Light-Duty Driving Test Cycle
WTT	well-to-tank
XPS	X-ray photoelectron spectroscopy
XRD	X-ray diffraction
YSZ	yttrium-stabilized zirconia
ZEA-1	Central Institute of Engineering, Electronics and Analytics – Engineering and Technology

Band / Volume 266

Real-time quantification of oxygen isotope exchange between carbon dioxide and leaf/soil water in terrestrial ecosystems with laser-based spectroscopy

L. Gangi (2015), XX, 156 pp

ISBN: 978-3-95806-061-6

Band / Volume 267

Secondary Uranium Phases of Spent Nuclear Fuel – CoXnite, $USiO_4$, and Studtite, $UO_4 \cdot 4H_2O$ – Synthesis, Characterization, and Investigations Regarding Phase Stability

S. Labs (2015), 153, xlii pp

ISBN: 978-3-95806-063-0

Band / Volume 268

Chemische, verfahrenstechnische und ökonomische Bewertung von Kohlendioxid als Rohstoff in der chemischen Industrie

A. Otto (2015), viii, 272 pp

ISBN: 978-3-95806-064-7

Band / Volume 269

Energetische und wirtschaftliche Optimierung eines membranbasierten Oxyfuel-Dampfkraftwerkes

Y. Nazarko (2015), IV, 337 pp

ISBN: 978-3-95806-065-4

Band / Volume 270

Investigation of light propagation in thin-film silicon solar cells by dual-probe scanning near-field optical microscopy

S. Lehnen (2015), 120 pp

ISBN: 978-3-95806-066-1

Band / Volume 271

Characterization of soil water content variability at the catchment scale using sensor network and stochastic modelling

W. Qu (2015), XVI, 123 pp

ISBN: 978-3-95806-067-8

Band / Volume 272

Light Absorption and Radiative Recombination in Thin-Film Solar Cells

T. C. M. Müller (2015), ii, 146 pp

ISBN: 978-3-95806-068-5

Band / Volume 273

Innenbeschichtung poröser Körper mittels Atomlagenabscheidung zur Redoxstabilisierung anodengestützter Festoxidbrennstoffzellen

T. Keuter (2015), XII, 133 pp

ISBN: 978-3-95806-069-2

Band / Volume 274

Thermochemical Modeling of Laves Phase Containing Ferritic Steels

A. Jacob (2015), 200 pp

ISBN: 978-3-95806-070-8

Band / Volume 275

Lithiumbatterien für stationäre und mobile Anwendungen: Benchmarking und experimentelle Umsetzung

T. Bergholz (2015), vi, 387 pp

ISBN: 978-3-95806-071-5

Band / Volume 276

Pyrochlore as nuclear waste form: actinide uptake and chemical stability

S. C. Finkeldei (2015), IX, 155 pp

ISBN: 978-3-95806-072-2

Band / Volume 277

Herstellung von Elektrodenstrukturen für Lithium-Ionen-Dünnschichtbatterien

A. Bünting (2015), v, 151 pp

ISBN: 978-3-95806-073-9

Band / Volume 278

Keramiken des Monazit-Typs zur Immobilisierung von minoren Actinoiden und Plutonium

J. M. Heuser (2015), viii, 212 pp

ISBN: 978-3-95806-076-0

Band / Volume 279

IEK-3 Report 2015

Systems Research and Engineering for a Sustainable Energy Supply
(2015), 182 pp

ISBN: 978-3-95806-077-7

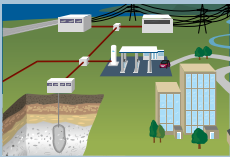
Weitere *Schriften des Verlags im Forschungszentrum Jülich* unter
<http://wwwzwb1.fz-juelich.de/verlagextern1/index.asp>

Institute of Energy and Climate Research – Electrochemical Process Engineering (IEK-3)

IEK-3 is one of the ten subinstitutes that currently constitute the Institute of Energy and Climate Research. Research work at IEK-3 focuses on providing technical solutions for a sustainable energy supply chain utilizing electrochemical energy conversion processes. Priority is given to electrochemistry and process engineering for solid oxide and polymer electrolyte fuel cells with and without reforming as well as for water electrolysis. These conversion technologies are investigated by an interdisciplinary team of scientists – from the underlying scientific principles to application in technical systems. IEK-3 not only has laboratories for imaging, physicochemical and electrochemical investigations, but also facilities for preparation and sample pretreatment. In addition, universal and specialized test setups enable extensive operational testing and characterization of diverse converters with dimensions ranging from a square centimetre to square metres. In anticipation of technology transfer, IEK-3 has established a technical facility to concurrently fabricate functional layer systems, such as electrodes, gas diffusion layers and membrane electrode assemblies, in a reproducible manner on an industrial scale. The facility also enables the precise assembly of multicomponent stacks. Process and systems analyses make it possible to identify and evaluate promising future R&D topics, to compare in-house technological developments with conventional technologies, to design energy pathways and energy supply networks, and to derive recommendations and provide guidance for interested sectors of society. IEK-3 cooperates closely with universities and other educational establishments, providing an extensive range of further education and training opportunities.



The future energy demand will be covered predominantly by renewables like wind, water and the sun in decentralized units. The associated fluctuating provision of energy necessitates the construction of industrial-scale electrolyzers, storage solutions and reserve power plants.



Electrolysis is a primary conversion process which converts renewable excess power into hydrogen for compressed gas storage in large salt domes. A pipeline network for transporting and distributing large quantities of H_2 will ensure the economic and safe supply of H_2 to filling stations and other places of use such as refineries and reserve power plants.



In addition the direct use of H_2 in cars, buses and transporters with fuel cell drives, its indirect use as a biofuel is a promising option for avoiding CO_2 emissions in the aircraft, truck, rail and marine sectors. To produce the fuel on an industrial scale, biomass-based carbon is processed together with H_2 in a refinery to create a liquid biofuel, which is then transported by trailers to the various dispersers at bio- or airport filling stations.